Università Politecnica delle Marche
Scuola di Dottorato di Ricerca in Scienze dell'Ingegneria
Curriculum in Ingegneria Civile, Ambientale, Edile e Architettura

---

Numerical analysis of traditionally excavated shallow tunnels

Ph.D. Dissertation of:

Alessandra Paternesi

Advisor:

Prof. Ing. Giuseppe Scarpelli

Curriculum supervisor:

Prof. Ing. Stefano Lenci

29th - 15th new series

Università Politecnica delle Marche
Scuola di Dottorato di Ricerca in Scienze dell'Ingegneria
Curriculum in Ingegneria Civile, Ambientale, Edile e Architettura

---

Analisi numeriche di gallerie superficiali scavate in tradizionale

Ph.D. Dissertation of:

Alessandra Paternesi

Advisor:

Prof. Ing. Giuseppe Scarpelli

Curriculum supervisor:

Prof. Ing. Stefano Lenci

29^{th} - 15^{th} new series

Università Politecnica delle Marche
Dipartimento di Scienze e Ingegneria della Materia, dell'Ambiente ed Urbanistica (SIMAU)
Via Brecce Bianche 12, 60131 Ancona (Italy)

Acknowledgements

I wish to thank Professor Scarpelli not only for giving me the opportunity and all the means I needed for developing this thesis but also for trusting me and supporting all the choices I had to take during this period as well as all the activities that could be useful for my personal growth. I appreciated his willingness to discuss with me and my colleagues about all the topics he had to deal with from both the research and professional side. All the projects and academic activities I was involved in represented an essential part of my knowledge. A huge thanks to Professor Schweiger, who welcomed me in Graz and contributed to turn my period as visiting PhD student into an extremely positive experience. He also played a decisive role in the definition of the path I could follow to develop an organic work and encouraged me to challenge myself, sharing my work with the scientific and professional community. His availability to share his knowledge and to discuss with PhD students and colleagues, as well as his passion for his work, represent an example for all those who have the luck to work with him.

Thanks to my colleagues Viviene, Paolo, David, Alessandro, Evghenia and Antonio for taking part in many useful discussions and providing important suggestions for improving my work.

Thanks to my family for recognising and supporting my inclination for research, for helping me in chasing my dreams and pursuing this path despite the difficult moments.

Thanks to Emanuele who was always in the front line for remembering me that I could make it, no matter how hard it was, and for his capability to lighten my mood and remember me not to take everything too seriously. Despite the distance, I never felt alone in facing good and bad moments.

Abstract

Among the problems that civil engineers have to face, the design and verification of an underground construction is one of the most challenging. A tunnel engineer has to tackle with a complex three-dimensional soil-structure interaction problem where many factors and uncertainties come into play. This is the reason why professional experience and engineering judgment usually play a crucial role.

In recent years, numerical calculation techniques, which can provide an important basis for a better understanding of the problem, have strongly improved. They have become a fundamental resource for underground construction design, but they also entail some drawbacks:

- only engineers with a strong numerical background can handle complex soil-structure interaction problems;
- numerical calculations, especially if 3D, can be very time-consuming;
- material parameters should be carefully evaluated, according to the particular problem and adopted constitutive law;
- numerical models need to be validated with field monitoring data
- it is not always clear how to tackle with numerical models in combination with design codes.

The goal of this thesis is to investigate the main issues regarding the applicability of numerical analyses to the design and verification of traditionally excavated shallow tunnels. The term traditional refers to any excavation technique not involving the use of tunnelling boring machines.

Despite the remarkable technological improvement in mechanised tunnelling, traditional techniques still represent, in some cases, the most suitable and convenient solution. The principal advantage of traditional techniques is the high flexibility in the choice of supports and reinforcement measures. However, design flexibility implies a deep understanding of the ground response to underground openings as well as a conscious use of numerical models. This work provides a contribution to the numerical design of shallow tunnels by focusing on three principal issues:

- stability of reinforced and unreinforced excavation faces;
- Eurocodes applicability to a numerically-based design of shallow tunnels;
- parameters calibration and numerical validation through comparison with monitoring data.

Riassunto

Lo scavo di gallerie rappresenta sicuramente una tra le sfide più impegnative che un ingegnere civile possa affrontare. Ciò è dovuto principalmente alla natura tridimensionale di questo problema di interazione terreno-struttura ma anche alle numerose incertezze che possono entrare in gioco nella progettazione. Come conseguenza di tali difficoltà, il giudizio ingegneristico e l'esperienza del progettista giocano spesso un ruolo forndamentale.
Recentemente, le tecniche di calcolo numeriche, che permettono una più ampia comprensione del problema, hanno subito un notevole sviluppo, diventando una risorsa fondamentale per la progettazione di scavi in sotterraneo. Tuttavia, è necessario valutare anche che:

- solo ingegneri con una buona preparazione numerica sono in grado di gestire la modellazione di problemi di interazione terreno-struttura così complessi;
- i calcoli numerici, in particolare quelli 3D, possono comportare un notevole dispendio di tempo, a volte non compatibile con le esigenze progettuali;
- i parametri del materiale devono essere calibrati accuratamente, tenendo in considerazione le peculiarità del problema analizzato e del legame costitutivo adottato;
- i modelli numerici devono essere validati con dati di monitoraggio;
- l'applicazione dei comuni codici progettuali ad una progettazione basata sulla modellazione numerica non è sempre chiara e lineare.

Lo scopo di questa tesi è quello di analizzare alcune delle problematiche principali legate alla progettazione di gallerie superficiali scavate in tradizionale. Lo scavo in tradizionale comprende tutte le tecniche che non prevedono un processo di industrializzazione dello scavo stesso, come avviene con l'utilizzo di una TBM (Tunnelling Boring Machine).
Nonostante il notevole sviluppo tecnologico dello scavo meccanizzato, quello in tradizionale rappresenta ancora, in alcuni casi, la soluzione più vantaggiosa. Il vantaggio principale è legato alla maggiore flessibilità nella scelta dei rivestimenti e delle techniche di rinforzo del cavo e del fronte della galleria. Tuttavia, una maggiore flessibilità progettuale è necessariamente legata ad una profonda conoscenza del comportamento deformativo dell'ammasso, nonché ad un utilizzo consapevole delle

tecniche di modellazione numerica. Il presente lavoro è principalmente incentrato sulle seguenti tematiche:

- l'analisi della stabilità di fronti di scavo rinforzati e non rinforzati;
- l'applicabilità degli Eurocodici ad una progettazione di gallerie superficiali condotta mediante tecniche di modellazione numerica;
- la calibrazione dei parametri del modello numerico e la sua validazione attraverso dati di monitoraggio.

Contents

List of Figures

List of Tables

Introduction

Traditionally excavated tunnels are underground openings built without the use of tunnelling boring machines. In these cases, the human intervention plays a major role and therefore, the workmanship skills and experience can have a significant influence on the construction process. The tunnel supporting techniques involve mainly sprayed concrete, steel ribs and grouted bolts. A further support made of reinforced or unreinforced concrete is usually cast at a certain distance from the tunnel face. Unlike mechanised tunnelling, traditional excavation allows for greater flexibility in the choice of structural supports and section geometries. The possibility to carry out face surveys while advancing leads to a deeper knowledge of the local geology and geomechanical properties. A greater awareness of the mechanical behaviour of the excavated ground can also be achieved by monitoring stresses and deformations of the tunnel support and the surrounding mass. The flexibility in defining the supporting techniques and the excavation sequence allows for on-going design evaluations and modifications, which might result in actual improvements only when based on an extensive monitoring and accurate back-analyses.

Regarding shallow tunnels (overburden lower than 3-5 tunnel diameters), they often involve soils or weathered rocks. This aspect raises the problem of guaranteeing face stability and workmanship safety, avoiding excessive deformations or the activation of failure mechanisms that could potentially cause important subsidence phenomena and building damages. The three-dimensionality of the problem and the frequent need to design face reinforcements require complex numerical calculations.

Nowadays, the development of user-friendly numerical codes and the growing computational capacity make possible to simulate complex geometries and excavation sequences both in two and three dimensions. Therefore, stress-deformation calculations, as well as safety analyses, can be easily performed by tunnel engineers both in the design phase and when updating the original design. Nevertheless, without a proper model parameter calibration carried out through laboratory and in situ tests, even the most accurate model would fail in providing reliable predictions. By back-analysing monitoring data, it is theoretically possible to reach a further refinement of the ground geotechnical properties.

Regarding numerical methods applied to tunnel construction analyses, no standard code currently regulates and define the most suitable procedure to ensure a safe design. Therefore, geotechnical engineers have to refer to other codes, defined for above structures or conventional geotechnical structures such as Eurocodes.
Given the previously mentioned issues, this thesis focuses on three principal aspects regarding traditionally excavated shallow tunnel:

- Eurocodes applicability to a numerically-based design of shallow tunnels;
- stability of reinforced and unreinforced excavation faces;
- parameter calibration and numerical validation through comparison with monitoring data concerning a specific case study.

The monitoring data considered for the present study refer to construction works of a new highway in Southern Italy.
All the previously mentioned issues were tackled using both 2D and 3D numerical calculations in combination with traditional or advanced constitutive models, depending on the final goal and on the specific problem to be analysed.
A comprehensive study of the state of the art regarding numerical analyses of underground constructions provided the basis for a more conscious definition of the numerical models. The literature review is included in the first two chapters.
Chapter 1 provides an overview of traditional excavation techniques and support measures.
Chapter 2 focuses on the design and verification methods commonly used in tunnelling with particular attention to numerical models. This part of the literature review covers each of the main topics that are analysed in the following chapters (face stability, Eurocodes based design and numerical predictions).
Chapter 3 deals with the application of Eurocodes to the design of shallow tunnels. A benchmark example, analysed through a 2D numerical model, enables some specific considerations.
Chapter 4 shows the results of 3D calculations aimed at assessing the stability and deformation behaviour of reinforced and unreinforced excavation faces. Comparisons with simpler models are provided.
Chapter 5 introduces the case study and the parameter calibration carried out before running numerical simulations. The case study deals with the construction works of a highway in Southern Italy.

Chapter 6 shows the model validation through field data, which are compared to numerical results.

Chapter 1. The construction of shallow tunnels through traditional techniques

The need to improve the transport network in increasingly congested urban areas, as well as the demand of new highway and motorway networks in hilly areas, often requires the construction of shallow tunnels. Despite tunnelling boring machines have become more flexible and reliable in the recent years, traditional excavation techniques are still widely used. In some cases, if the tunnel cover is thin (lower than 1-2 tunnel diameters), it can be built with the cut and cover method, which consists of trench excavation, tunnel construction and soil covering of the excavated tunnel. However, only mined tunnels will be considered in the following chapters.

1.1. Excavation techniques

Tunnel design includes, besides the definition of the supporting and reinforcement measures, the choice of the most appropriate excavation method and sequence. This choice is related to the characteristics of the tunnel itself as well as to the those of the surrounding environment (presence of pre-existing buildings and infrastructures, geomechanical and hydrological conditions). Irrespective of the context and the specific project, tunnel designers have to guarantee field safety conditions during both excavation and support installation. Regarding the excavation methods, it is often distinguished between traditional heading and mechanised heading. Both **Kolymbas (2005)** and **Lunardi (2000)** presented a comprehensive overview of the available excavation systems together with a discussion of the main factors involved in the selection of a particular method.

Mechanised tunnelling usually refers to the use of big machines allowing for a continuous and industrialised excavation process and therefore capable of reaching the fastest advance rates (up to 20 m/day).

The conventional methods are drill and blast and mechanically supported excavation (mechanical shovels, rippers, hydraulic and pneumatic hammers, roadheaders). Specific aspects regarding conventional heading are also addressed in the guidelines of **Ita Working Group Conventional Tunnelling (2009)**. After excavating and mucking, the primary support and, if necessary, soil reinforcements are applied to the cavity. Support and

reinforcement measures in conventional tunnelling will be addressed in the next paragraph.
The technique of drill and blast involves the detonation of explosive material placed in horizontal boreholes drilled by percussion or rotary-percussive means, according to a particular blasting sequence.

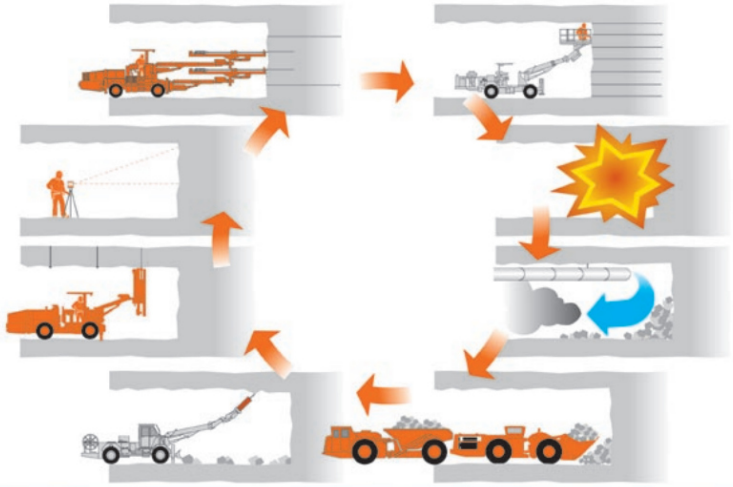

Figure 1. Drill and blast cycle (from Heiniö 1999)

When drill and blast is uneconomic or is not possible due to the ground mechanical properties or to the proximity to urban areas, the excavation may be carried out through mechanical or hydraulic tools, such as crawler excavators equipped with shovels, rippers, hammers, rotary cutters or roadheaders.

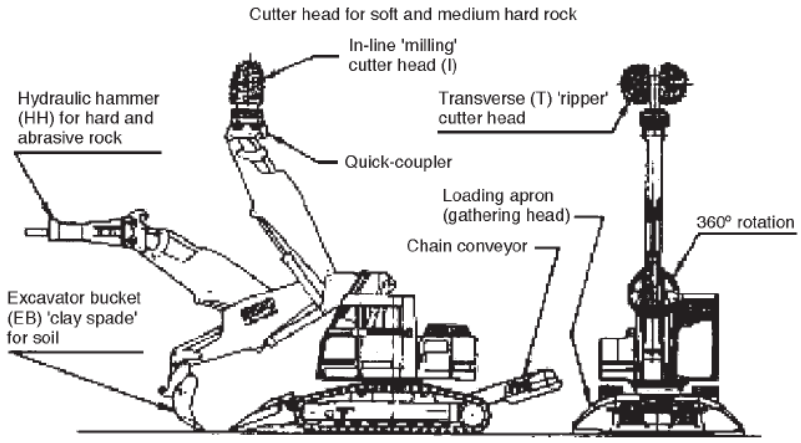

Figure 2. Excavator with attachment for multiple tasks (from Tatiya 2005)

Figure 3. Crawler excavator equipped with mechanical shovel

Figure 4. Crawler excavator equipped with rotary cutters

Figure 5. Crawler excavator equipped with hammer

Figure 6. Crawler excavator equipped with ripper

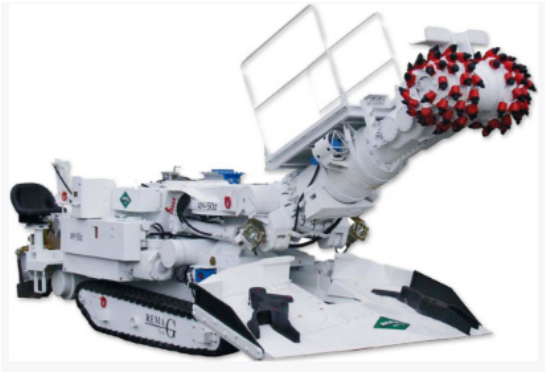

Figure 7. Roadheader

Wheel or crawler loaders and dumper are subsequently used to transfer the excavated material outside of the tunnel.

Figure 8. Wheeled loader and dumper.

The choice of the excavation tool or technique is strictly related to the ground properties and to the presence of pre-existing structures in the surroundings of the underground opening. Mechanical shovels are usually suitable for soils or weak rocks, whereas rippers can be used when hard rock inclusions are encountered and when RMR varies from 30 to 60 or P-waves vary from 1 to 2 km/s **(Kolymbas 2005)**. Roadheaders and hammers can be used for moderate rock strengths, but their efficiency decreases with the increase of rock mass strength.

Table 1. General indications about the suitability of different conventional excavation techniques according to the matrix UCS (from Lunardi 2000)

Parameter	Strength of the matrix [MPa]		
	<3	3–20	>20
Excavation system	ripper	hammer, roadheaders[1]	blasting

[1]useable only on small to medium cross section tunnels

As well as traditional tunnelling, also mechanised tunnelling involves excavation, mucking and support installation but the adopted tunnel machines can deal with all these three phases almost simultaneously, speeding up the construction process and requiring less workmanship.
The choice between conventional and mechanised heading depends on several factors: ground conditions, tunnel length, shape and dimensions of the cross section, environmental conditions, financial and time factors. The advantages of conventional excavation method compared to mechanised tunnelling are:

- greater flexibility and adaptability to different geotechnical conditions;

- possibility to excavate according to various shapes of the cross section;
- low installation costs.

On the other hand, traditional tunnelling usually requires workmanship operating close to the excavation face, advance rates do not exceed 5 meters/day and installation of the final support (after the primary lining) is often required.

However, despite the remarkable technological development regarding tunnel boring machines and the availability of very flexible and reliable TBMs, traditional excavation is still preferred when highly varying ground conditions are expected, for short tunnels and for tunnels with variable cross section shape.

The higher flexibility and adaptability to different ground types of conventional tunnelling lies in the possibility of changing excavation tool as well as other design characteristics such as:

- the strength and stiffness of the cavity support (shotcrete type and thickness, use of steel ribs or lattice girders, steel profile, ribs spacing);
- the length of the unsupported span;
- the primary support closure to form a closed ring (by installing providing the primary or temporary support with an invert);
- the distance of casting of the final concrete invert from the tunnel face;
- the adoption of partialised or full face section;
- the magnitude of face reinforcement (fibreglass bars, pipe umbrella, jet grouting, and so forth);
- radial reinforcement (bolts).

These variables can be defined and adjusted according to the encountered ground conditions and according to the deformation behaviour monitored while excavating (observational design method).

1.2. Supporting and reinforcement measures in conventional tunnelling

Supporting and reinforcement techniques aim at guaranteeing the stability of the excavation face and the cavity during the construction works and after

the excavation is completed. Figure 9 depicts the main supporting and reinforcement techniques employed in conventional tunnelling.

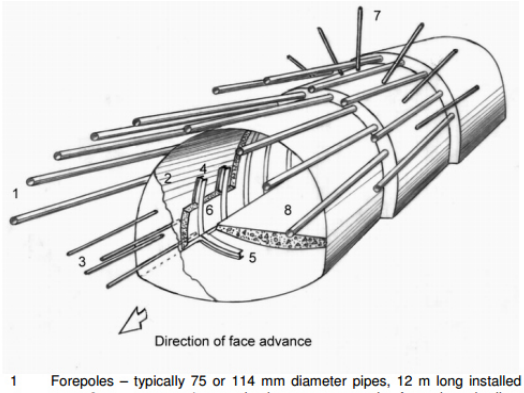

1 Forepoles – typically 75 or 114 mm diameter pipes, 12 m long installed every 8 m to create a 4 m overlap between successive forepole umbrellas.

2 Shotcrete – applied immediately behind the face and to the face, in cases where face stability is a problem. Typically, this initial coat is 25 to 50 mm thick and it is to prevent deterioration of the exposed rock surfaces.

3 Grouted fibreglass dowels – Installed midway between forepole umbrella installation steps to reinforce the rock immediately ahead of the face. These dowels are usually 6 to 12 m long and are spaced on a 1 m x 1 m grid.

4 Steel sets – installed as close to the face as possible and designed to support the forepole umbrella and the stresses acting on the tunnel.

5 Invert struts – installed to control floor heave and to provide a footing for the steel sets.

6 Shotcrete – typically steel fibre reinforced shotcrete applied as soon as possible to embed the steel sets to improve their lateral stability and also to create a structural lining. This shotcrete may be up to 300 mm thick.

7 Rockbolts as required. In very poor quality ground it may be necessary to use self-drilling rockbolts in which a disposable bit is used and is grouted into place with the bolt.

8 Invert lining – either shotcrete or concrete can be used, depending upon the end use of the tunnel.

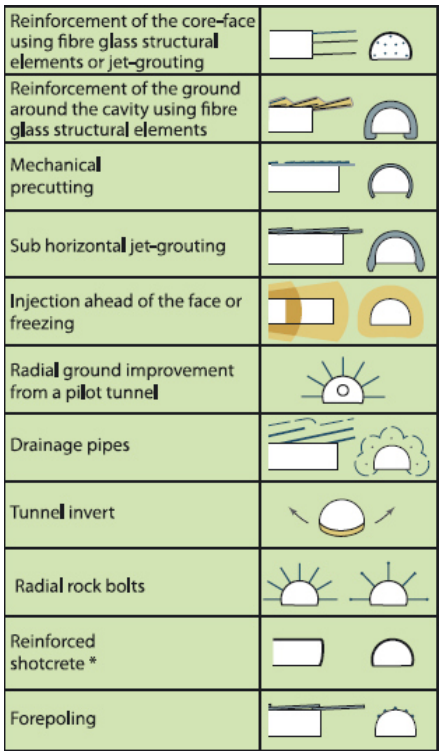

Figure 9. Support measures in conventional tunnelling (from Hoek 2001 and Lunardi 2000)

Supporting methods can be classified as temporary, primary or final linings. Temporary and primary supports are supposed to guarantee the tunnel stability while completing the construction works, whereas final lining aims at guaranteeing the long-term stability of the cavity. Temporary lining refers to those supports which are supposed to be removed before the tunnel completion (such as temporary inverts or central walls in partialised excavations). Most of the times traditionally excavated tunnels require both temporary/primary and final support, especially when dealing with soils and weak or medium strength rocks. The primary ground support is normally provided through a shotcrete shell reinforced with fibres, welded steel meshes, lattice girders and steel profiles. The final support is usually made of the primary lining and an inner cast-in-place concrete layer.

Thanks to the ground deformation and consequent stress relaxation occurring before and after lining installation (pre-convergence, Figure 10), the primary support is never loaded with the full initial stress the ground was subjected to. In fact, ground deformation implies the occurrence, in the zone surrounding the cavity, of the phenomenon called arching. It can be described as the stress redistribution caused by the tunnel excavation thanks to which the ground itself act as a cavity support.

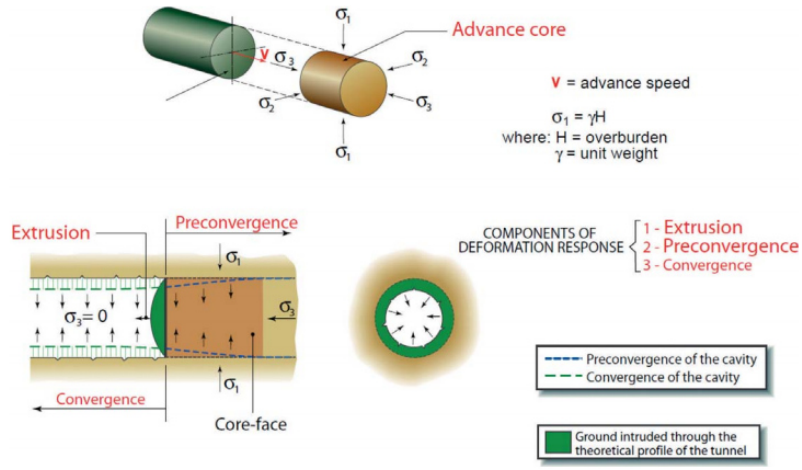

Figure 10. Tunnel deformation response (from Lunardi 2005)

Shotcrete, which is basically concrete projected at high velocity on the tunnel walls, is the main element constituting the primary or temporary lining. Its mechanical properties are similar as those of normal concrete. It is particularly suitable for tunnel construction because it can fit any shape of surface undergoing displacement and compaction at the same time. Furthermore, thanks to its deformability at early stages, it allows for ground deformation and stress redistribution.

As depicted in Figure 11, shotcrete can be reinforced with lattice girders or steel arches such as open steel profiles (IPN, HE, IPE). However, one of the major structural problems of these profiles is buckling (Figure 12, a). This is the reason why, in recent years, tubular hollow steel profiles (Figure 12, b) were tested and installed in some construction sites **(Zenti & Perlo 2015)**. These closed profiles, having the same moment of inertia in any direction, are more efficient in case of eccentric loads acting along a different axis. Both laboratory and in-situ tests proved the better performances of circular profiles compared to open profiles with the same cross section area.

Moreover, the concrete filling the hollow profile collaborates to the structural capacity of the section, which can, therefore, be assumed as a composite section. The circular shape also eliminates the shadow effects when projecting the shotcrete caused by the flanges of the open profile **(Zenti & Perlo 2015)**. Recently, a further technological innovation regarding the tubular steel profile allowed to improve the workmanship safety during tunnel construction, by introducing a semi-automatic installation procedure. The new steel rib is provided with automatically unfolding hinges and a special telescopic foot, enabling the arch installation entirely by machinery and avoiding the presence of workers close to the tunnel face (Figure 13).

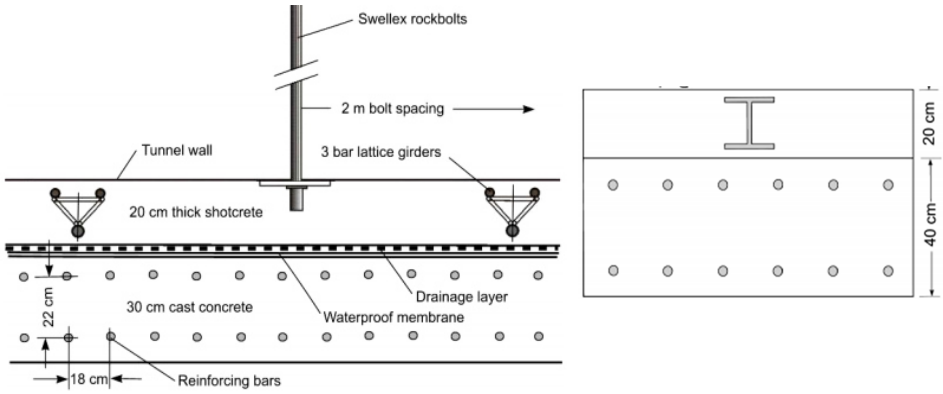

Figure 11. Sections of both primary and final tunnel support: shotcrete reinforced with lattice girders and cast in place concrete (left), shotcrete reinforced with steel ribs and cast in place concrete (right). Figures from (Hoek et al. 2008)

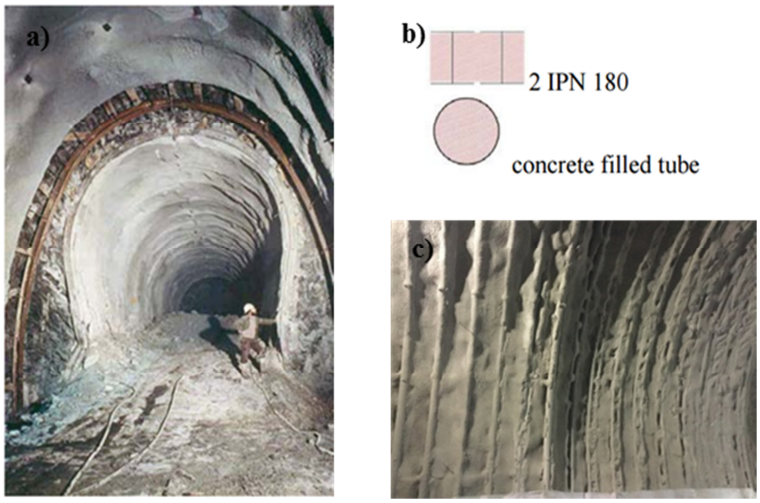

Figure 12. Case of open profile buckling (a, from Zenti & Perlo 2015), 2 coupled IPN profiles and tubular hollow profile (b, from Zenti & Perlo 2015), comparison between primary lining made of shotcrete reinforced with circular steel profiles on the left and shotcrete reinforced with coupled IPN on the right (c, from http://www.societaitalianagallerie.it)

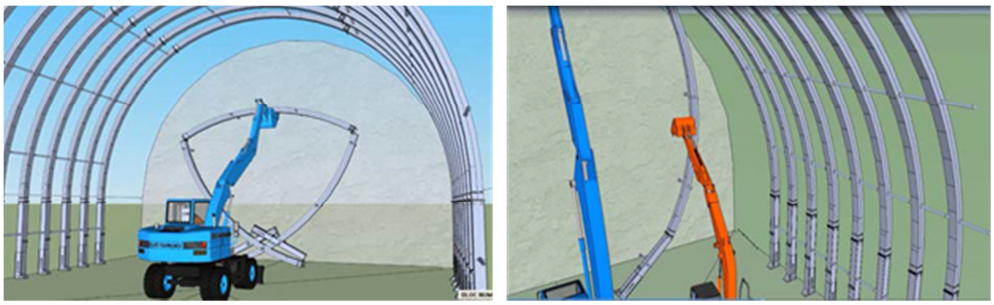

Figure 13. Installation of the semi-automatic tubular steel arch support (from Zenti & Cullaciati 2016)

In some cases, the shotcrete lining, due to significant radial displacement, can exceed the maximum compression deformation (around 1%) and reach failure. When significant convergences are expected (squeezing grounds), and damages to the primary support must be avoided, longitudinal slots in the shotcrete shell can be left open. The slots width can be up to 40 cm. In

this way, the cavity closure will deform only the steel reinforcement of the primary lining. These gaps can also be closed with special yielding joints, which represents predetermined failure points and enable a higher control of the final deformation as well as the redistribution of the ground pressure around the cavity (Figure 14). One of the first yielding element (Figure 15, left) was made of a group of steel tubes, installed with the axis in the circumferential direction **(Schubert 1996).** Later, some improvements (Figure 15, right) eliminated the problem of buckling affecting the tubes **(Schubert & Moritz 1998).**

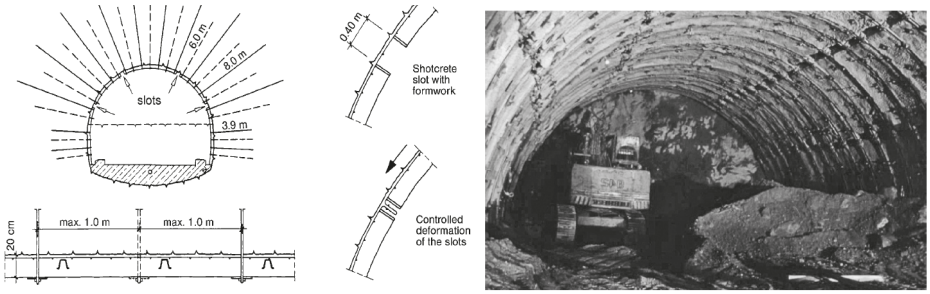

Figure 14. Longitudinal slots in the primary support (from Bernhard Maidl, Markus Thewes, Ulrich Maidl 2013)

Figure 15. Yielding supports (Schubert & Radoncic 2015)

A further support of the ground cavity can be provided through radial anchors, mainly used in rocky or very stiff soils. These reinforcements allow increasing the strength of the surrounding ground. Rock bolts can be divided into two main groups: end anchored and fully bonded. End anchored bolts are usually expanding bolts and are commonly used in materials that are fractured but have good mechanical properties to guarantee a stable anchorage. They work essentially in tension and can be pretensioned

(active) or left untensioned (passive, activated after cavity convergence starts to occur).
Fully bonded anchors, also called nails, are bars or tubes made of steel or fibreglass bonded to the wall for their whole length. They can, therefore, be used in poor quality rocks. The stress transfer between ground and bar can occur through the cement mortar used for filling the hole or through the tube itself as for Swellex bolts. They work both in shear and in tension and can significantly increase the cohesion of the reinforced material.

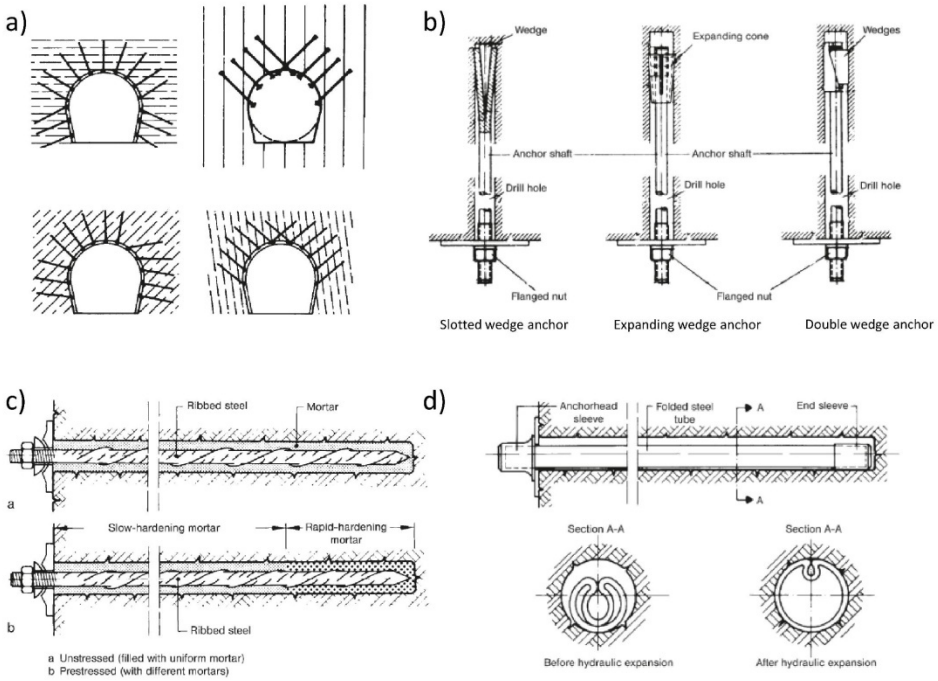

Figure 16. Correct arrangement of anchors (a), end anchored bolts (b), grouted anchors (c), Swellex anchors (d); figures from Bernhard Maidl, Markus Thewes, Ulrich Maidl 2013

When the primary lining is an open arch, an important construction detail that allows controlling vertical deformation is the thickening or the reinforcement of the lining foot (Figure 17). This structural detail enables to reduce the lining settlements providing an immediate bearing capacity to the primary support. It is particularly important in shallow tunnels, where limiting subsidence phenomena represents an important issue.

In any case, in soft grounds and urbanised areas, a fast ring closure either through a temporary or a permanent invert is very important for controlling deformations.

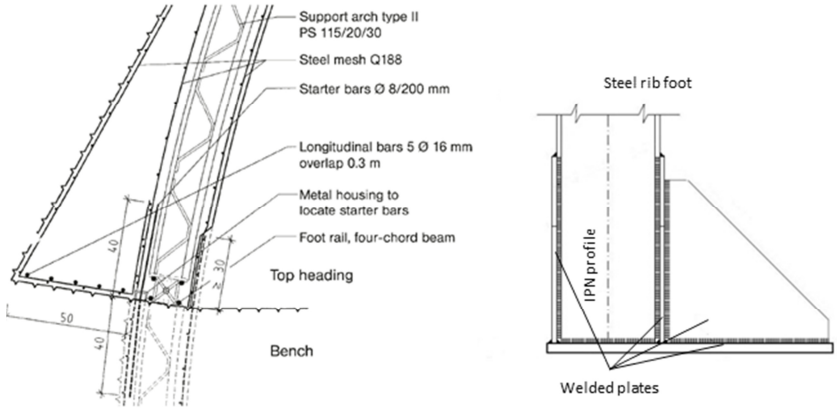

Figure 17. Construction detail of the primary support foot: shotcrete reinforced with lattice girder on the left (Bernhard Maidl, Markus Thewes, Ulrich Maidl 2013) and steel rib on the right.

Besides shotcrete or reinforced shotcrete linings, aimed at limiting the convergence of the tunnel cavity, other techniques can be implemented to provide further stability and limit ground deformations even before the face arrival.

Especially when the tunnel is excavated full face or with large unsupported spans, the surrounding ground may require some improvement to guarantee stability. When the final goal is to reinforce the tunnel face, limiting extrusion and pre-convergenge (Figure 10) and preserving the integrity of the advance core, the most common techniques implemented in traditional tunnelling are

- soil nailing;
- freezing;
- jet/grouting;
- mechanical pre-cutting.

Besides the previously described radial bolts, soil nailing can be performed in advancement. These nails are usually fibreglass bars inserted into a previously drilled hole and injected with grout (Figure 18). They can work as short-term reinforcements when they are inserted in the tunnel core or as long-term stabilisation technique when they are horizontally drilled around

the excavation profile in order to improve the stress redistribution capacity around the cavity. They remain unstressed until soil deformation occurs, causing the tensile stresses to be transferred to the nail through the lateral borehole surface. The properties that make fibreglass nails suitable for tunnel core reinforcement are:

- high tension strength;
- low weight;
- high fragility (easy to break during excavation).

This technique is mostly used in cohesive or semi-cohesive soils.

Recently, a new kind of fibreglass pipe characterised by an external corrugated profile was tested, developed and successfully used in tunnel construction works. The further improvement in this technology consisted in equipping the bar with an external textile sheath aimed at containing the injected cement grout (Figure 18, e). Furthermore, the bar was also provided with a coaxial drain designed to reduce the pore water pressures occurring at the tunnel face (Pressure Element Reinforcement Ground or PERGround®, Elas Geotecnica S.r.L.).

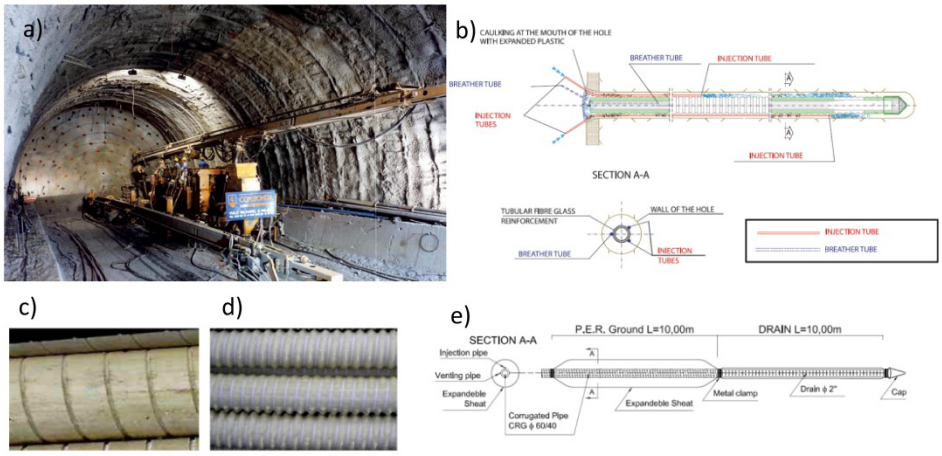

Figure 18. Drilling machine and reinforcement scheme (a, b; from Lunardi 2000); bar lateral surface (c), new corrugated profile (d) and P.E.R. Ground (e), from Zenti et al. 2012).

In granular or pseudo-cohesive soils, jet grouting is preferred to reinforce the advance core and to create a reinforced shell around the tunnel cavity (Figure 19). The only treatment used for horizontal injections in tunnels is normally the monofluid system, which consists of the injection, at high pressure (300 to 600 bar), of the cement suspension only. The high

pressures cause hydrofracturing (claquage) in the soil and create volumes of improved soil having the shape of columns. When very coarse soil is treated, the strength properties of the improved material are comparable to those of concrete. Injections can also be performed from the surface (for shallow tunnels) or from a pilot tunnel.

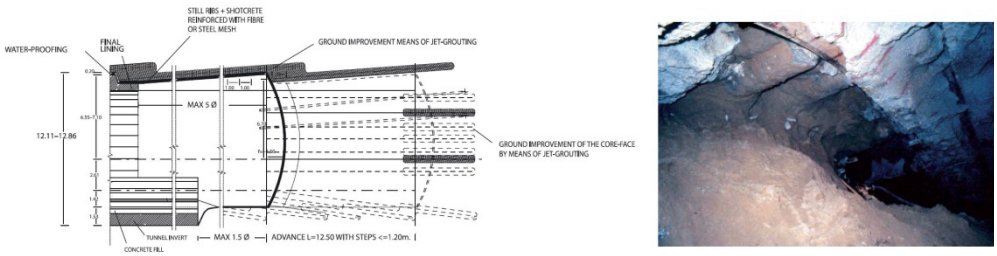

Figure 19. Longitudinal profile of the tunnel with jet-grouting reinforcements (left), detail of the columns on the tunnel crown (right); figures from Lunardi (2000)

In loose ground below the groundwater table, ground freezing is a convenient technique to temporary stabilise the ground surrounding the excavation. In contrast with jet grouting, it only alters the hydraulic conditions during the construction period.

Another application, mostly used to reinforce the tunnel roof in fractured rock or stiff soil is the so-called forepoling (Figure 20). It consists in the drilling, ahead of the face, of an umbrella of steel tubes, which are subsequently injected with grout. However, contrary to the reinforcement methods previously seen, forepoling does not contribute to arch effects because the structural elements are not connected to each other and therefore there is no collaboration between them.

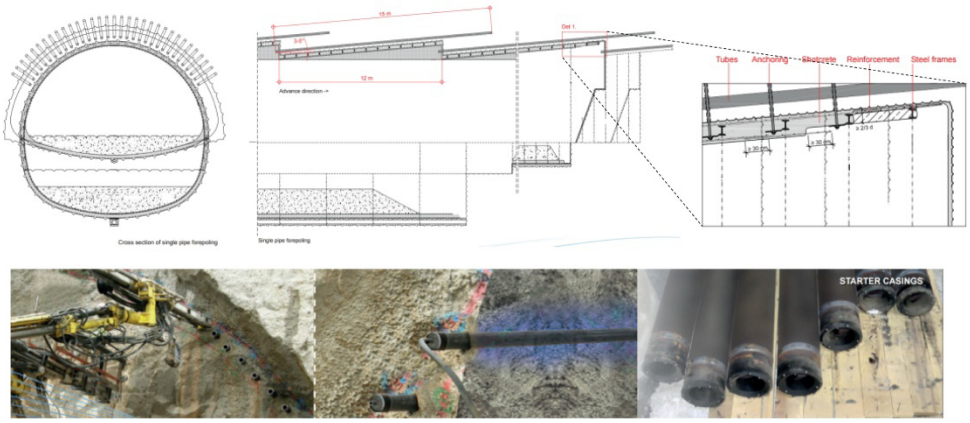

Figure 20. Forepoling with steel tubes (figures from www.robit.fi)

To avoid water inflow into the tunnel during the excavation phase, umbrellas of drainage pipes are usually installed, especially when the tunnel is below the water table. The slotted tubes are launched ahead of the face and create a zone of higher permeability around the tunnel to be excavated (Figure 21 a, b). This technique, when drained conditions take place, also has a positive effect on the mechanical properties of the surrounding ground. In fact, lowering the pore water pressures means increasing the effective stresses too. The drainage should be extended ahead of the tunnel face as deep as possible so that construction works are not interrupted too often. The drainage pipes consist of slotted hard PVC tubes installed into 35 to 100 mm diameter holes.

Regarding the final hydraulic conditions, the tunnel can be either drained (Figure 21, c) or sealed (waterproofed). An intermediate solution consisting in limiting the pressure to a prescribed value (through special valves) is also possible. This solution might be the best option when on the one hand it is necessary to reduce the disturbance to the surrounding soil and aquifer, but on the other hand, it would not be economically convenient to design the tunnel support to bear the full water pressure.

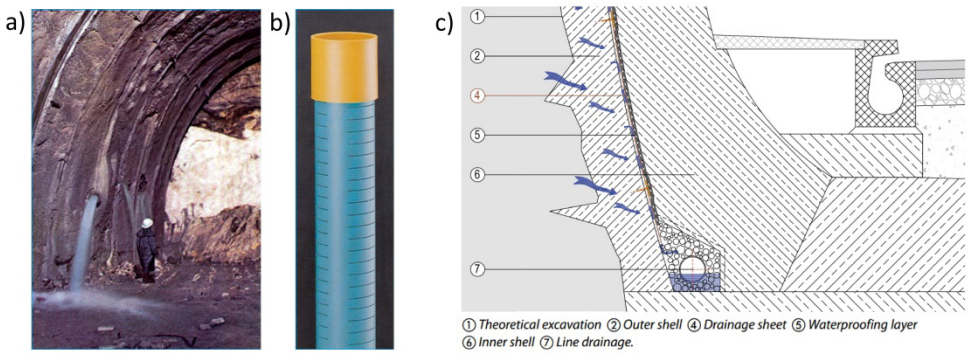

Figure 21. Drainage pipe bearing water (a) and slotted tube detail (b), from Lunardi 2000; detail of the final drainage on the tunnel sidewall (c), from www.cosella-dorken.com

1.3. Partialised vs. full face excavation

Conventional tunnelling allows the designer to choose between partial and full face excavation. However, it is largely debated, among tunnelling experts, whether tunnels should be driven full face or partialising the excavation face and which is the most suitable and economical solution with respect to different ground conditions. Furthermore, this topic is commonly associated with different construction methods, namely A.DE.CO-RS (acronym for Analysis of COntrolled Deformation in Rocks and Soils) and NATM (New Austrian Tunnelling Method).

The NATM, developed between the fifties and the sixties from the Austrian tunnelling specialists Rabcewicz, Pacher, Müller-Salzburg, entails that the tunnel is sequentially excavated and supported and the excavation face is partialised (Figure 22). The excavation sequences can be adapted to different ground conditions. The primary support is provided by shotcrete reinforced with fibres, welded-wire meshes or steel arches. Soil nails can be additionally used to improve the arching effect around the tunnel cavity. The fundamental principles are:

- maximisation of ground strength mobilisation (so to exploit arching effect to the maximum extent and reduce the thickness of the primary shotcrete support);
- intensive monitoring, necessary to adapt supporting measures to the encountered conditions and to check the correctness of the implemented solutions.

The exploitation of the load-bearing ring formed by the ground around the opening and the systematic measurements, leading to a construction process tailored to specific geotechnical conditions are, therefore, the pillars of NATM.
The ADECO-RS approach, developed more recently (1980s-1990s) from Lunardi, introduced some innovations. The philosophy behind this method is to act not only on the deformations occurring after the arrival of the advance face (namely the so-called convergence) but also on the pre-convergence and extrusion phenomena. Acting on these portions of the total deformation entails the adoption of reinforcement techniques aimed at improving or protecting the advance core (Figure 23), which represents the ground volume ahead of the face.
Unfortunately, since the number of the projects where both construction methods were used under similar conditions is low, it is very difficult to compare them through field data. However, it is possible to run numerical calculations as well as to make some general considerations aimed at comparing the two methods.
Marcher & Jiřičný (2005) carried out 3D numerical analyses of tunnel originally designed the NATM method, also with a plausible excavation sequence according to the ADECO RS approach. By comparing the results regarding crown settlements and subsidence, it turned out that the two methods yield comparable results, at least for the considered range of ground parameters. According to the same authors, if on the one hand the ADECO RS approach enables a faster and industrialised full face excavation, on the other hand it entails higher costs due to the use of face reinforcements and stiffer supports. However, in markedly poor geotechnical conditions, the advantages of the ADECO RS method can potentially increase. In fact, in these cases, preconfinement of the advance face, as well as the possibility of rapidly closing the arch supporting the cavity, can significantly contribute to minimize the deformations. This aspect could make the difference in shallow tunnels involving soils or weak rocks, especially in urban areas where surface settlements have to be minimised.
The minimization of displacements can also be pursued through the NATM by further partializing the advance face and adopting a temporary closure of the partial section (i.e. temporary invert). However, this method would increase the construction time, reducing the design cost-effectiveness.

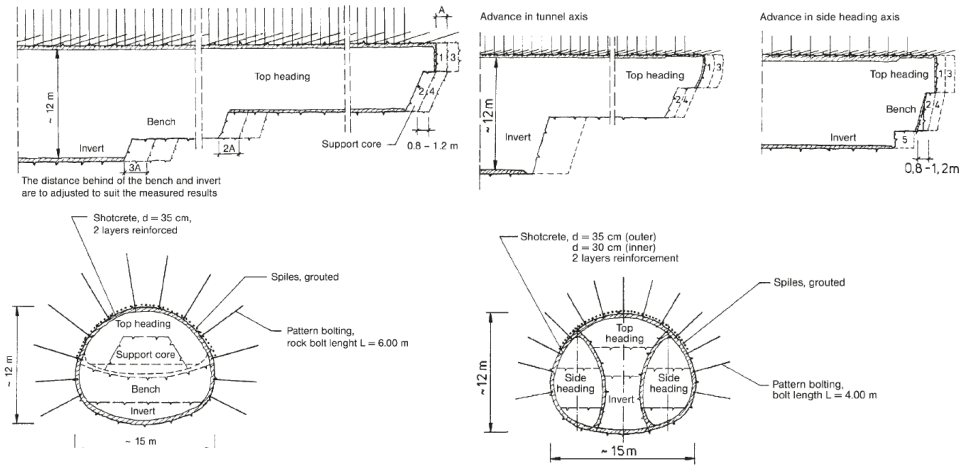

Figure 22. Examples of face partialisation and stabilisation through rock bolts: top heading-bench excavation on the left and side drift excavation on the right (after Bernhard Maidl, Markus Thewes, Ulrich Maidl 2013)

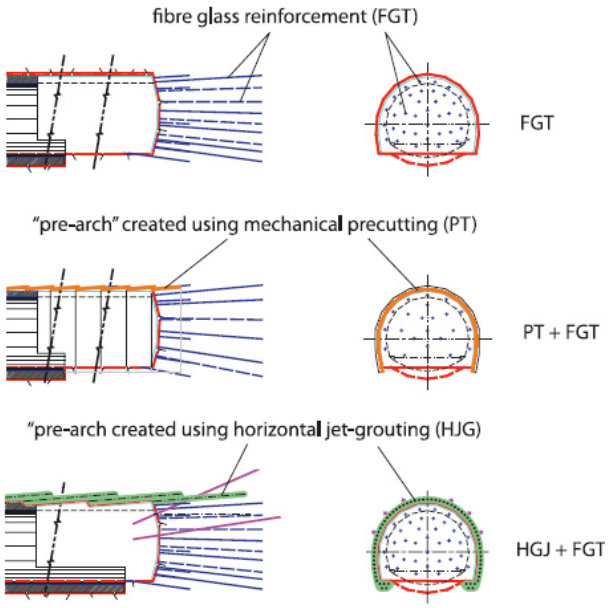

Figure 23. Reinforcement and protection techniques of the advance core (from Lunardi 2008)

1.4. Monitoring devices and techniques

In conventional tunnelling, field monitoring plays an important role. In fact, it is not only used for checking the goodness of the design but also for updating it whenever some adjustments of cavity supports, reinforcements or construction sequence are required. When the monitoring data are carefully back-analysed, they enable a more accurate definition of the geotechnical parameters and therefore an increase in the knowledge of the ground mechanical behaviour. Furthermore, monitoring also allows an early detection of unforeseen conditions and, when observation periods are sufficiently extended, the investigation of the long-term behaviour. If lining stress state is directly measured or back-calculate from deformation or displacement measurements, an evaluation of the structural safety is also possible.

The measurements normally carried out are:

- displacements of 5 points of the primary lining in 3 dimensions;
- displacements occurring in the surrounding ground;
- stress state on the primary and final lining;
- stress state on the anchors;
- tilt and cracks opening in surface structures (for shallow tunnels in urbanised areas)

Lining displacements, representing the standard monitoring, are usually measured through optical surveying. Monitoring sections can be 10-30 meters spaced and are installed at least at 1 m from the excavation face. Measurements are initially acquired every day, whereas the survey interval can be increased when the measured value show a stabilisation trend. Most of the times the measurement points are optical targets mounted on the primary lining (Figure 24, Figure 25). However, the measurement of distances between prescribed points would be more precise if carried out through invar wires or steel tapes (Kolymbas 2005, Table 2).

Table 2. Methods for monitoring of convergence (from Kolymbas 2005)

Method	Manufacturer	Resolution (mm)	System accuracy (mm)
Pins and invar wire	SolExperts	0.001	± 0.003
Steel tapes	Interfels	0.01	± 0.05
Geodetic tachymeter	e.g. Leica	1	$\pm(2-3)$
Tunnel scanner	DIBIT, GEODATA	1	± 10

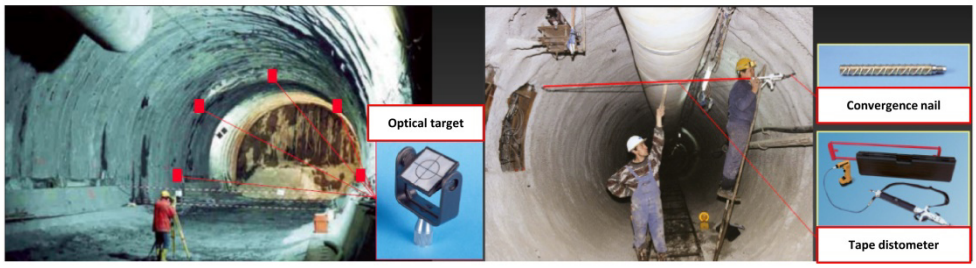

Figure 24. Optical targets (left) and tape distometer (right); courtesy of Sisgeo

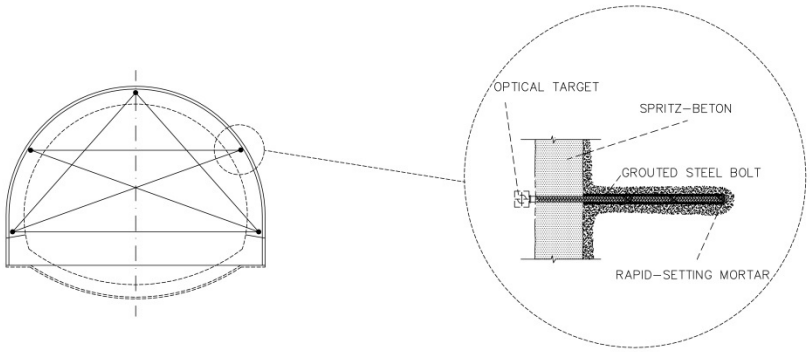

Figure 25. Details of optical targets installation on the primary lining

The monitoring of deformations and displacements in the ground surrounding the tunnel cavity is performed mainly by instrumenting boreholes with extensometers, sliding micrometres, inclinometers and extenso-inclinometers.

Extensometers and sliding micrometres allow for an estimation of deformations along the borehole axis, inclinometers provide horizontal displacements and finally extenso-inclinometers enables both measurements. Extensometers can be incremental, single or multipoint. The axial deformation profile is obtained by measuring the relative displacement of a prescribed point fixed to the ground respect to a reference point. Single and multipoint extensometers are equipped with one or more anchor points grouted to the surrounding ground. These points are connected to the head of the instrument through steel or fibreglass rods protected by an anti-friction sheath allowing the rods to slide and transfer the movement to the head (Figure 26, a). Incremental extensometers measure the distance

between the different pairs of magnetic rings fixed to an inclinometer tube cemented into the borehole (Figure 26, b).
These instruments can be installed either around the cavity or from the surface. Incremental extensometer horizontally installed into the tunnel core are also used to measure face extrusion and deformation of the advance core along the tunnel axis. In fact, the incremental extensometer tube can be partially demolished enabling extrusion measurements of the core during tunnel advance.

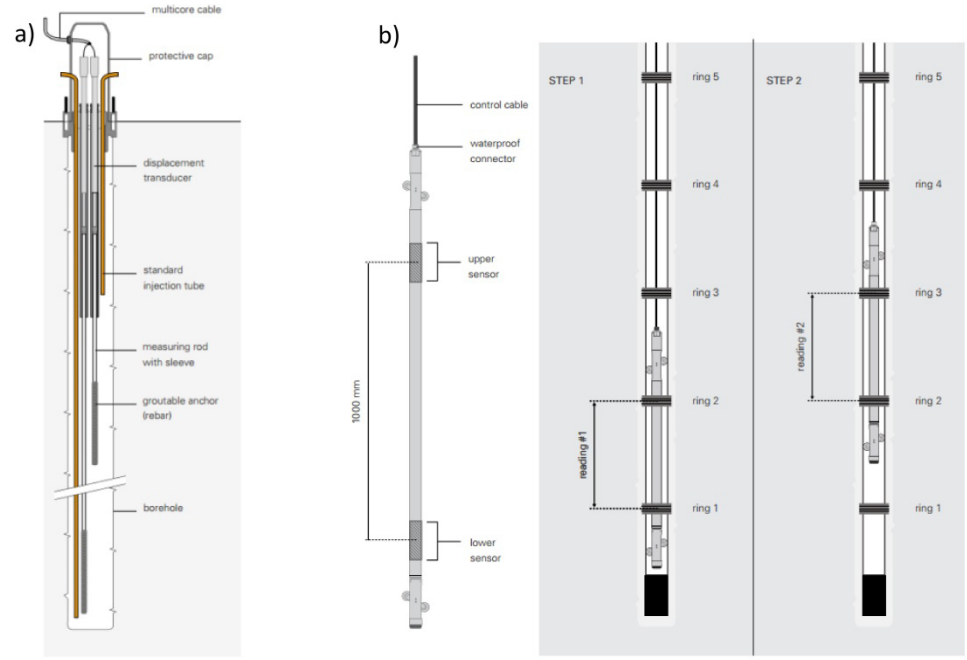

Figure 26. Multibase (a) and incremental extensometer (b)

Tunnels in urban areas also require subsidence measurements, normally carried out through precision levelling and monitoring of pre-existing structures through tiltmeters, DSM level measurement system (Differential Settlement Monitoring), crackmeters and jointmeters
Most of the times, traditional monitoring systems in underground excavations involve only displacements of the tunnel lining and of the surrounding ground at predefined monitoring sections. However, since tunnel design also includes the definition of the structural supports, the verification of the predictions regarding forces and stresses on the lining should also play an important role in the observational method. A

significant number of publications dealing with the interpretation of lining displacements and the consequent rock mass behaviour prediction are already present in the literature **(e.g. Schubert et al. 2004, Schubert & Moritz 2011)**. However, attempts aimed at interpreting and determining stresses or pressure recorded directly on the shotcrete lining are limited **(Clayton et al. 2002)**. Some tools are available in practice to obtain a good estimate of the degree of utilisation of the shotcrete based on measured displacements **(Rokahr & Zachow 1997, Hellmich et al. 2001, www.tunnelmonitor.com)**. However, the degree of utilisation of the primary lining can also be investigated through direct methods, such as strain gauges or load cells (Figure 27).
Strain gauges can be welded on steel sets, and they are usually coupled to provide a stress distribution along the section of the steel profile.
Load cells measure the pressure of a fluid within two steel plates and can be embedded in the shotcrete or between shotcrete and surrounding ground. When steel ribs are installed, these cells can also be placed under the ribs foot or between two components of the steel arch. Special load cells enable the measurements of anchors load.

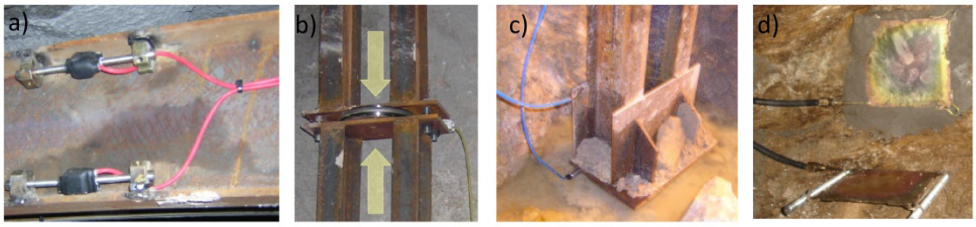

Figure 27. Strain gauges on the flanges of a steel rib (a), load cell placed between the upper arch and the lower part of the coupled steel ribs (b), load cell under the foot of the steel support, pressure cells before installation in the final lining (d) (Courtesy of SISGEO)

The technology of optical fibres (Figure 28) is also spreading rapidly, especially in construction sites that require an extended monitoring. This technology is based on the principle that when the light travels through an optical fibre, a small fraction is scattered back at every location of the fibre with a frequency that is linearly proportional to the temperature and strain applied at the scattering location. Therefore it is possible to obtain a continuous strain profile along the full length of the fibre.

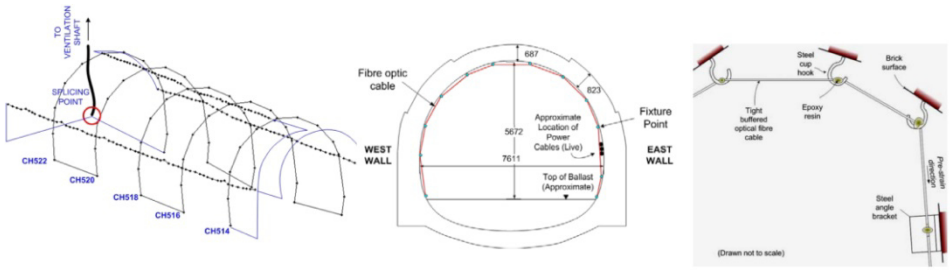

Figure 28. Longitudinal and transversal layout of fibre optic cable in Thameslink tunnel (after Soga et al. 2008)

Chapter 2. Numerical modelling of traditionally excavated shallow tunnels: state of the art

Analyses of underground constructions are aimed either at designing the tunnel supports and verifying the deformation behaviour or at validating design models through field data. In any case, both the ground deformations and the stress state on tunnel supports have to be determined or verified.
Difficulties in tunnel calculations arise from the fact that the ground is simultaneously loading and load-bearing medium. Moreover, this load is not prescribed from the outside and therefore its characteristics can be determined only through an accurate geological and geotechnical survey.
Many are the solutions for evaluating the stress-deformation behaviour associated with this complex soil-structure interaction problem. However, they do not have the same degree of accuracy, and they are not suitable for all the possible geometric and geotechnical conditions.
The following paragraphs include an overview of the calculation methods used in tunnelling. After a very general first paragraph (§2.1), summarising all the principle calculation methods, the focus of the chapter is on numerical modelling of traditionally excavated shallow tunnels. In particular §2.2 deals with a numerically based design according to Eurocodes, §2.3 summarises the state of the art regarding tunnel face stability and §2.4 reviews the previous works involving back-analysis of case studies.

2.1. Calculation methods in tunnelling

First of all, it should be distinguished between tunnels in rock and soft soil. Hard rocks frequently present discontinuities such as faults, joints and bedding planes. Therefore tunnel designers should take them into account when evaluating failure modes and lining loads. Soft rock and stiff soils may also present discontinuities that are likely to influence the overall behaviour, especially if the average stress state is low due to a low degree of confinement. In these cases, the choice between continuum and discontinuum approach depends on the joints persistence and spacing related to the opening diameter as well as on the average stress state characterising the underground construction. In soils or very weak rock, most of the times, the geotechnical behaviour can be described through a continuum model.

A further distinction has to be made between shallow and deep tunnels. In shallow tunnels, the most likely failure mechanism involves both the ground surrounding the cavity and the ground to be excavated up to the surface. On the contrary, in deep tunnels, the global failure mechanism can be seen instead as an excessive convergence of the cavity. It may happen that the ground surrounding shallow tunnels, especially when characterised by low cohesion and H<D, cannot form a load bearing ring and have a very low stand-up time. In these cases, the tunnel can be driven cut-and-cover, by excavating an open trench first and building the tunnel afterwards.
Peculiarities of shallow tunnels are low confinement stresses, fewer possibilities to form the arching in the ground surrounding the cavity and ground types varying, most of the times, between soils and weak rocks.
The analysis of shallow tunnels can be carried out through simplified models, numerical models and physical models. Some of these methods are also used for deep tunnels.
In this paragraph, they are briefly overviewed to show both their advantages and shortcomings. Afterwards, only the state of the art regarding numerical models applied to shallow tunnels will be considered and discussed. The only exception is face stability where simplified models (such as limit equilibrium models), widely used in practice, will be considered for comparison with the results of numerical models.
The principal calculation methods used in tunnel engineering can be classified as follow:

- Empirical methods;
- Analytical methods;
- Limit equilibrium methods;
- Bedded-beam-spring models;
- Numerical models.

2.1.1. Empirical methods

Empirical methods are based on previous experience and field observations. An example is represented by the design charts based on the RMR (Rock Mass Rating) or the Q system. These methods have proven to be successful when used by experienced engineers.
The most common method used to estimate the surface settlement trough, which is based on the Gaussian distribution function **(Schmidt 1969, Peck 1969)** can also be classified as empirical. Similarly, the simple methods

commonly adopted for a preliminary assessment of face stability, such as those based on the stability ratio **(Broms & Bennermark 1967)** associated with threshold values deriving from laboratory tests (e.g. centrifuge tests) and field observations are empirical design methods (Figure 29).

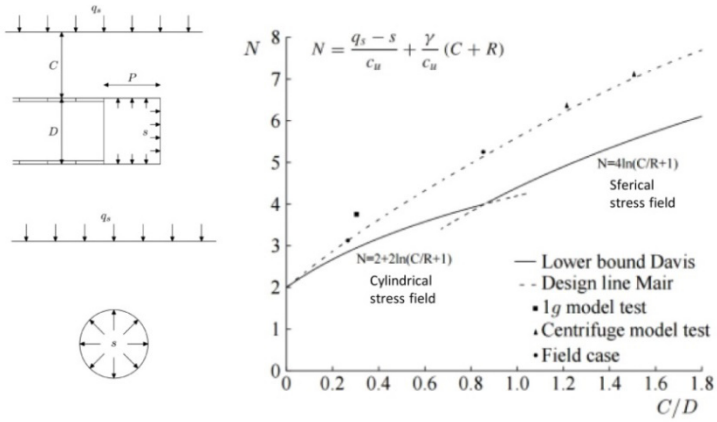

Figure 29. Stability numbers for a preliminary evaluation of face stability in cohesive soils (modified after Broere 2001)

2.1.2. Analytical methods

Analytical design tools entail strong initial hypotheses such as the schematization of the tunnel into a two-dimensional model, infinite medium, circular shape, homogeneous ground and elastic or elastoplastic behaviour. These features are usually more suitable for representing deep tunnels. Closed form solutions were derived both for continuum models and for the so-called Convergence-Confinement Method applied through the characteristic curves. An overview of solutions derived for continuum models (Figure 30) was provided by **Duddeck & Erdmann (1983)**.

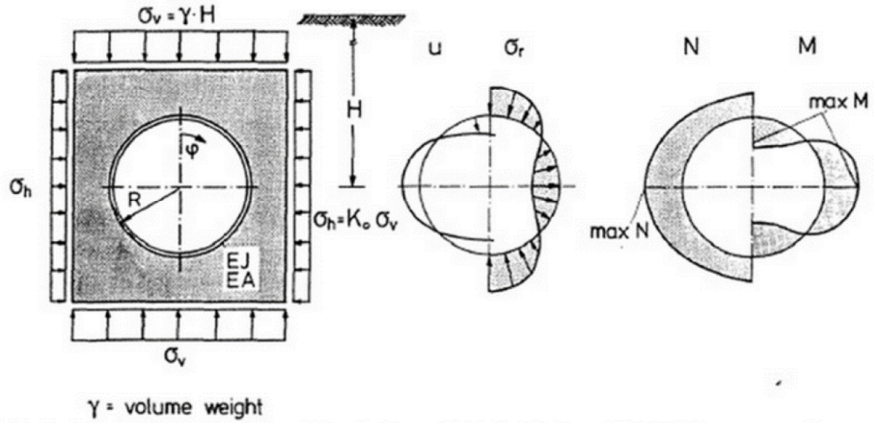

Figure 30. Plain strain continuum model and distributions of displacements, radial stresses, normal forces and bending moments (after Duddeck & Erdmann 1983)

The convergence-confinement method (Figure 31), based on the contraction of a spherical cavity, takes into account the delay of support installation but considers only hydrostatic stress states. Differently from continuum models, this second method provides only axial forces on the support and not bending moments.

The different deformation and failure mechanisms of tunnels with low overburden, compared to deep tunnels, is the reason why traditional design approaches, such as the convergence-confinement method, are not suitable for shallow tunnels.

Besides considering an hydrostatic stress state and a circular shape, this method also neglects the gravitational forces due to the weight of the failed material above the tunnel. Disregarding gravitational forces makes this calculation method even less applicable to shallow tunnels.

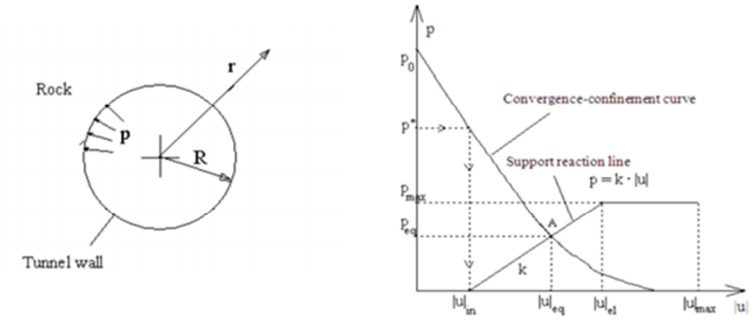

Figure 31. Convergence-confinement method with characteristic curves (after Oreste 2009)

Some analytical solutions were also derived for the stability number by applying the upper/lower bound plasticity theorems (**Davis et al. 1980**, Figure 29)

2.1.3. Bedded-beam-spring models

Bedded-beam-spring models simulate the tunnel lining through a beam element and the surrounding ground through springs. This simple structural model allows designers to take easily into account soil-structure interaction. However, it does not provide any information regarding soil deformations and displacements.

Differently from analytical solutions, different shapes of the cross section as well as different soil stratifications can be considered. The structural element is represented using either finite differences or finite elements, and the solution is usually obtained by iteration through a computational software.

With a bedded-beam-approach, it is also possible to consider geometries of cross-sections with partial areas that are not embedded (Figure 32, a). This model would be more realistic in the case of a shallow tunnel in poor material, compared to the fully bedded beam. An example of bedded beam model for shallow tunnels is shown in Figure 33.

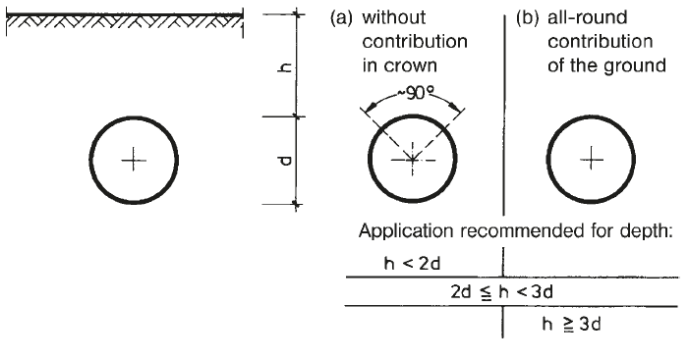

Figure 32. Approaches for the contribution of the ground to load-bearing (after Bernhard Maidl, Markus Thewes, Ulrich Maidl 2013)

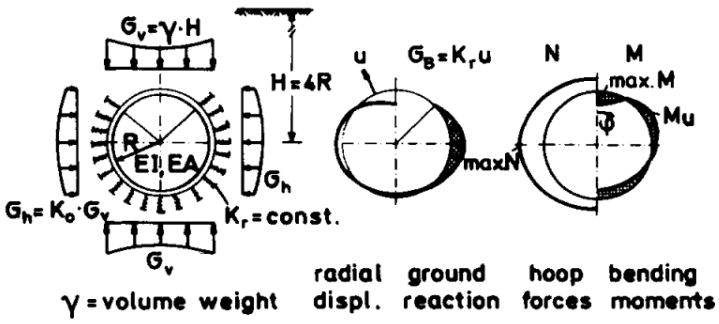

Figure 33. Example of bedded-beam-spring model for a shallow tunnel (H=4R), after (ITA 1988)

Traditional excavation in soils requires a certain amount of cohesion and a certain stiffness (unless special improvement techniques are adopted). These characteristics allow the excavation to be carried out either with a full or a partialised face, according to the value of soil cohesion. In these models, as well as in the continuum models previously mentioned, another difficult task that tunnel designers have to face is assessing the amount of stress release occurring before the lining installation. Similarly, in the Convergence-Confinement method estimating the tunnel displacement occurring before support installation and the corresponding stress release is not an easy task.

Higher or lower pressure are expected to act on the tunnel support depending on the soil cohesion and stiffness as well as on the unsupported

span, closure of the ring, lining stiffness and time-effects. The effect of all these factors on the stress release is very difficult to predict.

2.1.4. Limit equilibrium methods

Limit equilibrium methods assume an arbitrary failure surface and evaluate the equilibrium conditions of the blocks within this surface. The internal stress and strain distribution are disregarded. Limit equilibrium equations can be solved either manually or through calculation programs (e.g., UNWEDGE, Rockscience: Figure 34, right). For shallow tunnels in soils or weak rocks, a very common failure model is the chimney-like mechanism, frequently used to assess face stability (i.e. Figure 34, left).

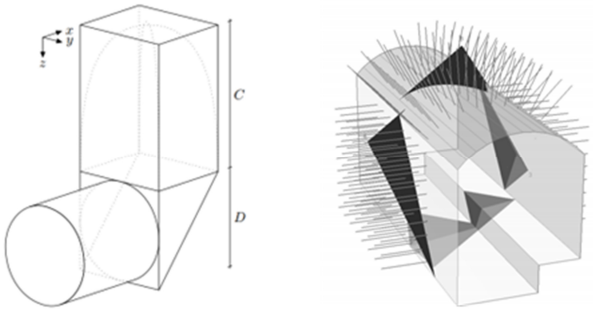

Figure 34. Failure mechanism for limit equilibrium analysis of face stability (left, after Broere 2001) and scheme for calculation of radial bolts (right, from www.rocscience.com)

2.1.5. Some considerations about simplified solutions

All the simplified solutions previously introduced may be used for a preliminary design and parametric studies.

Full numerical modelling is more suitable and therefore highly recommended for detailed soil-structure interaction studies or displacements predictions, as well as for back-analyses. Finite difference and finite element approaches are the most widely used in geotechnical engineering for numerical calculations. Besides allowing for the implementation of a wide range of constitutive models for both the soil and the structure, full numerical models enable the simulation of engineering problems characterised by complex geometries and construction sequences. Since the number of input data is remarkable, only an experienced user can properly

handle this kind of analysis, especially when non-linear behaviour and complex constitutive models are involved.
An additional difficulty in tunnelling calculations is represented by the three-dimensional stress state characterising the ground within 2-3 tunnel diameters from the excavation face (Figure 35).

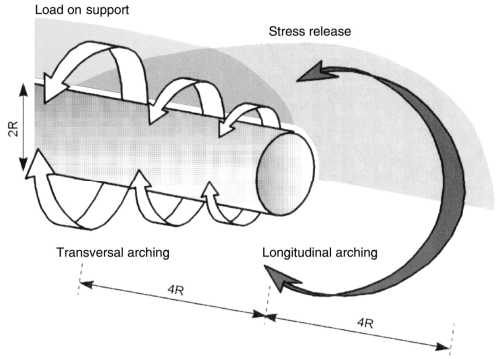

Figure 35. 3D arching effects occurring around underground constructions (after Potts 2002)

Neglecting this aspect can simplify the problem but can also lead to less accurate analyses. On the other hand, in some cases, approximations are necessary to reduce the computational effort. Therefore, the user must be aware of the consequences that some simplifications involve.
A **plain strain analysis** provides information only on transverse stress-strain behaviour but cannot provide information about tunnel face deformation or longitudinal behaviour. Moreover, it requires a strong hypothesis regarding the stress relaxation occurring before lining installation.
On the other hand, an **axis-symmetric analysis** could potentially provide information regarding both tunnel face and longitudinal stress-strain behaviour, but it is unsuitable for shallow tunnels because it assumes $k_0=1$ and homogeneous soil around the tunnel. Moreover, an axis-symmetric model entails the assumption of circular sections, which is far from most of the traditionally excavated tunnels and does not provide any information regarding surface subsidence.
In the light of these considerations, three-dimensional models would overcome the shortcomings of both plain strain and axis-symmetric analyses, requiring, however, a much higher computational effort.

In the following paragraphs, some specific aspects regarding the numerical analysis of shallow tunnels are discussed, and the state of the art is summarised. The literature review addresses, in particular, three main issues concerning the design of traditionally excavated shallow tunnels:

- Numerically based design in combination with Eurocodes;
- Face stability analysis;
- Numerical predictions and back-analyses.

2.2. Numerically based design in combination with Eurocodes

Currently, there is no generally accepted standard code which defines and regulates the design of underground openings. Therefore, geotechnical engineers have to refer to other codes, defined for conventional geotechnical structures (Eurocodes, BS, DIN, AASHTO, etc.) and engineering judgement still plays an important role.

Concerning tunnelling design, two different problems can be distinguished: the stability of the tunnel face and the stability of the lined excavation.

The stability of the tunnel face is a typical geotechnical problem, usually tackled using limit equilibrium methods (LEM) applied to predefined failure mechanisms **(Horn 1961)**. On the contrary, the stability of the supported excavation is primarily a problem of soil-structure interaction. This implies that strength and stiffness of both soil and structural support affect the stress-strain distribution and, consequently, the safety level of the tunnel.

In order to carry out this kind of analysis without neglecting the interaction effects between soil and support, numerical codes are usually required (e.g., Finite Element and Finite Difference Methods).

To guarantee a safe design, engineers often refer to Eurocode standards. Eurocode 7 **(CEN 2004 - EN 1997)**, devoted to geotechnical design, is based on the general framework of Limit State Design (LSD). Limit State Design consists in the verification that no limit state is exceeded under relevant design situations. Regarding tunnels, leaving aside serviceability limit states, two possible ultimate limit states should be primarily checked:

- exceeding limit strength or excess deformation in the soil (GEO);
- exceeding limit strength or excess deformation in the structural elements (STR).

The GEO-type limit state is appropriate for the verification of the face stability. On the contrary both GEO and STR-type limit states are relevant for the support design.
When the verification of the different limit states is performed through calculations, according to Eurocode 7, it is possible to use three different design approaches, synthesis of different design methods traditionally used in the European countries.
Deep tunnels and rock tunnels are explicitly excluded at this stage because other criteria govern their design and the role of the observational method in common practice plays a much more pronounced role than in shallow tunnelling **(Schubert 2010)**.

2.2.1. Overview of Eurocode 7

The current version of Eurocode 7 **(EN 1997-1)** provides the possibility to use three different design approaches (Table 3).

Table 3. Summary of Eurocodes design approaches.

Design approach	**DA1**		**DA2**	**DA3**
Combination	1	2		
Partial factors applied to	Actions	Variable actions and Material properties (x)	Actions and resistance	Structural actions and material properties
Partial factor sets	A1+M1+R1	A2+M2+R1/R4	A1+M1+R2	A1/A2(*)+M2+R3

Sets A1-A2= factors on actions/effects of actions
Sets M1-M2=factors on material properties
Sets R1-R3=factors on resistances
(x) for axially loaded piles and anchors sets M1 (unless specific situations) and R4
(*) A1 for structural load; A2 for loads derived from the ground

Design approach 1 requires the verification of two different combinations: in DA1-1 partial factors are applied to unfavourable actions whereas in DA1-2 they are applied mainly to ground strength parameters. Design approach 2 requires the application of partial factors on actions (or effects of actions) and ground resistances and design approach 3 requires partial factors on structural actions and ground strength parameters. The possibility to introduce partial factors on the sum of the effect of actions rather than on the action itself is usually referred to as DA2* approach.
In the current version of Eurocodes, partial coefficients for the actions (γ_F) and the effects of actions (γ_E) are the same. This implies the assumption of a linear relationship between action and effect of action, which is not always the case. In order to tackle this problem, according to a general principle of

Eurocode 1990 – Basis of structural design **(CEN 2002 - EN1990)**, the following procedure may be adopted: whenever the effect of an action increases faster than the action, the partial factor must be applied to the action; vice versa, if the effect of an action increases less than the action, the partial factor must be applied to the effect of the action. It is not always straightforward, however, to determine which of these two cases applies to a particular design situation.

From a general point of view the three approaches can be grouped into two main families **(Bauduin et al. 2005)**: Load and Resistance Factoring Approach (LRFA, also called Load Resistance Factor Design – LRFD according to **Shuppener et al. 2009**) and Material Factoring Approach (MFA). LRFA represented by DA2 requires partial factors to be applied both to actions and to resistances. Instead, in the MFA, represented by DA3, partial factors are mainly applied ground strength parameters. DA1, which includes two combinations, can be considered as LRFA for piles and anchors. However, for every other geotechnical work, DA1.1, appears to be a particular case of LRFA, in which values of partial factors on resistances are equal to 1, whereas DA1.2 is a MFA.

When defining the partial factors to be applied to the actions it is important to keep in mind the so-called single-source principle (EC7-1, Clause 2.4.2), which eliminates the need to distinguish between favourable and unfavourable permanent actions. In fact, it states that "*Unfavourable (or destabilising) and favourable (or stabilising) permanent actions may in some situation be considered as coming from a single source. If they are considered so, a single partial factor may be applied to the sum of these actions (or to the sum of their effects)"*. In the case of underground excavations, as well as for retaining structures, actions and resistances derive from the same source, namely the soil.

Unlike for foundations and retaining walls, there is no guidance provided for tunnels regarding resistance factors. Moreover, being the soil surrounding the tunnel both action and resistance, it would be extremely difficult to apply resistance factors in numerical computations. If partial factors on resistances are taken equal to 1, DA1-1 and DA2 are identical. DA3 and DA1-2 can also be considered identical when no structural actions (i.e., actions deriving from another structure applied directly to the retaining structure) are involved in the problem.

2.2.2. Current application of EC7 to tunnel design

Even if geotechnical design of tunnel excavations is not explicitly covered by Eurocode 7, the general procedure can still be applied and used as reference. In general two issues have to be addressed, namely, tunnel face stability and the stability of the lined excavation. Concerning the first problem, most of the considerations regarding slope stability can still be held valid. In this case, being the ground the main element providing resistance (GEO-type limit state), an approach requiring partial factors on material strength is recommended, although not explicitly stated in EN 1997-1.

The general tendency of geotechnical designers all over Europe is to prefer DA3 for this class of problems.

Concerning the design of the supported excavation, the approach DA2* is the most frequently used in Germany and Austria, even if the latter (contrary to Germany) also allows the use of DA3, when numerical methods are employed. In Italy, DA1 is prescribed for flexible retaining walls, but tunnels are not explicitly addressed; the current tendency of the practitioners for the design of the supported excavation is to use DA2*. The recent revision of the National Italian Code (not yet issued) requires the use of DA1. The recommendations of the French Tunnelling and Underground Space Association (AFTES) suggest, consistently with the French National Annex, the application of DA2 approach, in the form of DA2* (Colombet et al. 2007). Nevertheless, the National Annex leaves the possibility to use also DA3.

It should be noted that, if geotechnical failure governs the design as decisive ultimate limit state, an approach prescribing partial factors on forces may not be the most appropriate one to guarantee a sufficient margin of safety. Instead, considering the major role played by soil properties, it would be more logical to use safety factors on soil strength parameters. In other cases, the opposite situation can take place: factoring the strength of the ground leads to a less safe design when compared to the approach of factoring the effects of actions. This is particularly true when the rock or soil mass is competent enough to guarantee the formation of a good arching effect and, therefore, reducing soil resistance leads to a negligible increase of the structural forces. For this reason, it could be suggested to check both the combinations (DA2* and DA3) to avoid, on the one hand, the underestimation of the structural forces and detect, on the other, the possible failure mechanisms in the soil mass. Another design strategy, which would

allow applying partial factors on actions instead of the effect of actions, is to increase the soil unit weight. However, in the opinion of the authors, it is not suitable because it would have the double effect of increasing both actions and resistances. In fact, the effective stresses would raise and consequently the shear resistance would be higher. When using advanced constitutive laws with stress-dependent stiffness, the soil stiffness would increase too. Moreover, this design strategy is not in accordance with Eurocodes in their current form.

2.2.3. Application of EC7 approaches to numerical calculation of underground excavations

Focusing on the stability of the supported excavation, the application of Eurocode approaches should consider that:

- it is a soil-structure interaction problem;
- it is usually analysed using numerical methods;
- shotcrete, largely used in NATM excavations, is a material characterised by a strongly non-linear and time-dependent behaviour.

Referring to the soil-structure interaction, it is largely debated all over Europe which is the best approach for this kind of problems. Both in Italy and in France a material factoring approach (MFA) in combination with numerical codes raises some concerns about the unrealistic distribution of stresses and strains in the soil, due to the formation of plasticity zones much wider than the ones which can be expected in situ. Against this consideration, two objections can be expressed. First of all the goal of ULS checks, as defined in the Eurocodes, is not to reproduce a realistic stress-strain distribution in the soil mass, but to make sure that the soil-structure system is far enough from failure or collapse. Secondly, the application of partial factors only to actions or effects of actions does not allow the check of ground failure.

It is true that reducing soil parameters might lead to a different and less realistic distribution of structural forces as well as to a deviation from the real mass behaviour, but a material factoring approach would ensure a higher margin of safety against geotechnical failure, with respect to a load factoring approach. In fact, reducing material strength parameters seems to be a good strategy for checking how far the current problem is from geotechnical failure (e.g., punching of the lining footing into the ground). The current situation should be described through characteristic values.

The hostility of some practitioners towards partial factors on material strength derives from the fact that the material parameters commonly used for tunnel design are already quite conservative. This means that, in normal practice, engineers do not use "best estimates" of material parameters (**Simpson & Powrie 2001**). Therefore, a further reduction seems not appropriate because it would lead to uneconomic design. In any case, reducing soil parameters, as highlighted before, should not be judged as a too conservative way to consider soil strength properties. In fact, other uncertainties are implicitly included in these partial factors.

Being soil-structure interaction problems such as tunnelling governed to a large extent by stiffness and relative stiffness, it could be considered to introduce partial factors on soil stiffness, which in turn would have an influence on calculated internal forces of the lining. However, it has to be considered that reducing soil stiffness can have different effects depending on the particular soil model used in the calculation and therefore this approach would be difficult to control. Moreover, checking the ultimate limit states (normally associated with failure conditions) by just acting on parameters that control the soil deformation behaviour does not seem to be a consistent approach. In addition, it would not be in line with Eurocode7 in its present status.

For a general overview about the applicability of Eurocodes to a numerically based design, one can refer to **Bauduin et al. (2000)**, **Schweiger (2005)**, **Schweiger (2009)**, **Schweiger (2014)**, **Simpson (2000)**, **Simpson (2007)**, **Simpson & Junaideen (2013)**, **Potts & Zdravkovic (2012)**. Even if some studies have been already carried out to evaluate and compare different design approaches **(Schweiger et al. 2010, Schweiger 2010, Jones 2007, Walter 2007, Walter 2010, Hofmann et al. 2010)**, there is no general agreement, especially when it comes to apply these methods in combination with numerical analysis. It is clear that, when dealing with numerical calculations, neither actions nor resistances can be clearly distinguished and factorised. The soil surrounding the underground opening represents, in fact, a source of action and resistance at the same time. For this reason DA2*, which overcomes this issue by applying partial factors on the effect of actions (namely structural forces on the tunnel support) and allowing for a single check, has gained popularity among practitioners.

An important step towards the investigation of the applicability of Eurocodes to tunnel excavation is represented by the workshop organised by

the Austrian Society for Geomechanics, whose proceedings are included in Geomechanics and Tunnelling 3.1, 2010.
Another important contribution is provided by the French tunnelling association **(Colombet et al. 2007)**, whose recommendations deal with the compatibility of both EC7 and EC2 to tunnel construction and the applicability of EC2 to shotcrete and reinforced-shotcrete linings.
The main outcomes deriving from the previous works, regarding the application of Eurocode approaches in combination with numerical methods, show, as expected, that different results can be obtained from different combinations of partial safety factors depending on the soil constitutive model adopted and on the specific benchmark considered (soil properties and excavation sequence). However, differences in results due to the implementation of different design approaches seem to be smaller when advanced constitutive models are used **(Schweiger 2010)**. Therefore advanced soil models seem to have not only the merit to give more realistic SLS predictions but also advantages for ULS calculations.
As third aspect, it should also be considered that traditionally excavated (NATM) shallow tunnels are usually supported by shotcrete. This construction material is characterised by a strongly non-linear and time-dependent behaviour. However, how to deal with non-linear materials, in terms of design approach using numerical analysis, is not clearly defined anywhere. Therefore, this aspect should be further investigated. It is also of particular interest because assuming the shotcrete linear elastic could lead to a very uneconomic design. On the contrary, introducing non-linearity can lead to a reduction of structural forces due to the stress redistribution capacity of the support. Some calculations and preliminary results deriving from the application of Eurocodes design approaches in combination with advanced constitutive laws for the tunnel lining can be found in **Walter (2007** and **2010)**. It seems clear that the advantage of using such models is to exploit as much as possible the stress redistribution both in the soil and in the structural support, avoiding an excessive increase in lining forces, which could lead to an unreasonably conservative design.

2.3. Face stability calculations

The problem of face stability and deformation behaviour of shallow tunnels is particularly remarkable not only for the necessity to guarantee the workmanship safety but also because it is directly related to surface deformations, at least for shallow tunnels. The occurrence of excessive face

extrusion or the development of a failure mechanism could cause significant subsidence phenomena, damaging pre-existing buildings and infrastructures. Several experimental studies have been carried out in the past to assess the stability of an unreinforced face and different analytical or semi-empirical solutions have been formulated. A detailed overview of these studies for both drained and undrained conditions is provided in **Ruse (2004)**. Moreover, advantages and shortcomings of the most common methods employed for geotechnical stability analysis (namely limit equilibrium method, upper/lower bound limit analysis and displacement finite-element analysis) can be found in **Sloan (2013)**. The author summarises the main features of these methods in a concise and effective table (Table 4).

Table 4. Traditional methods used for geotechnical stability analysis: main features (from Sloan 2013)

Property	Limit equilibrium	Upper-bound limit analysis	Lower-bound limit analysis	Displacement finite-element analysis
Assumed failure mechanism?	Yes	Yes	–	No
Equilibrium satisfied everywhere?	No (globally)	–	Yes	No (nodes only)
Flow rule satisfied everywhere?	No	Yes	–	No (integration points only)
Complex loading and boundary conditions possible?	No	Yes	Yes	Yes
Complex soil models possible?	No	No	No	Yes
Coupled analysis possible?	No	No	No	Yes
Error estimate?	No	Yes (with lower bound)	Yes (with upper bound)	No

Concerning tunnel face stability, the solutions formulated by different authors are usually expressed in the form of stability numbers which can be introduced in Equation 1 to calculate the minimum support pressure required to reach face stability. These factors were mainly derived from upper/lower bound calculations or limit equilibrium methods.

$$p_f = -c'N_C + qN_Q + \gamma DN_\gamma \quad (1)$$

The choice between drained and undrained analysis should depend on the ratio between the ground permeability and the advance rate **(Anagnostou 1993)**. When long excavation standstills have to be considered, even a low permeability material should be analysed in drained conditions.

If necessary, the stability of the face, in traditionally excavated tunnels, can be improved either by a partial excavation of the cross section or by reinforcing the core ahead of the face. The first method allows for a reduction of the deconfinement inevitably induced by an underground excavation. The second provides an improvement in the mechanical characteristics of the ground to be excavated. For cohesive or semi-cohesive soils, bars made of Glass Fiber Reinforced Polymer (GFRP) are often adopted. They are basically pipes inserted in longitudinal holes drilled into

the core and immediately grouted using a shrink controlled or an expansive mixture. During the excavation, a certain length of these elements should always be guaranteed to have beneficial effects. For this reason, when a new series of fibreglass bars is installed, a prescribed overlap length should be kept. The success of this material is due to the considerable strength and stiffness properties combined with high fragility. Therefore, it is easy to excavate the core with the same tools regularly used for an unreinforced material, but at the same time, excessive de-confinement is avoided by improving ground stiffness and strength. The reliability of this method has been proved by many successful projects completed over the past 30 years, especially in Italy and France. For a complete overview of the method and its applications in different projects, one can refer to **(Lunardi & Bindi 2004)**. The design of reinforcing elements is commonly carried out through limit equilibrium calculations which allow, given a prescribed failure mechanism, an evaluation of the safety factor. The advantage of the LEM is to be a very simple and fast method to assess the stability conditions of an excavation. However, being based on several simplifying hypotheses, it cannot always guarantee realistic estimations of the face stability. Performing a 3D numerical analysis, on the other hand, implies a significant computational effort, given the level of mesh fineness necessary to achieve a satisfactory accuracy of the results and the high number of structural elements required to simulate the reinforcements. Considering that an optimisation of their design features requires several trials, this effort increases considerably.

The design implies the definition of the number, length and arrangement of reinforcements. One criterion to define these characteristics could be a target safety level to be reached. Nevertheless, when the limitation of the surface settlements is a major concern, it makes sense to adopt a criterion based on limiting the volume loss. This design criterion would prevent an excessive volume loss and consequently excessive surface subsidence. Either way, the evaluation of the deformation behaviour of the reinforced tunnel requires, at least for shallow tunnels, a full 3D numerical analysis including direct modelling of the face reinforcements. Alternative ways to consider the presence of these elements in a 3D model could be the application of a face pressure or the definition of equivalent material properties for the clusters belonging to the tunnel core.

2.3.1. Application of the limit equilibrium method for tunnel face stability

The principal hypothesis characterising the limit equilibrium method regards the definition of a failure mechanism, which is represented by rigid blocks sliding along surfaces where the maximum shear resistance is assumed to be mobilised. A mechanism commonly assumed to represent a potential tunnel face failure is the Horn mechanism **(Horn 1961)**, represented in Figure 36.

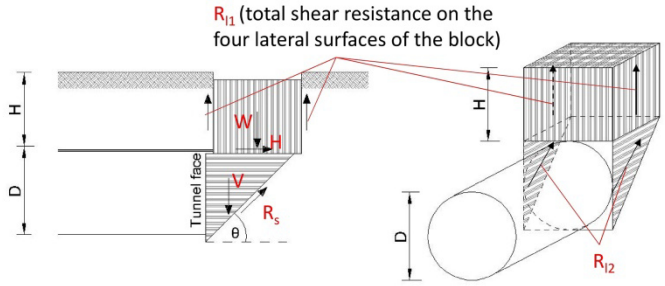

Figure 36. Horn failure mechanism and forces involved in the calculation of the safety factor

The sides of the square front of the sliding wedge can be taken of equal length as the diameter of the tunnel cross-section or, alternatively, an equivalent area can be calculated. On the lateral surfaces of the sliding wedges, the shear forces depend on the geostatic stress distribution, which can be evaluated according to the Silo's theory **(Janssen 1895),** as shown in Figure 37. In particular, the vertical stress at a certain depth (z) is computed as:

$$\sigma(z) = \frac{\gamma r}{2K_0\mu}\left(1 - e^{-\frac{2k_0\mu z}{r}}\right) \quad (2)$$

where γ is the soil unit weight, K_0 the at-rest earth pressure coefficient, r the silo's radius and μ the friction coefficient. Given a silo's geometry and prescribed values of γ and K_0, the maximum value reachable by the vertical stress is $\gamma r/(2K_0\mu)$.

The safety factor can be calculated as the ratio between forces and resistances acting along the sliding surface, whose angle (θ) has to be defined by minimising this ratio. The Horn's model has been widely used in the past for both conventional and mechanised tunnelling **(Oreste 2011,**

Anagnostou & Kovari 1994, Anagnostou & Kovari 1996, **Anagnostou & Serafeimidis 2007, Segato et al. 2015)**.

One of the main limits of the LEM is that the failure mechanism is apriori defined whereas, as shown in previous works carried out by means of numerical calculations **(Vermeer et al. 2002, Kavvadas & Prountzopoulos 2009)**, the potential failure mechanism depends on the specific case, in particular on the material strength properties and on the overburden.

In the LEM, the wedge mechanism can be properly modified in order to consider an unsupported span, whereas the presence of reinforcements can be taken into account by considering an equivalent force S supporting the excavation face. The value of this force, which is necessary to guarantee a prescribed safety factor, can be assessed by considering the force itself in the equilibrium of the sliding wedge. Once the supporting force has been determined, one can easily define the minimum number of reinforcements necessary to reach that safety level. The procedure usually adopted takes into account only the axial force developed in the bars, while the flexural stiffness is assumed to be negligible **(Oreste 2011)**. Each bar can develop a force equal to the minimum between the axial force bearable by the structural element (calculated with the admissible axial stress), the frictional force that can be mobilized between the ground and grout in the segment inside the sliding block and the one which can be mobilized in the segment falling in the stable part of the core (respectively Equations 3,4 and 5):

$$S \leq n \cdot \sigma_{adm} \cdot A_{bar} \quad (3)$$

$$S \leq n \cdot \tau_{adm} \cdot (\pi \cdot \phi_{hole} \cdot L_a) \quad (4)$$

$$S \leq n \cdot \tau_{adm} \cdot (\pi \cdot \phi_{hole} \cdot L_p) \quad (5)$$

where σ_{adm} is the admissible tensile stress of the element, τ_{adm} is the maximum shear stress at the contact ground-grout, ϕ_{hole} is the hole diameter, n is the number of bars, L_a and L_p are the bar lengths falling inside and outside the sliding prism (Figure 37).

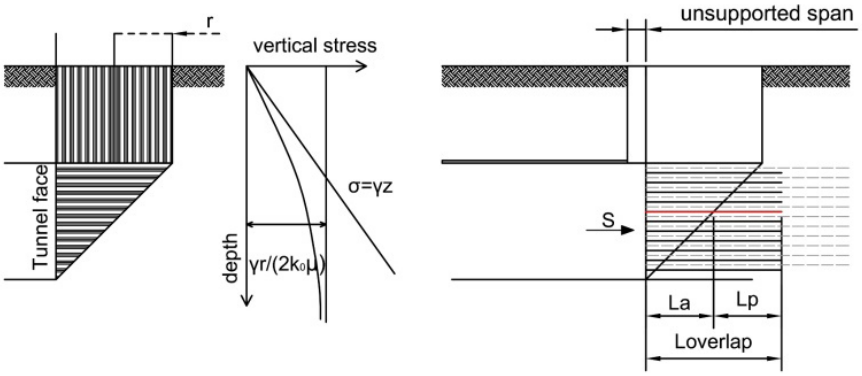

Figure 37. Silo's theory and scheme for the calculation of face stability with LEM in the case of face reinforcements and unsupported span

Another failure mechanism which could theoretically occur is the pull-out of the bar along the contact surface between structural element and injection material. However, given the very high values of the pull-out resistances, especially for corrugated profiles, deriving from laboratory tests **(Zenti et al. 2012)**, this mechanism does not govern the reinforcements design. Moreover, considering the structural properties of these elements, the common overlap lengths adopted (0.5D-D) and the average ultimate bond strength between grout and ground for mainly clayey and silty soils (τ_{adm} <150kPa), the structural failure is not likely to occur either, being the structural strength higher than the pull-out resistance (calculated considering the contact grout-ground). Therefore Equation 4 and 5 usually govern the design of fiberglass dowels. In general, in order to optimize the intervention and obtain the design parameters, pull-out tests should be performed. These tests would allow to determine the shear resistance developed at the borehole boundaries, between soil and grout.

Anagnostou & Serafeimidis (2007) proposed a computational method for tunnel face reinforcements based on the LEM combined with the method of slices, providing design nomograms for homogenous ground and uniform reinforcements. This method allows for considering also layered grounds as well as different reinforcement layouts.

Oreste (2009) developed a method for performing a detailed analysis of the interaction between dowels and surrounding material, simulated through a Winkler approach for both normal and axial directions.

2.3.2. State of the art on numerical calculations of stability and face deformation behaviour

Numerical calculations aimed at determining face stability conditions are usually carried out through the so-called strength reduction method. This procedure consists in reducing the ground strength properties until the computational program is not able to reach convergence. In this cases, the user should be careful in checking that the non-convergence is due to an actual global collapse rather than to numerical problems or local failure.

An extensive numerical study regarding unreinforced excavation faces has been conducted by **(Ruse 2004)**. On the basis of the numerical calculations performed, the author provided the stability factors to be introduced in Equation 1 and consequently derived analytical formulations of the failure pressure for closed face tunnelling (Equation 6) as well as an analytical expression of the safety factor for open-face tunnelling (Equation 7). The second one was derived from the first one by considering p_f=0 and the definition of the factor of safety as the ratio between the available shear strength and the shear strength mobilised at failure.

$$p_f = -c'\cot\varphi' + \gamma D\left(\frac{2+3\left(\frac{d}{D}\right)^{6\tan\varphi'}}{18\tan\varphi'} - 0{,}05\right) \qquad (6)$$

$$\eta = \frac{0.9\tan\varphi' + 18c'/\gamma D}{2+3(d/D)^{6\tan\varphi'/\eta}} \qquad (7)$$

This solution is valid for $\varphi'>20°$ and $d/D < 0.5$ (where "d" and "D" are respectively the unsupported length and the tunnel diameter), and applies to a homogeneous soil. It does not consider the destabilising effect of pore water pressures. The theoretical derivation of the dimensionless coefficient $\cot\varphi'$, which multiplies the effective cohesion, comes from the assumption of a Mohr-Coulomb failure criterion. The adoption of this factor, however, does not take into account possible tensile failure in the soil. By neglecting this, an overestimation of the necessary face pressure or of the safety factor is expected, especially in highly cohesive soils. In fact, when tensile stresses are allowed in the calculations, the soil can count on strength resources that lead to a different and wider stress redistribution around the disturbance zone created by the underground opening. This effect has also been proven by **Tschuchnigg & Schweiger (2015)** for slope stability problems. Nevertheless, the suggested formula represents a reasonable way to check the plausibility of FEM stability analyses.

Other important outcomes of the study carried out by **Ruse (2004)** can be summarised as follows:

- if the friction angle is higher than 20°, stability is independent from the ground cover, because the stress distribution is dominated by arching;
- for open face tunnels with small cutting length, stability is guaranteed when $\gamma D<10c'$;
- when tensile stresses are allowed, the safety factor is overestimated (the overestimation depends on the specific problem);
- dilatancy angle, Poisson's ratio, Young's modulus and K_0 influence the computed displacements but have a negligible effect on the failure load (the very low influence of dilatancy angle and K_0 is also confirmed by **Perazzelli & Anagnostou (2012)**.

It must be pointed out that, based on recently published results of slope stability analysis **(Tschuchnigg et al. 2015)**, dilatancy may have an influence for high values of internal friction angles ($\varphi' > 35°$).

Among the previous works regarding the evaluation of the behaviour of a reinforced tunnel face, some focus on the assessment of the tunnel face stability in terms of safety factor, whereas others deal with the analyses of face extrusion and surface settlements.

Ng & Lee (2002) studied the effect of soil nailing in minimising ground movements and reducing volume loss. They conducted a parametric study with a series of three-dimensional elastoplastic coupled-consolidation analyses involving a circular excavation in uniform over-consolidated London clay. The performance of the nailing system was evaluated by changing their axial stiffness and analysing the results in terms of extrusions, surface settlements, nail forces and pore water pressures. The authors defined optimum values of the nails axial rigidities as those values beyond which no significant improvement in the stress-deformation behaviour is gained.

Yoo (2002) performed 3D elastoplastic numerical analyses to study the effects of different soil nail configurations on the deformation behaviour. A wide range of geometrical, soil and reinforcement conditions were analysed. For the different cases, the author provided values of critical density and critical reinforcement length, which appear to be independent from the tunnel cover depth. The critical values are defined as those providing a maximum reinforcing effect. According to these calculations, the minimum

overlapping length normally adopted in practice (0.3D - 0.4D), may be a non-conservative assumption for soils with small friction angle.

Schweiger & Mayer (2004) investigated face stability with full 3D analyses, using the so-called strength reduction technique. They showed that this method could be successfully applied also to reinforced tunnel faces, provided that also the properties characterising the interface between structural elements and ground are subjected to the same reduction of c' and φ' during the safety calculation. In this work, the authors used the geomembrane elements implemented in Plaxis to model face reinforcement. These elements do not have bending stiffness, but they allow for the limitation of the maximum axial force. In this work, considering a specific case study, the influence of the reinforcement length on the safety factor was evaluated.

Kavvadas & Prountzopoulos (2009), having performed 3D deformation analyses of a circular tunnel in elastoplastic material reinforced with fibreglass dowels, provided values of optimum nail length and density. Different strength properties and cover depth were taken into account. The main outcomes of the work are that the optimum length shows a strong dependency on friction angle and in soils with low friction angle a minimum value of around 0.8D should be considered in order to have a significant effect on the deformations. The authors also studied the possibility to model a dense and homogeneous nail pattern using an equivalent pressure, proposing some reference values according to the friction angle and cover depth.

Oreste & Dias (2012) carried out stability analyses including face reinforcements and comparing the results of 3D numerical calculations with those deriving from a new calculation procedure based on the LEM method and the elastic line of one-dimensional element combined with Winkler springs. The 3D analyses, referring to two real projects, were performed using the φ-c reduction technique and modelling both the ground and the structural reinforcements as elastoplastic elements. The authors showed a good agreement between the numerical results and the proposed LEM procedure.

Perazzelli & Anagnostou (2012) compared the results of the LEM method, according to the procedure proposed by **Anagnostou & Serafeimidis (2007)**, with those provided by FEM calculations both in the case of reinforced face and unreinforced face. The calculations involved a square tunnel with fixed overburden and excavated in a cohesive-frictional soil.

The reinforcements were modelled with infinite tensile strength so that only bond failure could occur. The results are presented in terms of minimum cohesion needed to obtain face stability for a given bolt pattern. Different criteria for considering the bond strength were implemented and compared.
Li et al. (2015) performed five series of parametric studies to define the influence of length, density, axial stiffness and reinforcement area of soil nails on face deformation behaviour. Their results are in accordance with the previous works. An important outcome regards the improvement area: installing face reinforcements in the tunnel periphery seems to be more effective than reinforcing the central area.
The results of centrifuge tests **(Kamata & Mashimo 2003)** and small-scale experiments **(Yoo & Shin 2003)** of reinforced tunnel faces, also demonstrated the effectiveness of this technique in reducing face deformation and the existence of optimum values of the design parameters.

2.4. Numerical predictions and back-analyses

The prediction of displacements and lining stresses in underground openings represents a challenging task. The main reason is primarily related to the complexity of this soil-structure interaction problem and secondly to the difficulties in obtaining from the beginning a reliable geotechnical characterization of the soil or the rock. In any case, especially when class A predictions fail in forecasting the system behaviour, performing class B or C predictions, which rely on a higher level of knowledge of the surrounding ground, can represent a useful resource for identifying and reducing model deficiencies.
Numerical modelling of tunnel construction relies in most cases on 2D plane strain analyses. In fact, three-dimensional calculations are still too time-consuming with respect to the common design and construction deadlines. Especially when the observational method has to be applied, and the main goal of the back-analysis is to promptly update the original design, it is usually not possible to run very time-consuming calculations.
Considering the problem from a geotechnical point of view, tunnelling usually induces mainly deviatoric and unloading stress paths in the surrounding medium. Moreover, with respect to the ground surface, the soil response to underground openings involves most of the time a deformation level from medium to very low. On the contrary, close to the underground opening, the deformation level can be much higher. The complexity of loading paths and the wide deformation range involved in tunnelling

excavations make the choice of the constitutive model and the selection of the soil parameters quite challenging and demanding.
Since many variables are involved in this problem, the choice of each parameter or calculation hypothesis should be justified through a preliminary calibration or back-calculation. The higher the number of available field measurements is, the more accurate a back-calculation or a model validation will be. When performing back-analyses, it is, therefore, important to have a complete set of monitoring data, regarding both the soil mass and the tunnel lining. Nevertheless, one should also keep in mind that the discrepancy between calculation and field measurements might be due to construction deviations and workmanship quality.
Performing numerical calculations during and after tunnelling works represents a useful resource to update the design and improve future predictions in similar conditions. Many attempts have been made in the past three decades to numerically back-analyse monitoring data from different construction sites or to validate predictions.
Negro & Queiroz (2000) reviewed more than 60 case histories studied up to the end of the last century. The numerical predictions of shallow tunnels were classified according to soil type, construction method, numerical model, constitutive model and available field measurements. Moreover, for each study, the class of prediction according to the classification proposed by **Lambe (1973)** was also identified. Most of the predictions were classified as class C1, which means back-analyses. A further distinction was made between actual back-analyses and predictions carried out using previously calibrated models, finding that the latter provided good quality predictions, not far from proper back-analyses. These findings prove that a proper calibration is essential to obtain good predictions. By the way, no clear correlation could be found between accuracy of predictions and model quality, soil type or construction process.
In the last 15 years, substantial progress has been made on constitutive modelling and computational capacity. Thus, three-dimensional models have become more popular **(Galli et al. 2004, Möller 2006, Segato & Scarpelli 2006, Yeo et al. 2009, Svoboda & Masin 2011, Do et al. 2014, Fargnoli et al. 2015, Janin et al. 2015).** However, their practical application is still limited to the design of geometrically complex cases or back-calculations, mainly due to the high computational effort required. Especially when it comes to studying the interaction between multiple tunnels, performing 3D calculation might be prohibitive. As a consequence,

most of these analyses have been performed in plane strain conditions **(Addenbrooke & Potts 2001, Karakus et al. 2007)**, whereas the number of studies adopting 3D simulations of multiple excavations is very low **(Ng et al. 2004, Do et al. 2014, Fargnoli et al. 2015)**. A further need for 3D studies of underground excavations derived from the necessity of modelling face reinforcements, which has become a frequently and successfully implemented technique for improving face stability. This topic is also investigated in the present thesis.
In the following paragraphs, a brief overview of the main factors influencing numerical simulations of conventional underground excavations is provided. In comparison to simple analytical or empirical solutions, many more aspects can influence the validity of the results. This is the reason why a high level of competency is required to obtain reliable results.

2.4.1.1. 2D versus 3D calculations

In standard practice, 2D analyses are still widely adopted for tunnel design, whereas 3D calculations are limited to complex geometries like intersections. The most common way to simulate such a 3D process with a plane strain calculation, at least for conventional excavation, is the stress reduction method or convergence-confinement method **(Panet & Guenot 1983)**. According to this approach, the radial stress acting on the tunnel boundary is reduced to simulate the arrival of the excavation face at the analysed section. The reduction factor of the initial stress is usually referred to as relaxation factor λ.
Other methods adopted to consider the 3D effect due to the volume loss are described in **Karakus (2007)**. Besides the stress reduction method, it is possible to adopt the stiffness reduction method, the softening method, the hypothetical modulus of elasticity method, the gap method and the volume loss control method. The author compared the results of back-calculations aimed at matching subsidence measurements of an NATM excavation in London Clay. The analyses were performed using the previously mentioned methods, except for the gap method, mainly employed for shield tunnelling. The lining was modelled with both beam and continuum elements. A better match of settlement trough was obtained using the convergence-confinement method in combination with beam elements, whereas continuum elements showed a stiffer behaviour.
Möller (2006) showed the merits and shortcomings of both plane strain and full three-dimensional simulations of shallow tunnels. The author calibrated

the unloading factors (or β-values, where β =1-λ) by comparing 2D and 3D analyses. They were found to be strictly dependent on some soil mechanical properties such as cohesion and stiffness but less on the soil friction angle. In particular, β increases with increasing cohesion and with decreasing stiffness. As expected, there is also a connection with the adopted excavation sequence, especially with the excavation round length. The further away from the excavation face the lining is installed, the bigger is the amount of induced stress relief. Another important outcome of this research is the dependency of the unloading factors on the back-analysed quantity: three different β values were necessary to match surface settlements, normal forces and bending moments. Finally, the unloading factor also depends on the geometry of the excavated section.

Also **Svoboda & Masin (2011)**, by comparing surface settlements from two-dimensional and three-dimensional analyses, showed that the optimum value of the stress reduction factor depends both on the mechanical properties of the soil and on the simulated problem. This factor was also found to be strongly dependent on the small strain shear modulus, more than on the large strain modulus, whereas the initial stress state seems to have a minor influence.

As far as the design phase is concerned, in standard practice, a range of β-factor is adopted to cover the uncertainties on the simplification of the 3D behaviour and to obtain a cautious estimate of displacements and structural forces. Lower unloading factors maximise displacements, whereas higher unloading factors maximise structural forces. In this way, a conservative design is ensured. However, when geotechnical parameters have to be updated during or after the tunnel construction, the uncertainties and the non-uniqueness of this value do not allow for a proper back-analysis. If on the one hand, 2D analyses are relatively fast and potentially accurate enough to match field data, on the other hand, assumptions have to be made to coop with the 3D nature of the problem. Given a certain set of geotechnical parameters, different hypotheses regarding stress reduction factor or stiffness reduction factor obviously lead to different results. This aspect does not allow to correctly back-calculate soil strength and stiffness and can potentially represent a source of inaccuracy in the model. Three-dimensional analyses, on the contrary, would avoid initial assumptions regarding the amount of stress relief or pre-convergence occurring before the lining installation.

If the main goal is to obtain a reliable estimate of surface settlements, a combination of a 2D and a fast 3D analysis (so-called all-in-one installation) also represents a relatively fast alternative as suggested by **Vermeer et al. (2002)**. This procedure leads to an estimate of the relaxation factor which allows reproducing precisely the 3D subsidence phenomena by using a 2D analysis. However, the so calibrated λ-value does not guarantee the match of lining forces and displacements as calculated with a full 3D analysis. Furthermore, the λ value obtained from a certain back analysis would not be valid anymore if, for instance, ground conditions remain the same but one of the other conditions changes (e.g. geometry, excavation sequence, overburden). For example, the λ value that is found by back analysing the monitoring data of an exploratory adit could not be used for a reliable prediction of the real tunnel displacements **(Svoboda & Masin 2011)**.
In conclusion, if the stress reduction factor is carefully chosen, a plain strain analysis carried out through the stress reduction method can reproduce some aspects of a full 3D simulation, but a small variation of the λ value strongly affects the results **(Galli et al. 2004)**. In any case, plane strain analyses represent an extremely useful and fast method for carrying out parametric studies aimed at better understanding the influence of each parameter or model detail on the calculation results.

2.4.1.2. Mesh dependency

The main factors governing the influence of the mesh size on numerical results are tunnel diameter, ratio between tunnel depth and tunnel diameter, k_0 coefficient and soil constitutive model.
Regarding three-dimensional simulations, the initial vertical boundary of the model causes a significant disturbance. Therefore, a certain excavation length is necessary to reach the so-called steady-state condition of displacement as highlighted by **Vermeer et al. (2002)**. The authors performed three-dimensional simulations in low k_0 conditions. They showed that for a circular tunnel, a 4.5D long excavation (with D=tunnel equivalent diameter) has to be simulated before reaching a stationary solution, whereas a top heading-invert excavation requires even longer models. **Franzius & Potts (2005)** performed calculations in high k_0 regimes, showing that, although the simulation was carried out up to a 24D from the vertical boundary, no steady state settlements were reached.
Pang et al. (2005), performing 2D calculations, showed that tunnelling induced settlements become more extended as the tunnel gets deeper and the

K_0 coefficient increases. Therefore, the higher overburden and K_0 are, the wider is the mesh width required to minimise the boundary influence.
Möller (2006), according to two different criteria for the vertical and bottom boundaries, defined the minimum mesh dimensions for both 2D and 3D models. Although the study considers only one K_0 condition, one tunnel geometry and one soil constitutive model, it is a useful reference for an initial definition of the boundaries in the case of shallow tunnel simulations.

2.4.1.3. The role of K_0

Several class C predictions mainly based on surface settlement and horizontal displacements in the soil mass, showed that the assumed earth pressure coefficient plays a crucial role in the accuracy of the back-calculation.
An extensive literature regarding the short-term behaviour in London clay investigated the problem of the overestimation of the settlement trough in high K_0 regimes.
Franzius et al. (2005) compared field observations from the Jubilee Line Extension (London) and the results of 2D and 3D calculations varying both K_0 and soil anisotropy. It turned out that only assuming unrealistic values of K_0 and degree of anisotropy, it was possible to obtain a reasonable shape of the settlement trough and a steady-state condition of displacements, despite the considerable longitudinal length of the 3D model. Moreover, neither anisotropy nor the implementation of a 3D model instead of a simple 2D one could avoid the overestimation of the width of the transverse settlement trough.
Mašín (2009) carried out a simulation of the Heathrow Express trial tunnel construction in stiff clays with high K_0 conditions. The author implemented the hypoplastic model for clays and a shotcrete model that considers the time dependency of stiffness and strength. Soil parameters were calibrated against laboratory tests and field measurements. The so-calibrated soil parameters combined with a 3D model provided a reasonable agreement between numerical predictions and soil displacements, both vertical and horizontal. Besides highlighting the deficiencies of the simple Mohr-Coulomb model in predicting reasonable settlement troughs and horizontal displacements in high K_0 regimes, the results show the effect of the G_0 degradation curve on the deformation response.
An interesting evaluation of the K_0 value and its effects on predictions in a stiff clay deposit is provided by **Rott et al. (2015).** The authors also

highlight how the evaluation of K_0 coefficient through different methods might lead to significantly different values. In particular, methods deriving K_0 from OCR can lead to an overestimation of the horizontal stress state. In fact, the overconsolidation can be due not only to mechanical unloading but also to ageing processes. The performed back-analyses confirmed the discrepancy between the K_0 estimated through the OCR and the K_0 providing a reasonable agreement between predicted and measured displacements.

2.4.1.4. Drainage conditions

Before running a numerical calculation, the drainage conditions should also be defined. The hypothesis of fully drained or fully undrained conditions disregards the evolution of pore water pressures with time, avoiding time-consuming consolidation analyses. Regarding the deformation response to underground excavations in fine-grained materials, besides ground permeability, other factors should be taken into account to evaluate the drainage conditions correctly: position of the phreatic level with respect to the tunnel, saturation degree, presence of thin sandy interlayers, advancement rate, lining permeability, use of drainage systems installed in advancement during the excavation and so forth. In general, high advancement rates and low permeabilities lead to smaller deformations, since the excess pore pressures around the tunnel face do not have enough time to dissipate. **Anagnostou et al. (1993)** suggested, by running some parametric analyses, that drained conditions can be expected with permeability higher than 10^{-7} to 10^{-6} m/sec and excavation advance rate lower than 0.1-1 m/hour. However, in the case of excavation standstill, it is strongly recommended to consider drained conditions, which usually represent the critical ones for both stability and deformation problems. Further three-dimensional consolidation calculations carried out by **Anagnostou (2008)**, showed the influence of the excavation rate on the surface settlements. The author highlighted the strong effect of negative pore pressures in the proximity of the tunnel face, where high ratios between advance rate and permeability tend to reduce the deformations significantly. The analyses were carried out by reformulating the consolidation equations in a reference system fixed to the moving tunnel face. This method allows the time-variable to be eliminated from the equations governing the steady state, in the case of homogeneous conditions in the longitudinal direction, thus avoiding extremely time-consuming calculations.

Considering traditional tunnelling, the advance rate is usually between 1 and 2 m/day, depending on the magnitude of improvement interventions and the adopted excavation technique (hammer, ripper, blasting, etc.). Therefore, according to the consolidation analyses carried out by **Anagnostou (2008),** the undrained behaviour is likely to influence the deformation response when k is lower than 10^{-7} m/s, especially in the soil volume surrounding the excavation face. Nevertheless, the presence of thin sandy layers might reduce this influence by facilitating the dissipation of excess pore water pressures. Furthermore, the presence of permeable linings, as well as drainage systems installed before advancing, can locally lower the phreatic level.

2.4.1.5. Soil Constitutive Modelling

Only in the last two decades, the implementation and verification of advanced constitutive models (e.g. hardening plasticity models or hypoplastic models) as well as a considerable improvement in the computational capacity, contributed significantly in providing more realistic numerical results. A general overview of the most common constitutive models used in practice can be found in **Schweiger (2008)** and **Lade (2005)**. The accuracy of predictions carried out by using advanced constitutive models is strictly dependent on the level of knowledge of the ground conditions. The calibration of a sophisticated constitutive model should, therefore, rely on an accurate geotechnical model. Nevertheless, even if the soil behaviour is not well defined, advanced constitutive models have the merit of providing more realistic results in terms of stress-strain behaviour when compared to simple soil models, leading to a better understanding of complex soil-structure interaction problems. Moreover, in most cases, the model parameters have a clear physical meaning, allowing the user to calibrate them using standard soil tests. On the other hand, although simple elastic-perfectly plastic models require fewer input values, their correct definition involve more engineering judgement. This fact is due to the necessity to synthesise different mechanical behaviours of the soil over a wide range of stresses, strains and loading patterns by using a small number of material parameters. As long as failure conditions of an engineering problem are concerned, basic models such as the Mohr-Coulomb or Tresca models represent a suitable choice. However, when the soil response under working loads has to be predicted or back-analysed, the non-linear pre-failure behaviour has to be considered for obtaining more realistic

predictions. Moreover, when the problem is governed by deviatoric deformations (e.g. retaining walls and underground excavations involving stiff clays), another aspect which should be considered is the irreversible response due to primary deviatoric loading. Another feature that considerably improves displacement predictions is the implementation of high stiffness under very small strains. The use of a non-linear constitutive relation including small strain stiffness in tunnelling simulations has the advantage of predicting narrower settlements troughs, concentrating strains around the tunnel cavity and reducing them far from its boundary. The implementation of this feature also contributes to avoiding unrealistic heave at the tunnel bottom and reduces the influence of the mesh boundaries on the results **(Brinkgreve 2006)**.

The most common advanced constitutive models for geotechnical applications involving continuum problems have been formulated both in the framework of the classic plasticity theory and according to the theory of hypoplasticity. In general, they have proved to be quite effective in predicting soil pre-failure deformations in the case of underground openings. **Puzrin et al. (1997)** considered linear and non-linear, isotropic and anisotropic pre-failure behaviour for modelling the twin Jubilee Line Extension Project tunnels. The authors highlighted the importance of including pre-failure non-linearity for obtaining a narrower and deeper surface settlement thanks to the strain concentration at the tunnel boundary combined with a strain dependent stiffness.

Mašin & Herle (2005) carried out plain strain FE simulations of the Heathrow Express trial tunnel in London clay adopting both traditional and advanced constitutive models such as combined isotropic and kinematic hardening plasticity and hypoplasticity. The results demonstrate that displacements are better predicted when pre-failure non-linearity (including small strains), anisotropy and stress path dependency are considered in the stiffness calculation.

Despite the significant improvement in subsidence prediction introduced by these models and their capability of reproducing most facets of real soil behaviour, they still fail most of the time in matching ground surface distortions. This issue is probably related to the difficulties in modelling shear strain concentrations leading to the development of shear bands **(Negro & Queiroz 2000).** Recently developed and numerically implemented constitutive models such as the multilaminate soil model can potentially overcome this problem **(Galavi & Schweiger 2010)**.

Among the advanced constitutive models, one of the most used in practice is the Hardening Soil Model **(Schanz et al. 1999).** The HS Model includes ten parameters, but they all have a clear physical meaning and the experimental data needed for the calibration can be acquired through conventional laboratory tests. The implementation of the small strain stiffness in the Hardening Soil Model is described in **Benz (2007)** and requires two additional parameters, namely the maximum small-strain shear modulus G_{max} and the shear strain $\gamma_{0.7}$ at which G decays to $0.7G_{max}$. The possibility to give G_{max} as a direct input in the HSS model (i.e. Hardening Soil Model with Small Strain Stiffness) is consistent with the finding that this parameter is more effective in normalising stiffness decay curves in fine-grained soils when compared to p' or c_u **(Vardanega & Bolton 2013).** The authors also showed that G_{max} is better predicted when defined as a function of the specific volume and mean effective stress. This procedure should be preferred in practice when compared to analytical expressions requiring OCR, being this value harder to estimate reliably.
Nowadays small strain soil parameters are often available, and they can be therefore exploited not only for seismic purposes but also for static analyses. In fact, seismic in situ tests are commonly carried out in practice, due both to the enhanced soil investigation technologies and to the necessity of defining the ground seismic response according to design codes requirements.

2.5. Concluding remarks

In §2.1 an overview of the wide range of methods commonly used in tunnel design have been presented. Besides numerical calculations, many simplified calculation or prediction methods are available. The main properties, as well as advantages and shortcomings of all of them, have been briefly pointed out. Concerning shallow tunnels and traditional excavation, most of the non-numerical approaches present remarkable disadvantages deriving from a very restrictive set of assumption. This explains the intensive use in previous works, as well as in this thesis, of computational programs. In particular, in the present thesis, three of the most crucial problems regarding traditionally excavated shallow tunnels are investigated: the application of standard codes to a numerically-based tunnel design, the stability of reinforced and unreinforced tunnel face and the possibility to use numerical methods for model validations or back-calculations. §2.2, §2.3 and §2.4 summarised the main achievements concerning the previously

listed topics. The analysis of the state of the art regarding design codes suggested that despite Eurocode 7 aims at standardising geotechnical design all over Europe, there is no agreement about how to deal with tunnels. The main difficulty derives from the application of Eurocodes approaches in combination with numerical programs. This problem is complicated by the fact that actions and resistances derive from the same source and both the soil and the structural support present a non-linear behaviour.
Concerning face stability, the previous works seem to provide already a quite complete framework to evaluate the influence of several factors on face stability and to design face reinforcements. However, most of the collected research results involve only face deformation behaviour. Lower is the number of papers involving face stability calculations. Therefore, it is necessary to further investigate the problem of evaluating the safety level of the tunnel face through numerical analyses.
Finally, the review of the case studies including numerical validations or back-calculations pointed out the difficulty in obtaining reliable predictions. Plain strain models, independently from the initial assumptions, fail in matching all the results of a full 3D model. Moreover, to obtain reliable predictions or back-analyses, it is important to take into account several aspects: above all, the high variety of the stress paths and deformation levels involved in tunnelling problems. This aspect requires an appropriate choice of the constitutive model, depending on the level of accuracy to be achieved.

Chapter 3.
Eurocodes applicability to numerical calculation of shallow tunnels: calculation examples

Although Eurocode 7 is not meant to be applied to the design of tunnels, the lack of standard codes explicitly focusing on tunnelling leads to the situation that Eurocode 7 is increasingly used in practice, at least for shallow tunnels in soils. However, there is no general agreement on which of the approaches defined in EC7 is the most suitable for the design of shallow tunnels, in particular when it comes to applying them in combination with numerical analyses. In this chapter, the results of numerical calculations aimed at assessing ultimate limit state conditions of a shallow tunnel in soil are presented. The focus of the present work is firstly on the verification of the applicability of the Eurocodes in combination with numerical analyses and the comparison of different design approaches. Secondly, the consequences of the choice of a nonlinear material model for the shotcrete lining are discussed.

The results obtained from the application of different design approaches and modelling strategies for the lining design of a typical shallow tunnel are compared, and the limits of each of them are pointed out. The interaction with Eurocode 2, as well as the possibility to take into account the non-linear and time-dependent behaviour of the shotcrete, is also considered by applying a non-linear constitutive model for shotcrete and comparing the results with those obtained by using an elastic material.

3.1. Calculation benchmark

This contribution originates from an initiative supported by the Austrian Society for Geomechanics (OeGG), aimed at investigating the compatibility between Eurocodes approaches and numerical analyses applied to shallow tunnels. The current version of the Austrian guideline **RVS 09.01.42 (Tunnel structures in soft soil under built-up areas)** specify that for standard cases, like 2-D finite element analyses of tunnel excavations, carried out through non-linear constitutive models for the soil and linear for the support, DA2* approach should be applied. If the tunnel support is modelled with a non-linear constitutive model, these guidelines are not directly applicable. Therefore, the goal of the calculation example here

presented is not only to compare different design approaches but also to evaluate different possibilities for their application in combination with non-linear models for the tunnel support. This example also provided the opportunity to assess the impact of these models on the design, regarding safety and cost-effectiveness.

The benchmark problem here considered is a shallow NATM tunnel characterised by an equivalent diameter of 10 m and overburden of about one diameter. Geometry and material parameters have been taken based on an actual project but have been slightly modified for the purpose of this study. The model, shown in Figure 38 and the prescribed excavation sequence, schematically represented in Figure 39, have been analysed through the finite element code Plaxis 2D **(Brinkgreve et al. 2014)**. 15-noded triangular elements were used. The calculations focus only on the primary lining, normally designed to fully support the excavation before the construction of the final lining.

The excavation area is divided in right side drift (excavated first) and left side drift. Each side drift has been excavated in two phases: top heading and bench. In order to simulate the three-dimensional effects of the face advancement, a pre-relaxation factor of 0.4 has been adopted for each section. The surface load of 15 kN/m^2, applied after the completion of the excavation, has been considered as a permanent load. The analyses aim at assessing the applicability of different design approaches and the impact of different modelling strategies given a certain set of characteristic parameters. The analyses aim at assessing the applicability of different design approaches and the impact of different modelling strategies given a certain set of characteristic parameters. The constitutive model assigned to each soil layer and the corresponding soil parameters are provided in Table 5.

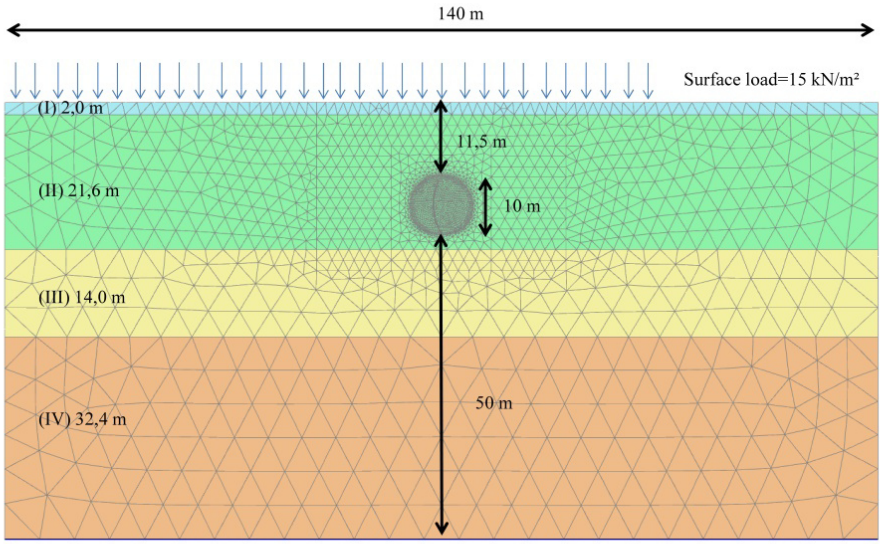

Figure 38. FEM model of the calculation example

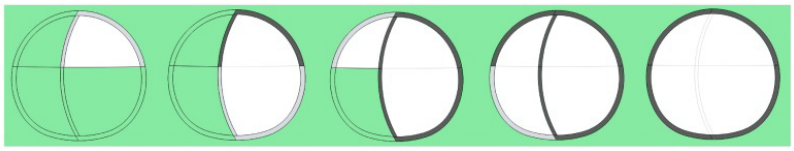

Figure 39. Schematic representation of the excavation sequence

Table 5. Soil parameters

		I	II	III	IV
		Backfill	Loess	Sandy gravel	Clayey silt
Parameter		MC*	HSS#	HSS	HSS
γ_k	kN/m³	19.00	19.00	21.00	20.00
$K_{0,NC}$	-	-	0.5	0.5	0.5
φ	°	20.00	25.00	35.00	23.00
c	kN/m²	0,00	50.00	0.00	50.00
E	kN/m²	5,000	-	-	-
ν	-	0.2	-	-	-
$E_{50,ref}$	kN/m²	-	25,000	100,000	50,000
σ_{ref}	kN/m²	-	100	100	350
E_{ur}	kN/m²	-	75,000	250,000	150,000
ν_{ur}	-	-	0.2	0.2	0.2
m	-	-	0.6	0.5	0.6
$E_{0,ref}$	kN/m²	-	200,000	800,000	450,000
G_{0ref}	kN/m²	-	83,333	333,333	187,500
$\gamma_{0,7}$	-	-	0.0002	0.0002	0.0002
$E_{oed,ref}$	kN/m²	-	25,000	100,000	50,000

*Mohr-Coulomb Model
#Hardening Soil Model with Small Strain Stiffness

The shotcrete primary lining has a thickness of 35 cm at the tunnel circumference and of 25 cm at the central support. In the FE analysis, it has been modelled using volume elements. The calculation of lining forces derives from the stress integration along the different cross sections of the lining, automatically performed by a special tool implemented in the software.

With the use of continuum elements for modelling the shotcrete lining, it has been possible to assign both a linear elastic constitutive model and an advanced constitutive model. The latter takes into account the non-linear and time-dependent behaviour of the shotcrete, which plays a very important role in tunnel constructions since, unlike normal concrete structures, the shotcrete is loaded at very early age. This model considers the time-dependency of both stiffness and strength, creep and shrinkage effects as well as plastic deformations before and after reaching the maximum strength. More details about the model formulation can be found in **Schaedlich & Schweiger (2014)** and **Schaedlich et al. (2014)**. The material parameters adopted for the non-linear shotcrete model are given in Table 6.

Table 6. Material parameters adopted for the non-linear shotcrete model.

Parameter	Description	value	
E_{28}	Young's modulus of cured shotcrete at t_{hydr}	kN/m²	2.50E+07
ν	Poisson's ratio		0.2
$f_{c,28}$	Uniaxial compressive strength of cured shotcrete at t_{hydr}	kN/m²	2.00E+04
$f_{t,28}$	Uniaxial tensile strength of cured shotcrete at t_{hydr}	kN/m²	2,000
ψ	Dilatancy angle	°	0
E_1/E_{28}	Time dependency of elastic stiffness	-	0.648
$f_{c,1}/f_{c,28}$	Time dependency of strength	-	-2
$f_{c0,n}$	Normalized initially mobilised strength	-	0.15
ε_{cp}^{p} **at 1h**	Uniaxial plastic failure strain at 1h	-	-0,03
ε_{cp}^{p} **at 8h**	Uniaxial plastic failure strain at 8h	-	-2.00E-03
ε_{cp}^{p} **at 24h**	Uniaxial plastic failure strain at 24h	-	-1.00E-03
φ_{max}	Maximum friction angle	°	35
t_{hydr}	Time for full hydration	day	28

In the following analyses, only the time-dependency of stiffness and strength and the pre-peak plastic deformation behaviour of the material have been taken into account. Therefore no creep and shrinkage effects, as well as no softening behaviour, have been considered. The increase of Young's Modulus follows the recommendation of **CEB-FIP model code (1990)** whereas, for the strength evolution, the J2 range defined in **EN 14487-1 (2006)** has been chosen (Figure 40).

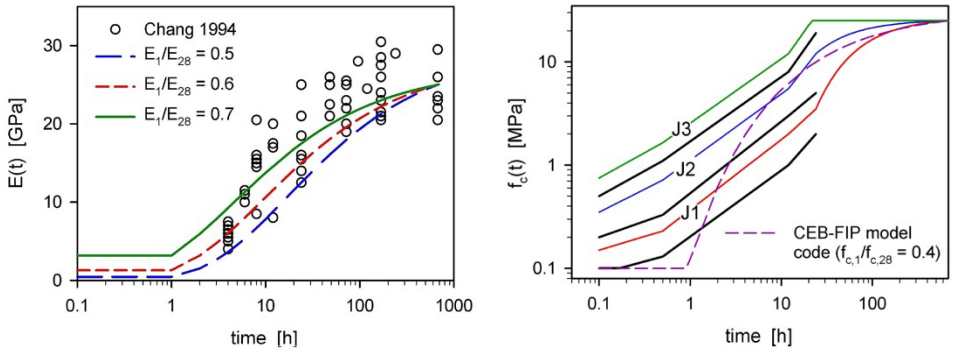

Figure 40. Time dependency of shotcrete stiffness and strength

The model, as implemented in Plaxis, takes automatically the mean values of the ranges defined in the standard. The steel reinforcements are considered in the model as an equivalent tensile strength of the shotcrete

material. In the calculations where the shotcrete has been modelled as linear elastic, a stepwise increase of the Young's Modulus has been adopted: 5 GPa and 15 GPa for young and old shotcrete respectively. A detailed list of the performed calculation phases can be found in Table 7.
No interface has been modelled between soil and structure. Therefore they are tied together, and no relative displacements can occur. This approach is not conservative when the goal is to estimate soil displacements. However, when the structural support has to be designed, it is a cautious assumption. Moreover, it is not easy to define the properties of the interface. Even though assuming soil and structure fully tight might lead to an overestimation of the structural forces, the comparison between design approaches or between different modelling strategies is still valid.
The calculations have been carried out both according to DA2* approach (which is identical to DA1-1 when resistance factors are neglected) and to DA3 approach (which corresponds to DA1-2).
All the combinations taken into account in the present example are listed in Table 8.
The verification of the tunnel support is usually carried out using the interaction diagrams between normal force and bending moment (M-N check). In order to be fulfilled, this check requires the structural forces to fall inside the diagram.
When DA3 has been adopted in combination with a shotcrete lining modelled as non-linear material, the analysis has been carried out both using the characteristic shotcrete strength (this requires an M-N check at the end) and reducing it by the 1.5 factor, prescribed in **EN 1992-1-1**. The advanced shotcrete model implemented in Plaxis offers the possibility to directly introduce, in the model settings, partial safety factors on both tension and compression strength. These factors automatically scale the strength envelope during its evolution with time. The reduction of shotcrete strength, performed directly during the analysis, as previously described, instead of performing the final M-N check, could be considered an alternative way to apply the DA3 approach in combination with non-linear models for the structural support.

Table 7. Calculation phases performed

PHASE	description	Δ days (time necessary to develop each phase)	Total number of days (Σ Δ days of each phase)
0	Initial stress	0	0
1	pre relaxation (area 1)	1.5	1.5
2	total relaxation (area 1) and shotcrete activation	1.5	3
3	pre relaxation (area 2)	1.5	4.5
4	total relaxation (area 2) and shotcrete activation	1.5	6
5	pause	7	13
6	pre relaxation (area 3)	1.5	14.5
7	total relaxation (area 3) and shotcrete activation	1.5	16
8	pre relaxation (area 4)	1.5	17.5
9	total relaxation (area 4) and shotcrete activation	1.5	19
10	Removal of the central support	1	20
11	Activation of the surface load	0	20

Table 8. Design calculations performed

Combination		Actions		Soil parameters		Structural resistances	
		Partial factor on effect of actions	Partial factor on surface load(+)	Partial factor on cohesion	Partial factor on friction angle (tanφ')	Shotcrete model	Partial factor on shotcrete resistance(#)
1	DA2*	1.35	-	-	-	Linear elastic	-
2	DA2*	1.35	-	-	-	Non-linear	-
3	DA3	-	-	1.25	1.25	Linear elastic	-
4	DA3	-	-	1.25	1.25	Non-linear	-
5	DA3	-	-	1.25	1.25	Non-linear	1.5

(+)considered as a permanent geotechnical action
(#)directly given as input in the calculation

3.1.1. Results and discussion

In order to compare the results obtained from the different calculations, not only the final stage of the construction process but also an intermediate stage, namely the end of the excavation of the right drift (phase 4), is

considered. In fact, it represents a critical stage, showing particularly severe stress conditions, especially at the upper junction between the circumferential lining and the central support. In the figures below, the different calculations are identified by the corresponding numbers of Table 8. The shotcrete modelled as a linear elastic material is referred to as LES, whereas the new shotcrete model is referred to as NSM. The structural forces depicted in the graphs are design forces, which means that they include the factor on the effect of actions (namely 1.35 for DA2*). In the legend, a further distinction is made between calculations with characteristic or design shotcrete strength (respectively 20 MPa and 13.3 MPa at 28 days of curing).

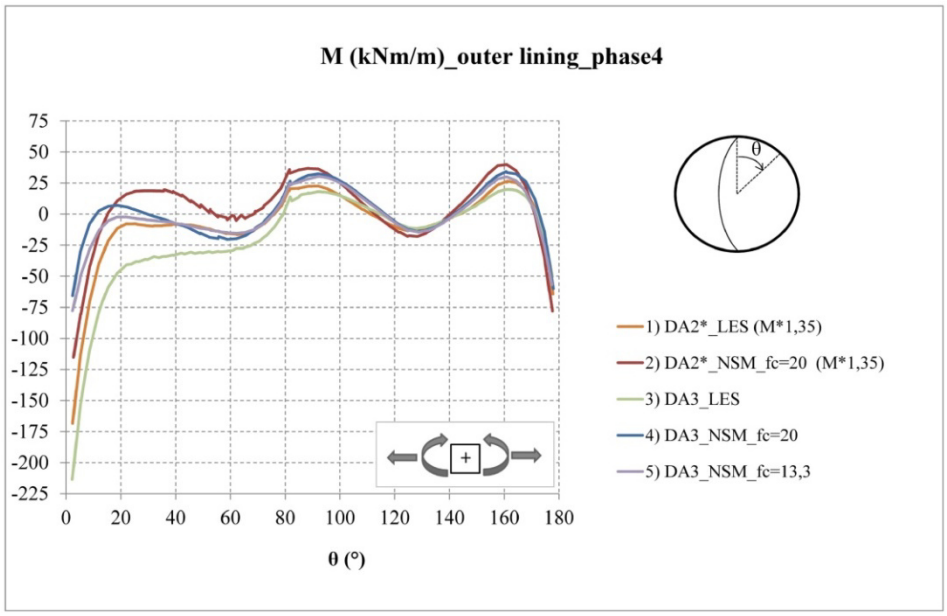

Figure 41. Bending moments from phase 4 (outer lining)

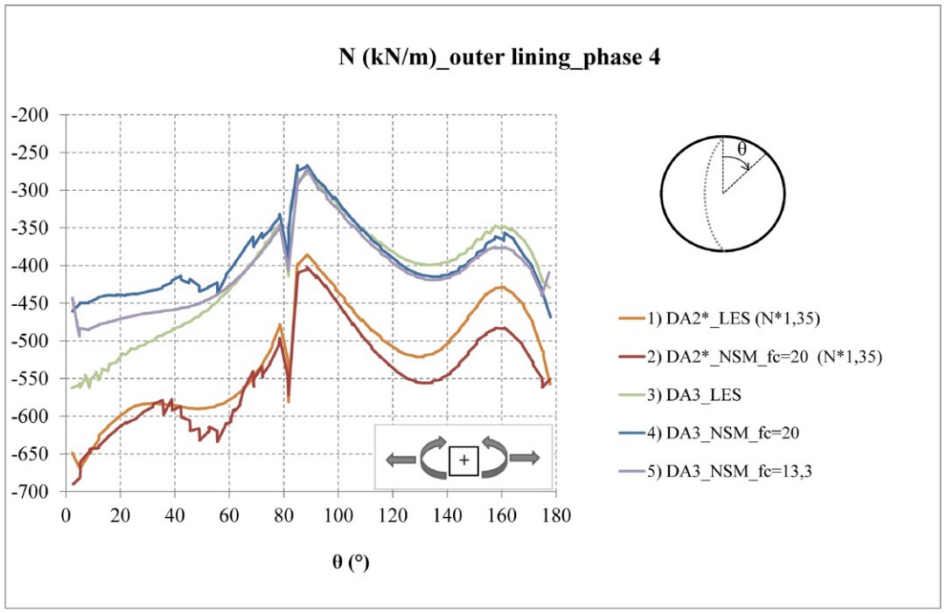

Figure 42. Normal forces from phase 4 (outer lining)

From Figure 41, showing bending moments obtained from phase 4, it can be seen that modelling the lining as a stepwise elastic material leads to much higher bending moments when compared to the non-linear shotcrete model. In the case of elastic shotcrete, DA3 results are more conservative. This means that, in this specific phase, the plasticity of the soil induced by a reduction of soil strength properties plays a major role, leading to higher bending moments when compared to DA2* approach, where the factor 1.35 is applied to the calculated forces. The opposite situation holds for the case of non-linear shotcrete, where DA2* results in higher bending moments. The differences between design approaches are less pronounced when the lining is modelled with the advanced constitutive model. Concerning normal forces (Figure 42), differences in calculated values are not significant independently from the shotcrete model and the use of characteristic or design strength parameters for the soil. Therefore DA2* results in higher normal forces due to the application of the partial factor 1.35 on structural forces.

In the final phase, the differences in the calculated forces due to the use of a specific lining model or to soil characteristic parameters instead of design parameters are less remarkable. Therefore, also in this case, the main

difference in the curves plotted in Figure 43 and Figure 44, stems from the 1.35 factor applied on the computed values of the lining forces.
The maximum and minimum values of the lining forces obtained from each combination for both the intermediate and the final phase are listed in Table 9.

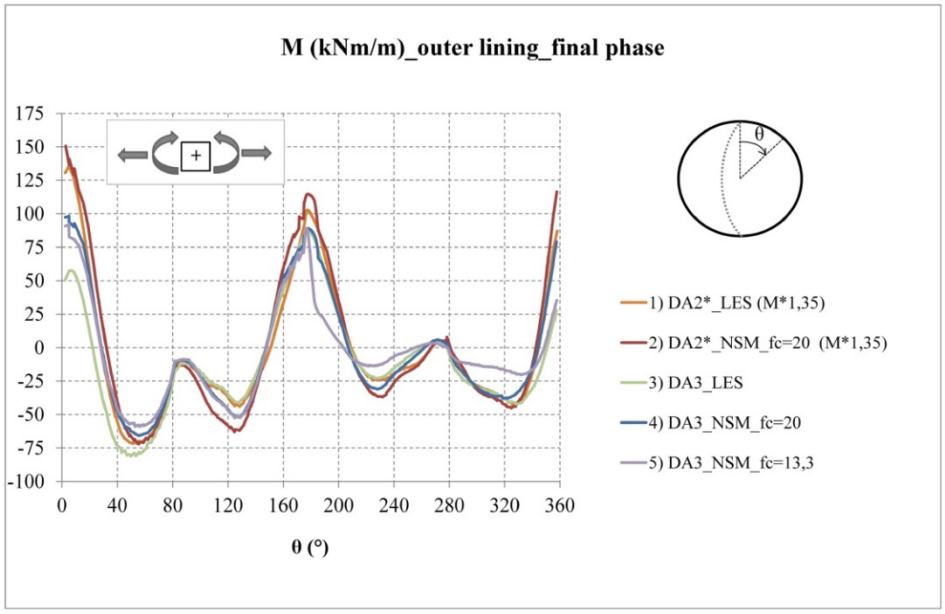

Figure 43. Bending moments from the final phase (outer lining)

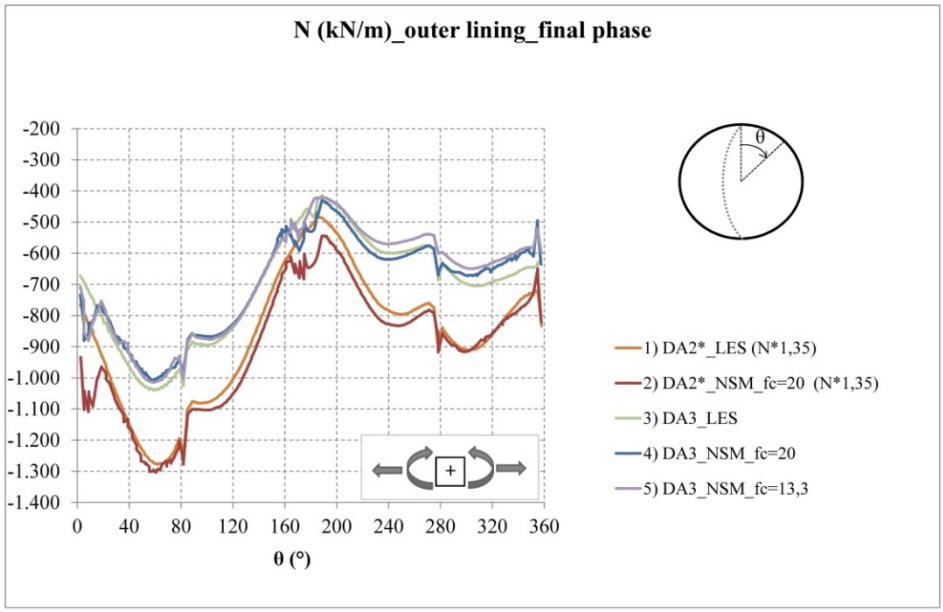

Figure 44. Normal forces from the final phase (outer lining)

Table 9. Maximum and minimum values of the lining forces from phase 4 and from the final phase (outer lining)

Combination	Intermediate phase (n°4)				Final phase			
	M_{max}	M_{min}	N_{max}	N_{min}	M_{max}	M_{min}	N_{max}	N_{min}
1	26	-168	-386	-669	136	-72	-484	-1278
2	40	-115	-402	-690	151	-72	-544	-1304
3	20	-214	-273	-562	89	-81	-415	-1040
4	34	-66	-267	-468	98	-66	-430	-1008
5	30	-78	-272	-494	92	-59	-419	-1015

For the central support, whose critical conditions are also reached at the end of the right drift excavation (i.e. phase 4), similar results to those emerged for the outer lining have been obtained (Figure 8, Figure 9). This is reasonable considering that the central support is rigidly connected to the circular lining. The maximum and minimum values of the lining forces deriving from each combination are listed in Table 10.

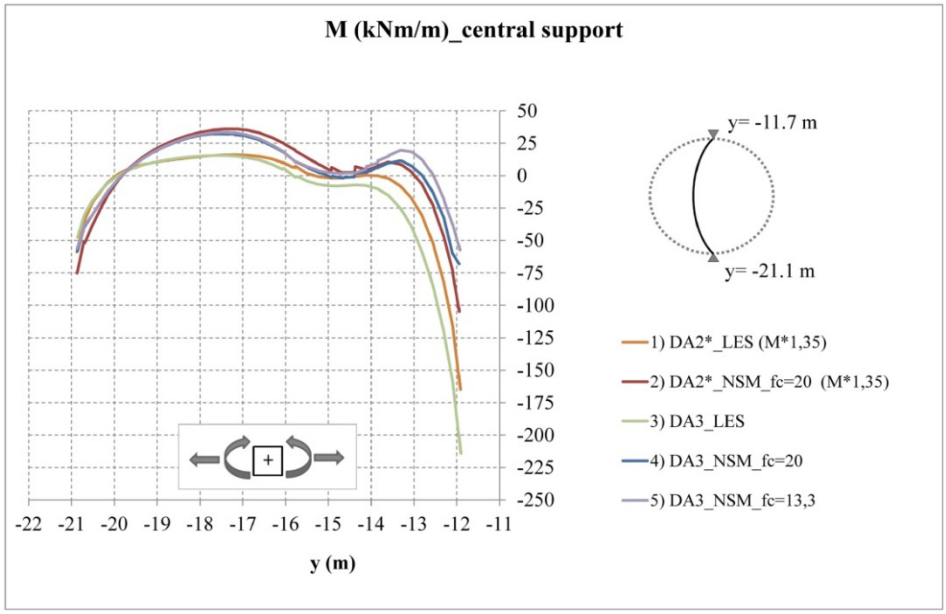

Figure 45. Bending moments from phase 4 (central support)

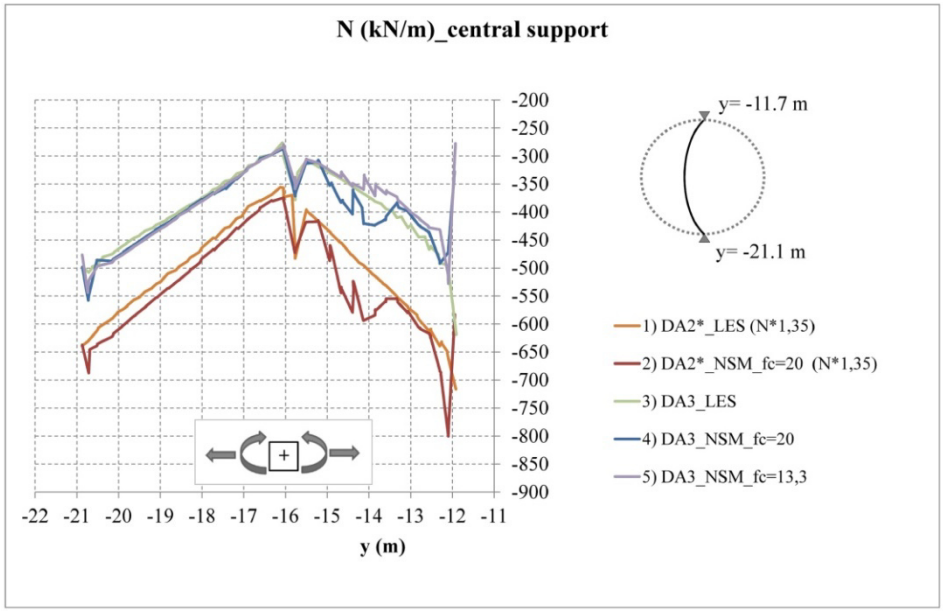

Figure 46. Normal forces from phase 4 (central support)

Table 10. Maximum and minimum values of the lining forces from phase 4 (central support)

Combination	Intermediate phase			
	M_{max}	M_{min}	N_{max}	N_{min}
1	16	-165	-356	-717
2	36	-105	-374	-687
3	15	-214	-276	-619
4	32	-68	-287	-558
5	34	-57	-277	-544

For all the analysed combinations, the M-N interaction diagrams have been plotted to evaluate the structural margin of safety. The different calculations, whose results are shown in Figure 47, Figure 48 and Figure 49, are identified with the corresponding number indicated in Table 8. The reference sections are the most critical ones and coincide with the upper corner for phase 4 and with the lowest section of the lining for the final phase. The black curve represents the characteristic domain, whereas the grey one is the design domain, reduced by the partial safety factor on material strength, namely 1.5. For the intermediate phase (i.e. phase 4), a different domain has been considered because, after the excavation of the right drift, the shotcrete curing process is not completed and the shotcrete resistance is around 90% of the final one.
The combination DA3 with partial factors applied on shotcrete resistance (combination 5) was also included in the graphs, even though it does not require an M-N check, being the design criteria implicitly satisfied. All the other combinations are supposed to fall in the grey domain to fulfil the structural ULS requirements.

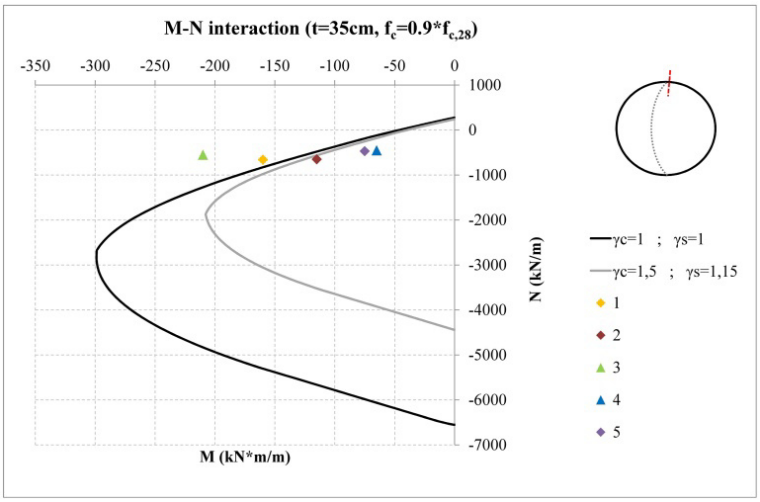

Figure 47. M-N check for the outer lining (phase 4)

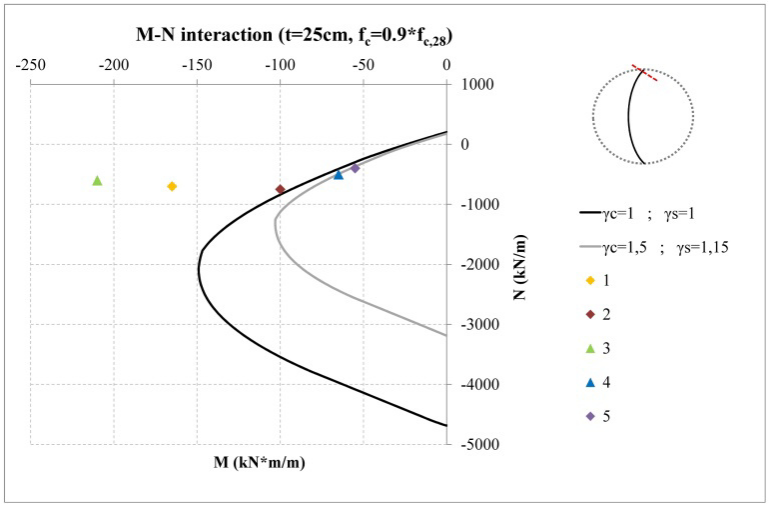

Figure 48. M-N check for the central support (phase 4)

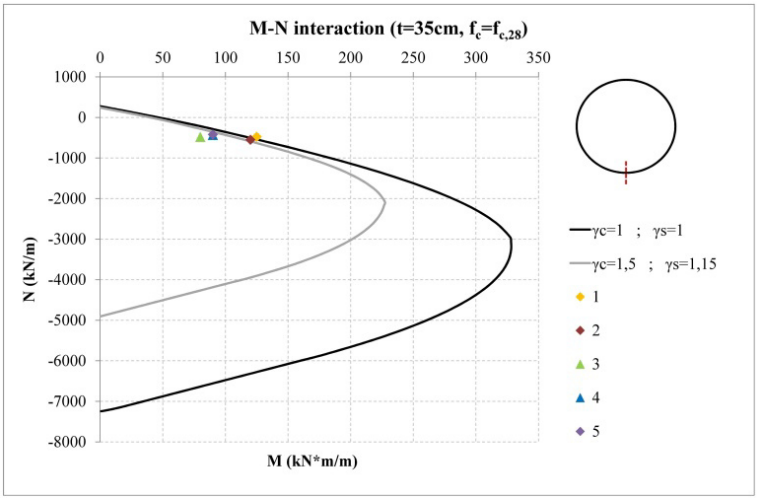

Figure 49. M-N check for the outer lining (final phase)

As previously underlined, phase 4 represents one of the most critical conditions the tunnel support is subjected to. From Figure 47 and Figure 48, it can be noticed that both calculations with purely elastic shotcrete are outside the design domain in both the outer lining and the central support. In the latter case, also combination 2, including a non-linear structural support, does not fulfil the structural requirements. This means that the initially designed and analysed section has not enough strength to sustain the calculated forces increased by 1.35 and therefore the structural design should be reviewed.

Considering the final phase, the first two combinations (i.e., all those with characteristic soil parameters and partial factors applied on the computed lining forces) fall slightly outside the design domain, as it can be seen from Figure 49.

It seems clear, from these results, that no general rule can be established regarding which approach governs the structural design. In general, when adopting the advanced shotcrete model, the differences between DA2* and DA3 in terms of distance with respect to the M-N domain seem to be smaller.

In some cases, the adoption of an elastic model for the structural support with a stepwise increase of stiffness can lead to an extremely conservative design.

Considering the 1.35 factor to be applied to the calculated internal forces, DA2* approach in combination with non-linear shotcrete would theoretically allow for a lower exploitation of the redistribution capacity of the tunnel support, with respect to DA3. However, this issue is attenuated due to the application of the 1.35 factor to both bending moments and normal forces that, in most cases, increase the bending capacity of the section.

The possibility to exploit plasticity and stress redistribution capacity in both the soil and shotcrete lining, by using non-linear constitutive models is shown in Figure 50, where plastic point are plotted.

The advantage of using design soil material parameters, instead of the characteristic ones, is that at those stages where geotechnical failure seems to be approached (e.g., phase 2 where a diffused plasticity takes place at the lining footing), the designer can be more conscious about the possible failure mechanisms that are likely to develop and about the available margin of safety.

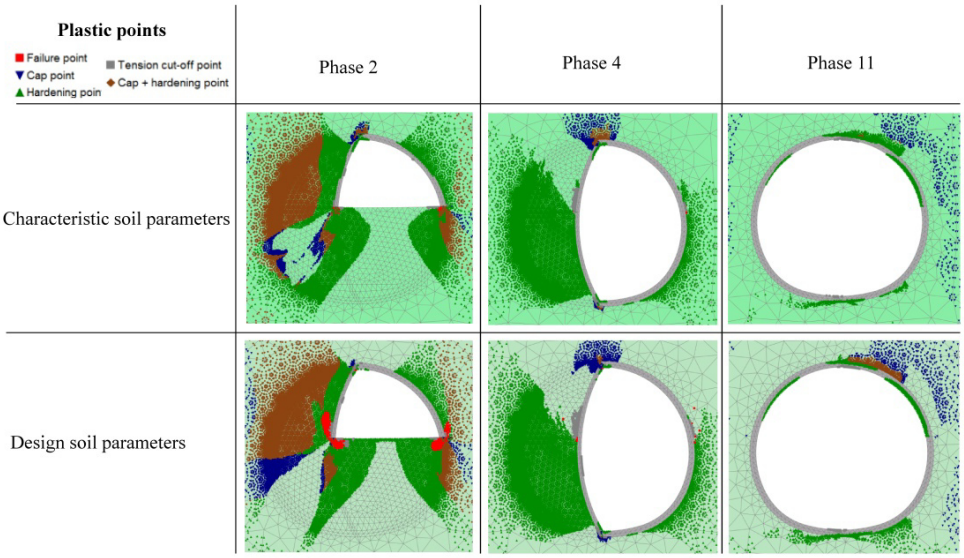

Figure 50. Plasticity distribution in both the soil and shotcrete (modelled with an advanced constitutive model)

3.1.2. Concluding remarks

In the present chapter, after an overview on the applicability of Eurocodes to a numerically-based design for underground excavations, the results of a calculation example regarding a NATM shallow tunnel are discussed.

It has been shown that a nonlinear shotcrete model can be applied in combination with design approach DA2*, the approach intuitively favoured by many geotechnical engineers in the common practice. On the other hand, at least to the opinion of the author, DA3 approach in combination with a partial factor on the shotcrete strength directly applied in the numerical calculation would also be in accordance with the material factoring approach as defined in EC7 for soils. Moreover, it would allow performing a completely implicit design, meaning that no further M-N check is required.

The benefits, in terms of cost-effectiveness, of a design carried out by using a constitutive model that accounts for the non-linear and time dependent behaviour of shotcrete can be considerable, especially when high stress concentrations cause an unrealistic increase of structural forces. Furthermore, provided that it is common practice to use non-linear material models for soils in numerical calculations, considering non-linearity and plasticity also in the structural support seems to be consistent. This is particularly true when dealing with highly non-linear and time dependent lining materials such as shotcrete, for which stress redistributions capabilities have to be considered to avoid uneconomic designs.

After analysing the diagrams of structural forces resulting from the calculations performed in this study, the following conclusion can be drawn:

- in some cases, the adoption of a linear elastic material for modelling the tunnel support leads to considerably higher bending moments when compared to the advanced shotcrete model;
- DA2*, except for bending moments of phase 4, provided higher internal forces.
- DA3 approach is feasible, in particular when considering the nonlinear material behaviour of both soil and shotcrete, resulting in a consistent (implicit) design.

In any case, when structural safety has to be assessed, an M-N check is required, unless all the partial factors are introduced in the calculation, and the design is therefore totally implicit (as for combination 5). Considering the M-N interaction domains the structural verifications still show that DA2* is the critical combination, i.e. the one governing the support design.

The only exception is represented by the results obtained from the linear elastic shotcrete model. In fact, in this case, the material factoring approach DA3, at the intermediate stage (phase 4), exceeds the design domain much more than DA2*.
Concerning the question which is most suitable and conservative design approach to be used for shallow tunnel projects, it can be concluded that it depends not only on the specific example but also on the excavation stage considered. Using only one of the two analysed approaches might lead to a less safe design either from a geotechnical or a structural point of view. In this sense, a combination of both DA2* and DA3 would achieve the purpose of ensuring a safe design from both the geotechnical and structural side. This goal would be accomplished by concentrating the uncertainties once on the effect of actions and once on the material properties. This design strategy seems to be the most suitable according to the present status of Eurocode 7.

Chapter 4.
Analyses of reinforced and unreinforced excavation face

Considering the main outcomes from previous researches on tunnel face behaviour (§2.3), some potential lines of development of this topic can be drawn. First of all, past research works involving numerical calculations regard more the analysis of the face deformation behaviour, rather than face stability. In particular, very few are the analyses involving face reinforcements in the numerical calculation. This fact is mainly due to the computational and time resources required to carry them out. Therefore, after a first paragraph introducing the Limit Equilibrium Method applied to tunnel face stability (used for comparison with FEM analyses), the focus of the present work in on the assessment of face stability through the so-called φ-c reduction procedure available in Plaxis 3D. The main reason why the LEM method is considered and used for comparison is that it is still one of the most used calculation methods for this kind of problems, at least in a first design stage. The only case of H=D was investigated because, if the friction angle is higher than 20°, stability is independent from the ground cover (§2.3.2).

Regarding the reinforced face, both LEM and FEM analyses were used to assess face stability. In the FEM models face reinforcements can be directly modelled or simulated by assigning a face pressure or equivalent material properties (e.g., increased cohesion).

On the contrary, the evaluation of the deformation behaviour of the reinforced tunnel requires a full 3D numerical analysis including direct modelling of the face reinforcements. Also in this case, alternative ways to consider the presence of these elements in a 3D model could be the application of a face pressure or the definition of equivalent material properties for the core clusters. Besides the detailed 3D model, the second option was considered in the present study for both stability assessment and evaluations of the deformation behaviour.

With respect to the previous literature, the present work includes a more extensive study covering a wide range of material properties and reinforcement configurations and providing safety factors for both unreinforced and reinforced face. The so-called strength reduction technique is adopted for analysing face stability. An important outcome of this study is

that the results obtained from limit equilibrium methods may be non-conservative for these types of problems. This aspect, however, is not common knowledge, at least not in practice. A further series of numerical calculations is aimed at investigating the effectiveness of face reinforcement in reducing both extrusion and subsidence phenomena. In this way, both the behaviour under working conditions and the ultimate limit state of the excavation face are taken into account.
The present work focuses mainly on fine-grained soils, where full face excavation can be carried out and the fibreglass technique is frequently adopted.

4.1. LEM analyses

In order to establish a basis for comparison with numerical analyses some parametric analyses, performed by applying the LEM and adopting the standard Horn mechanism, are presented in the following section. The first series regards unreinforced excavation faces and the second one deals with reinforced faces. The latter was analysed by accounting for the force S in the overall equilibrium of the sliding wedge. The characteristics of the fibreglass bars and the system ground-grout considered in the LEM calculations are listed in Table 11.
The values of L_a and L_p (Figure 37) depend on the minimum reinforcement length guaranteed during the excavation (namely the overlapping length) and on the inclination of the sliding block. Therefore, they are calculated case by case. In particular, L_a is taken as the average value of the bars length inside the sliding wedge and L_p is assumed equal to the average length of the bars in the stable ground. Figure 51 shows some results regarding safety factors calculated with the LEM according to the simple Horn model and the Silo's theory (§2.3.1). The factor of safety, in the case of c'=20 kPa and unreinforced face, is close to 1. Face reinforcement provides an increment in the safety factor between 0.4 and 0.8, depending on the soil properties and the reinforcement density. The influence of the friction angle on face stability is very low, at least for the considered variation range.

Table 11. Characteristics of the fibreglass reinforcement system.

properties		value
$\sigma_{adm,\ fibreglass\ bar}$	(MPa)	600
$\phi_{ext,\ fibreglass\ bar}$	(mm)	60
$\phi_{int,\ fibreglass\ bar}$	(mm)	50
ϕ_{hole}	(mm)	100
$\tau_{adm,\ ground\text{-}grout}$	(kPa)	100

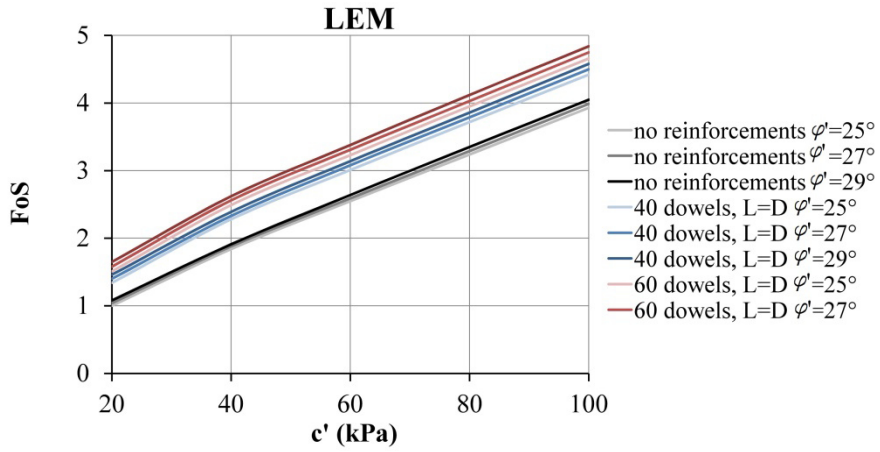

Figure 51. Factors of safety for reinforced and unreinforced excavation faces from LEM calculations

4.2. 3D FEM safety analyses

The numerical calculations presented in this paper were performed with Plaxis 3D 2013 **(Brinkgreve et al. 2013)**. A Mohr-Coulomb failure criterion was adopted for the soil whereas the fibreglass reinforcements have been modelled as 3D embedded pile elements. These structural elements are basically beam elements provided with a special interface to model the interaction between the surrounding soil and the element itself. A spring element at the pile base allows for considering a base resistance if required (in this case it was neglected). The interface can simulate relative displacements between the structural element and soil and it is characterised by an elasto-plastic constitutive law. The ultimate skin resistance can be introduced by means of two input values, at the top and at the bottom of the

embedded pile. The shear force acting on the pile circumference is calculated by multiplying the elastic shear stiffness of the interface for the relative displacement between soil and pile. This value cannot exceed the maximum shear force calculated according to the Mohr-Coulomb failure criterion or the value T_{max}, which can be defined by the user.

$$|t_s| < \left(\sigma_n^{avg} \tan\varphi_{int} + c_{int}\right)\pi D \quad \text{and} \quad |t_s| < T_{max} \quad (8)$$

The interface strength properties are calculated from the surrounding soil properties by means of the reduction factor for interfaces R_{inter}.

$$\tan\varphi_{int} = R_{int}\tan\varphi_{soil} \quad (9)$$
$$c_{int} = R_{int}c_{soil} \quad (10)$$

In the specific case R_{inter}=1 was adopted, and a constant limitation of the skin resistance (T_{max}) along the pile was introduced. Limiting the maximum axial force was not possible in this case, since the element is an elastic beam. Anyway the axial forces, in the performed calculations, never exceeded the maximum axial capacity, denoting that failure is governed by the strength of the interface (i.e., geotechnical failure).
The analyses were performed in 3 phases: stress initialization, excavation of the tunnel in one-go for a length of two tunnel diameters, φ-c reduction. The latter consists of an incremental reduction of both soil and interface strength parameters. The safety factor can be defined as the ratio between the tangent of the available friction angle, and the tangent of the friction angle mobilised at failure (Equation 11). This factor is equal to the ratio between the corresponding values of cohesion. In fact, both $\tan\varphi'$ and c' are reduced with the same increments during the φ-c reduction procedure.

$$\eta = \frac{\tan\varphi_{available}}{\tan\varphi_{failure}} = \frac{c_{available}}{c_{failure}} \quad (11)$$

In the safety calculations, the value of the ultimate skin resistance assigned to the embedded piles was iteratively changed to have the same reduction factor of that obtained from the φ-c reduction. The mesh dimensions of the model adopted for this study (Figure 52, a) are larger than those suggested by **Ruse (2004)** because, considering the presence of the embedded piles, the disturbed zone is more extended. The analysed excavation section is

circular (D=14 m) and characterised by an equivalent area comparable to that of a two lanes highway tunnel (Figure 52, b).
The movements in x, y and z directions are restrained on the bottom boundary, the surface boundary is free, and the movements on the other boundaries are restrained in the orthogonal directions by roller supports.

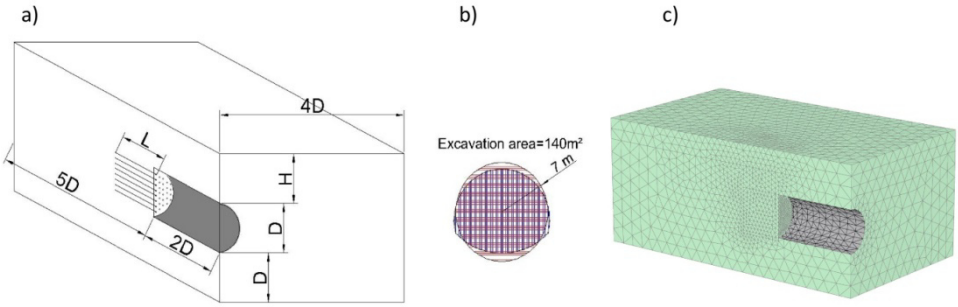

Figure 52. Model dimensions, excavation cross-section and FEM mesh

The mesh (Figure 52, c) consists of about 50000 10-noded tetrahedral elements and it is locally refined where the failure mechanism is supposed to occur (i.e., behind the excavation face).
In order to verify the accuracy of the simplified methods previously described, both reinforced and unreinforced excavation faces were analysed. The cases analysed without activating soil reinforcement are described in Table 12 and cover mainly soils characterised by a silty-clayey matrix and a wide range of effective cohesion. Since for cohesive-frictional soils with $\varphi' > 20°$ the factor of safety seems to be independent from the ground cover, only one value of overburden was taken into account (i.e., H=D). The k_0 applied in all the analyses is 0.6 and the soil unit weight is 19 kN/m^3. Different initial stress states were not considered since it has been shown that it does not influence the safety of the excavation face **(Ruse 2004, Perazzelli & Anagnostou 2012)**. In all the analyses, the tension cut-off is activated and no tensile stresses are allowed. Moreover, the unsupported span is neglected, and the lining is activated close to the tunnel face. In fact, it turned out that this aspect of the excavation sequence has a negligible influence on the face stability **(Ruse 2004)**, at least for values of the ratio d/D commonly adopted in practice.

Table 12. Analysed cases for an unreinforced excavation face

Unreinforced excavation face – analysed cases		
properties		**value**
H	(m)	D
d	(m)	0
φ	(°)	25-27-29
c	(kPa)	20-40-60-80-100

In Figure 53, it is clearly shown that the limit equilibrium method leads to a significant overestimation of the safety factor (up to 60%) when compared to the numerical calculations.

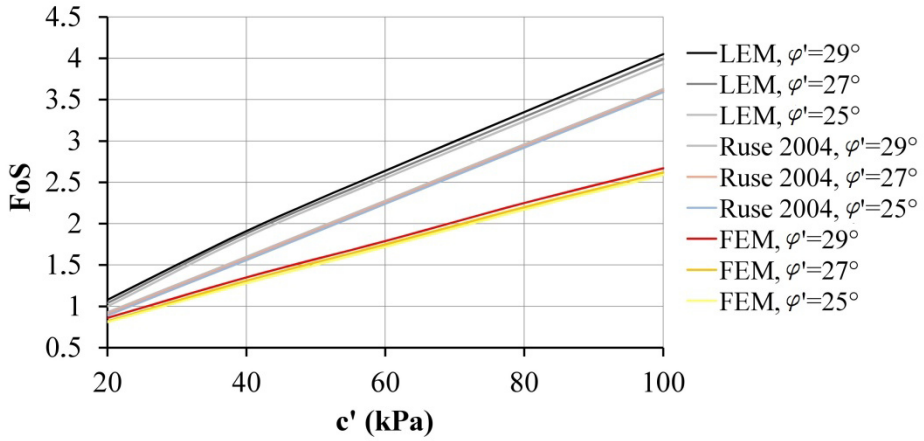

Figure 53. Factors of safety from LEM analyses, Ruse's formula and FEM analyses for unreinforced excavation faces

Also Equation 7 **(Ruse 2004)** provides higher safety factors because, as pointed out by the author, it does not consider tensile failure and therefore always overestimates face stability when compared to numerical calculations in which tension cut-off is activated, and no tensile strength is considered. In addition, Equation 6, from which Equation 7 derives, is based on the principle of superposition between two different contributions associated to soil cohesion and friction angle and therefore the overestimation increases with the increase of soil cohesion.

In order to match the numerical results obtained from the φ-c reduction procedure, Equation 7 was modified into Equation 12. In particular, Ruse's equation was modified by only acting on the term including soil cohesion and searching the function that provides a better match of the numerical results.

$$\eta = \frac{0.9\tan(\varphi') + 11.2 \cdot \left(\frac{c'}{\gamma D}\right)^{-0.13} \cdot \frac{c'}{\gamma D}}{2 + 3(d/D)^{6\tan\left(\frac{\varphi'}{\eta}\right)}} \quad (12)$$

The results obtained from different calculations are shown in Figure 54 and listed in Table 13, for a soil with φ′=25°. In this case, the same analyses were also carried out allowing for tensile stresses, to assess the impact of neglecting tensile failure. It turned out that, for the specific problem, when performing a φ-c reduction with Plaxis 3D, the overestimation of FoS varies from 8 to 14%.

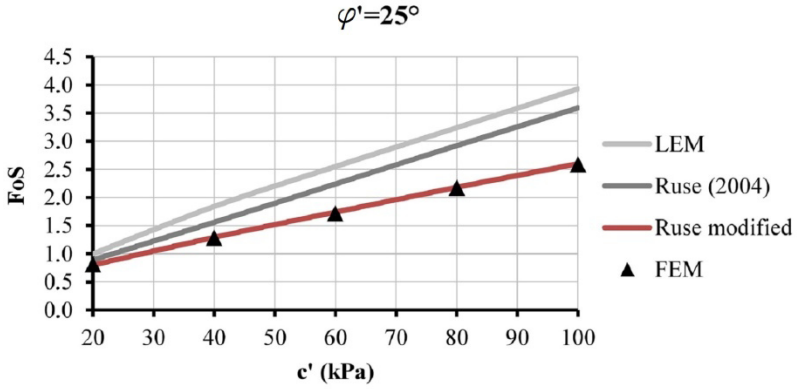

Figure 54. Comparison between the FoS obtained from LEM, Ruse's equation, FEM and equation 12

Table 13. Factors of safety for the case of unreinforced face from different analysis methods (case φ'=25°)

φ'=25°	c'=20	c'=40	c'=60	c'=80	c'=100
LEM (Horn)	1.00	1.84	2.55	3.24	3.93
Ruse (2004)	0.89	1.56	2.24	2.92	3.59
FEM	0.81-0.9*	1.28-1.46*	1.73-1.92*	2.17-2.37*	2.59-2.79*
Ruse modified	0.80	1.29	1.74	2.18	2.60

*tensile stresses allowed

The results of the other analysed cases (φ'=27°-29°) are listed in Table 14 and Table 15.

Table 14. Factors of safety for the case of unreinforced face from different analysis methods (case φ'=27°)

φ'=27°	c'=20	c'=40	c'=60	c'=80	c'=100
LEM (Horn)	1.04	1.88	2.59	3.29	3.99
Ruse (2004)	0.91	1.58	2.26	2.94	3.61
FEM	0.82	1.31	1.75	2.20	2.62
Ruse modified	0.82	1.31	1.76	2.20	2.62

Table 15. Factors of safety for the case of unreinforced face from different analysis methods (case φ'=29°)

φ'=29°	c'=20	c'=40	c'=60	c'=80	c'=100
LEM (Horn)	1.08	1.91	2.64	3.35	4.05
Ruse (2004)	0.93	1.60	2.28	2.96	3.63
FEM	0.86	1.35	1.79	2.25	2.67
Ruse modified	0.84	1.33	1.78	2.22	2.64

Regarding the overestimation of safety factor in LEM calculations, it can be mainly attributed both to the considered failure mechanism and to the hypothesis of maximum shear stresses acting along the prisms surfaces. In fact, in FEM analyses, the tension cut-off causes a drop in shear stresses

when tensile failure is reached. If no tension failure criterion is considered, high cohesion can induce significant tensile stresses, altering the shear stress distribution along a prescribed failure surface. The high deviations between LEM and FEM calculations, due to the tensile failure criterion adopted in the calculation, have been already highlighted by **Tschuchnigg & Schweiger (2015)** for slope stability problems. The magnitude of the deviation is related to the value of soil cohesion and can potentially increase with the slope steepness.
Displacement contours and plastic points obtained from FEM analyses allowing or not for tensile stresses are plotted in Figure 55 and Figure 56 respectively. From this figures, it is possible to notice how the tension failure influences the kinematics of the problem.

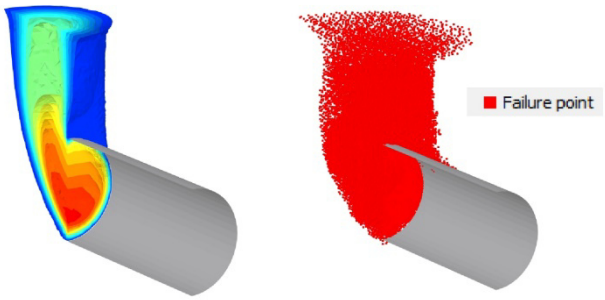

Figure 55. Displacements contours at failure (left) and plastic points (right) for the case φ'=25° and c'=40kPa, tensile stresses allowed

Figure 56. Displacements contours at failure (left) and plastic points (right) for the case φ'=25° and c'=40kPa, tensile stresses not allowed

The same geometry adopted for the analyses with an unreinforced face has been used to assess the impact of structural reinforcements on face stability. Different nails lengths and densities are considered (Table 16). The

properties listed in Table 17 are assigned to the embedded piles used to model the structural elements. Two reinforcement densities are analysed: 0.29 dowels/m^2 and 0.43 dowels/m^2 corresponding to 40 and 60 dowels respectively. The values of nail length adopted in the calculations are based on those commonly used in practice.
In Figure 57, the FoS values for all the different cases considered in the study are shown. The same graph also shows the values calculated using the limit equilibrium method. This method, for the specific case, does not provide different results for different reinforcement lengths because Equation 4 governs the problem and the minimum dimension of the sliding wedge is always smaller than 0.5D (i.e. the lower value of the reinforcement length considered in these calculations). Anyway, for the lower value of soil cohesion adopted in the study (20 kPa) and L=D, the LEM provides FoSs comparable to those obtained from the FEM analyses. However, when shorter dowels are considered, the FoS is overestimated. Concerning the calculations performed with the higher value of soil cohesion (40 kPa) the overestimation is much more significant.

Table 16. Analysed cases for a reinforced excavation face

Reinforced excavation face - analysed cases		
properties		**value**
H	(m)	D
d	(m)	0
Bars number	-	40-60
L	(m)	0.5D-0.7D-D
φ	(°)	25
c	(kPa)	20-40

Table 17. Properties of the fibreglass bars considered in the FEM calculations

Embedded pile elements		
properties		**value**
E	(MPa)	30,00E6
Diameter	(m)	0.1
Skin resistance	-	Linear
$\mathbf{T_{top,max}}$	(kN/m)	31.40
$\mathbf{T_{bot,\ max}}$	(kN/m)	31.40

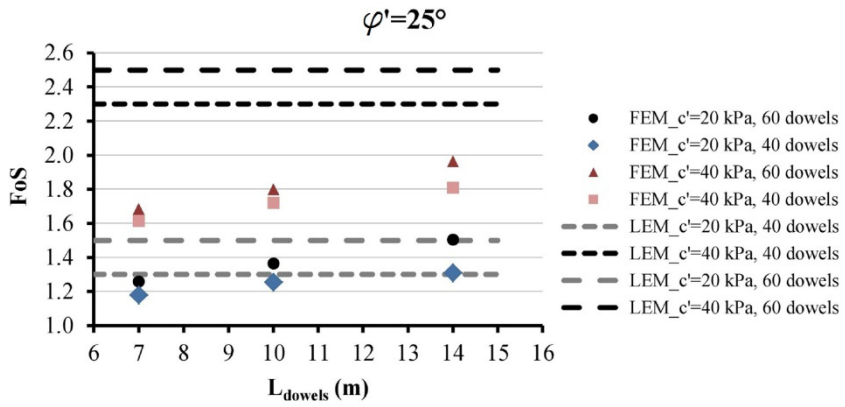

Figure 57. Factors of safety for a reinforced excavation face (comparison between FEM and LEM) according to different reinforcement lengths and densities

When the structural elements are activated the failure mechanism radically changes. While without face reinforcements the instability involves just the tunnel core (Figure 58, a), in the case of reinforced face the failure mechanism is much more extended and characterised by a chimney type shape (Figure 58, b). The skin friction after φ-c reduction is fully mobilised for all the embedded piles but the axial force never exceeded the maximum value the fibreglass bars (around 500 kN) can take. In Figure 58 (c), skin friction and axial force diagrams for a central structural element are shown.

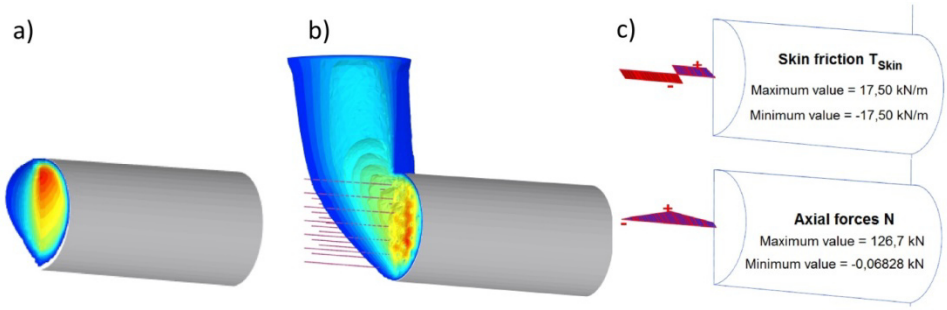

Figure 58. Total displacements plot for an unreinforced (a) and a reinforced face (b), skin friction and axial force on an embedded pile (c) (case c'=40, φ'=25°, L=D, 40 dowels, after φ-c reduction)

Comparing the results from FEM and LEM analyses performed in the present study, it seems clear that LEM overestimates the FoS, especially for

high values of soil cohesion and low values of nails length. The LEM, therefore, cannot always guarantee a safe design. Numerical calculations seem to be the only way to get a reliable estimate of the excavation face stability for a wide range of soil conditions and reinforcement patterns. However, given the high computational effort required when modelling the reinforcements in a FEM calculation, some attempts to simplify the model have been done in the past. **Kavvadas & Prountzopoulos (2009)** provided values of equivalent face pressures, while **Grasso et al. (1989)** suggested calculating an equivalent cohesion for the reinforced zone, leaving the friction angle unchanged:

$$c^* = c' + \frac{\Delta\sigma_3}{2}\tan(45 + \frac{\varphi}{2}) \qquad (13)$$

where $\Delta\sigma_3$ is the average longitudinal confining pressure which can be calculated dividing the force S by the area of the excavation face. The supporting force can be calculated as the minimum value obtained from Equations 3,4 and 5 (§2.3.1).
Using this equation for the specific case study with φ'=25°, it is possible to calculate an increment in the cohesion of around 24 kPa for the lower reinforcement density and 37 kPa for the higher one.
The same evaluation can be made exploiting the curves that provide the FoS for unreinforced excavation faces as a function of cohesion. From Figure 59 it can be seen that the increment of cohesion required to obtain the same safety factor evaluated by modelling the structural elements is not constant. In particular, it varies between 14 and 24 kPa for the higher reinforcement density and between 15 and 22 kPa for the lower one. Therefore Equation 13 always overestimates the increment of cohesion when compared to FEM calculations.

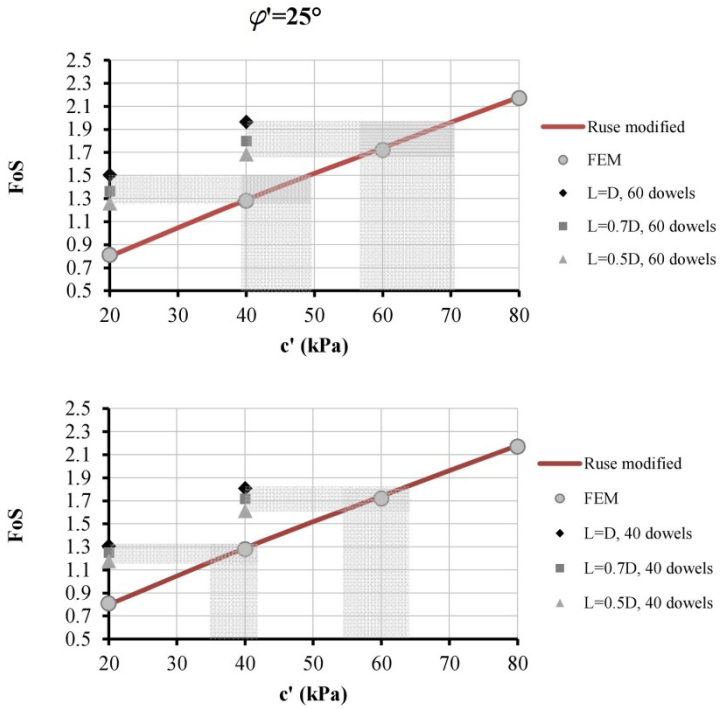

Figure 59. Evaluation of the equivalent soil cohesion necessary to obtain the same safety factor of the calculations including face reinforcements

4.3. Deformation analyses

Previous works concerning the stress-deformation behaviour of reinforced tunnel faces provided a significant contribution to the definition of the optimum length, density and stiffness of the face reinforcement **(Yoo 2002 and Kavvadas & Prountzopoulos 2009)**, where the optimum values are defined as those beyond which no significant improvement in the stress-deformation behaviour is obtained. According to **Kavvadas & Prountzopoulos (2009),** the optimum nail length mainly depends on soil friction angle and less on soil cohesion and density of the nail distribution. According to **Yoo (2002),** both the ratio between overburden and tunnel diameter and the initial stress condition should be taken into account when

analysing the deformation behaviour of a reinforced face. Therefore, since the impact of face reinforcement on deformations changes not only with soil strength and nails characteristics but also according to overburden and initial stress state, it seems difficult to quantify, by using parametric analyses, the effectiveness of soil reinforcement in reducing face extrusion. Only a general assessment of the efficacy of these bars in reducing both extrusion and surface settlement and an optimisation of the reinforcement design are possible, as already shown by many experimental and numerical studies.

In the present work the same model used for the stability analyses (H/D=1, d=0, Mohr-Coulomb soil model) was adopted to analyse face extrusion. A Young's Modulus of 100 MPa was assigned to the excavated soil. An all-in-once excavation with temporary structural elements activation was modelled, meaning that the real excavation sequence is disregarded. Therefore, the aim of these calculations is not to evaluate realistic extrusion values but only the effectiveness of the fibreglass reinforcements in reducing tunnel face deformations. In fact, to accurately evaluate the deformation behaviour of a reinforced excavation face, a larger model and a realistic excavation sequence would be required.

According to the results of this work, the maximum extrusion obtained with face reinforcement can be up to one-half of the one calculated for an unreinforced face (Figure 60, Figure 61). The same effect could be potentially obtained assigning equivalent material properties to the reinforced soil clusters, without modelling the structural elements. For example, an excavation face characterised by c'=40 kPa and reinforced with 40 14m-long dowels presents the same maximum extrusion of an unreinforced face with c'=100 kPa. However, when dealing with deformations, it is not possible to define a general rule to correctly evaluate equivalent properties of the reinforced material, since they would depend not only on the reinforcement density and length but also on the geometry of the specific problem and on the soil characteristics as well as on the constitutive model adopted. Moreover, fibreglass dowels improve both resistance and stiffness of the reinforced material. Thus, to define an equivalent material, both strength and deformation parameters would have to be increased.

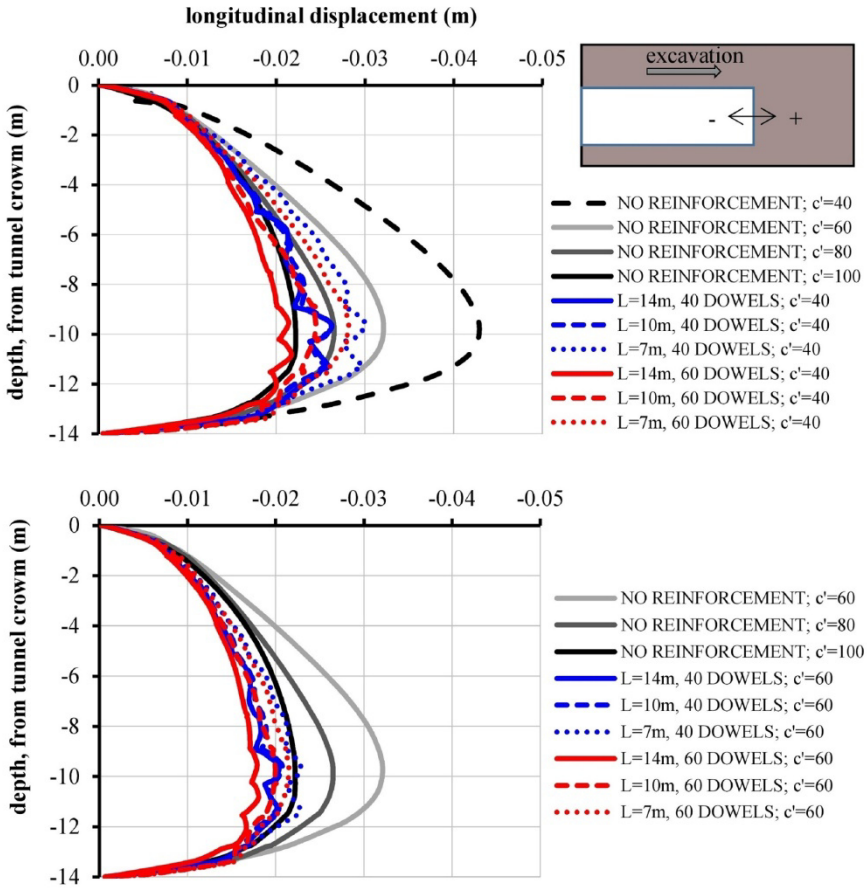

Figure 60. Extrusion profiles for reinforced and unreinforced excavation face; the curves representing reinforced faces refer to the case of φ'=25° and c'=40 kPa (upper graph) or c'=60kPa (lower graph)

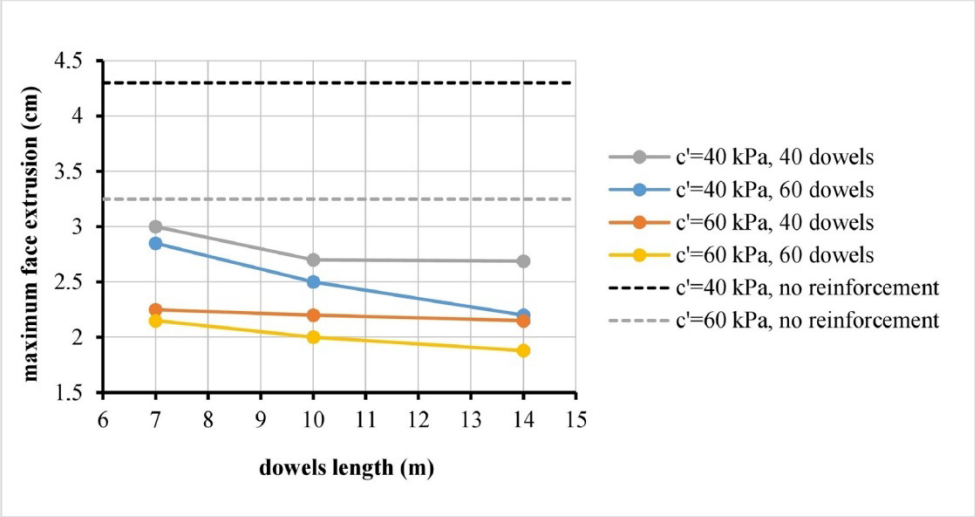

Figure 61. Maximum face extrusion versus dowels length

However, if the goal of the analysis is to assess the beneficial effect of face reinforcement on surface deformations, a simple Mohr-Coulomb failure criterion, does not seem appropriate. In fact, this criterion, especially when dealing with unloading problems and low strain levels, fails in realistically reproducing the soil deformation behaviour. Therefore further calculations aimed at comparing subsidence deformation with and without face reinforcements were performed by modelling the ground with the Hardening Soil Model Small Strain **(Schanz et al. 1999, Benz 2007)**. The material properties assigned to the soil are listed in Table 18. The reinforcement scheme adopted in this calculation is characterised by 40 dowels with L=D. The results show a remarkable reduction in face extrusion as well as in surface settlements (Figure 62, Table 19). In particular, face extrusion shows a reduction of 25% and the maximum surface settlement of 48%. These results prove that controlling the deformations of the advance core is an effective strategy for reducing subsidence phenomena.

Table 18. Material properties for the HSS model.

parameter		value
E_{50}^{ref}	(kN/m^2)	15,000
E_{oed}^{ref}	(kN/m^2)	15,000
E_{ur}^{ref}	(kN/m^2)	45,000
m	(-)	1
p_{ref}	(kN/m^2)	100
ν_{ur}	(-)	0.2
$\gamma_{0.7}$	(-)	0.0002
$G_{0,ref}$	(kN/m^2)	100,000
c'	(kN/m^2)	40
φ'	(°)	25
ψ	(°)	0
R_f	(-)	0,9

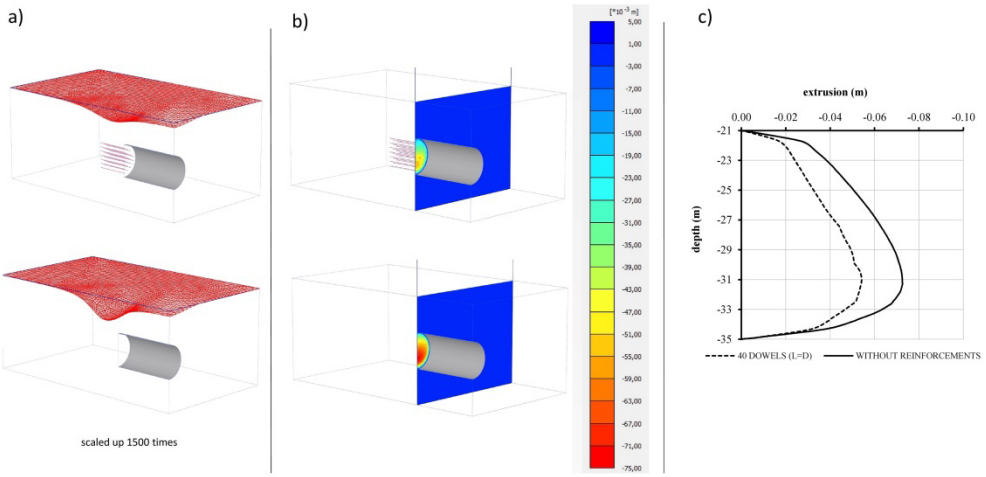

Figure 62. Extrusion and surface settlements for an unreinforced (left and a reinforced excavation face (HSS model)

Table 19. Maximum surface settlements and face extrusion (HSS model)

Face reinforcements	Maximum surface settlement (cm)	Maximum extrusion (cm)
40 dowels (L=D)	3.3	5.4
-	6.3	7.2

4.4. Concluding remarks

In the present study, some numerical and limit equilibrium calculations regarding the stability of both unreinforced and reinforced excavation faces have been presented. The considered range of soil properties covers mainly soils characterised by a silty-clayey matrix. Only drained behaviour has been taken into account.

Previous works carried out through numerical analysis concerned mainly the face deformation behaviour. The few works concerning face stability were limited to preliminary studies or specific case studies. The systematic analyses shown in the present paper, covering both different material properties and reinforcement configurations, provided a further contribution to the topic of face stability analysis and face reinforcement design. This kind of calculation is necessary to evaluate the tunnel face behaviour not only in working conditions but also with respect to the ultimate limit state of face collapse.

The calculations concerning unreinforced faces showed that the basic formulation of the LEM method, adopting the Horn mechanism, may significantly overestimate safety factors. From the results of the numerical calculations performed with Plaxis 3D, an analytical formulation of the safety factor has been derived by modifying the equation proposed by **Ruse (2004)**. Also the calculations regarding reinforced excavation faces showed that the LEM method overestimates face stability, except for the case of low cohesion and high overlapping length of the bars.

The 3D numerical analyses carried out by modelling the structural elements allowed for an estimation of the increase in the factor of safety which can be gained with this technique. Two different soil types, as well as different nail lengths and densities, have been analysed. For the cases considered in the present study, the increase in FoS calculated with FEM analyses varies

between 0.4 and 0.7. An evaluation of the equivalent cohesion needed to obtain the same FoS, without directly modelling the structural elements, is also shown. In particular, the necessary increment of cohesion varies from 14 to 24 kPa, from the lower to the higher values of nail length and density. Not only for assessing limit conditions but also for analysing working conditions, equivalent material properties could be evaluated. These would allow an important simplification in the numerical simulation of reinforced faces, avoiding an excessive computational effort. However, especially when the deformation behaviour is considered, the equivalent soil properties would depend on many different factors like initial stress state, problem geometry, overburden and soil constitutive model adopted, making general assumptions quite difficult. Nevertheless, FEM analyses including face reinforcements showed the effectiveness of this technique in reducing both extrusion and surface settlements.

Given a Eurocodes-based design, since the different methods to assess face stability (i.e., LEM and FEM) are characterised by different accuracy levels and margins of safety, the application of different partial factors could be discussed. Anyway, being the ground the main element providing resistance (GEO-type limit state), an approach requiring partial factors on material strength would be recommended, although not explicitly stated in EN 1997-1.

Whether the density and length of these elements should be evaluated according to face stability or according to a criterion based on minimizing deformations depends on the specific case. For underground excavations in urban areas, it is extremely important to minimise subsidence phenomena. Therefore the check of serviceability limit states is likely to govern the reinforcement design.

Chapter 5.
Case study: introduction and parameter calibration

The case study presented in this thesis deals with the construction works of twin tube shallow tunnels, excavated in a stiff and fine-grained deposit. The work initially focuses on the soil parameters calibration against experimental data which, together with the choice of an appropriate constitutive model, plays a major role in the assessment of tunnelling induced deformations.

The simulation relies on a preliminary calibration of the parameters of the soil constitutive model against laboratory tests.

The calibration is presented in this chapter, whereas the numerical results are presented in the following one, where FEM calculations are compared with monitoring data of displacements and deformations during the excavation.

The importance of assessing the deformation behaviour in case of twin tunnels excavation lies in the fact that quite often, due to design constraints it is not possible to place the tunnels at such a distance that they do not influence each other. Furthermore, in an urban environment, it is likely that new tunnels have to be built in the proximity of existing ones.

Since two-dimensional analyses, in order to to take into account the effect of the 3D excavation, imply some initial assumptions, three-dimensional finite element analyses have been preferred. Comparisons between monitoring data and results of numerical simulations are provided. The available field data include displacements and deformation measurements regarding both the soil and the tunnel lining.

The tunnels analysed in this study were excavated during the construction works of a new dual carriage highway in Southern Italy, close to the Ionian coast. This infrastructure is an upgrade of the existing S.S.106 Jonica national road. The considered stretch goes from Marina di Gioiosa Jonica to Ardore, and it is 11 km long. It includes five twin tube tunnels (Gerace, Trigoni, Timpa, Pergola and Limbia) for a total underground excavation length of 5 km. The equivalent diameter of the tunnels is around 13-14 m.

The location, the geology of the area and the road longitudinal profile are shown in Figure 63.

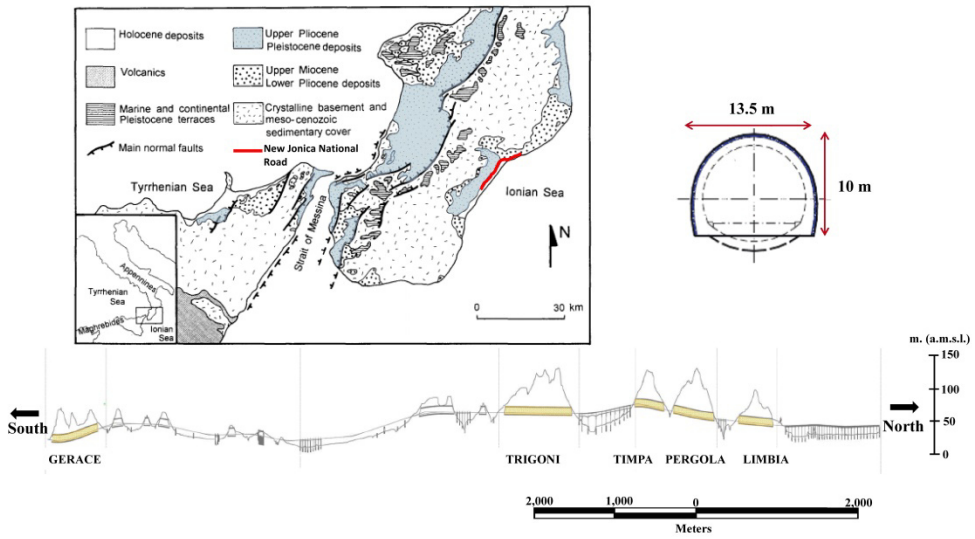

Figure 63. Geological map of the area (modified from Monaco et al., 1996), tunnel dimensions and road longitudinal profile (natural tunnels in yellow)

The underground openings are mainly located in the Trubi formation, a Pliocene fine-grained slightly overconsolidated deposit. The plasticity index of this formation varies between 20 and 40 and the clay fraction between 40 and 60. In some cases, the sandy fraction grows up to 30-40%.
Some grain size distribution curves and the Casagrande plasticity chart are shown in Figure 64 and Figure 65 respectively.
The rhythmic alternation of dark and pale grey layers observed during the construction, due to a variation in the carbonate content, does not seem to affect the mechanical properties **(Segato et al. 2015).** This alternation can be clearly seen from the excavation surveys presented in Figure 66. Some of these surveys also show the presence of discontinuity systems (Figure 66, b and c) or a higher sandy fraction (Figure 66, h). In most cases, the excavation face appeared to be dry and did not show any water inflows.

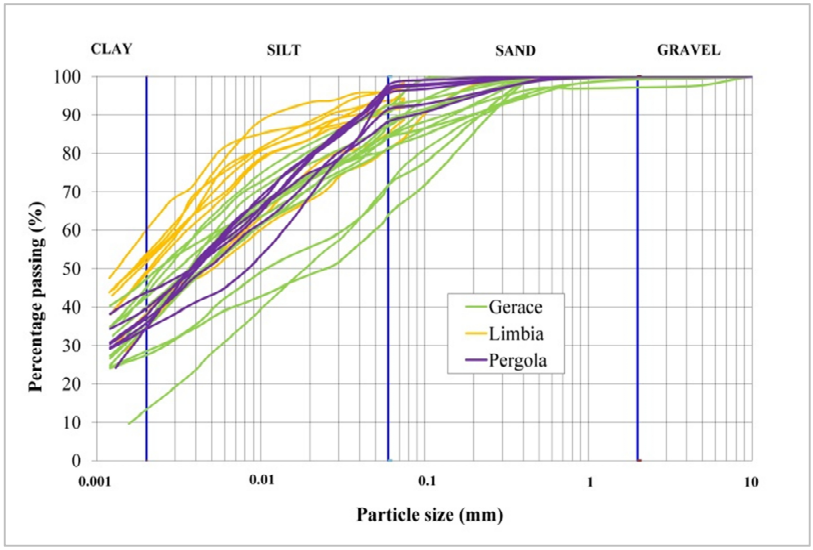

Figure 64. Grain size distribution curves

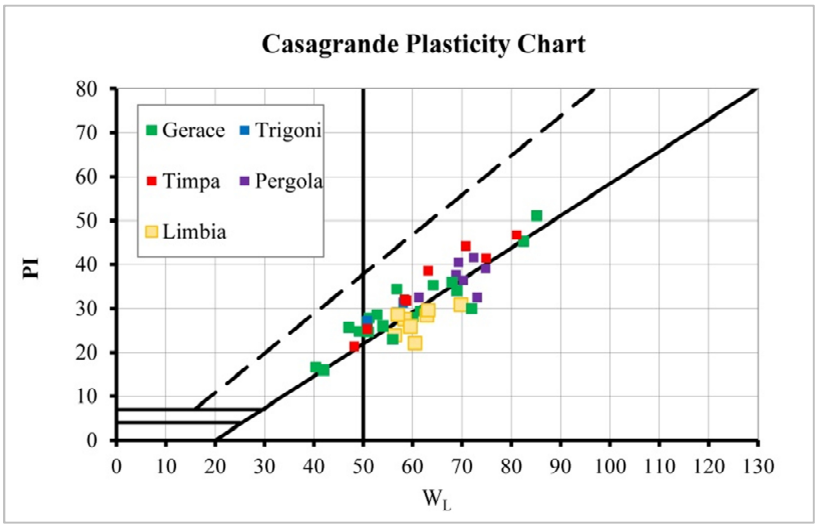

Figure 65. Casagrande plasticity chart

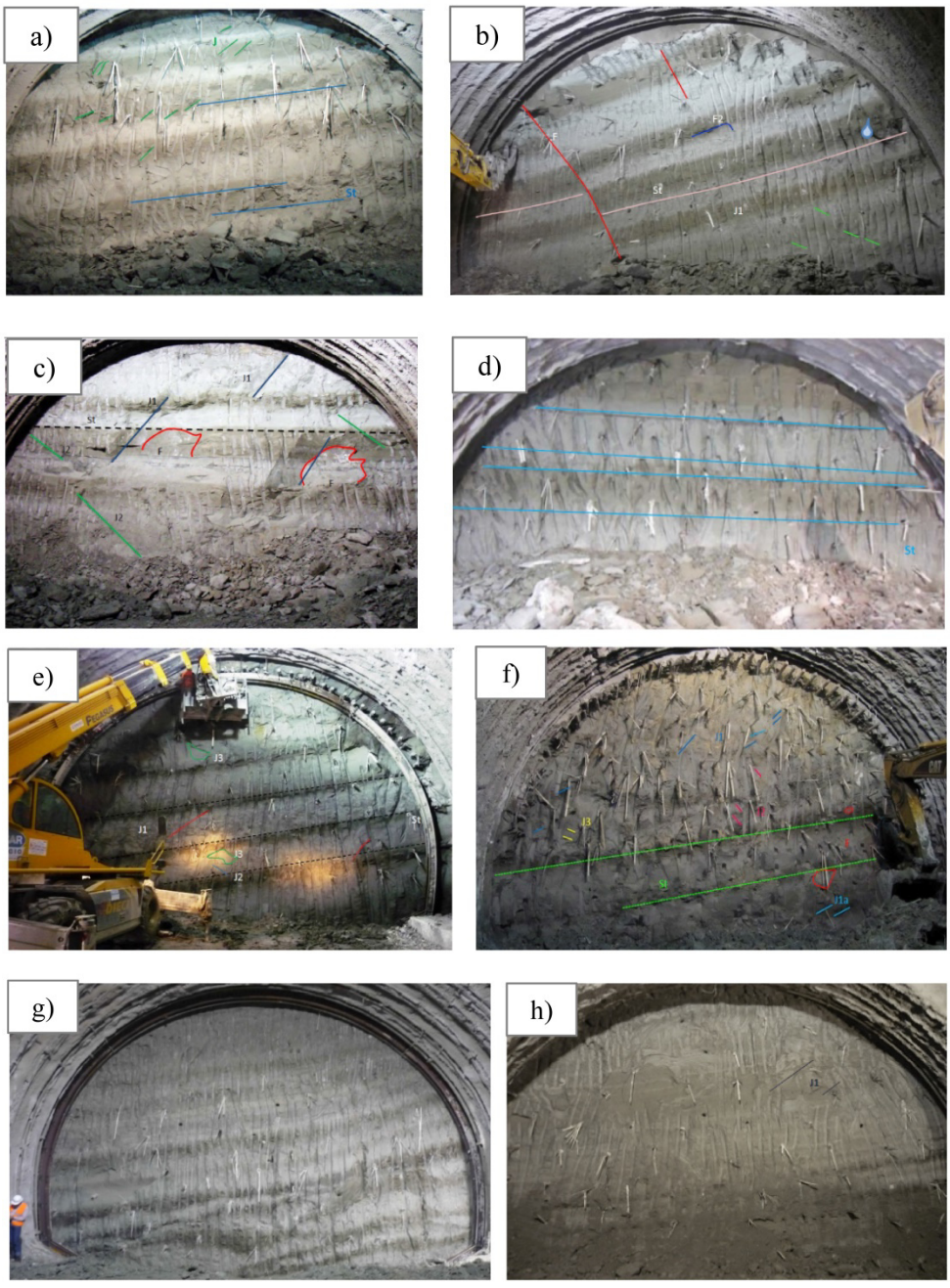

Figure 66. Tunnel face surveys (courtesy of Dott. Pasqualino Notaro).

The tunnels were excavated according to the ADECO method **(Lunardi 2008).** The excavation was carried out full face, supporting the cavity with an open arch made of coupled steel sets and a 20-30 cm thick shotcrete layer. The open ring was closed with cast-in-place sidewalls and invert at a few diameters from the tunnel face. The final concrete lining was cast at a much greater distance. A schematic representation of the tunnel support is provided in Figure 67.

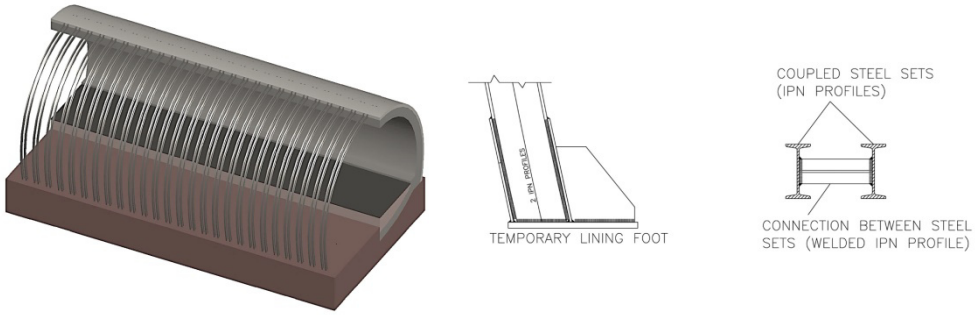

Figure 67. Three-dimensional scheme of temporary and final lining (left); details of the temporary support (right)

In order to reinforce and improve the stability of the excavation face, in some cases, fibreglass reinforcements and drainage pipes were installed before advancing. By lowering the water level in the proximity of the excavation, the shear strength is increased and the lining pressures reduced. Anyway, the water level, during the geological investigation, was found to be located, most of the times, below the tunnel axis.
By using face bolts, extrusion is limited and face instability is prevented.
While excavating, no significant water inflow occurred, probably due to the predominant fine-grained nature of the deposit, to the use of drainage pipes while advancing and to the low initial water level. The tunnel itself in the long term also has a draining effect thanks to the membrane placed in between the preliminary and the final lining, consisting of drainage panels and a PVC sheath. The drained water is collected laterally using slotted PVC tubes embedded in the sidewalls and connected to a central drainage pipe. A scheme of the drainage system during and after construction is provided in Figure 68.

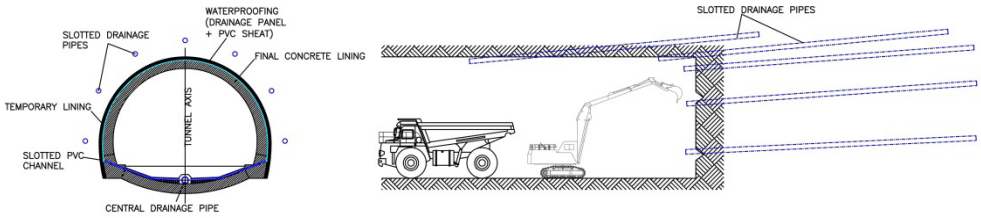

Figure 68. Drainage system and umbrellas of drainage pipes

5.1. Calibration of the HSS model

The geotechnical characterization and the parameter calibration were carried out exploiting all the laboratory and in situ tests involving the Trubi formation. The mechanical behaviour of the upper layer, belonging to the Monte Narbone Formation, is not described in detail because its thickness is not significant in the sections that will be considered. In fact, the properties of the first 5-10 m of soil have little influence on the overall response of the deposit to the tunnel excavation, at least for overburden of 2-3D.

The Hardening Soil Model with Small Strain Stiffness **(Schanz et al. 1999, Benz 2007)** was chosen for modelling both layers. This choice is based on the possibility to define soil stiffness according to the stress path (loading and unloading, compression and deviatoric), stress level and deformation level. Moreover, despite the considerable number of soil parameters required to define the constitutive model, they have a precise physical meaning and can be determined through common laboratory and in situ tests.

The HSS model is currently implemented in the numerical code Plaxis, and it is defined in terms of effective stresses and therefore requires both effective stiffness parameters and effective strength parameters. The model involves 12 input parameters:

- three stiffness moduli defined at the reference pressure p^{ref} (E_{50}^{ref}, which governs the plastic straining due to primary deviatoric loading, E_{oed}^{ref}, which controls the plastic straining due to primary compression and E_{ur}^{ref}, which represents an elastic unloading-reloading stiffness);
- the exponent *m*, governing the stress dependency of stiffness;
- ν_{ur} or unloading-reloading Poisson's ratio;

- the Mohr-Coulomb strength parameters (c' and ϕ') and the dilatancy angle ψ;
- k_0^{nc}, coefficient of earth pressure at rest in primary one-dimensional compression;
- the failure ratio R_f;
- G_0^{ref} or stiffness at very small strain and $\gamma_{0.7}$ or shear strain at which G drops to $0.7G_0$.

For more details about the model, the reader is referred to Appendix A.
All the laboratory tests used for the calibration in the present study were carried out at Marche Polytechnic University, in Italy.
The strength properties of the mainly fine-grained soil layer have been defined through isotropically consolidated drained triaxial tests. The average effective strength envelope, shown in Figure 69, is characterised by c'=90 kPa and φ′=25°. The high values of effective cohesion are mainly due to the marly component of the deposit.

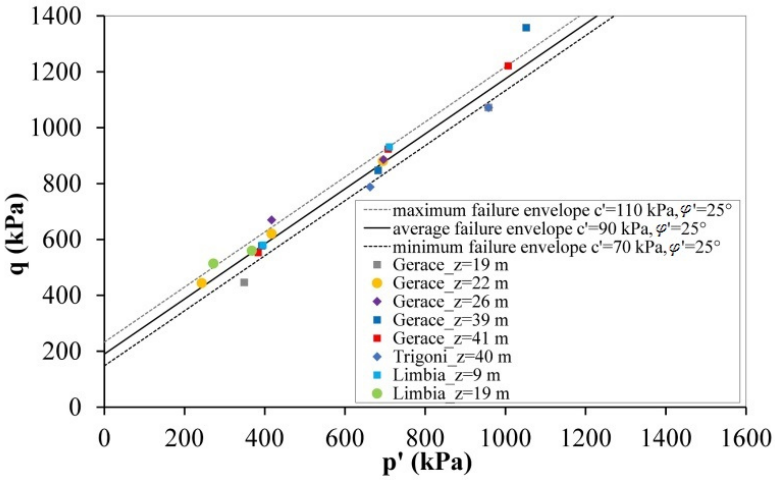

Figure 69. Failure envelope from drained triaxial tests on the invariants plane

Regarding the soil deformability, **Soos & Bohac (2001)** suggested some reference values for the stiffness properties according to soil type. In Table 20, the values regarding fine-grained normally consolidated soils and sandy soils are listed. The stiffnesses refer to a reference pressure of 100 kPa**. Ohde (1939)** suggested m≈1 for fine-grained soils and m=0.5-0.7 for coarse-grained soils. These values can be used as reference values to

identify a range of variability for the expected behaviour of soils according to their grain size distribution and plasticity.

Table 20. Suggested soil parameters according to soil type and plasticity (after Soos, 2001)

Soil type	W_l (%)	W_p (%)	I_p (%)	E^{ref} (Mpa) $E = E^{ref} \cdot \left(\frac{p}{p_{at}}\right)^{w_e}$	m (-)
low plasticity silt	25	21	4	4	0.8
	35	28	11	11	0.6
medium to high plasticity silt	35	22	7	3	0.9
	20	25	25	7	0.7
low plasticity clay	28	15	7	2	1
	14	25	16	5	0.9
medium plasticity clay	38	18	16	1	1
	18	25	28	3	0.85
high plasticity clay	55	20	33	0.6	1
	20	35	55	2	1
uniform fine sand	-	-	-	15	0.75
				30	0.60
uniform coarse sand	-	-	-	25	0.7
				70	0.55
well graded sand and gravelly sand	-	-	-	20	0.7
				60	0.55
silty sand	20	16	4	15	0.8
	45	25	25	50	0.65

In the present case study, the required deformation parameters have been further evaluated using both laboratory (mainly triaxial and oedometric tests) and in situ tests (Menard pressuremeter tests). The latter enabled a soil mass characterization at a larger scale. All these tests can be considered as ordinary, meaning that they are commonly used in practice to investigate the soil mass behaviour in case of underground construction.

Regarding primary loading stress paths, the HSS model treats one-dimensional compression and deviatoric loading separately and therefore it requires different reference stiffnesses (i.e. E_{50}^{ref} and E_{oed}^{ref}). Unloading stress paths are associated with a higher stiffness, namely E_{ur}, which describes the elastic deformation behaviour inside the yield surface.

Mathematically, the soil stress dependency is dealt with through the following equations:

$$E_{50} = E_{50}^{ref} \left(\frac{\sigma'_3 + c \cdot \cot\varphi}{\sigma_{ref} + c \cdot \cot\varphi} \right)^m \qquad (14)$$

$$E_{oed} = E_{oed}^{ref} \left(\frac{\sigma'_1 + c \cdot \cot \varphi}{\sigma_{ref} + c \cdot \cot \varphi} \right)^m \quad (15)$$

$$E_{ur} = E_{ur}^{ref} \left(\frac{\sigma'_3 + c \cdot \cot \varphi}{\sigma_{ref} + c \cdot \cot \varphi} \right)^m \quad (16)$$

In Figure 70, the triaxial moduli at 50% of failure deviatoric stress and the oedometric moduli are plotted against the corresponding normalised minor and major effective stresses respectively. The normalisation involves the reference pressure and the strength properties. This logarithmic representation of the laboratory results allows to determine representative values of the reference moduli as well as to define the stress dependency factor whereas, the strength properties derived from the minimum failure envelope have been assumed here (c'=70 kPa and φ′=25°).

The average y-intercepts are around 9.3 and 9, for triaxial and oedometric tests respectively. These values give an E_{50}^{ref} of 11,000 and an E_{oed}^{ref} of around 8,000 kPa. Regarding the stress dependency, m=0.8 seems to provide a good match for both triaxial and oedometric moduli.

The unloading-reloading modulus E_{ur} cannot be plotted in the case of oedometric tests as a function of the minor principal stress σ_3 (Equation 16), being the stress path not know apriori during the test, unlike triaxial tests. Unfortunately, the available triaxial tests did not involve unloading stress paths. Nevertheless, by simulating oedometric tests and CRS tests, E_{ur}^{ref} was found to vary from 45,000 to 70,000 kPa.

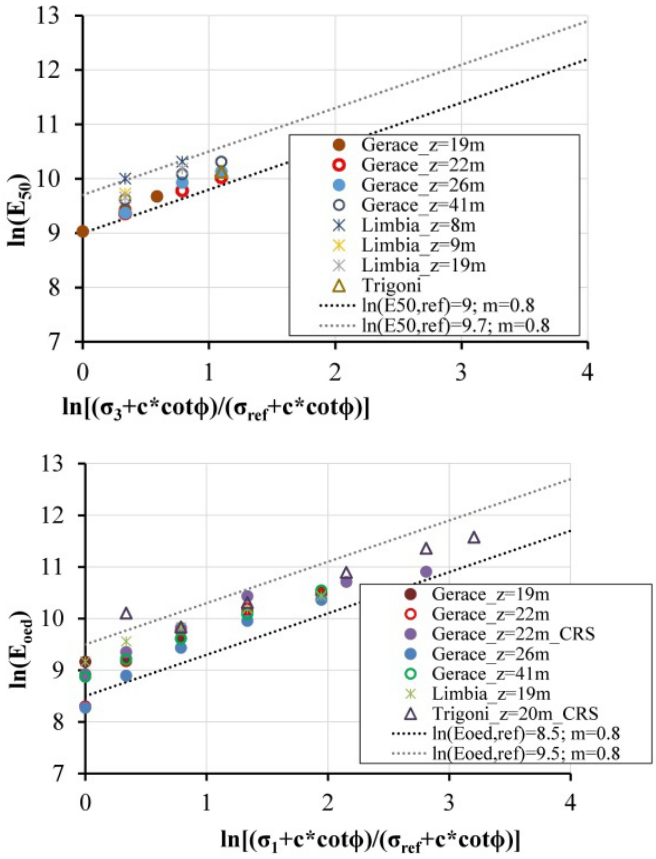

Figure 70. Determination of $E_{50,ref}$, $E_{oed,ref}$ and stress dependency of the two moduli

Further information on the soil deformation behaviour can be derived from pressuremeter tests. Being the data quite scattered, they were just used for a comparison with the stiffness profiles computed according to the chosen constitutive model. Assuming $E_{50}^{ref} = E_{oed}^{ref} = 11{,}000$ and $E_{ur}^{ref} = 45{,}000$ kPa, it is possible to plot the three stiffness profiles with depth, according to equations 14, 15, 16 and valid for initial stress conditions. The so calculated curves are superimposed to the pressuremeter moduli in Figure 71. Most of the pressuremeter loading moduli fall between the E_{ur}^{ref} and the E_{oed}^{ref} curve. Unloading moduli are too scattered to define a clear trend.

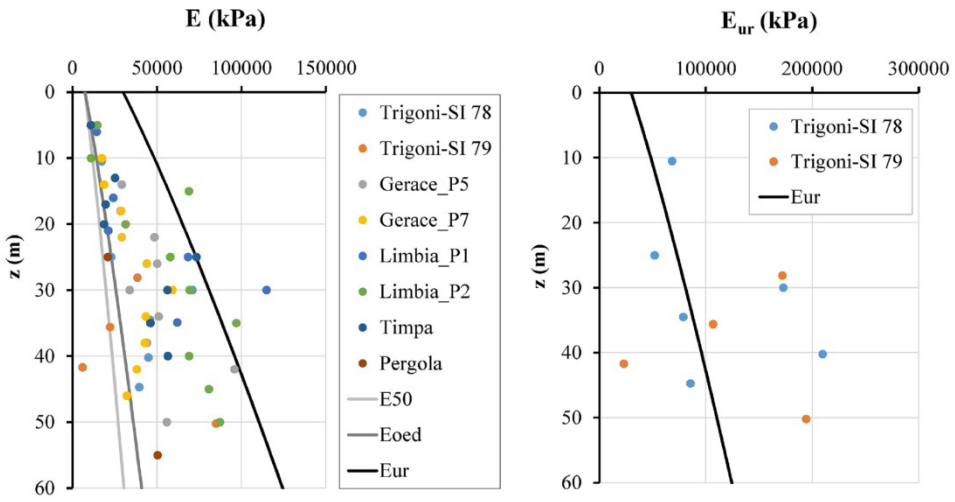

Figure 71. Deformability from pressuremeter tests carried out in the Trubi formation

The Ménard modulus should be theoretically corrected by applying the rheological factor, to partially take into account the soil disturbance and derive the elastic modulus. However, for overconsolidated silts and clays, this factor can be assumed close to 1.

Besides the deformability of the deposit, the pressuremeter test can also give qualitative information on the initial stress state. Different methods can be used to obtain the initial horizontal stress from a pressuremeter curve. However, it should be kept in mind that this value, in the case of Menard pressuremeter, can be strongly affected by the disturbance induced in the soil by digging the borehole. In this case, it was calculated considering the initial point of the straight line **(Baguelin 1978)**. In Figure 72, it can be seen that both k_0 and OCR decrease with depth. These features are typical of soils overconsolidated due to the removal of overburden. Therefore, assuming a constant value of POP, instead of a constant value of OCR, seems to be consistent with the investigation results. The overconsolidation ratio of the deposit was also estimated through oedometric tests and CRS tests which provided values between 1 and 4, in agreement with the pressuremeter tests. The oedometric tests provided lower OCR values when compared to CRS tests. This can be due to the fact that the oedometer, reaching lower vertical stresses, may not be able to catch a significant variation of curve slope in correspondence of the pre-consolidation pressure.

Considering the specific case, assuming POP=300 kPa and k_0=0.7 seems to be appropriate, especially for overburden varying between 20 and 40 m.

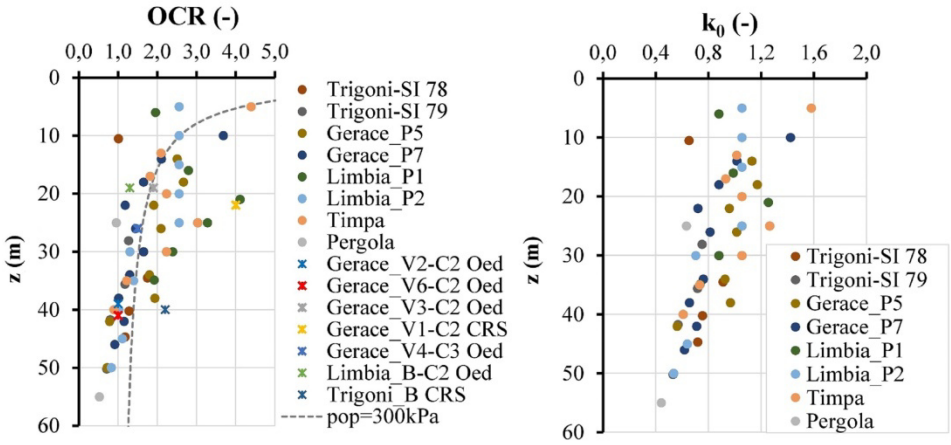

Figure 72. Initial stress state from pressuremeter tests: OCR on the left and k_0 on the right (from pressuremeter, CRS and Oedometric tests)

Besides defining the average values of soil properties and combining all information coming from different tests, each test can be individually simulated. In Figure 73, Figure 74, Figure 75, Figure 76, Figure 77, Figure 78, Figure 79, Figure 80, Figure 81, Figure 82, Figure 83, Figure 84, Figure 85 and Figure 86, some examples of parameter calibration by direct simulation of triaxial, oedometric and CRS test is shown. The tables included in the pictures provide the model parameters used for each calibration and in particular only those that have an actual influence on the corresponding test curves. In some cases (e.g., Figure 82) more sets of parameters provided a good match. Slightly different model parameters were necessary to fit the curves obtained from the different laboratory tests and subsequently some engineering judgement was necessary to choose a parameter set for the numerical simulations.

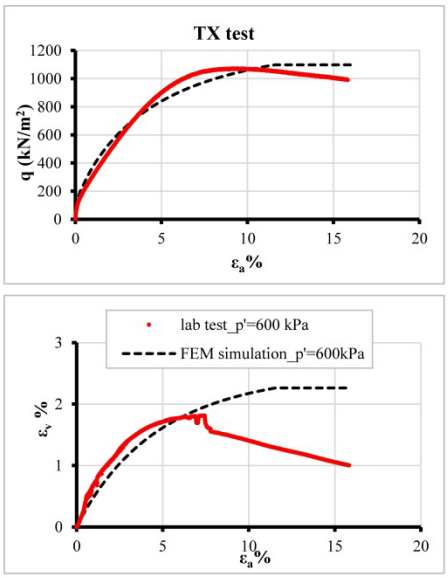

E_{50}^{ref}	kPa	11,000
E_{oed}^{ref}	kPa	11,000
m	-	0.8
c'	kPa	70
ϕ'	°	25
ψ	°	0
R_f	-	0.8

Figure 73. Calibration of the HSS parameters through the simulation of a triaxial test (Trigoni, z=40 m)

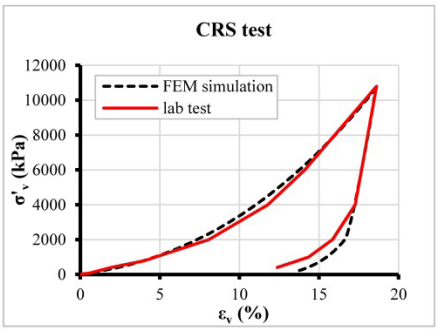

E_{50}^{ref}	kPa	12,000
E_{oed}^{ref}	kPa	12,000
$E_{ur,}^{ref}$	kPa	70,000
m	-	0.6
v'_{ur}	-	0.2
c'	kPa	70
ϕ'	°	25
ψ	°	0
R_f	-	0.8

Figure 74. Calibration of the HSS parameters through the simulation of a CRS test (Trigoni, z=40 m)

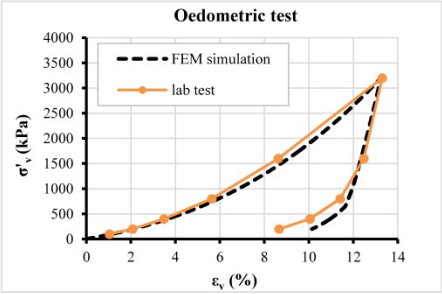

E_{50}^{ref}	kPa	8,000
E_{oed}^{ref}	kPa	7,500
$E_{ur,}^{ref}$	kPa	40,000
m	-	0.7
v'_{ur}	-	0.2
c'	kPa	70
ϕ'	°	25
ψ	°	0
R_f	-	0.8

Figure 75. Calibration of the HSS parameters through the simulation of an oedometric test (Limbia, z=19 m)

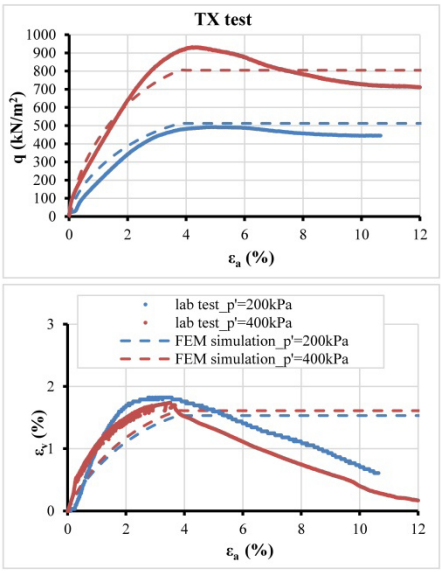

E_{50}^{ref}	kPa	30,000
E_{oed}^{ref}	kPa	15,000
m	-	0.8
c'	kPa	70
ϕ'	°	25
ψ	°	0
R_f	-	0.8

Figure 76. Calibration of the HSS parameters through the simulation of a triaxial test (Limbia, z=19 m)

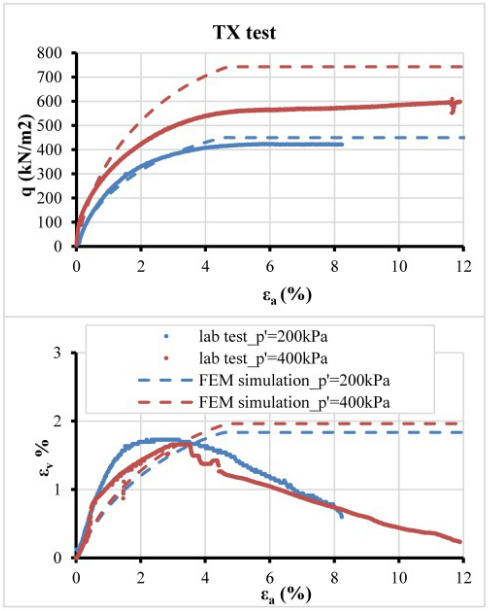

E_{50}^{ref}	kPa	20,000
E_{oed}^{ref}	kPa	10,000
m	-	0.8
c'	kPa	50
ϕ'	°	25
ψ	°	0
R_f	-	0.8

Figure 77. Calibration of the HSS parameters through the simulation of a triaxial test (Limbia, z=8.5 m)

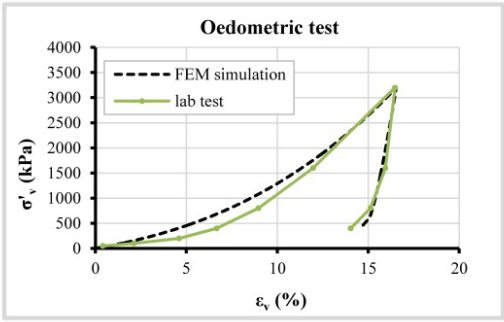

E_{50}^{ref}	kPa	8,000
E_{oed}^{ref}	kPa	6,000
$E_{ur,}^{ref}$	kPa	45,000
m	-	0.7
v'_{ur}	-	0.2
c'	kPa	70
ϕ'	°	25
ψ	°	0
R_f	-	0.8

Figure 78. Calibration of the HSS parameters through the simulation of an oedometric test (Gerace, z=22 m)

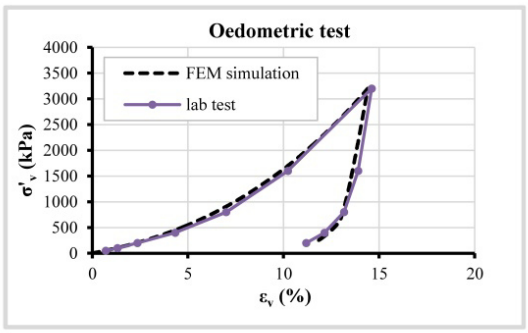

E_{50}^{ref}	kPa	8,000
E_{oed}^{ref}	kPa	6,800
$E_{ur,}^{ref}$	kPa	45,000
m	-	0.7
ν'_{ur}	-	0.2
c'	kPa	70
ϕ'	°	25
ψ	°	0
R_f	-	0.8

Figure 79. Calibration of the HSS parameters through the simulation of an oedometric test (Gerace, z=19 m)

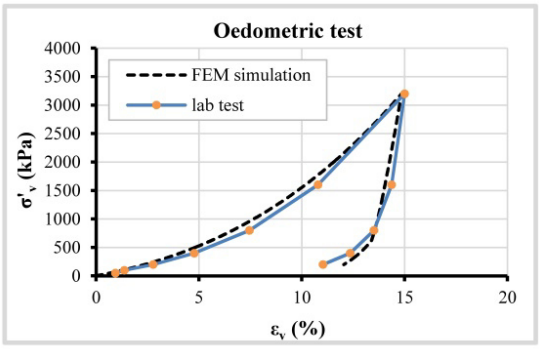

E_{50}^{ref}	kPa	8,000
E_{oed}^{ref}	kPa	6,600
$E_{ur,}^{ref}$	kPa	45,000
m	-	0.7
ν'_{ur}	-	0.2
c'	kPa	70
ϕ'	°	25
ψ	°	0
R_f	-	0.8

Figure 80. Calibration of the HSS parameters through the simulation of an oedometric test (Gerace, z=41 m)

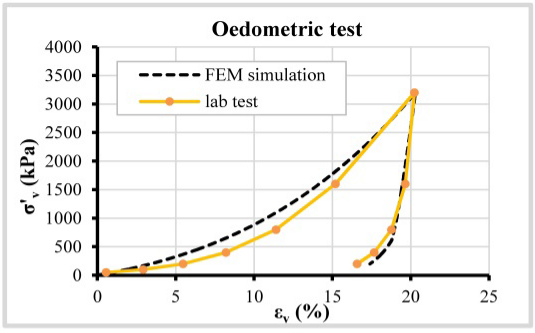

E_{50}^{ref}	kPa	8,000
E_{oed}^{ref}	kPa	4,500
$E_{ur,}^{ref}$	kPa	40,000
m	-	0.75
ν'_{ur}	-	0.2
c'	kPa	70
ϕ'	°	25
ψ	°	0
R_f	-	0.8

Figure 81. Calibration of the HSS parameters through the simulation of an oedometric test (Gerace, z=26 m)

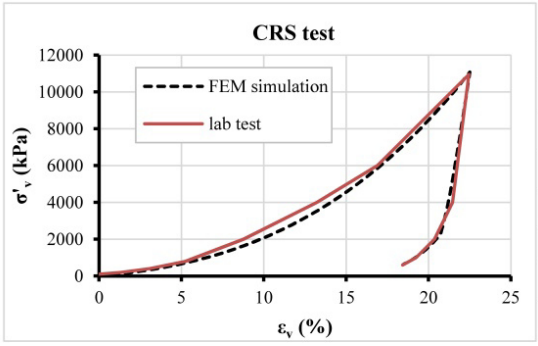

E_{50}^{ref}	kPa	8,000
E_{oed}^{ref}	kPa	7,900
$E_{ur,}^{ref}$	kPa	55,000
m	-	0.7
ν'_{ur}	-	0.2
c'	kPa	70
ϕ'	°	25
ψ	°	0
R_f	-	0.8

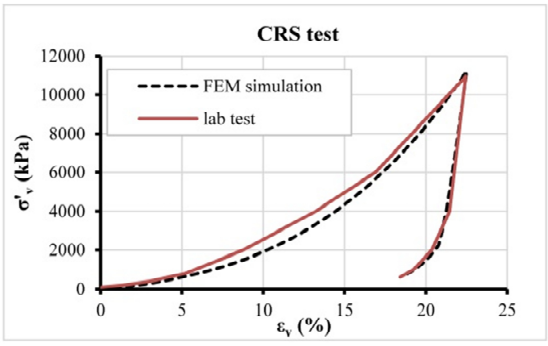

E_{50}^{ref}	kPa	9,000
E_{oed}^{ref}	kPa	7,100
$E_{ur,}^{ref}$	kPa	55,000
m	-	0.75
ν'_{ur}	-	0.2
c'	kPa	70
ϕ'	°	25
ψ	°	0
R_f	-	0.8

Figure 82. Calibration of the HSS parameters through the simulation of a CRS test (Gerace, z=22 m)

In the case of Gerace oedometric tests, a further calibration attempt was made by superposing all the sperimental curves and making the last loading

points coincide.

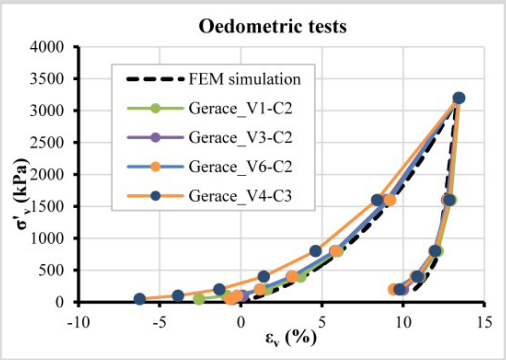

E_{50}^{ref}	kPa	8,000
E_{oed}^{ref}	kPa	7,000
$E_{ur,}^{ref}$	kPa	45,000
m	-	0.75
ν'_{ur}	-	0.2
c'	kPa	70
ϕ'	°	25
ψ	°	0
R_f	-	0.8

Figure 83. Calibration of the HSS parameters through the simulation of oedometric tests (Gerace)

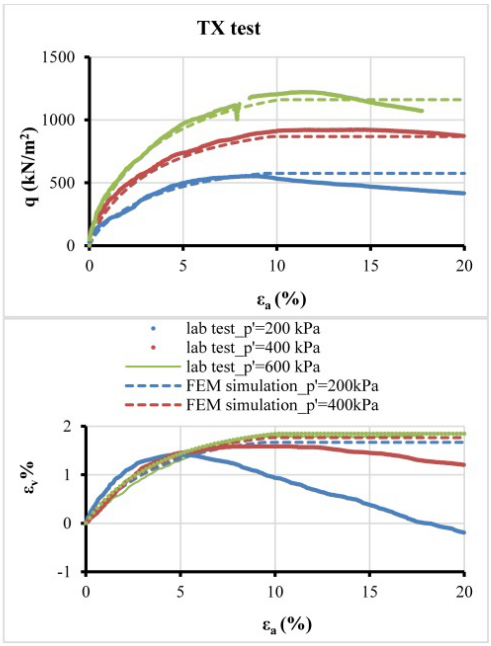

E_{50}^{ref}	kPa	30,000
E_{oed}^{ref}	kPa	15,000
m	-	0.8
c'	kPa	70
ϕ'	°	25
ψ	°	0
R_f	-	0.8

Figure 84. Calibration of the HSS parameters through the simulation of a triaxial test (Limbia, z=41 m)

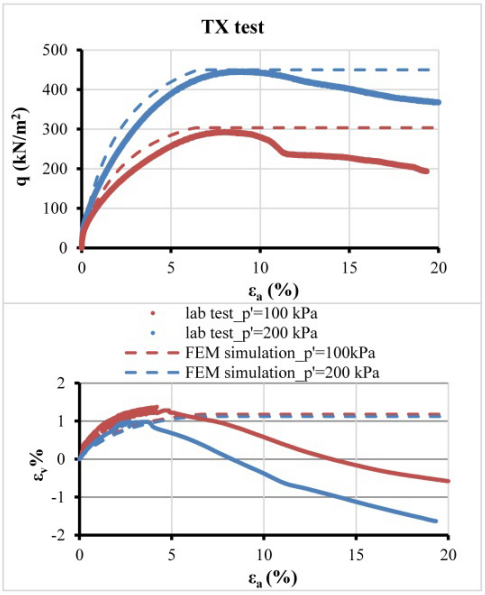

E_{50}^{ref}	kPa	15,000
E_{oed}^{ref}	kPa	15,000
m	-	0.8
c'	kPa	50
ϕ'	°	25
ψ	°	0
R_f	-	0.8

Figure 85. Calibration of the HSS parameters through the simulation of a triaxial test (Gerace, z=19 m)

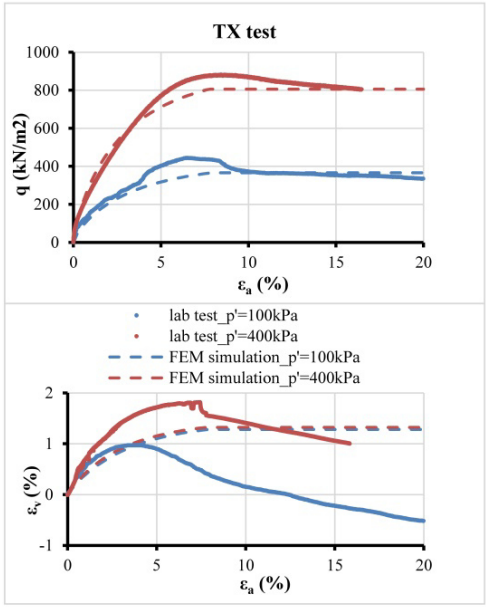

E_{50}^{ref}	kPa	15,000
E_{oed}^{ref}	kPa	15,000
m	-	0.8
c'	kPa	90
ϕ'	°	25
ψ	°	0
R_f	-	0.8

Figure 86. Calibration of the HSS parameters through the simulation of a triaxial test (Gerace, z=22 m)

The same curve fitting can be carried out for a pressuremeter test. In this paper, some of the tests involving both loading and unloading paths and the corresponding curve-fitting trials are presented. Pressuremeter tests were simulated by running drained axis-symmetric analyses with Plaxis 2D 2015 **(Brinkgreve et al. 2015)**.

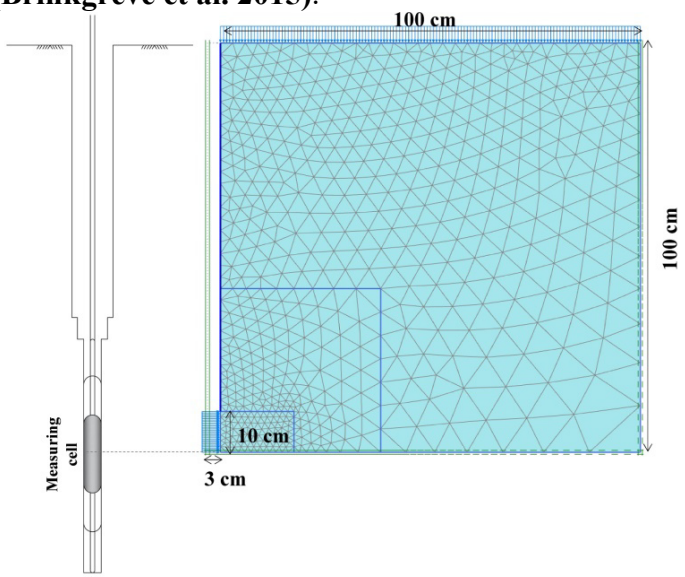

Figure 87. FEM model for the pressuremeter test simulation

The calculation model is represented in Figure 87. The simulations were carried out in 5 phases. After an initial phase, the overconsolidation was imposed by applying a surface load equal to the vertical effective stress plus the pre-overburden pressure (Phase 1) and by subsequently removing the POP (Phase 2). In the same phase, the borehole excavation was simulated and a horizontal pressure equal to the horizontal at rest pressure applied. Phase 3, 4 and 5 are initial loading, unloading and final loading respectively. These phases were simulated by increasing or decreasing the horizontal pressure. The curve refers to the mean radial displacement of the vertical boundary where the horizontal load is applied. The analyses were run by using the updated mesh option, which allows taking into account large deformations.

Empirical curves have been shifted to the left so that the origin of the x-axis coincide with the assumed horizontal earth pressure. In this way Phase 1 of the classis pressuremeter curve (Figure 88, left) disappears from the graph. Two different sets of deformability parameters within the variability range

detected through laboratory tests as well as two different POP values have been adopted to match the experimental curves.
In MPM tests, the shape of the experimental curve is highly influenced by the disturbance induced by the borehole (Figure 88, right). Because of this unavoidable disturbance, the true elastic strains cannot be measured during the test, but only pseudo-elastic strains can be measured instead. High degrees of disturbance can make the test not usable for evaluating soil mechanical properties. For example, when the borehole is oversized or too small the experimental curve shows a very different shape when compared to the ideal one.

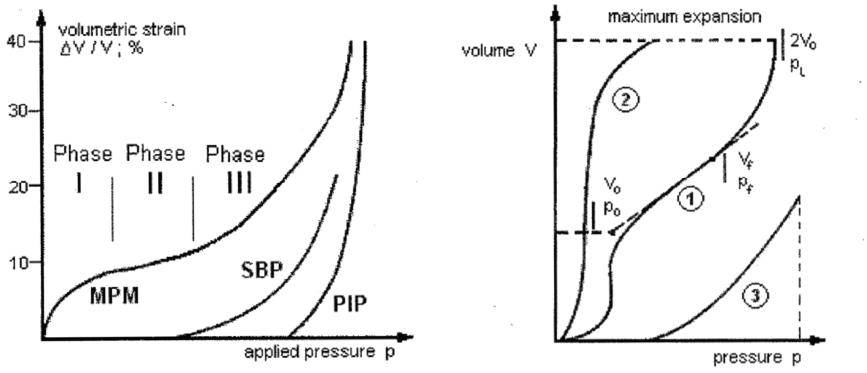

Figure 88. Typical pressuremeter curves on the left, from Clarke (1994) (MPM: Ménard Pressuremeter test, SBP: Self-Bored pressuremeter, PIP: Pushed-In Pressuremeter). Influence of the soil disturbance on the shape of the pressuremeter curves (right, from S. Amar, B.G. Clarke, M.P. Gambin (1991)): 1. Ideal curve, 2.oversized borehole, 3 .too small borehole

Only the curves showing a low degree of disturbance and covering a sufficient range of deformation were exploited for this comparison. Initially, this validation was performed through the MPM tests carried out in the proximity of the Trigoni tunnel, because they included both loading and unloading curves. The test simulations seems to be in good agreement with the experimental curves.

Soil parameters		Set 1	Set 2
E_{50}^{ref}	kPa	11,000	14,000
E_{oed}^{ref}	kPa	11,000	14,000
$E_{ur,}^{ref}$	kPa	45,000	70,000
m	-	0.8	0.8
ν'_{ur}	-	0.2	0.2
c'	kPa	70	90
ϕ'	°	25	25
ψ	°	0	0
R_f	-	0.8	0.8

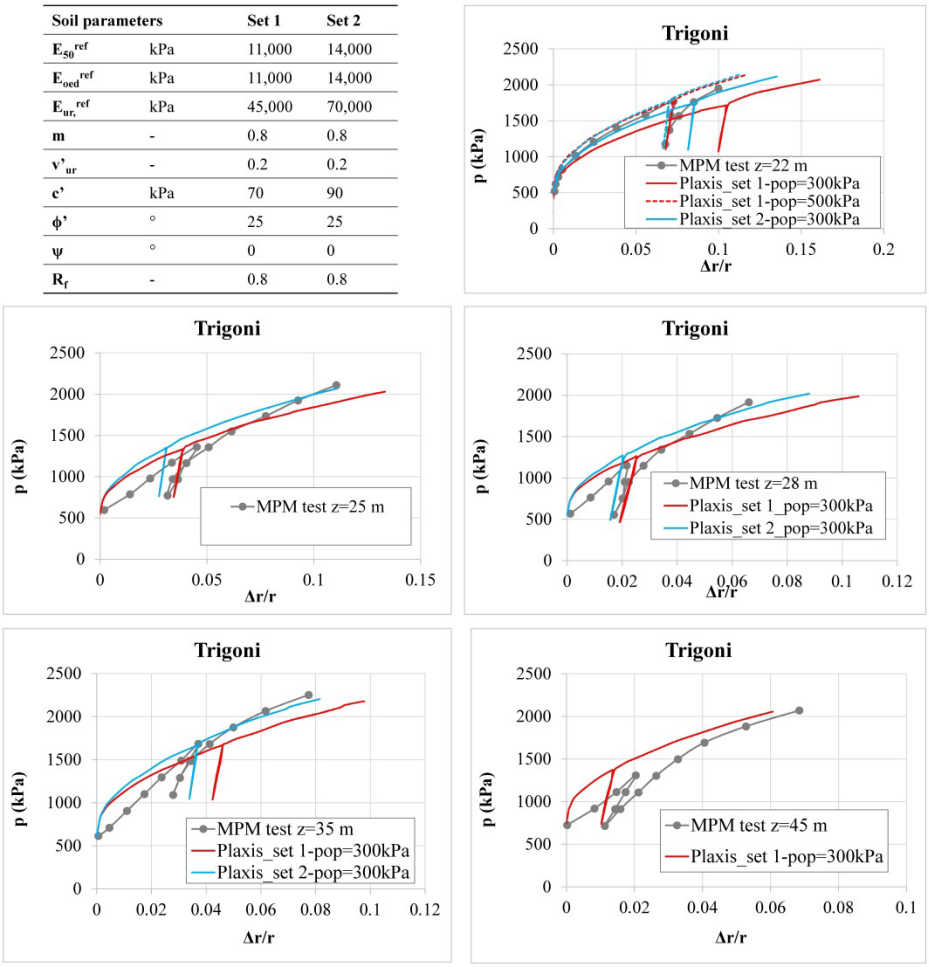

Figure 89. Pressuremeter curve fitting through numerical simulation of pressuremeter tests with both loading and unloading curve

The same parameter sets were used to check the compatibility with other pressuremeter curves. The pressuremeter tests shown in the following were carried out in boreholes located in the proximity of other tunnels but unfortunately they do not include unloading paths.

Soil parameters		Set 1	Set 2
E_{50}^{ref}	kPa	11,000	14,000
E_{oed}^{ref}	kPa	11,000	14,000
$E_{ur,}^{ref}$	kPa	45,000	70,000
m	-	0.8	0.8
ν'_{ur}	-	0.2	0.2
c'	kPa	70	90
ϕ'	°	25	25
ψ	°	0	0
R_f	-	0.8	0.8

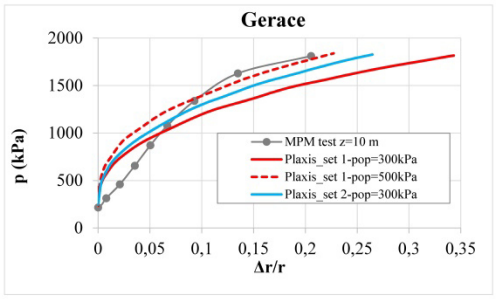

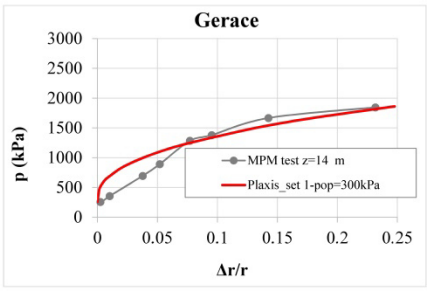

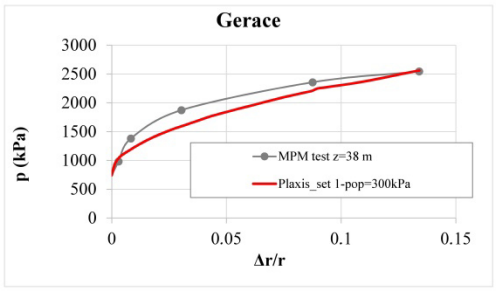

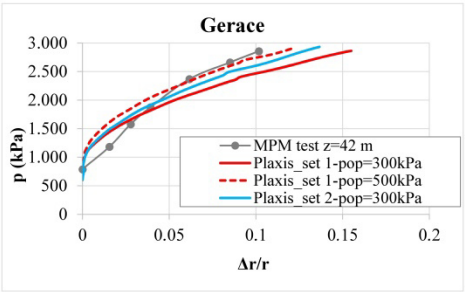

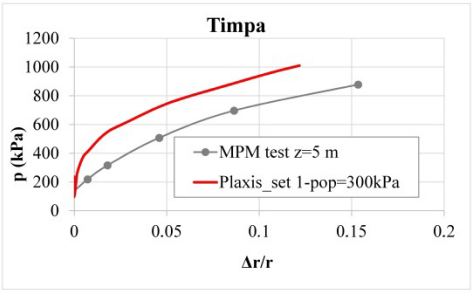

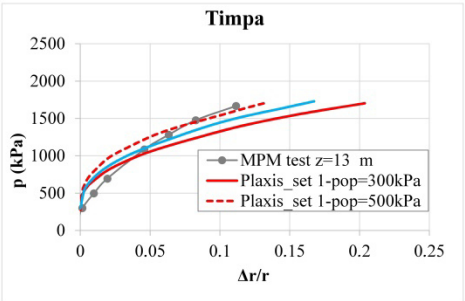

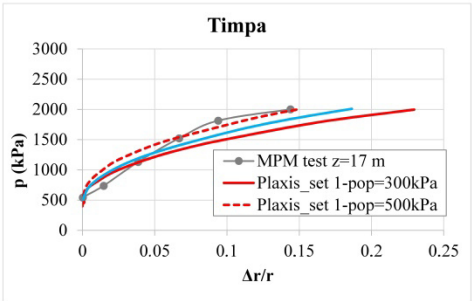

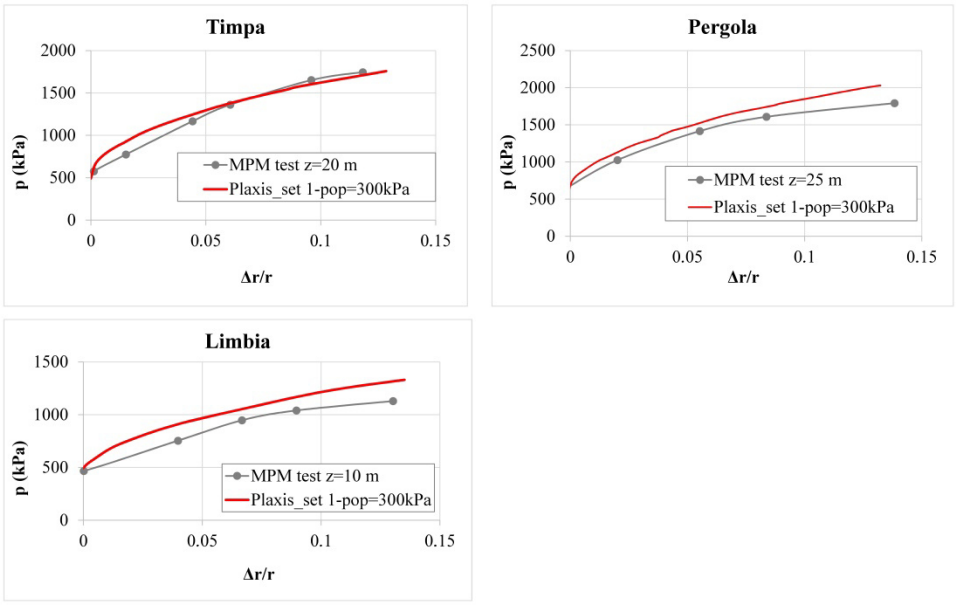

Figure 90. Pressuremeter curve fitting through numerical simulation of pressuremeter tests with only loading curve

Even tough it is difficult to define which parameter set provides a better match, these test simulations confirmed the variation range of the stiffness parameters already identified through laboratory tests.

The calibration of the HSS model parameters also includes the definition of soil behaviour in the small strain range. The implementation of the small strain behaviour in Plaxis requires only two additional parameters: the initial shear modulus at the reference pressure ($G_{0,ref}$) and the shear strain level $\gamma_{0.7}$ at which the shear modulus drops to 70% of the initial value. The definition of the soil properties in the small strain range is nowadays considered necessary not only for earthquake engineering and but also for static problems since it might strongly affect the accuracy of serviceability predictions. The model takes into account the stress dependency of the small-strain shear modulus through the same power law implemented for E_{50} and E_{ur}.

The empirical relations for estimating G_0 usually link this value to the mean effective stress (p') and either the void ratio (e) or the OCR. The advantage of dealing with void ratios instead of over-consolidation ratios lies in the fact that the first ones can be easily estimated from the soil natural water

content, whereas OCR is less easy to assess **(Vardanega & Bolton 2013)**. An equation commonly adopted to describe the small strain stiffness profile according to the average effective stress p' is the following:

$$\frac{G_0}{p_a} = Sf(e)\left(\frac{p'}{p_a}\right)^{0.5} \quad (17)$$

Several authors, on the basis of experimental tests, provided different values for the coefficient S and analytical expressions for f(e). Some of the most commonly used are listed in Table 21.

Table 21. Analytical expressions for the coefficient function f(e) and reference values for the coefficient S

Reference	f(e)	S	Soil type investigated
Hardin & Black, 1969 (Hardin & Black 1969)	$\frac{(2.97-e)^2}{1+e}$	330	Undisturbed clayey so and crushed sands
Jamiolkowski, 1994 (Jamiolkowski et al. 1995)	$e^{-1.3}$	275-1174	Six undisturbed Itali clays
Shibuya et al., 1997 (Shibuya et al. 1997)	$(1+e)^{-2.4}$	1800-3000	Soft clays
Shibuya et al., 1997 (Shibuya et al. 1997)	$(1+e)^{-2.4}$	5000	Overconsolidated Itali clays

The value of $\gamma_{0.7}$ can be estimated through the stiffness degradation curves proposed by **Vardanega & Bolton (2013)** as an update of the commonly used **Vucetic & Dobry (1991)** curves. The decay curve suggested for static applications is:

$$\frac{G}{G_0} = \frac{1}{1+\left(\frac{\gamma}{\gamma_{ref}}\right)^{0.736}} \quad (18)$$

$$\gamma_{ref} = 22\left(\frac{I_p}{1000}\right) \quad (19)$$

According to this equations and considering an average plasticity index of 30, the reference strain $\gamma_{0.7}$ can be assumed equal to $2 \cdot 10^{-4}$.
The small strain modulus was evaluated by taking into account the G_0 profile obtained from a cross-hole test, the corresponding soil stratigraphy and the literature curves for fine-grained materials based on the void ratio

(Figure 91). The average void ratio, of the clayey and silty material, derived from undisturbed samples taken in the silty-clayey deposit from different boreholes, is around 0.85 (Figure 91, right). The G_0 profile computed according to the HSS model is also plotted in the same figure. 200 MPa and 100 MPa were chosen as G_0 reference values respectively for the upper and lower soil layer.

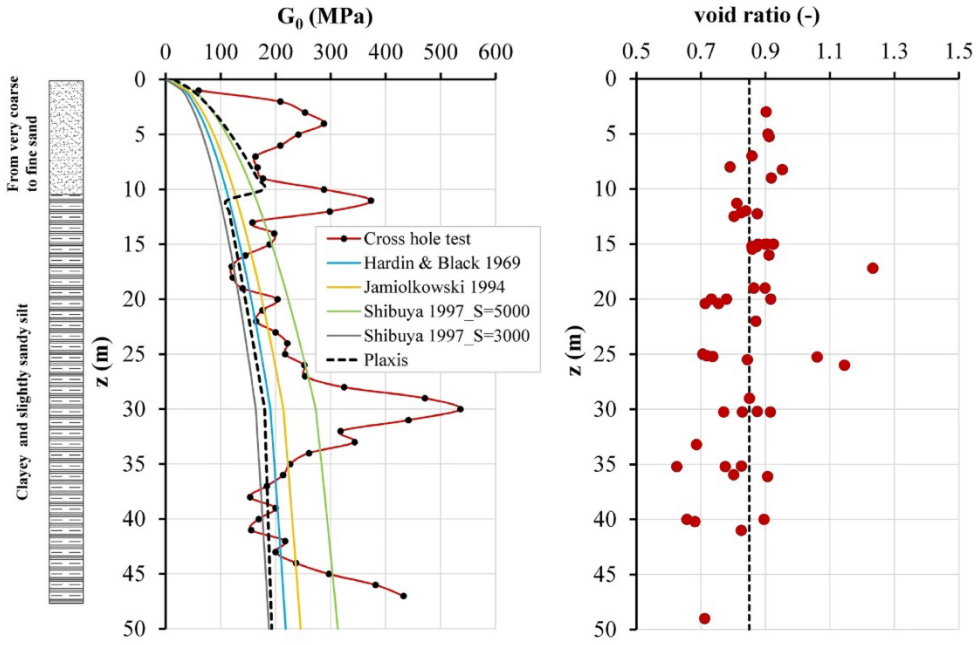

Figure 91. Cross-hole test and void ratio

The geotechnical characterization of the upper soil layer, belonging to the Monte Narbone Formation, was not as accurate as for the fine-grained deposit, in which 90% of the tunnels were excavated. Nevertheless, it was previously verified that its properties do not have a remarkable influence on the results, because, in the considered stretch, the thickness of this deposit is not significant compared to the total overburden.

5.2. Tunnel stress paths

If on the one hand advanced soil constitutive models allow designers to reduce the number of initial hypotheses by directly modelling different aspects of the soil behaviour, on the other hand it is necessary to be aware of the influence that each parameter has on the stress-strain response.

Moreover, the magnitude of this influence varies according to the specific stress-paths involved in the problem. Therefore, the parameters governing the problem change according to the peculiar case. Stress-paths characterizing a traditionally excavated tunnel were analysed by means of a 3D numerical calculation. The excavation was simulated in one go. The tunnel lining is an open arch modelled as plate element. The considered points are showed in Figure 92 and the soil parameters are listed in Table 22. As it can be seen from Figure 93, most of the points, in the close proximity of the excavation, undergo deviatoric primary loading or unloading. The single stress paths also change during the calculation, as the relaxation due to soil removal proceeds. This analysis suggests that particular attention should be paid to correctly define the deviatoric stiffness and the unloading-reloading modulus.

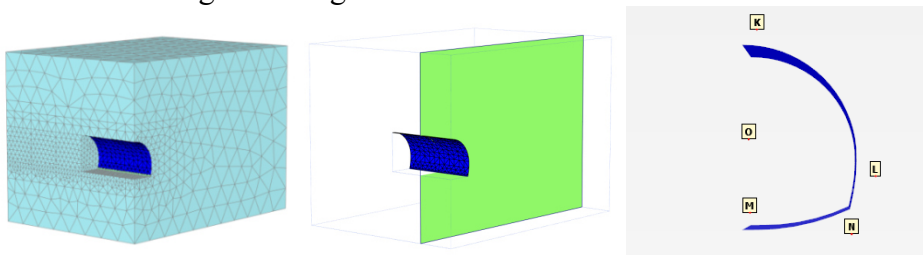

Figure 92. FEM model (left); considered section (center); points location (right)

Table 22. Soil parameters used for the stress path analysis

Soil parameter		Trubi formation
γ_{unsat}	kN/m^3	19
γ_{sat}	kN/m^3	20
$E_{50,ref}$	kPa	11,000
$E_{oed,ref}$	kPa	11,000
$E_{ur,ref}$	kPa	45,000
m	-	0.8
v'_{ur}	-	0.2
k_0	-	0.65
k_0^{nc}	-	0.5774
$G_{0,ref}$	kPa	100,000
$\gamma_{0.7}$	-	0.0002
c'	kPa	70
φ'	°	25
ψ	°	0
R_f	-	0.8
POP	kPa	300

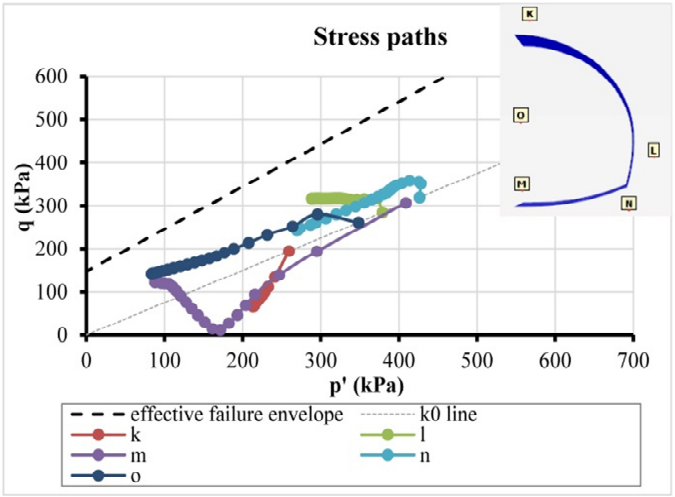

Figure 93. Stress paths

5.3. Concluding remarks

This chapter included the description of the case study and the soil parameter calibration carried out using both laboratory and in situ tests.
The material mainly involved in the underground excavations is a fine-grained slightly marly and overconsolidated deposit. Given the characteristics of both the material and the particular engineering problem here considered, the HSS model was chosen to numerically model the soil behaviour.
By simulating the single tests, as well as by averaging all the results, it was possible to define a variation range for all the required soil parameters. The identification of the main stress-paths involved in such a complex problem helps in identifying the most important parameters for the specific situation.
Further details regarding the constitutive model as well as some sensitivity analyses involving both the soil and the lining parameters are shown in Appendix B.

Chapter 6.
Numerical calculations and comparisons with monitoring data

In the following paragraphs, the field data acquired during the excavation of the Trigoni and Pergola tunnel are analysed and used for validating 3D numerical models.

6.1. Trigoni tunnel

This paragraph focuses on the 840 m long Trigoni tunnel, NE-SW oriented and excavated from both entrances. During the construction of the first tunnel, the temporary lining was closed with a cast in place concrete invert at a maximum distance of 2D. In the secondly excavated tunnel, this distance was usually reduced to 1-1.5D. The excavation of the twin tunnels was not carried out contemporary, but keeping a distance up to 8D between the two advance faces while excavating from South and 4-5 D while excavating from North. Moreover, the second tunnel was excavated only after the final lining of the first tunnel was cast in place (at least sidewalls and invert). This procedure avoided overstressing of the central pillar and excessive deformations in the soil mass.
The water level was found to be roughly located between the tunnel crown and the invert.
In the present study, to set the model geometry and define the excavation phases, two reference segments were considered (Figure 94). The first goes from chainage 12+140 to chainage 12+180, and it is close to the Southern entrance. The second goes from chainage 12+540 to chainage 12+580, and it is close to the Northern entrance. The choice of these locations stretches is due to the intensified monitoring system adopted, consisting not only of convergence measurements but also of surface settlement measurements and a vertical incremental extensometer placed between the two tunnels.
From the geological profile shown in Figure 94, it is possible to see that both the stretches mainly involved the Trubi formation with overburden varying from 25 to 40 m.

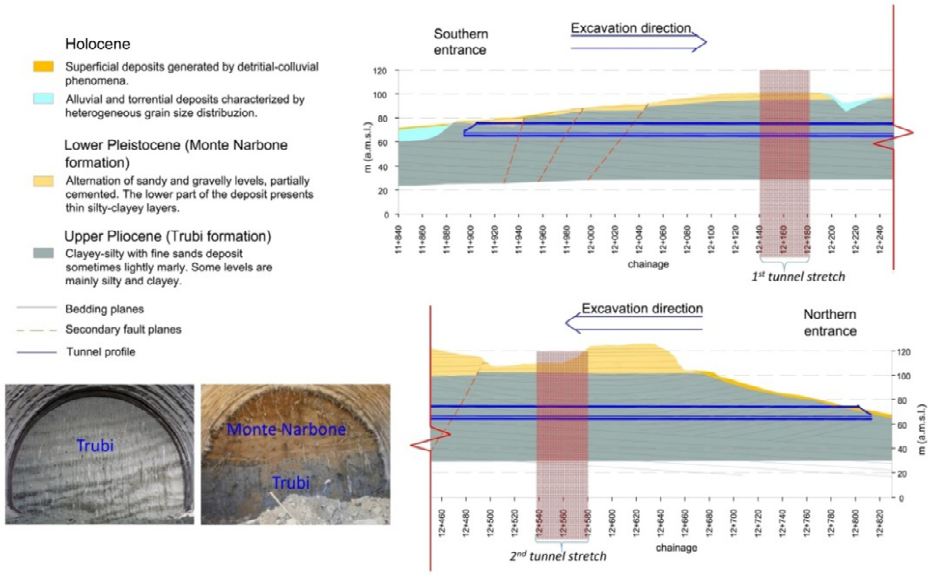

Figure 94. Geological profile of the Trigoni tunnel (Northern carriageway)

6.1.1. Numerical analysis

The numerical calculations, aimed at reproducing the observed behaviour were carried out employing the numerical code Plaxis 3D 2013 **(Brinkgreve et al. 2013)**. The use of a 3D model made it possible to avoid initial assumptions regarding the stress release occurring before the support activation.

Given the different overburden characterising the two considered tunnel stretches (as described before), two different models were generated. The first one, closer to the Southern entrance, is characterised by overburden varying between 30 and 35 m and the second one, closer to the Northern entrance, presents overburden from 35 to 40 m. Both the models consist of around 400000 10-node tetrahedral elements and are 300 m long and 200 m wide, corresponding to 23D and 15D respectively (Figure 95, left). The bottom boundary is around 3D from the tunnel invert. The mesh dimensions satisfy the minimum values suggested by **Möller (2006)**.

The calculation was carried out using the so-called step by step approach **(Katzenbach and Breth 1981),** usually adopted to simulate traditionally excavated tunnels. The real excavation sequence was simulated by

deactivating a 1 m thick cluster of the advance core and activating, within the same phase, a plate element representing the primary lining at a distance of 1 m from the excavation face.
Regarding the final support, every 10 excavation steps, 10 clusters, each 1 m thick, belonging to the lower part of the section were deactivated. In the following phase, the final invert, simulated through plate elements, was activated. While excavating from South, a maximum distance of 2D and 1.5D between the face and concrete invert was kept for the firstly and secondly excavated tunnel, respectively. While excavating from North, the maximum distances between excavation face and invert were 1.5D for the Southern carriageway and 1D for the Northern carriageway.

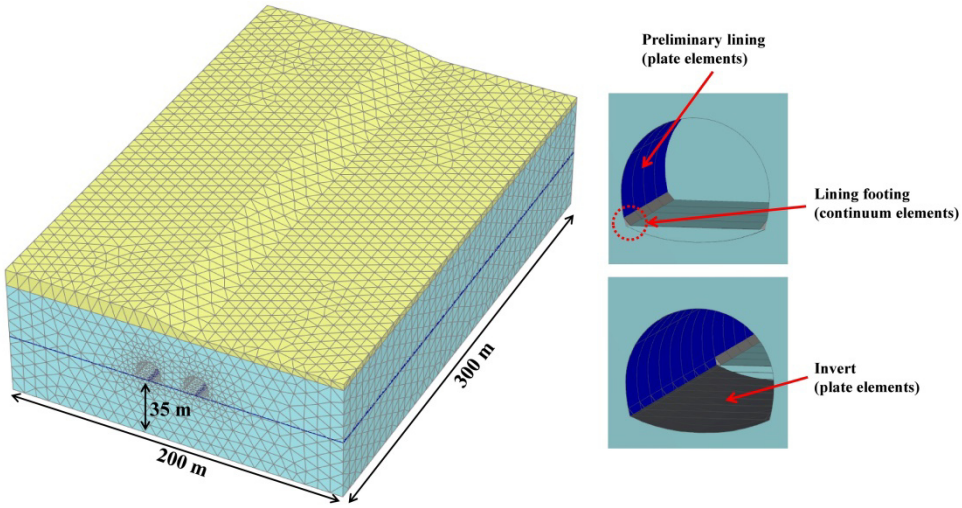

Figure 95. 3D FEM mesh of the model generated for the first stretch (left); details of preliminary lining and invert arc (right)

Only in the central 100 m of the model, the real excavation sequence has been simulated. The first 100 m were excavated in 20 phases by removing 5 m thick soil clusters of the tunnel core while simultaneously installing the temporary lining, keeping the cavity completely supported. This procedure allows getting away from the initial vertical boundary, which, similarly to the other boundaries, has a significant influence on the results. The lateral vertical boundaries are fixed in the horizontal direction whereas the bottom boundary is fixed in both the horizontal and the vertical direction. No fixities were applied to the upper horizontal boundary.

Both the preliminary and the final lining were modelled with linear-elastic plate elements. Since the temporary lining is made of steel sets and sprayed concrete, an equivalent homogeneous section was considered. In the present case study, the steel represents the main element providing stiffness and resistance, especially at early stages. Therefore, the adoption of a linear elastic material with an equivalent Young's modulus instead of using an advanced constitutive model should not significantly influence the results. On the contrary, in those cases where the temporary lining is primarily made of shotcrete, it might be necessary to take into account its rheological behaviour to get realistic results, at least with respect to the lining stress state.

Being the temporary lining, before the construction of the concrete invert, an open arch, it is also important, in order to avoid excessive punching into the soil clusters, to correctly model the lining footing. For this reason, the model was enhanced by adding continuum elements to the foot of the plate elements, thus restoring the bearing capacity of the open ring (Figure 95, right). In this way, a compromise between plate and continuum elements was reached, allowing to optimise the total number of mesh elements without losing the benefits of modelling the original thickness in correspondence of the lining foot. Modelling the lining with continuum elements would have had the disadvantage of increasing significantly the number of degrees-of-freedom necessary to reach a good mesh quality and avoid a poor geometric conditioning. Moreover, an integration tool allowing to determine the structural forces in curved volumes is currently not available in Plaxis 3D.

The plate stiffnesses, governed by the thickness and Young's modulus, were defined according to the main steel profile installed in each section (Table 23). For modelling the temporary lining of the first and the second stretch, the homogeneous stiffnesses of 2 coupled IPN 220/m and IPN 180/m combined with a shotcrete thickness of 25 cm were adopted respectively.

Table 23. Steel shotcrete homogenization

	1st stretch	2nd stretch
profile	2 IPN 220/m	2 IPN 180/m
shotcrete thickness (cm)	25	25
$EA_{shotcrete}$ (kN)	1.75E+06	1.75E+06
EA_{steel} (kN)	1.66E+06	1.17E+06
$EJ_{shotcrete}$ (kN*m^2)	9.11E+03	9.11E+03
EJ_{steel} (kN*m^2)	1.29E+04	6.09E+03
s_{hom} (m)	0.278	0.250
E_{hom} (kPa)	1.23E+07	1.17E+07

Curved structural elements are modelled in Plaxis as faceted shell elements, meaning that they consist of more plane facets. These elements allow for an easier numerical formulation when compared to the implementation of a proper shell theory, but the accuracy of the results depends on a fine discretization of the structure. Advantages and disadvantages of using a specific type of element for modelling the tunnel lining are presented in **Augarde & Burd (2001)**.

In the present study, the interface between plate elements and surrounding ground is rigid.

Given the results of the previously described parameter calibration, a first attempt to simulate the Trigoni tunnel excavation was carried out by using the model parameters listed in Table 24 and assuming drained conditions.

Table 24. Soil parameters adopted for the model validation

Soil parameter		Trubi formation	Monte Narbone formation
γ_{unsat}	kN/m^3	19	19
γ_{sat}	kN/m^3	20	20
$E_{50,ref}$	kPa	11,000	30,000
$E_{oed,ref}$	kPa	11,000	30,000
$E_{ur,ref}$	kPa	45,000	90,000
m	-	0.8	0.6
ν'_{ur}	-	0.2	0.2
k_0	-	0.7	-
k_0^{nc}	-	0.5774	0.4264
$G_{0,ref}$	kPa	100,000	200,000
$\gamma_{0.7}$	-	0.0002	0.0002
c'	kPa	70	0
ϕ'	°	25	35
ψ	°	0	0
R_f	-	0.8	0.9

The initial stress state was generated by applying the so-called k_0-procedure and performing a nil step afterwards to restore equilibrium conditions (the ground surface is not horizontal). The water table is located slightly below the tunnel invert in both models, as shown in Figure 95, left.
Regarding the accuracy of the FEM results, it depends on the prescribed tolerance on both global and local error. The first one is represented by the ratio between the out-of-balance vector of nodal forces and external forces, whereas the second one corresponds to the out-of-balance stress **(Vermeer & Langen 1989)**. For big meshes and small excavation steps, being the total amount of external forces remarkable and therefore the global error quite small, the accuracy is usually guaranteed by the tolerance on the out-of-balance stress.

6.1.2. Results and comparison with monitoring data

The monitoring data regarding the preliminary lining (i.e. convergences and strain gauge measurements) have been already analysed by **Buselli et al.**

(2013). The authors focused on the statistical elaboration of relative displacements recorded through topographical targets and strain gauge measurements. Despite the strong data scattering, they identified some correlations between tunnel convergences and advancement rate, soil stratification and construction procedure. Compared to relative displacements, absolute vertical displacements of the preliminary lining appear to be less scattered and more suitable for comparison with numerical calculations (Figure 96). The horizontal displacements and consequently the convergence between sidewalls present a stronger scattering, especially in the Southern part of the tunnel (Figure 97). The scattering can be due to the fact that, even though the optical targets are nailed to the shotcrete, there might be some gap between the primary lining and tunnel cavity. Furthermore, when there are gaps between lining and cavity, the contact between the primary lining and the ground cavity is likely to be reached faster in the crown than in the sidewalls, due to the effect of the gravity forces. Therefore, lining settlements usually present more consistent and reliable values.

The primary lining displacements were initially filtered, disregarding both the data with a short measuring time and those with delayed zero readings.

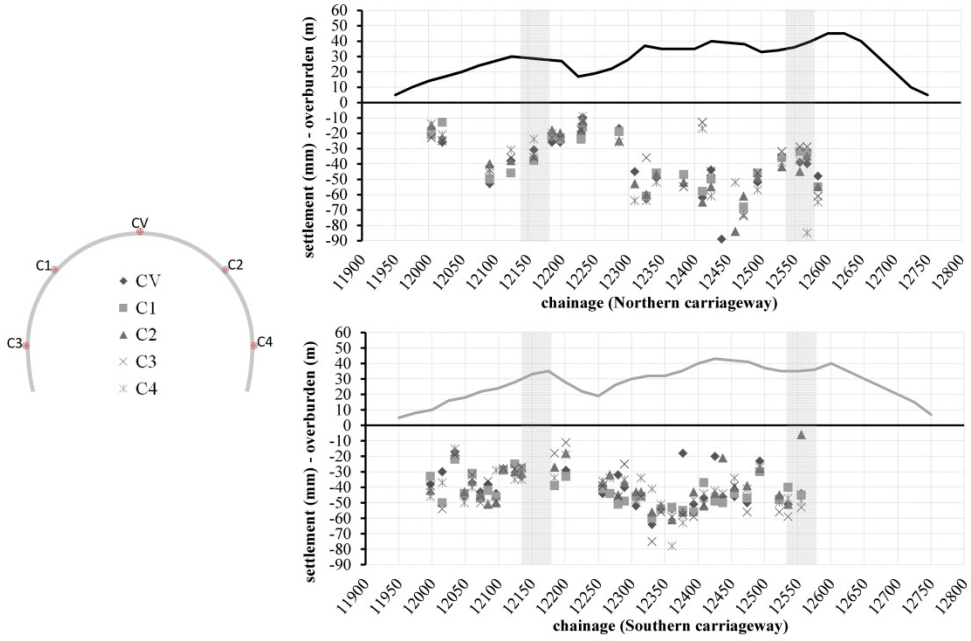

Figure 96. Trigoni tunnel: settlements of the temporary lining - measurements

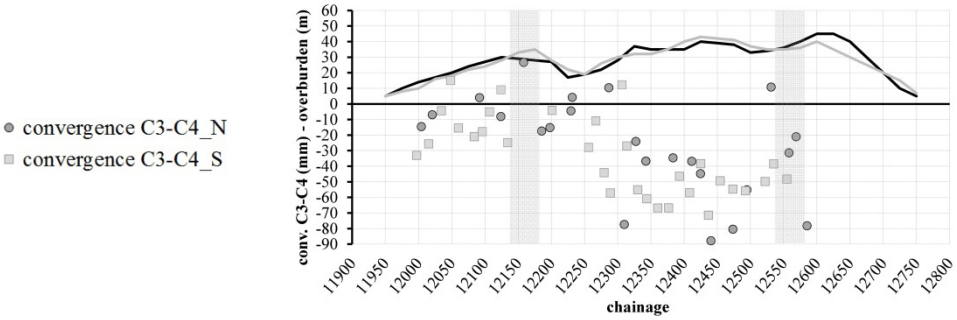

Figure 97. Trigoni tunnel: lateral convergences of the temporary lining - measurements

Considering vertical settlements (Figure 96), most of the measured values vary between 2.5 and 4.0 cm in the first stretch and between 3.0 and 6.0 in the second stretch, characterised by higher overburden and thus higher initial stress state.

The stress state on the temporary lining was investigated through coupled strain gauges placed on the steel sets, precisely on both the crown and sidewalls. Strain measurements can be converted in structural forces by considering a linear elastic constitutive behaviour for the steel and by multiplying the average stress state for the steel cross-section area as follows:

$$N = \frac{\varepsilon_1+\varepsilon_2}{2} EA \qquad (20)$$

where ε_1 and ε_2 are the recorded strains and EA is the axial rigidity of the steel profile installed in the considered monitoring section. In Figure 98 the calculated normal forces are plotted versus the tunnel chainage. The axial rigidity used to convert strains in structural forces includes two coupled steel sets. It can be observed that, close to the first tunnel stretch (from chainage 12+140 to chainage 12+180), the primary lining carries an average normal force of -600 kN on the sidewalls and -1000 kN on the crown. In correspondence of the second tunnel stretch (from chainage 12+540 to chainage 12+580), where values are more scattered, the average normal force is equal to -900 kN on the sidewalls and -1300 kN on the crown. Analysing all the instrumented sections, the highest values of normal forces were measured between ch 12400 and ch 12550. This can be attributed both to the higher overburden and to the construction sequence here adopted. In fact, in this section, the second tube was excavated before the shotcrete vault was cast in place. Therefore, the stress state on the temporary lining of the tunnel excavated first is also influenced by the second excavated tube.

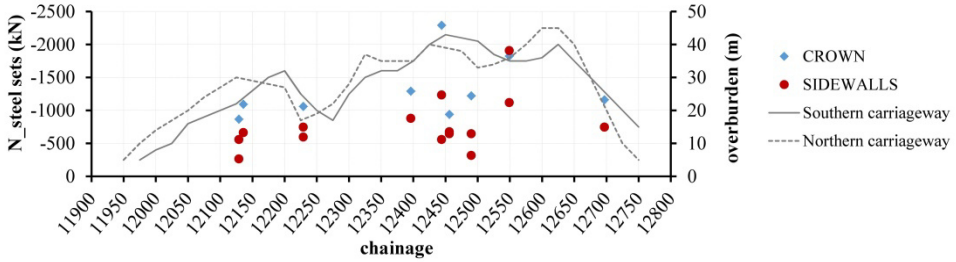

Figure 98. Trigoni tunnel: normal forces from strain gauge measurements (compression is negative)

In Figure 99 and Figure 100, the results of the calculations carried out with the first and the second model respectively, are represented. The vertical displacements of the temporary lining deriving from the FEM simulations are in good agreement with those monitored during the excavation. The calculated horizontal displacements are similar to the vertical ones, whereas the monitored horizontal displacements are too scattered for a comparison.
Regarding the computed structural forces, provided that the ratio between the axial stiffnesses of shotcrete and that of the coupled steel sets is close to 1 when IPN 220 profiles are adopted and close to 1.5 for IPN 180 (Table 23), the total axial force can be respectively divided by 2 and 2.5 to get the contribution of the steel ribs only. The so-calculated structural forces are similar to the average values derived from strain gauge measurements (Figure 98). Computed displacements and structural forces regarding the second excavated tubes are very close to those of the first tube.
The irregularities that characterise the computed N profiles, especially in the crown can be mainly associated with the use of faceted shell elements, whose accuracy depends on the mesh discretization. Unfortunately, for such big models, a further mesh refining would make the calculation prohibitively time-consuming.

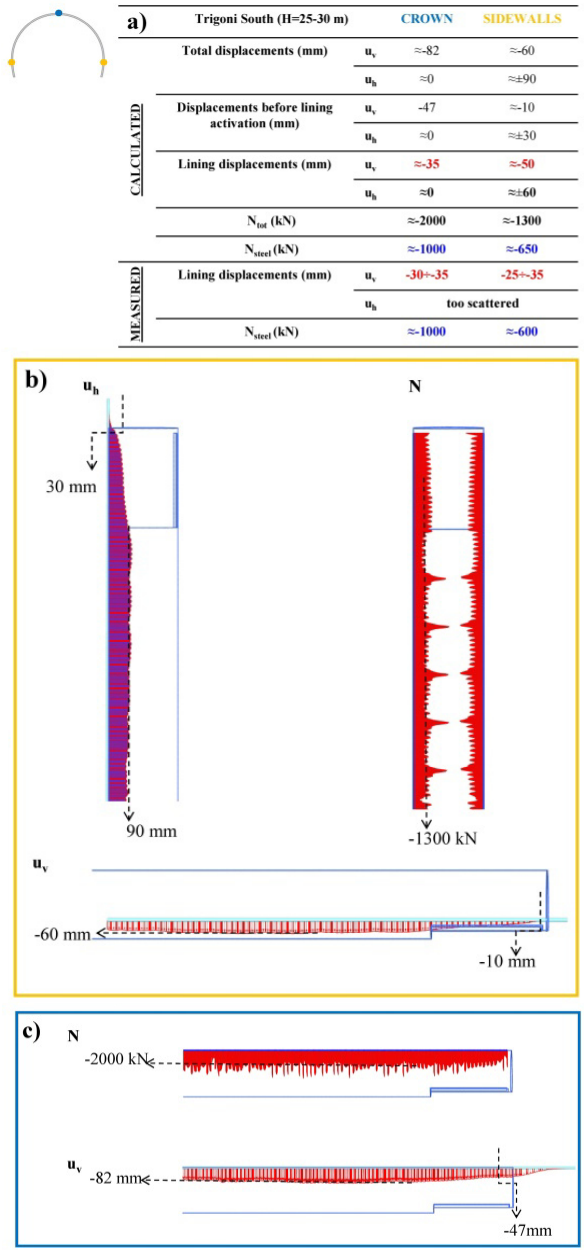

Figure 99. Trigoni tunnel, model 1: a) Measured and calculated lining displacements and forces; b) plot of calculated values at the sidewalls; c) plot of calculated values at the crown (first tunnel stretch, first excavated tube)

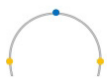

a)

Trigoni North (H=30-40 m)			CROWN	SIDEWALLS
CALCULATED	Total displacements (mm)	u_v	≈-110	≈-65
		u_h	≈0	≈±125
	Displacements before lining activation (mm)	u_v	≈-72	≈-5
		u_h	≈0	≈±45
	Lining displacements (mm)	u_v	≈-38	≈-60
		u_h	≈0	≈±80
	N_{tot} (kN)		≈-3300	≈-2000
	N_{steel} (kN)		≈-1320	≈-800
MEASURED	Lining displacements (mm)	u_v	-40÷-50	-30÷-60
		u_h	too scattered	
	N_{steel} (kN)		≈-900	≈-1300

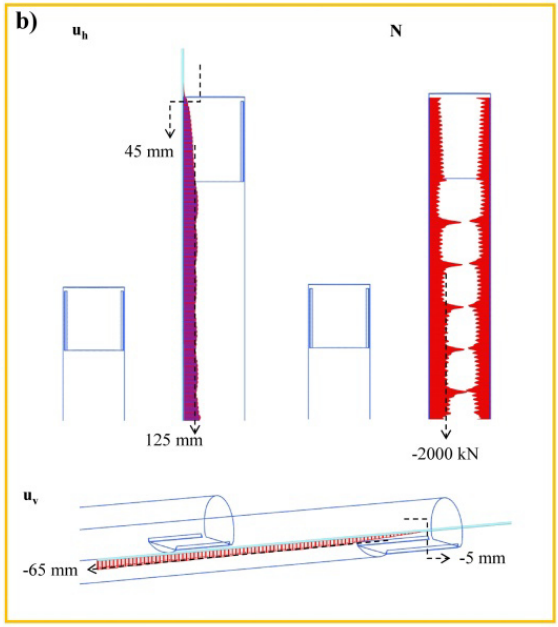

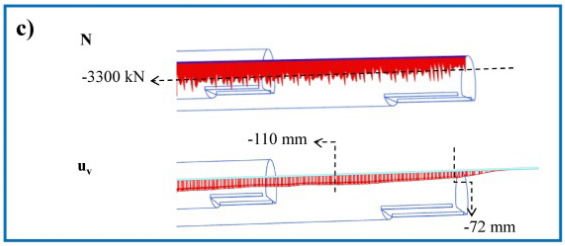

Figure 100. Trigoni tunnel, model 2: a) Measured and calculated lining displacements and forces; b) plot of calculated values at the sidewalls; c) plot of calculated values at the crown (second tunnel stretch, first excavated tube)

The section at ch 12697, which fall outside the previously considered stretches, was instrumented with both strain gauges (Figure 98) and pressure cells placed under the lining feet (Figure 101). However, being both overburden and structural support similar to those of the first stretch (from chainage 12+140 to chainage 12+180) the first numerical model was adopted as reference for comparison with the observed data. As depicted in Figure 101, the calculated axial forces at the lining feet and the measured ones are in good agreement.

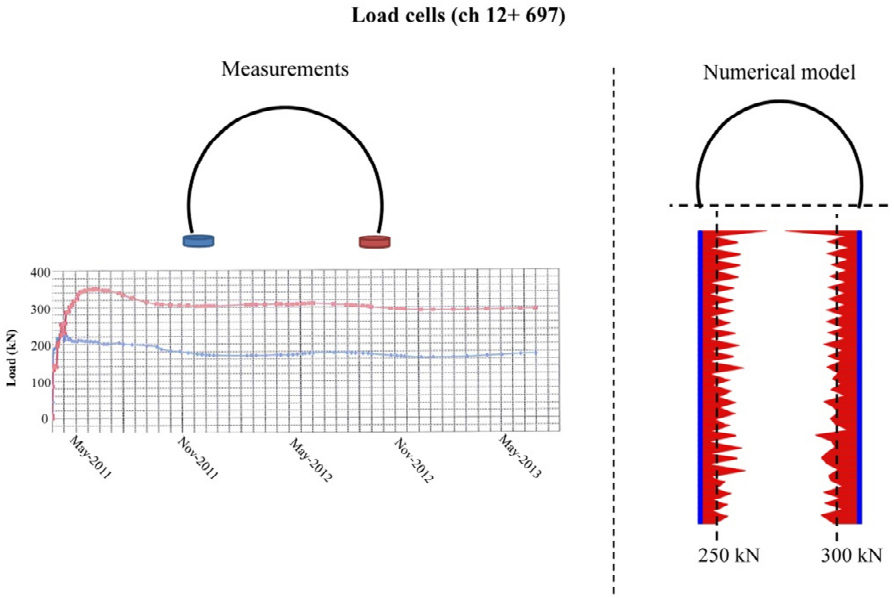

Figure 101. Load cells: measurements and FEM results

Concerning the deformation behaviour at a certain distance from the tunnel cavity, both subsidence and incremental extensometer measurements are available.

The subsidence measurements carried out at chainages 12180, 12540 and 12570 (Figure 102, Figure 103), showed maximum settlements lower than 7 cm. However, the monitoring period does not cover the whole excavation of both tunnels. Regarding the first analysed stretch, close to the Southern entrance, the time period includes the excavation of the first tunnel and the

arrival of the second tunnel at the corresponding chainage. In the second stretch, close to the Northern entrance, the monitoring period starts when the first excavation face is already at chainage 12540 and the second tunnel face at chainage 12580 (both advancing from North) and finishes when they are both more than 3D beyond the monitored sections.
Despite the monitoring periods do not allow to catch completely the effects of both tubes on surface settlements, 3D FEM calculations represent a valid instrument for validating the model parameters with subsidence data. This goal can be achieved by taking into account the tunnel face position at the beginning and the end of the available period.
The numerically computed settlement trough matches very well the field measurements for both chainage 12180 (Figure 102) and chainage 12570 (Figure 103). This consideration holds in particular for the monitoring points located far from pre-existing buildings, which can be associated with a free-field condition.

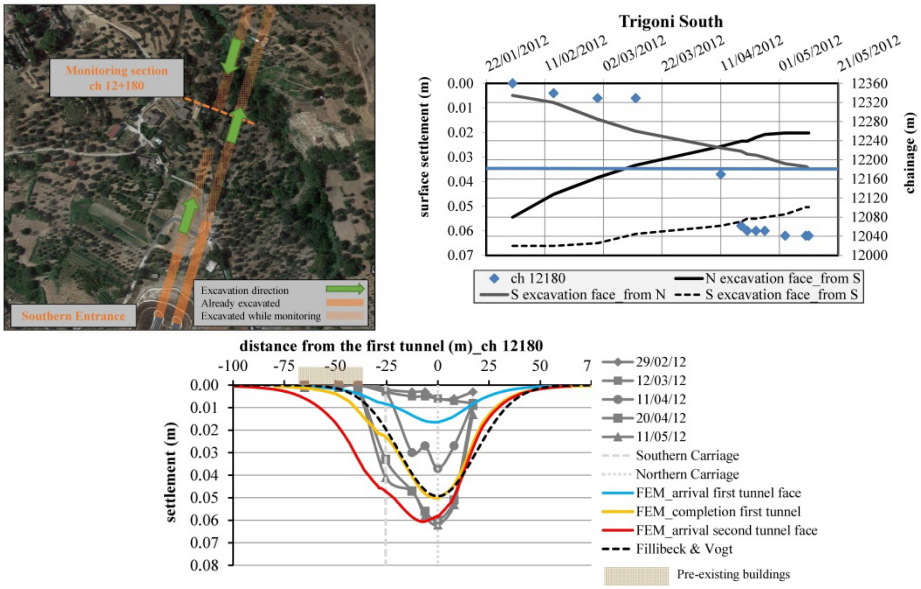

Figure 102. Subsidence monitoring section at ch 12180: measured and calculated settlements. Photo from Google Earth

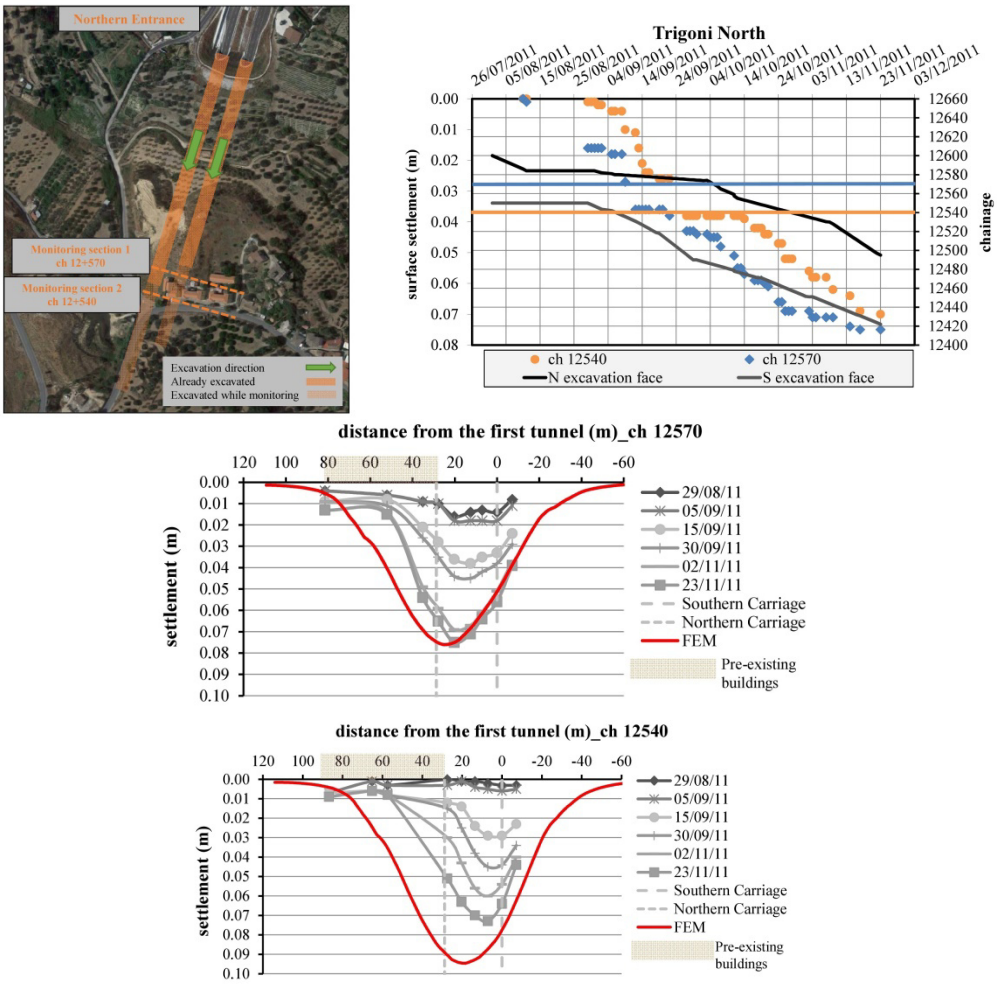

Figure 103. Subsidence monitoring section at ch 12580 and 12540: measured and calculated settlements. Photo from Google Earth

The settlements measured in the proximity to pre-existing structures tend to be much lower than the predicted ones. The main reason is most probably that the numerical model does not consider the interaction between soil mass and buildings, whereas in reality surface structures strongly affect settlements. Regarding the chainage 12540, the difference between measured and computed subsidence is more remarkable, probably due to a

stronger influence of both pre-existing buildings and a minor road crossing the monitoring section. The computed surface settlements associated with the single tunnel excavation (Figure 102, yellow curve) were also compared to the empirical solution proposed by **Fillibeck & Vogt (2012)**. This empirical method is based on the classic function of Gaussian distribution, which requires the definition of two input parameters, namely point of inflexion and volume loss. The authors suggested some reference values for both shotcrete and shield excavations. Regarding traditionally excavated tunnels, they collected data from more than 200 measurement sections of the Munich subway and other 50 sections from sites with different geological conditions. For atmospheric shotcrete excavations in fine-grained materials, they provided two different formulations for calculating the volume loss:

$$VL_{s,50\%} = (0.016 \cdot z_0 + 0.31) \cdot \frac{100}{E_{100}^{ref}} \quad \text{at a confidence interval of 50\%}$$

$$VL_{s,99\%} = (0.016 \cdot z_0 + 0.61) \cdot \frac{100}{E_{100}^{ref}} \quad \text{at a confidence interval of 99\%}$$

where E_{100}^{ref} represents the stiffness (in MPa) of the excavated soil at the reference normal pressure of 100kPa.

According to the same authors, the point of inflexion of a multi-layer system can be calculated as:

$$i = 0.82 d_{cl} + 0.57 \cdot (z_0 - d_{cl})$$

where z_0 is the total overburden and d_{cl} is the thickness of the fine-grained.

Applying the previously described solution to the present case study and considering $E_{100}^{ref} = E_{ur}^{ref} = 40MPa$ (which refers to σ_1=100kPa), the calculated subsidence curve at a confidence interval of 50% was found to be in good agreement with the surface settlements predicted by the model for the single tunnel. Making the same comparison with the measured displacements seems to be more complicated due to the difficulty in distinguishing the fraction of total settlement associated with the second tunnel excavation.

The vertical deformations of the first stretch of the Trigoni tunnel were also investigated through an incremental extensometer. The measuring tube, equipped with 1 m spaced magnet rings, was vertically installed between the two tunnels. The available monitoring period does not cover the excavation of both tunnels but only the approaching of the second excavation face to the monitored chainage (ch 12540). The tube was modelled as embedded pile, as shown in Figure 104 (left). In the same figure, the measured vertical

deformation and displacements are superimposed to those calculated through the first FEM model.

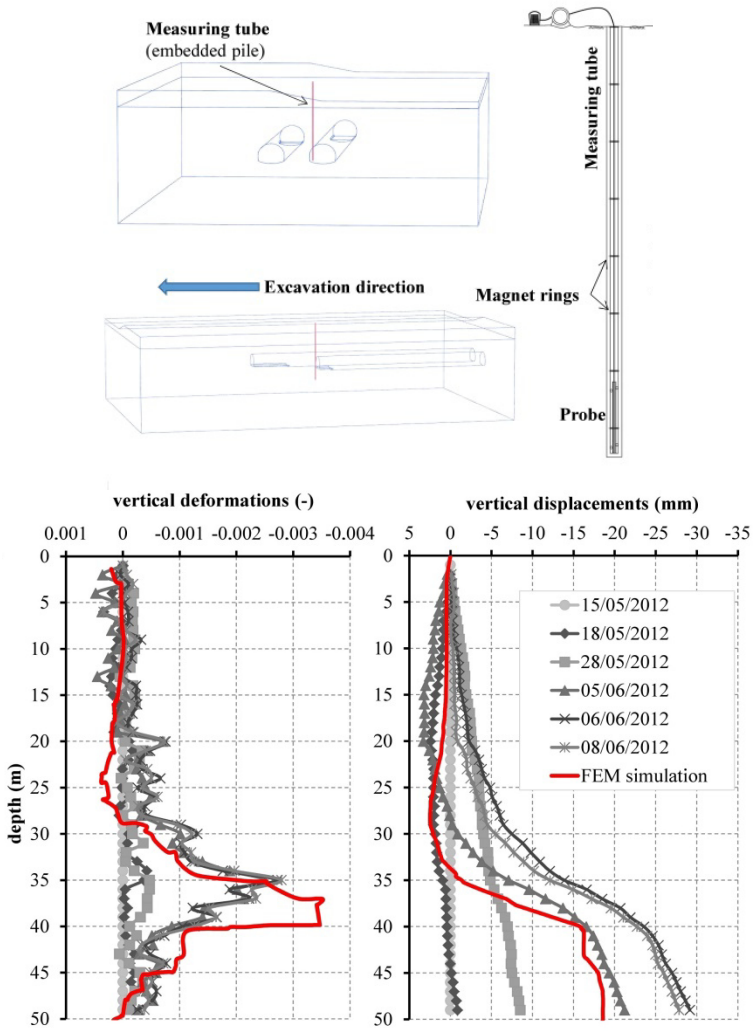

Figure 104. Incremental extensometer modelled as embedded pile (left); comparison between measured and computed vertical deformations (centre) and vertical displacements (vertical incremental extensometer at ch 15+140)

The model predicts very well the maximum value of vertical deformations as well as the depth where it concentrates, whereas the total vertical displacement is underestimated. However, the magnitude of the calculated

deformations and displacements depends also on the axial stiffness and bond strength assigned to the embedded pile. In this case, the rigidity provided by the grout between the borehole and measuring tube and literature values for the bond strength were considered. In particular, EA=1.29E+04 kN and τ_{max}=100 kPa were assigned to the structural element used in the simulation.

An efficient way to evaluate the deformation behaviour along the tunnel axis is to place a horizontal incremental extensometer into the tunnel core. This instrument allows monitoring longitudinal deformations of the ground to be excavated by measuring the relative distance between the magnet rings. During the excavation of the Trigoni tunnel, a measuring tube was installed at ch 11986 into the core of the southern tube (excavated after the northern tube). This section is characterised by H= 15 m. Before excavating from ch 11986 to ch 12000, the tunnel face was reinforced using 80 fibreglass bars. Moreover, an umbrella of 31 fibreglass bars was also installed to support the tunnel crown. Even though the position of the water table is not clearly defined, some water inflow that occurred during the drilling operation for face reinforcement and plastic piles construction (reinforcement from the ground surface) suggests a phreatic level higher than the tunnel top.

In order to compare the measured extrusion with FEM calculation results, a third model was generated (Figure 105). For the sake of simplicity, the model involves only one tube and includes embedded pile elements to simulate face reinforcement. Similarly, the measuring tube is also modelled as embedded pile element (same properties as before were adopted). To take into account that the extensometer was installed in the second excavated tunnel, the calculation was carried out neglecting the small strain behaviour and assigning POP=100 kPa instead of 300 kPa. In fact, being the two tubes only 1D spaced, the influence of the first excavation on the second is remarkable, and the ratio G/G_{ur} as well as the OCR tend to be close to 1. These settings concerning POP and OCR derive from the findings of previous calculations and refer to the tunnel axis depth. The water level, originally higher than the tunnel crown, was locally lowered inside the tunnel core while simulating the excavation. Seepage towards the excavation is disregarded, and phreatic conditions are imposed. Figure 105 shows the calculation model and a comparison between results of the FEM simulation and monitored longitudinal displacements recorded during the excavation. The quality of the match, except for the last measurement, is

good and the FEM curves reproduce the recorded displacements both in magnitude and shape (Figure 105).

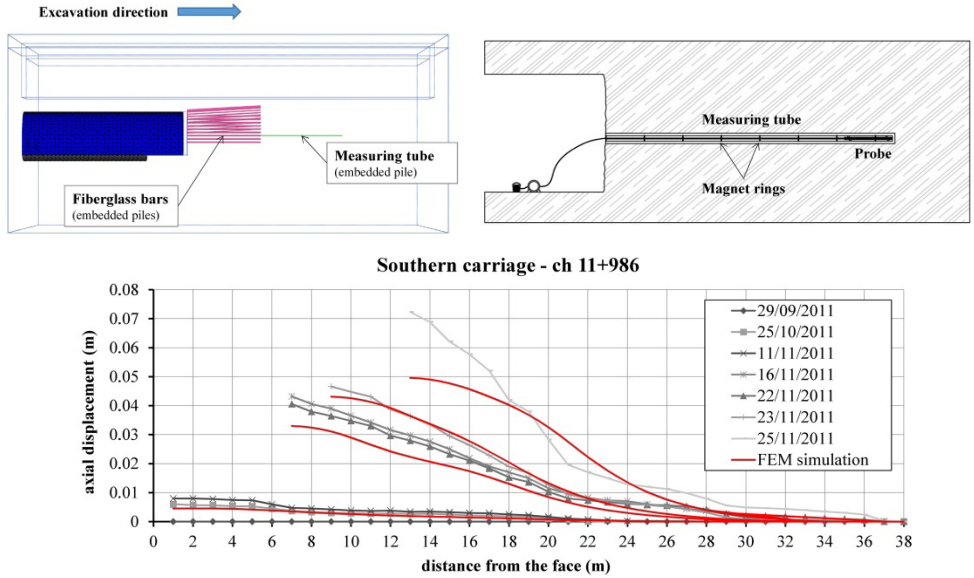

Figure 105. Numerical simulation of a reinforced excavation face instrumented with horizontal extensometer: calculation scheme and comparison between monitoring data and numerical results

6.1.3. Calibration of the stress release factor for 2D analyses

Concerning the possibility to reproduce the results of 3D models through 2D calculations, it was already investigated by **Möller (2006).** Since 3D model are still too time-consuming with respect to average design schedules and computational capacities, this issue is still of interest. **Möller**, considering the case study of a subway tunnel, found out that three different unloading factors were necessary to match surface settlements, bending moments and normal forces as computed by the 3D model.

In this paragraph, an attempt to calibrate the 2D stress relaxation factor was performed by considering the first 3D model generated for the Trigoni tunnel. The 2D model was generated by considering a slice of 5 m of the corresponding 3D model (thus still using Plaxis 3D, as shown in Figure 106). The initial goal of this calibration was to match surface settlements for all the excavation stages (arrival first tunnel, completion first tunnel, arrival second tunnel and completion second tunnel).

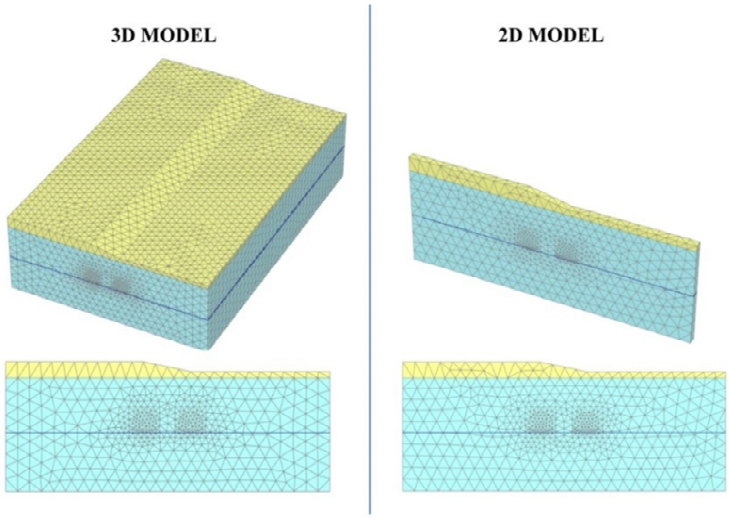

Figure 106. 3D and 2D model used for calibrating the stress relaxation factors

The simulation of the tunnel excavation in the 2D model was performed through the 9 phases listed in Table 25. The set of stress relaxation factor that allowed to obtain a good match of the surface settlements, as depicted in Figure 107, is also shown in Table 25. In turned out that this combination of stress relaxation factors matches quite well not only the surface settlements but also the axial forces at the tunnel crown (Figure 108, Figure 109). However, the axial forces on the sidewalls and the vertical displacements of the tunnel cavity (Figure 110, Figure 111, Figure 112, Figure 113) are, in some cases significantly different. The match of vertical displacements, in particular, seems to be less precise for intermediate phases but it gets better when plane strain conditions are reached (the excavation faces are far from the analysed section). This discrepancy between the two model can be mainly attributed to the longitudinal redistribution capacity (arching effect) that is developed in the 3D model but not in the 2D. Thus, 3D and 2D results, no matter which stress relaxation factor is adopted, will always have some differences.

It should be underlined that the stress relaxation factors listed in Table 25 were determined by trial and error and that a small variation causes a significant change in the computed vertical displacements. Less remarkable, for the present case study, seems to be the sensitivity of the axial force to

changes in λ. A further investigation on the influence of the stress relaxation factor on the model response is included in Appendix C.

Table 25. Simulation of the excavation sequence through the 2D model and stress relaxation factors adopted for each phase

Phase	Description	λ
0	K_0 procedure	-
1	Nil step	1
2	Deactivation of the upper cluster of the core (first tunnel)	0.5
3	Primary support activation (open arch, first tunnel)	0.95
4	Deactivation of the lower cluster of the core (first tunnel)	0.3
5	Invert activation (first tunnel)	1
6	Deactivation of the upper cluster of the core (second tunnel)	0.35
7	Primary support activation (open arch, second tunnel)	0.8
8	Deactivation of the lower cluster of the core (second tunnel)	0.3
9	Invert activation (second tunnel)	1

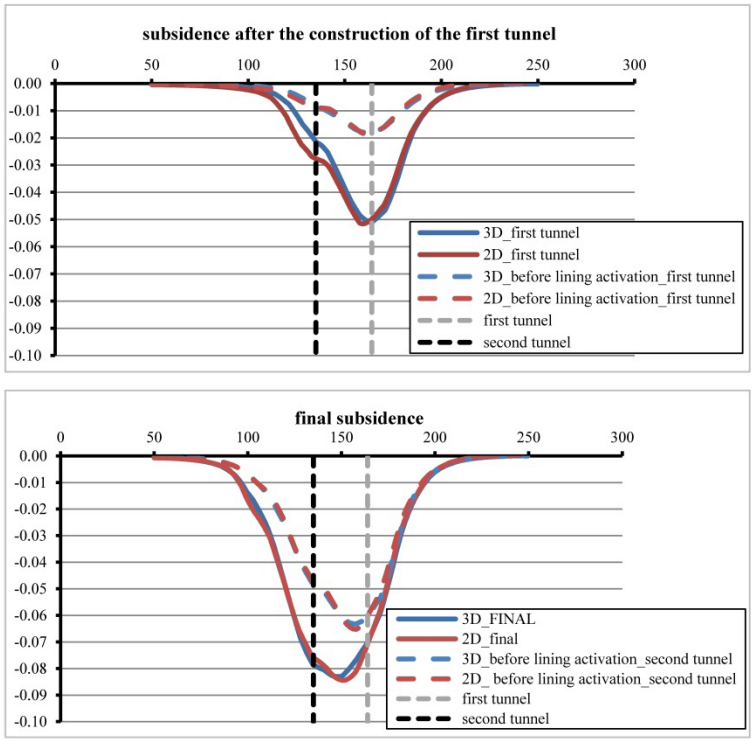

Figure 107. Comparison between the surface settlements obtained from the 3D and 2D model

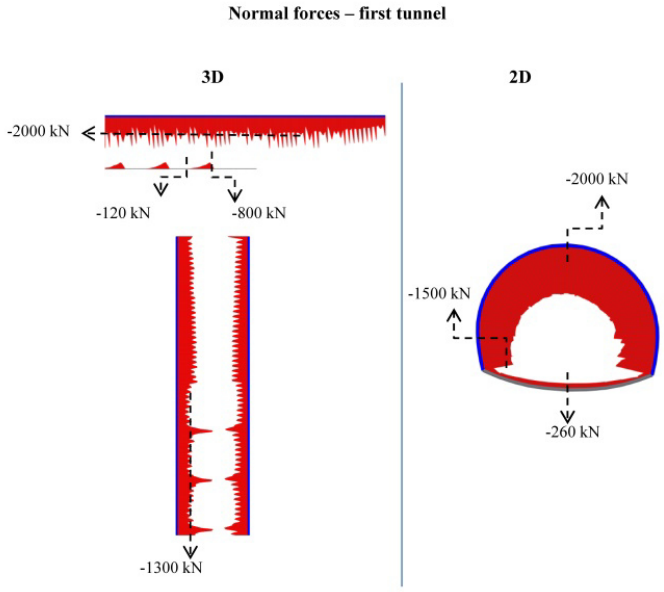

Figure 108. Comparison between axial forces from the 3D and 2D model (first tunnel)

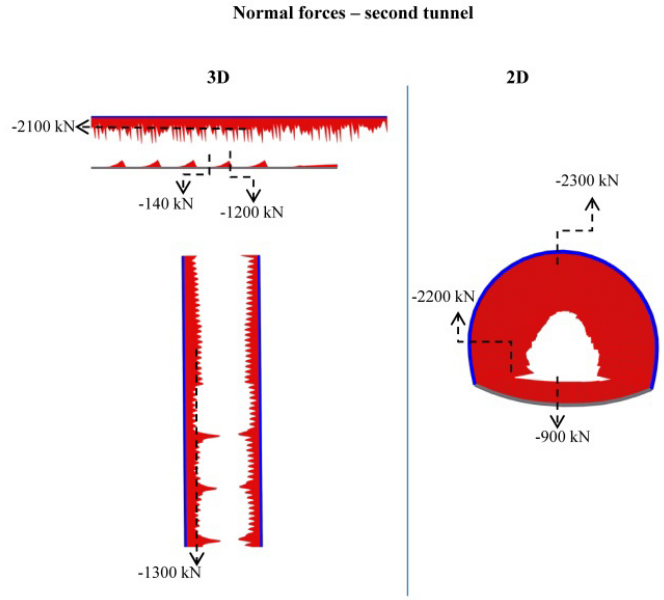

Figure 109. Comparison between axial forces from the 3D and 2D model (second tunnel)

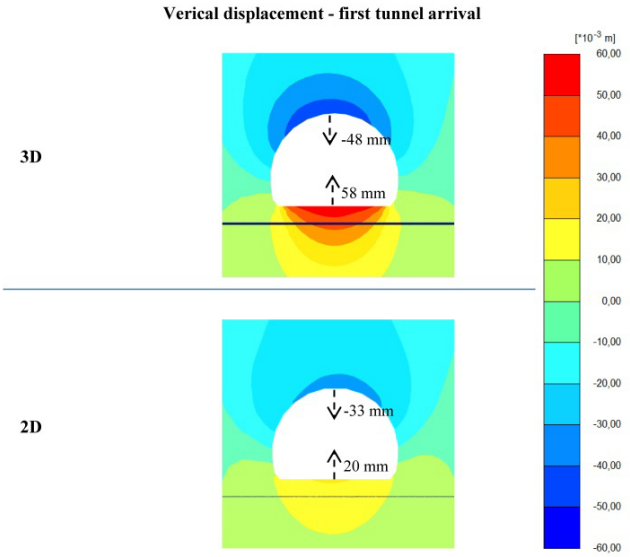

Figure 110. Comparison between vertical displacements from the 3D and 2D model (first tunnel arrival)

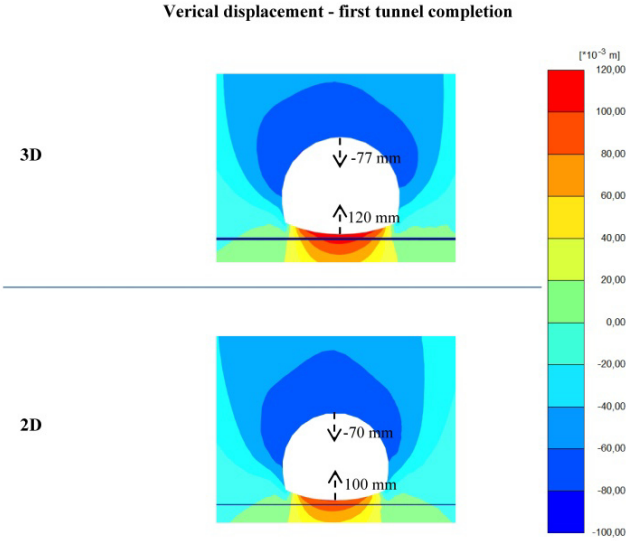

Figure 111. Comparison between vertical displacements from the 3D and 2D model (first tunnel completion)

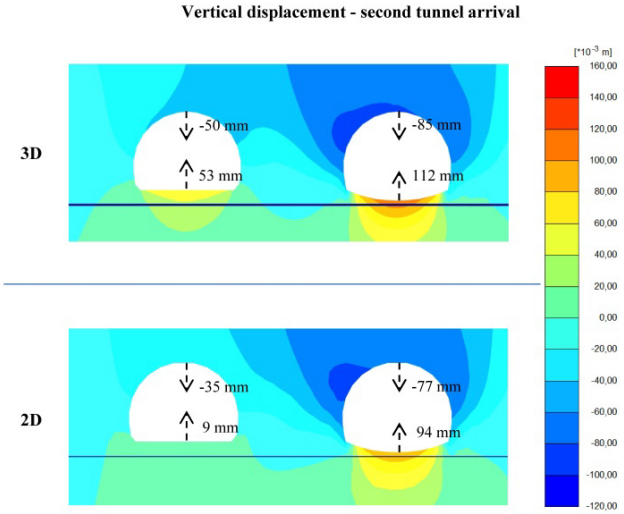

Figure 112. Comparison between vertical displacements from the 3D and 2D model (second tunnel arrival)

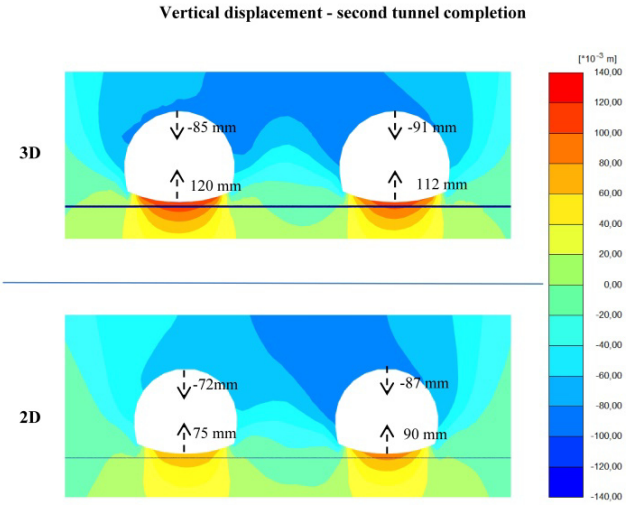

Figure 113. Comparison between vertical displacements from the 3D and 2D model (second tunnel completion)

6.2. Pergola tunnel

Similarly to what has been presented in the previous paragraphs, the monitoring data recorded while excavating the Pergola tunnel have been analysed and compared with numerical results. The total tunnel length is around 500 m, and the maximum overburden is 60 m. The excavation was carried out from both entrances and with the excavation faces of the two carriageways advancing almost contemporarily.
In the present study, to set the numerical model geometry and define the excavation phases, two reference segments were considered. The first goes from chainage 14+250 to chainage 14+280, and it is close to the Southern entrance. The second goes from chainage 14+510 to chainage 14+560, and it is closer to the Northern entrance (Figure 114).

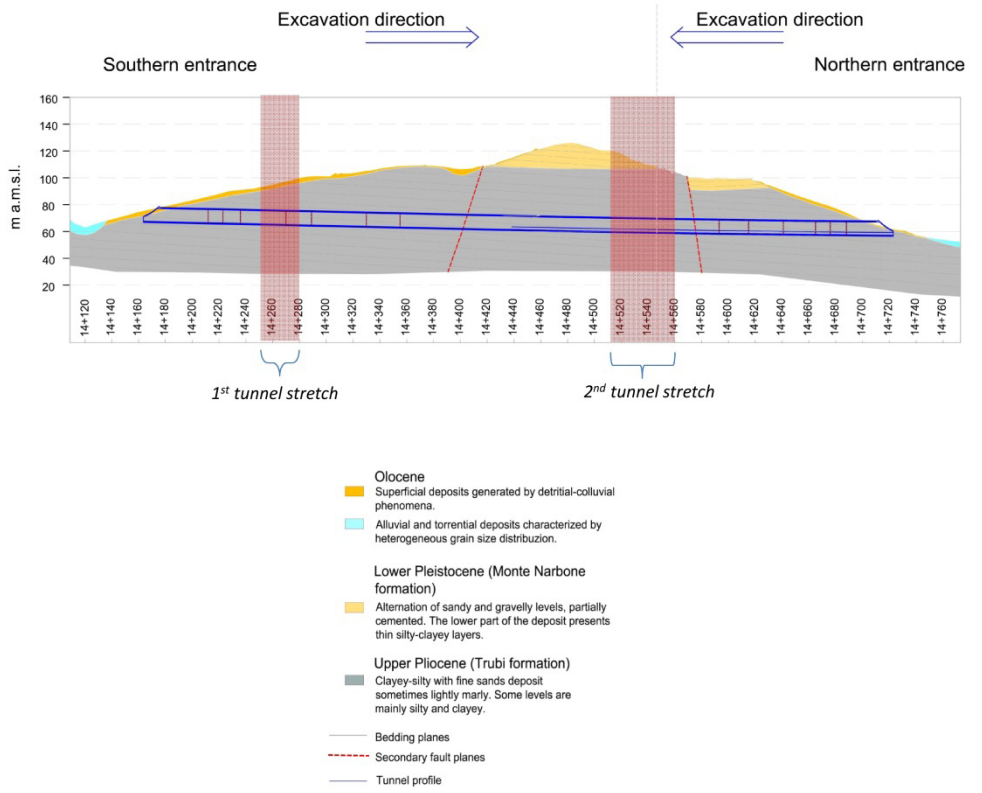

Figure 114. Geological profile of the Pergola tunnel (Northern carriageway)

In this case, as well as for the Trigoni tunnel case, the choice of these stretches is due to the intensified monitoring system adopted, consisting not only of convergence measurements but also of surface settlement measurements and a horizontal incremental extensometer placed between the two tunnels.
From the geological profile shown in Figure 114, both the tubes mainly involved the Trubi formation with overburden varying from around 15 to around 60 m.

6.2.1. Numerical analysis

The numerical calculations, aimed at reproducing the observed behaviour were carried out employing the numerical code Plaxis 3D 2013 **(Brinkgreve et al. 2013)**. Given the different overburden characterising the two considered tunnel stretches, two different models were generated. The first one, close to the Southern entrance, is characterised by an overburden of 20 m and the second one, closer to the Northern entrance, presents an overburden varying from 37 to 48 m. Both the models consist of around 400000 10-noded tetrahedral elements. The first one is 300 m long and 200 m wide corresponding to 23D and 15D respectively, whereas the second one is 300 m long and 250 m wide, corresponding to 23D and 18D respectively (Figure 115). The bottom boundary is around 3D from the tunnel invert. The mesh dimensions satisfy the minimum values suggested by **Möller (2006)**.
Similarly to the previous case study (Trigoni tunnel), the calculation was carried out using the so-called step by step approach **(Katzenbach & Breth 1981)**. Removal of continuum elements at the tunnel face and support activation follow the adopted excavation sequence; excavation length, as well as unsupported span, are equal to 1 m. The model details regarding the primary lining are the same of the numerical model adopted for the Trigoni tunnel (Figure 95, right).

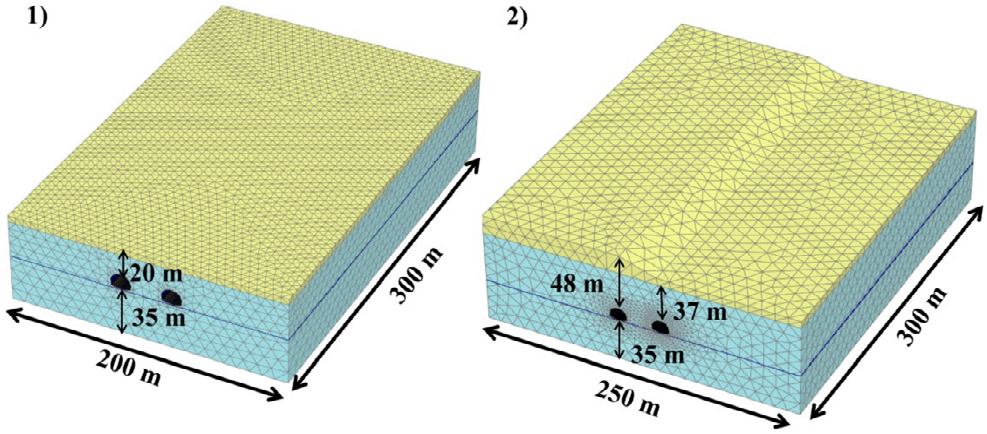

Figure 115. 3D FEM mesh of the model generated for the first stretch (left) and second stretch (right)

Concerning the model fixities, the lateral vertical boundaries are fixed in the horizontal direction whereas the bottom boundary is fixed in both the horizontal and the vertical direction. No fixities were applied to the upper horizontal boundary. As for the Trigoni tunnel model, only in the central 100 m of the model, the real excavation sequence has been simulated. The first 100 m were simulated in 20 phases by removing 5 m thick soil clusters of the tunnel core while simultaneously installing the temporary lining, keeping the cavity completely supported. This procedure allows getting away from the initial vertical boundary, which, similarly to the other boundaries, has a significant influence on the results.

Both the preliminary and the final lining were modelled with linear-elastic plate elements. Since the temporary lining is made of steel sets and sprayed concrete, an equivalent homogeneous section was considered. The final invert was activated at 3D from the tunnel face.

The plate stiffnesses, governed by the thickness and Young's modulus, were defined according to the main steel profile installed in each section. Similarly to the Trigoni tunnel case, coupled IPN 220 profiles were installed in the first stretch and coupled IPN 180 profiles were installed in the second stretch. Therefore, the homogeneous stiffnesses of 2 coupled IPN 220/m and IPN 180/m combined with a shotcrete thickness of 25 cm were adopted respectively (Table 23). The interface between plate elements and surrounding ground is rigid.

Given the results of the previously described parameter calibration and model validation carried out for the Trigoni tunnel, this further attempt of parameter validation was also carried out by using the soil parameters listed in Table 24 and assuming drained conditions.
The initial stress state was generated by applying the so-called k_0-procedure and, for the second model, performing a nil step afterwards to restore equilibrium conditions (the ground surface is not horizontal). The water table is located slightly below the tunnel invert in both models, as shown in Figure 115.

6.2.2. Results and comparison with monitoring data

This model validation, as well as the one carried out by using the monitoring data of the Trigoni tunnel, is mainly based on absolute vertical displacements of the preliminary lining. In fact, they still appear to be less scattered, compared to relative displacements, and more suitable for comparison with numerical calculations (Figure 116). The horizontal displacements and consequently the convergence between sidewalls present a stronger scattering (Figure 117), but the general trend is in accordance with the measurements of vertical displacements. Data with a short measuring time and those with delayed zero readings were disregarded.

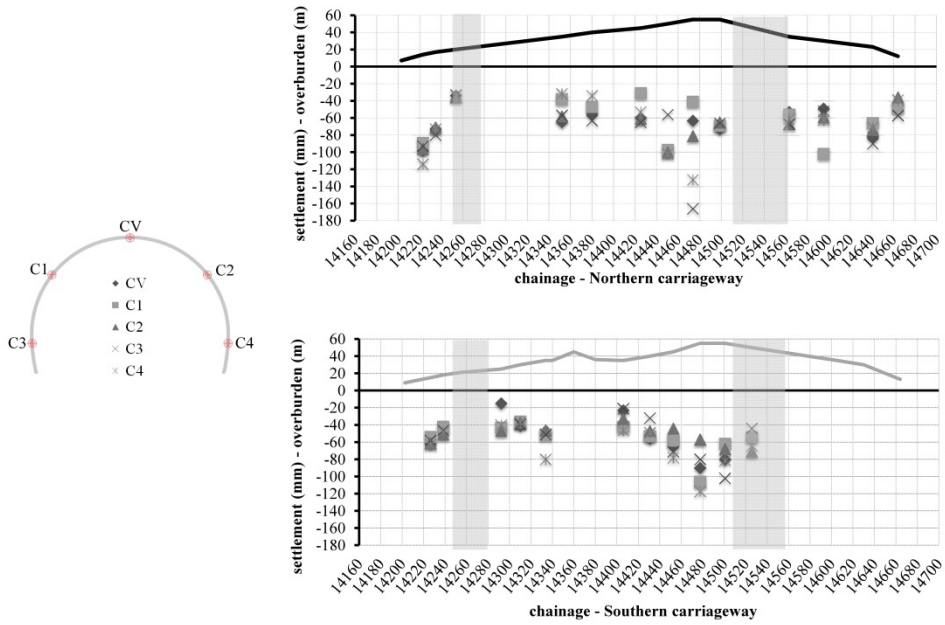

Figure 116. Pergola tunnel: settlements of the temporary lining - measurements

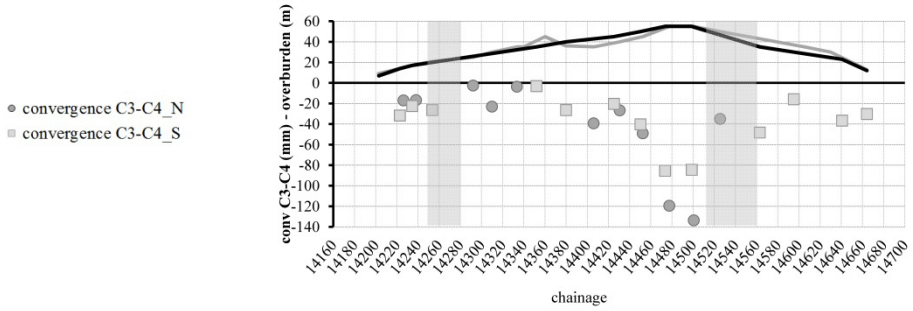

Figure 117. Pergola tunnel: lateral convergences of the temporary lining - measurements

Considering vertical settlements (Figure 116) and the measuring sections close to the analysed stretches, most of the measured values vary between 3.0 and 4.0 cm in the first stretch and between 4.0 and 7.0 in the second stretch, characterised by higher overburden and thus higher stress state.

By elaborating strain gauge measurements, it was possible to obtain some information about the stress state of the steel sets. Strain measurements on both the crown and sidewalls were converted in structural forces by

considering a linear elastic constitutive behaviour for the steel and by multiplying the average stress state for the steel section, as previously explained.
In Figure 118, the calculated normal forces are plotted versus the tunnel chainage.

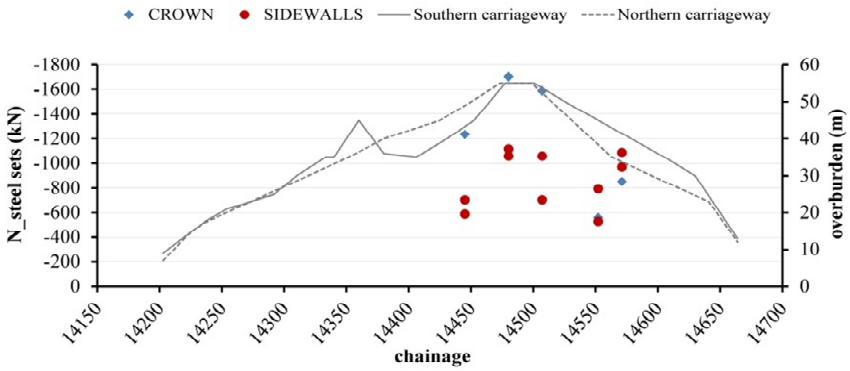

Figure 118. Pergola tunnel: normal forces from strain gauge measurements (compression is negative)

The axial rigidity used to convert strains in structural forces includes two coupled steel sets. It can be observed that these measurements are concentrated in the area with high overburden. The measurements present an average value of around -1200 kN in the crown and -900 kN in the sidewalls. These values are quite close to those recorded for the Trigoni tunnel, in the sections with the highest overburden. In Figure 119 and Figure 120, the results of the calculations carried out with the first and the second model respectively, are represented.

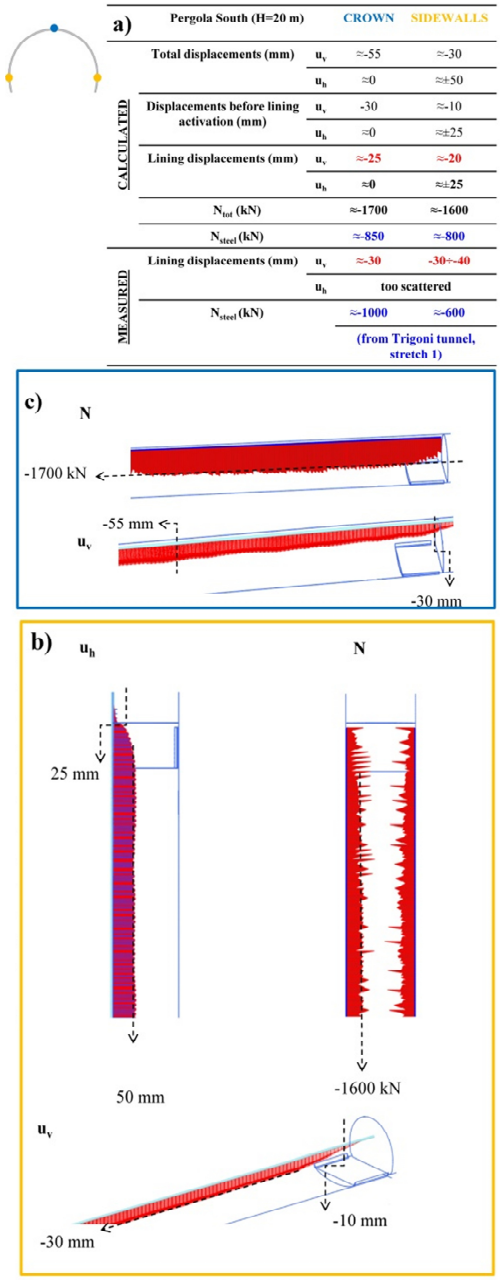

Figure 119. Pergola tunnel, model 1: a) Measured and calculated lining displacements and forces; b) plot of calculated values at the sidewalls; c) plot of calculated values at the crown (first tunnel stretch, first excavated tube)

The vertical displacements of the temporary lining deriving from the FEM simulations seem to slightly underestimate the monitored ones, especially at the sidewalls. However, only few sections covering a significant monitoring time are available in the proximity of the considered stretch. The calculated horizontal displacements are similar to the vertical ones, whereas the monitored horizontal displacements are too scattered for a comparison.
Regarding the computed axial forces, to get the contribution of the only steel sets, it is necessary to divide the total axial forces by 2 and 2.5, when IPN 220 and IPN 180 are adopted respectively. This operation allows to compare them with the monitored ones. However, concerning the first monitoring section here considered, no strain gauges were installed on the primary lining. It is only possible to compare the computed forces with those recorded during the Trigoni tunnel construction under low overburden (Figure 98). Structural forces seem to be slightly overestimated by the numerical model shown in §6.1. However, it should be noted that the strain gauge measurements of the first stretch of the Trigoni tunnel are associated with a slightly higher overburden than that characterising the first stretch of the Pergola tunnel. Therefore an underestimation of the numerical model is expected.
Regarding the second analysed tunnel stretch (Figure 120), measurements and computed values seem to be more consistent. This consideration holds true for both displacements and lining axial forces.

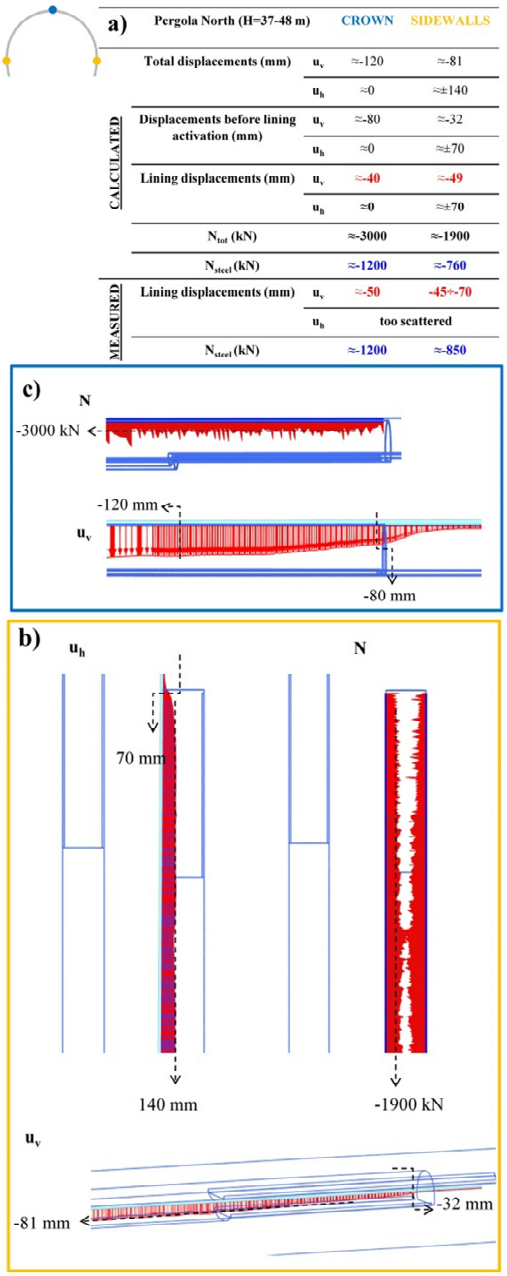

Figure 120. Pergola tunnel, model 2: a) Measured and calculated lining displacements and forces; b) plot of calculated values at the sidewalls; c) plot of calculated values at the crown (second tunnel stretch, first excavated tube)

Concerning the deformation behaviour of the ground surface, two subsidence measurements were carried out within the first tunnel stretch (ch 14260 and ch 14270). The measurements started when both excavation faces were around 20 m before the monitoring chainages. The observed vertical displacements are shown in Figure 121. The computed vertical settlements are quite in good agreement with the measured ones. Only in the central part of the subsidence curve, they seem to be slightly overestimated. This might be due to the presence of pre-existing buildings exactly between the two carriageways. In fact, the presence of structures on the surface usually tends to reduce the magnitude of greenfield settlements.

3D FEM calculations represented once again a valid instrument to simulate the subsidence phenomenon. It would have been difficult to carry out the same analysis with a 2D model, mainly because assumptions on the displacements occurring before the beginning of the monitoring would have been necessary. These hypotheses are not necessary when using 3D models, which allow taking into account the tunnel face position at the beginning and the end of the available monitoring period.

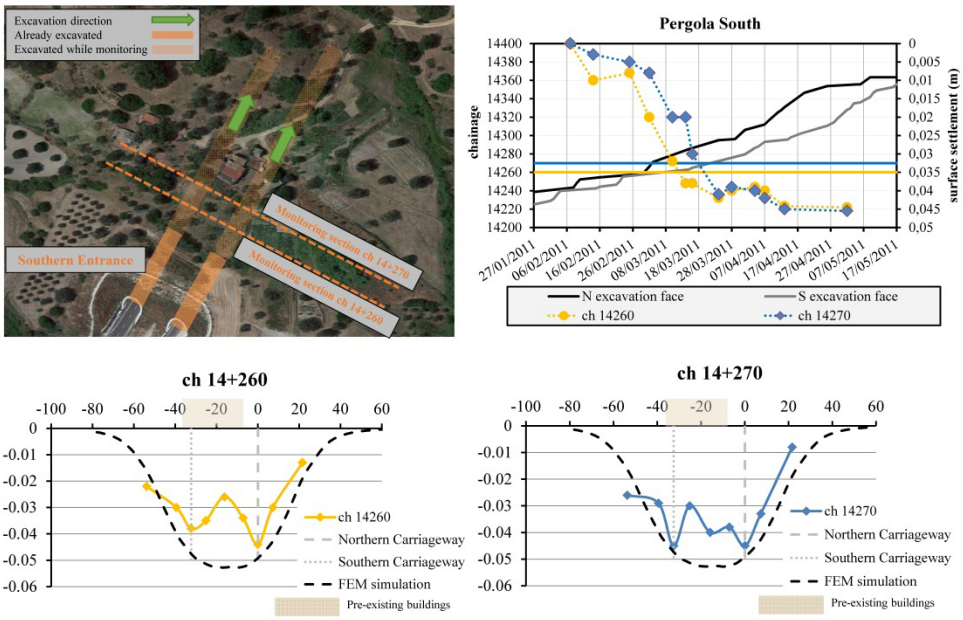

Figure 121. Subsidence monitoring sections at ch 14260 and 14270: measured and calculated settlements. Photo from Google Earth

The horizontal deformations of the second stretch of the Pergola tunnel were also investigated through an incremental extensometer. The measuring tube, equipped with 1 m spaced magnet rings, was horizontally installed between the two tunnels, as shown in Figure 122. The model in the figure also shows that, when the instrument was installed, the Southern tunnel has already been excavated, whereas the Northern one was being excavated from both entrances. These conditions would have been quite difficult to reproduce through a simple 2D model. On the contrary, even though it is quite complicated, it is possible to reproduce these conditions by using a 3D model.

The measuring tube was modelled as an embedded pile in Plaxis 3D. The measurements started when the excavation face of the Northern carriageway was already 5-6 meters beyond the reference chainage (ch 14520). As shown in Figure 123, the model predicts very well both the horizontal displacements along the central soil pillar only if the maximum bond strength is not limited. When the bond strength is limited to 100 kPa, which represents a reasonable value for this kind of soils, the displacements close to the Northern tube are underestimated. Probably, limiting the bond strength along the whole length of the pile is not a realistic hypothesis. This might be due to particularly high-stress conditions occurring close to the tunnel boundaries due to the arching effect and to the presence of a closed lining.

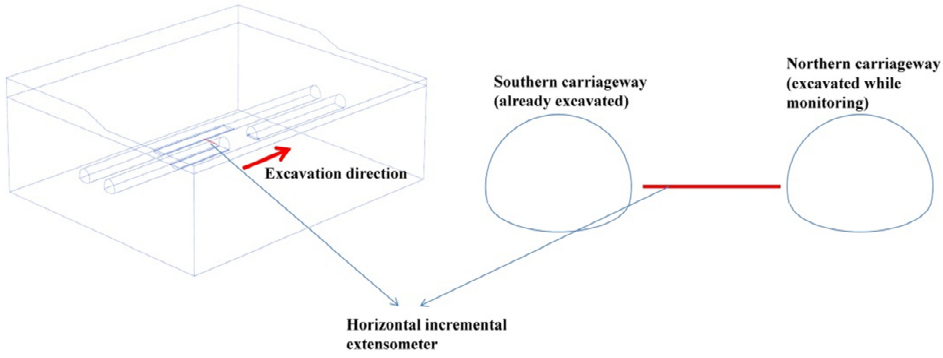

Figure 122. Modelling of the horizontal incremental extensometer through an embedded pile

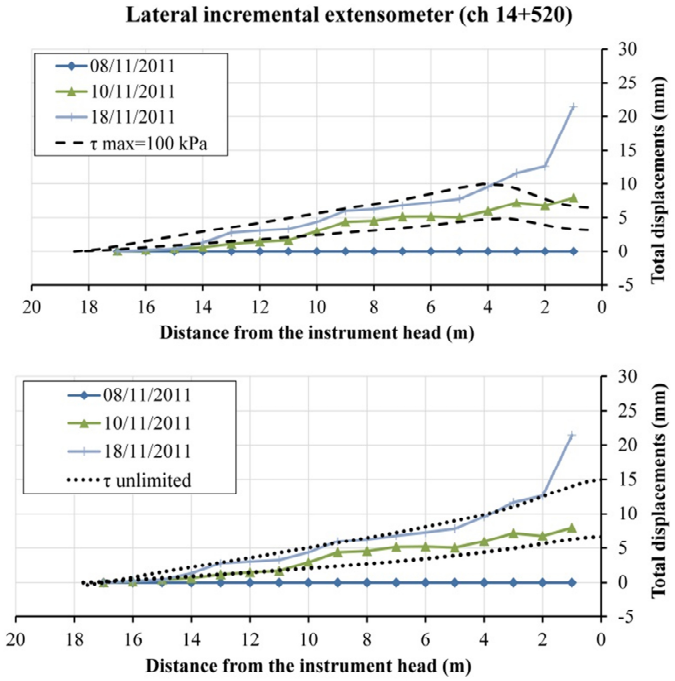

Figure 123. Comparison between measured and computed horizontal displacements (horizontal incremental extensometer at ch 14+520); the dashed lines represent the FEM results

6.3. Concluding remarks

This chapter focused on the numerical analysis of the deformation behaviour of twin tube shallow tunnels. After introducing the case study and carrying out a preliminary parameter calibration (chapter 5), it was possible to validate 3D numerical models through field measurements. The 3D numerical calculations adopted the previously calibrated constitutive model (Hardening Soil Model with Small Strain Stiffness). All the analyses were carried out in drained conditions.

The works involved the excavation of five twin tube tunnels in fine-grained deposits. The monitoring data recorded during the excavation of the Trigoni tunnel and Pergola tunnel were compared with the results of 3D FEM calculations aimed at simulating the real excavation sequence and geometry

along different tunnel stretches. Adopting simple 2D models would have had the advantage of being less time-consuming but also the significant shortcoming of a strong dependence of the results on the so-called stress relaxation factor.
The available tunnel monitoring included subsidence and convergence measurements as well as three incremental extensometers and several strain gauges welded on the steel ribs. The different type of observed phenomena allowed for a full validation of the FEM models. Even though in some cases there is some discrepancy between the observed behaviour and calculation results, the good general agreement shows that a detailed model calibration is a fundamental step to obtain reliable results from numerical analyses. A further adjustment of the model parameters through back-analysis could probably improve the quality of the predictions. Moreover, further comparisons between in situ measurements from other tunnels excavated in the same deposit and numerical simulations could provide an additional verification of the model effectiveness in describing the deformation behaviour of this deposit. Regarding the surface settlements, an important aspect affecting both the subsidence magnitude and the settlement trough shape is the interaction with pre-existing buildings, which was disregarded, however, in the present study.
It should also be considered that the soil stratification and the presence of different families of discontinuities, as suggested by other authors **(Buselli et al. 2013)** might have played a role in the deformation response.

Final conclusions and recommendations

This thesis addressed three of the main issues regarding traditionally excavated shallow tunnels. The identification of these issues and of the possible ways they should be developed was possible thanks to a preliminary analysis of the state of the art concerning shallow tunnels. This analysis entailed a collection of previous works regarding the topic as well as a critical detection of their points of strength and weakness. With respect to the latter, it seemed necessary to further develop the following issues:

1. the evaluation of Eurocodes applicability to a numerically-based design of shallow tunnels, especially when both soil and structure are treated as non-linear materials;
2. the evaluation of tunnel face stability through FEM numerical analyses (for both reinforced and unreinforced excavation faces);
3. the validation of 3D numerical models of twin shallow tunnels through field data, after calibrating the model parameters.

Chapter 1 focused on the technological aspects of traditional underground excavations.

Chapter 2 summarised the state of the art concerning tunnel calculations. In particular, it described the main outcomes of previous works concerning the three previously listed issues.

Chapter 3 showed the results of a calculation example aimed at verifying the applicability of Eurocodes to the design of shallow tunnels. The benchmark tunnel was analysed through a 2D model. The implementation, in Plaxis, of a new shotcrete model provided the possibility to consider plasticity and non-linearity in both the soil and the lining. Comparisons between different design approaches and also between different modelling strategies for the shotcrete allowed to draw the following conclusions:

- in some cases, the adoption of a linear elastic material for modelling the tunnel support leads to considerably higher bending moments when compared to the advanced shotcrete model;
- the benefits, in terms of cost-effectiveness, of a design carried out by using a constitutive model that accounts for the non-linear and time dependent behaviour of shotcrete can be considerable;
- DA2*, in most cases, provided higher internal forces, due to the 1.35 factor on the effect of actions;

- DA3 approach is feasible, in particular when considering the nonlinear material behaviour of both soil and shotcrete, resulting in a consistent (implicit) design, where no M-N check has to be performed;
- a combination of both DA2* and DA3 would achieve the purpose of ensuring a safe design from both a geotechnical and a structural point of view; this goal would be accomplished by concentrating the uncertainties once on the effect of actions and once on the material properties;
- considering non-linearity and plasticity not only in the soil but also in the structural support seems to be a consistent design strategy.

Chapter 4 showed the results of numerical and limit equilibrium calculations regarding both unreinforced and reinforced excavation faces. The numerical analyses exploited the so-called strength reduction technique and were carried out using a 3D FEM program, to take into account the three-dimensionality of the problem and the presence of face bolts. The parametric calculations covered mainly soils characterised by a silty-clayey matrix. In this type of soil, it is very common, at least in Italy and France, to use fibreglass bolts for the tunnel face reinforcement. The calculations concerning unreinforced faces showed that the basic formulation of the LEM method, adopting the Horn mechanism, may significantly overestimate the safety factor. Also the calculations regarding reinforced excavation faces showed that the LEM method overestimates face stability, except for the case of low cohesion and high overlapping length of the bars. An evaluation of the equivalent cohesion needed to obtain the same FoS, without directly modelling the structural elements, is also shown. All these considerations should be kept in mind by tunnel designers, which very often have to exploit simplified models due to very tight design schedules.

By analysing the tunnel face under working conditions (deformation analyses), it was possible to verify the effectiveness of this technique in reducing both extrusion and surface settlements. Also in these conditions equivalent material properties could be evaluated. However, when the deformation behaviour instead of face stability is considered, the equivalent soil properties would depend on many different factors like initial stress state, problem geometry, overburden and soil constitutive model adopted, making general assumptions quite difficult.

Chapter 5 introduced the case study and the parameter calibration carried out before running numerical simulations. The case study involved the excavation of twin tube tunnels in fine-grained deposits in Southern Italy. The chosen constitutive model (Hardening Soil Model with Small Strain Stiffness) was calibrated by exploiting both laboratory and in-situ tests.

Chapter 6 focused on the numerical analysis of the deformation behaviour of twin tube shallow tunnels. The different type of observed phenomena (convergences, subsidence, extensometer measurements) allowed for a full validation of the FEM models, which seemed to well reproduce most of these aspects. The previous model calibration turned out to be fundamental for obtaining such a good match.

Generally speaking, using simplier 2D models instead of time-consuming 3D ones is possible but only after calibrating the so-called stress relaxation factor (λ value). By trial and error, it was possible to find, for one of the reference sections, the λ value that allowed matching some aspects of the 3D model through a 2D one. However, it was observed that a small variation of λ causes strong variations in the computed value. Furthermore, there is no reliable way to find the λ values. In the light of these findings, a good back-analysis or model validation cannot rely on such an arbitrary parameter. Therefore, 3D models should be preferred.

Considering both the state of the art and the outcomes of the present work, some general recommendations can be formulated. First of all, in-situ measurements of stresses and deformations should be used not only for comparison with threshold and alarm values but also for successive adjustment of design hypotheses and for validating the geotechnical parameters. Moreover, engineering judgment and critical evaluations of the results are necessary for analysing such a complex soil-structure interaction problem. Running sensitivity analyses might help in leading the designer to a higher awareness of the critical parameters governing the problem. Tunnel designers should also be aware that some simplified solutions may not be conservative or represent correctly the analysed problem. Therefore, in some cases, running more complex calculations (such as 3D FEM calculations) might be worthwhile.

References

Addenbrooke, T. & Potts, D., 2001. Twin Tunnel Interaction: Surface and Subsurface Effects. *International Journal of Geomechanics*, 1(2), pp.249–271.

Anagnostou, G., 1993. Modeling seepage flow during tunnel excavation. In N. Ribeiroesousa, L and Grossmann, ed. *EUROCK 93, Lisboa, Portugal - Proceedings : safety and environmental issues in rock engineering, vol 1*. rotterdam: a a balkema, pp. 3–9.

Anagnostou, G., 2008. The effect of tunnel advance rate on the surface settlements. In *12th international conference of IACMAG, Goa, India*.

Anagnostou, G. & Kovari, K., 1996. Face stability conditions with earth-pressure-balanced shields. *Tunnelling and Underground Space Technology*, 11(2), pp.165–173.

Anagnostou, G. & Kovari, K., 1994. The face stability of slurry-shield-driven tunnels. *Tunnelling and Underground Space Technology*, 9(2), pp.165–174.

Anagnostou, G. & Serafeimidis, K., 2007. The dimensioning of tunnel face reinforcement. In *Proc. 33rd ITA-AITES World Tunnel Congress WTC*. pp. 291–296.

Augarde, C.E. & Burd, H.J., 2001. Three-dimensional finite element analysis of lined tunnels. *International Journal for Numerical and Analytical Methods in Geomechanics*, 25(3), pp.243–262.

Baguelin, F., 1978. *The pressuremeter and foundation engineering*, Trans Tech public.

Bauduin, C., Bakker, K. & Frank, R., 2005. Use of Finite Element Methods in geotechnical ultimate limit state design. In *Proceedings of the International Conference on Soil Mechanics and Geotechnical Engineering*. aa balkema publishers, p. 2775.

Bauduin, C., Simpson, B. & De Vos, M., 2000. Some considerations on the use of finite element methods in ultimate limit state design. In *Int Workshop on Limit State Design, LSD*.

Benz, T., 2007. *Small-strain stiffness of soils and its numerical consequences. PhD dissertation*, Univ. Stuttgart, Inst. f. Geotechnik.

Bernhard Maidl, Markus Thewes, Ulrich Maidl, D.S.S., 2013. *Handbook of Tunnel Engineering I: Structures and Methods.*

Brinkgreve, R.B.J. et al., 2015. PLAXIS 2015.

Brinkgreve, R.B.J., Engin, E. & Swolfs, W.M., 2014. PLAXIS 2D AE

manual. *Rotterdam, AA Balkema*.
Brinkgreve, R.B.J., Engin, E. & Swolfs, W.M., 2013. Plaxis 3D User Manuals.
Broere, W., 2001. *Tunnel face stability & new CPT applications*, TU Delft, Delft University of Technology.
Broms, B.B. & Bennermark, H., 1967. Stability of clay at vertical openings. *Journal of Soil Mechanics & Foundations Div*.
Buselli, F. et al., 2013. Observations from monitoring of tunnel excavations in clayey silt. In *Underground. The Way to the Future*. CRC Press, pp. 2078–2085.
Clarke, B.G., 1994. *Pressuremeters in geotechnical design*, CRC Press.
Clayton, C.R.I. et al., 2002. The performance of pressure cells for sprayed concrete tunnel linings. *Géotechnique*, 52(2), pp.107–115.
Colombet, G. et al., 2007. Compatibilité des recommandations AFTES relatives aux revêtements des tunnels en béton avec les Eurocodes: Recommandations du Groupe de Travail n° 29. *Tunnels et ouvrages souterrains*, (204), pp.378–390.
Davis, E.H. et al., 1980. The stability of shallow tunnels and underground openings in cohesive material. *Geotechnique*, 30(4), pp.397–416.
Do, N.-A. et al., 2014. Three-dimensional numerical simulation of a mechanized twin tunnels in soft ground. *Tunnelling and Underground Space Technology*, 42, pp.40–51.
Duddeck, H. & Erdmann, J., 1983. Structural design models for tunnels: Tunnelling 82, proceedings of the 3rd international symposium, Brighton, 7–11 June 1982, P83–91. Publ London: IMM, 1982. In *International Journal of Rock Mechanics and Mining Sciences & Geomechanics Abstracts*. Pergamon, p. A15.
Duncan, J.M. & Chang, C.-Y., 1970. Nonlinear analysis of stress and strain in soils. *Journal of Soil Mechanics & Foundations Div*.
Fargnoli, V., Boldini, D. & Amorosi, A., 2015. Twin tunnel excavation in coarse grained soils: Observations and numerical back-predictions under free field conditions and in presence of a surface structure. *Tunnelling and Underground Space Technology*, 49, pp.454–469.
Fillibeck, J. & Vogt, N., 2012. Prediction of tunnel-induced settlements in soft ground. *parameters*, 1, p.T2.
Franzius, J. & Potts, D., 2005. Influence of Mesh Geometry on Three-Dimensional Finite-Element Analysis of Tunnel Excavation. *International Journal of Geomechanics*, 5(3), pp.256–266.

Franzius, J.N., Potts, D.M. & Burland, J.B., 2005. The influence of soil anisotropy and K0 on ground surface movements resulting from tunnel excavation. *Géotechnique*, 55(3), pp.189–199.

Galavi, V. & Schweiger, H.F., 2010. Nonlocal multilaminate model for strain softening analysis. *International Journal of Geomechanics*, 10(1), pp.30–44.

Galli, G., Grimaldi, A. & Leonardi, A., 2004. Three-dimensional modelling of tunnel excavation and lining. *Computers and Geotechnics*, 31(3), pp.171–183.

Grasso, P., Mahtab, A. & Pelizza, S., 1989. Riqualificazione della massa rocciosa: un criterio per la stabilizzazione delle gallerie. *Gallerie e Grandi Opere Sotterranee*, 29(38), pp.35–41.

Hardin, B.O. & Black, W.L., 1969. Closure on vibration modulus of normally consolidated clay. *Journal of Soil Mechanics & Foundations Div*.

Hardin, B.O. & Drnevich, V.P., 1972. Shear modulus and damping in soils: measurement and parameter effects. *Journal of Soil Mechanics & Foundations Div*, 98(sm6).

Heiniö, M., 1999. Rock excavation handbook.

Hellmich, C., Mang, H.A. & Ulm, F.-J., 2001. Hybrid method for quantification of stress states in shotcrete tunnel shells: combination of 3D in situ displacement measurements and thermochemoplastic material law. *Computers & Structures*, 79(22), pp.2103–2115.

Hoek, E., 2001. Big Tunnels in Bad Rock: 2000 Terzaghi Lecture. *ASCE Journal of Geotechnical and Geoenvironmental Engineering*, 127, pp.726–740.

Hoek, E. et al., 2008. The 2008 Kersten Lecture Integration of geotechnical and structural design in tunneling. In *56th Annual Geotechnical Engineering Conference*. pp. 1–53.

Hofmann, R., Suda, J. & Poisel, R., 2010. Interaction of EC7 with EC2 in tunnelling. Interaktion des EC7 mit dem EC2 beim Tunnelbau. *Geomechanics and Tunnelling*, 3(1), pp.11–23.

Horn M., 1961. Horizontaler Erddruck auf senkrechte Abschlussflächen von Tunneln. *Landeskonferenz der ungarischen Tiefbauindustrie, Budapest (German translation, STUVA, Düsseldorf)*.

Horn, M., 1961. Horizontal earth pressure on perpendicular tunnel face. In *Hungarian National Conference of the Foundation Engineer Industry. Budapest.* pp. 7–16.

Hun YEO, C. et al., 2009. Three dimensional numerical modelling of a NATM tunnel. *International Journal of the JCRM*, 5(1), pp.33–38.

Ita Working Group Conventional Tunnelling, 2009. *General Report on Conventional Tunnelling Method*,

ITA, working group on general approaches to the design of tunnels, 1988. Guidelines for the design of tunnels. *Tunnelling and underground space technology*, 3(3), pp.237–249.

Jamiolkowski, M., Lancellotta, R. & Lo Presti, D.C.F., 1995. Remarks on the stiffness at small strains of six Italian clays. In *Pre-failure Deformation of Geomaterials. Proceedings of the International Symposium, 12-14 September 1994, sapporo, Japan. 2 vols*.

Janin, J.P. et al., 2015. Numerical back-analysis of the southern Toulon tunnel measurements: A comparison of 3D and 2D approaches. *Engineering Geology*, 195, pp.42–52.

Janssen HA, 1895. Versuche über Getreidedruck in Silozellen. *Zeitschrift des Vereins deutscher Ingenieure 35: 1045-1049*.

Jones, B.D., 2007. Design of SCL tunnels in soft ground using Eurocodes. *EURO:TUN 2007, ECCOMAS Scientific Conference on Computational Methods in Tunnelling, August 27-29, Vienna, Austria. Vienna University of Technology.*

Kamata, H. & Mashimo, H., 2003. Centrifuge model test of tunnel face reinforcement by bolting. *Tunnelling and Underground Space Technology*, 18(2), pp.205–212.

Karakus, M., 2007. Appraising the methods accounting for 3D tunnelling effects in 2D plane strain FE analysis. *Tunnelling and Underground Space Technology*, 22(1), pp.47–56.

Karakus, M., Ozsan, A. & Ba\csar\ir, H., 2007. Finite element analysis for the twin metro tunnel constructed in Ankara Clay, Turkey. *Bulletin of Engineering Geology and the Environment*, 66(1), pp.71–79.

Katzenbach, R. & Breth, H., 1981. Nonlinear 3-D analysis for NATM in Frankfurt Clay. In *Proceedings of the International Conference on Soil Mechanics and Foundation Engineering, 10th.*

Kavvadas, M. & Prountzopoulos, G., 2009. 3D analyses of tunnel face reinforcement using fibreglass nails. In *Eur: Tun 2009 Conference. Bochum*.

Kolymbas, D., 2005. *Tunnelling and tunnel mechanics: A rational approach to tunnelling*, Springer Berlin Heidelberg.

Lade, P., 2005. Overview of Constitutive Models For Soils. In *Calibration*

of Constitutive Models. American Society of Civil Engineers, pp. 1–34.
Lambe, T.W., 1973. Predictions in soil engineering. *Géotechnique*, 23(2), pp.151–202.
Li, B. et al., 2015. Numerical parametric study on stability and deformation of tunnel face reinforced with face bolts. *Tunnelling and Underground Space Technology*, 47, pp.73–80.
Lunardi, P., 2008. Design and construction of tunnels. *Analysis of controlled deformation in rock and soils (ADECO-RS)*.
Lunardi, P., 2005. Extrusion control of the ground core at the tunnel excavation face as a stabilisation instrument for the cavity. *Gallerie e Grandi Opere Sotterranee – Muir Wood Lecture 2015*.
Lunardi, P., 2000. The design and construction of tunnels using the approach based on the analysis of controlled deformaton in rocks and soils. *Tunnels and Tunnelling*, 1.
Lunardi, P. & Bindi, R., 2004. The evolution of reinforcement of the advance core using fibre-glass elements. *Gluckauf Forschungshefte*, pp.91–100.
Marcher, T. & Jiřičný, F., 2005. ADECO RS versus NATM – A 3D numerical study. *Tunel*.
Mašín, D., 2009. 3D Modeling of an NATM Tunnel in High K0 Clay Using Two Different Constitutive Models. *Journal of Geotechnical and Geoenvironmental Engineering*, 135(9), pp.1326–1335.
Mašin, D. & Herle, I., 2005. Numerical analyses of a tunnel in London clay using different constitutive models. In *Proceedings of the 5th international symposium TC28 geotechnical aspects of underground construction in soft ground, Amsterdam, The Netherlands*. pp. 595–600.
Möller, S.C., 2006. *Tunnel induced settlements and structural forces in linings*, Univ. Stuttgart, Inst. f. Geotechnik.
Negro, A. & Queiroz, P.I.B., 2000. Prediction and performance: A review of numerical analyses for tunnels. *Geotechnical Aspects of Underground Construction in Soft Ground*, pp.409–418.
Ng, C.W.W. & Lee, G.T.K., 2002. A three-dimensional parametric study of the use of soil nails for stabilising tunnel faces. *Computers and Geotechnics*, 29(8), pp.673–697.
Ng, C.W.W., Lee, K.M. & Tang, D.K.W., 2004. Three-dimensional numerical investigations of new Austrian tunnelling method (NATM) twin tunnel interactions. *Canadian Geotechnical Journal*, 41(3),

pp.523–539.
Obrzud, R.F. & Eng, G.C., 2010. On the use of the Hardening Soil Small Strain model in geotechnical practice. *Numerics in Geotechnics and Structures*.
Ohde, J., 1939. *Zur theorie der druckverteilung im baugrund*,
Oreste, P., 2009. The convergence-confinement method: roles and limits in modern geomechanical tunnel design. *American Journal of Applied Sciences*, 6(4), p.757.
Oreste, P., 2011. The stability of the excavation face of shallow civil and mining tunnels. *Acta Geotechnica Slovenica*, 8(2), pp.57–65.
Oreste, P.P., 2009. Face stabilisation of shallow tunnels using fibreglass dowels. *Proceedings of the Institution of Civil Engineers-Geotechnical Engineering*, 162(2), pp.95–109.
Oreste, P.P. & Dias, D., 2012. Stabilisation of the excavation face in shallow tunnels using fibreglass dowels. *Rock mechanics and rock engineering*, 45(4), pp.499–517.
Panet, M. & Guenot, A., 1983. Analysis of convergence behind the face of a tunnel: Tunnelling 82, proceedings of the 3rd international symposium, Brighton, 7--11 June 1982, P197--204. Publ London: IMM, 1982. In *International Journal of Rock Mechanics and Mining Sciences & Geomechanics Abstracts*. p. A16.
Pang, C.H., Yong, K.Y. & Dasari, G.R., 2005. Some considerations in finite element analysis of tunneling. *Underground Space Use: Analysis of the Past and Lessons for the Future, ITA-AITES, Turkey*.
Peck, R.B., 1969. Deep excavations and tunnelling in soft ground. In *Proc. 7th int. conf. on SMFE*. pp. 225–290.
Perazzelli, P. & Anagnostou, G., 2012. Comparing the limit equilibrium method and the numerical stress analysis method of tunnel face stability assessment. *Geotechnical Aspects of Underground Construction in Soft Ground*, p.463.
Potts, D., 2002. *Guidelines for the use of advanced numerical analysis*, Thomas Telford.
Potts, D. & Zdravkovic, L., 2012. Accounting for partial material factors in numerical analysis. *Géotechnique*, 62(12), p.1053.
Puzrin, A.M., Addenbrooke, T.I. & Potts, D.M., 1997. The influence of pre-failure soil stiffness on the numerical analysis of tunnel construction. *Géotechnique*, 47(3), pp.693–712.
RBJ Brinkgreve, 2006. The relevance of small-strain soil stiffness in

numerical simulation of excavation and tunnelling projects. In *Numerical Methods in Geotechnical Engineering*. Taylor & Francis, pp. 133–139.

Rokahr, R. & Zachow, R., 1997. Ein neues Verfahren zur täglichen Kontrolle der Auslastung einer Spritzbetonschale [A new method for the daily monitoring of the stress intensity of a sprayed concrete lining]. *Felsbau*, 15(6), pp.430–434.

Rott, J. et al., 2015. 3D FEM analysis of a NATM tunnel with shotcrete lining homogenization and stiffness anisotropy. In *Geotechnical Engineering for Infrastructure and Development - Proceedings of the XVI European Conference on Soil Mechanics and Geotechnical Engineering, ECSMGE 2015*. ICE Publishing, pp. 3723–3727. Available at: http://www.scopus.com/inward/record.url?eid=2-s2.0-84964475916&partnerID=tZOtx3y1.

Ruse, N.M., 2004. *Räumliche betrachtung der standsicherheit der ortsbrust beim tunnelvortrieb*, Institut für Geotechnik.

S. Amar, B.G. Clarke, M.P. Gambin, T.L.L.O., 1991. The Application of Pressuremeter Test Results to Foundation Design in Europe. *A-state-of-the-art Report by ISSMFE European Technical Committee on Pressuremeters, Part I: Predrilled Pressuremeters and Self-Boring Pressuremeters. Balkema, Rotterdam*.

Dos Santos, J.A. & Correia, A.G., 2001. Reference threshold shear strain of soil. Its application to obtain a unique strain-dependent shear modulus curve for soil. In *Proceedings of the Fifteenth International Conference on Soil Mechanics and Geotechnical Engineering, Istanbul, Turkey, 27-31 August 2001. Volumes 1-3.* AA Balkema, pp. 267–270.

Schaedlich, B. et al., 2014. Application of a Novel Constitutive Shotcrete Model to Tunneling. In *ISRM Regional Symposium-EUROCK 2014*. International Society for Rock Mechanics.

Schaedlich, B. & Schweiger, H.F., 2014. A new constitutive model for shotcrete. *Numerical Methods in Geotechnical Engineering*, p.103.

Schanz, T., Vermeer, P.A. & Bonnier, P.G., 1999. The hardening soil model: formulation and verification. *Beyond 2000 in computational geotechnics*, pp.281–296.

Schmidt, B., 1969. *Settlements and ground movements associated with tunneling in soil. PhD Thesis*, University of Illinois.

Schubert, W., 1996. Dealing with squeezing conditions in Alpine tunnels. *Rock Mechanics and Rock Engineering*, 29(3), pp.145–153.

Schubert, W., 2010. Is the OeGG guideline for geotechnical design compatible with the EC7? *Geomechanics and Tunnelling*, 3(1), pp.73–76.

Schubert, W., Grossauer, K. & Button, E.A., 2004. Interpretation of displacement monitoring data for tunnels in heterogeneous rock masses. *International Journal of Rock Mechanics and Mining Sciences*, 41, pp.882–887.

Schubert, W. & Moritz, B., 1998. Controllable ductile support system for tunnels in squeezing rock. *Felsbau*, 16(4), pp.224–227.

Schubert, W. & Moritz, B., 2011. State of the art in evaluation and interpretation of displacement monitoring data in tunnels/Stand der Auswertung und interpretation von verschiebungsmessdaten bei tunneln. *Geomechanics and Tunnelling*, 4(5), pp.371–380.

Schubert, W. & Radoncic, N., 2015. Tunnelling in "Squeezing" Ground Conditions–Problems and Solutions. In *13th ISRM International Congress of Rock Mechanics*. International Society for Rock Mechanics.

Schweiger, H., 2005. Application of FEM to ULS design (Eurocodes) in surface and near surface geotechnical structures. In *Proc. 11th Int. Conf. Computer Methods and Advances in Geomechanics*.

Schweiger, H., 2009. Influence of constitutive model and EC7 design approach in FEM analysis of deep excavations. In *Proceeding of ISSMGE International Seminar on Deep Excavations and Retaining Structures, Budapest*. pp. 99–114.

Schweiger, H., 2010. Numerical analysis of deep excavations and tunnels in accordance with EC7 design approaches. In *Proc. Int. Conf. Geotechn. Challenges in Megacities, Moskau*.

Schweiger, H.F., 2014. Influence of EC7 design approaches on the design of deep excavations with FEM. *geotechnik*, 37(3), pp.169–176.

Schweiger, H.F., 2008. The Role of Advanced Constitutive Models in Geotechnical Engineering. *Geomechanik und Tunnelbau*, 1(5), pp.336–344.

Schweiger, H.F., Marcher, T. & Nasekhian, A., 2010. Nonlinear FE-analysis of tunnel excavation–comparison of EC7 design approaches. *Geomechanics and Tunnelling*, 3(1), pp.61–67.

Schweiger, H.F. & Mayer, P.M., 2004. FE-analysis of reinforced tunnel face. *Felsbau*, 22(4), pp.47–51.

Segato, D. et al., 2015. Excavation works in stiff jointed clay material:

examples from the Trubi formation, southern Italy. *Landslides*, 12(4), pp.721–730. Available at: http://dx.doi.org/10.1007/s10346-014-0505-x.

Segato, D. & Scarpelli, G., 2006. Morphological effects on settlements induced by shallow tunnelling. In *Numerical Methods in Geotechnical Engineering: Sixth European Conference on Numerical Methods in Geotechnical Engineering (Graz, Austria, 6-8 September 2006)*. p. 299.

Shibuya, S., Hwang, S.C. & Mitachi, T., 1997. Elastic shear modulus of soft clays from shear wave velocity measurement. *Geotechnique*, 47(3), pp.593–601.

Simpson, B., 2007. Approaches to ULS design–The merits of Design Approach 1 in Eurocode 7. In *ISGSR2007 First International Symposium on Geotechnical Safety & Risk, Oct. 18-19, 2007 Shangai Tongji University, China*. pp. 527–538.

Simpson, B., 2000. Partial factors: where to apply them. In *Proceedings of the LSD 2000: International Workshop on Limit State Design in Geotechnical Engineering*. Citeseer, pp. 125–136.

Simpson, B. & Junaideen, S., 2013. Use of Numerical Analysis with Eurocode 7. In *Proc. Int. Conf. Advances in Geotechnical Infrastructure. Geotechnical Society of Singapore (GeoSS). Research Publishing*.

Sloan, S.W., 2013. Geotechnical stability analysis. *GEOTECHNIQUE*, 63(7), pp.531–572.

Soga, K., Mohamad, H. & Bennett, P.J., 2008. Distributed fiber optics strain measurements for monitoring geotechnical structures.

Soos, P. von & Bohac, J., 2001. Properties of soils and rocks and their laboratory determination. *Geotechnical Engineering Handbook, Ernst und Sohn, Berlin*, pp.116–206.

Svoboda, T. & Masin, D., 2011. Comparison of displacement field predicted by 2D and 3D finite element modelling of shallow NATM tunnels in clays. *geotechnik*, 34(2), pp.115–126.

Tatiya, R., 2005. *Civil excavations and tunnelling*, Thomas Telford Publishing. Available at: http://www.icevirtuallibrary.com/doi/abs/10.1680/ceat.33405.

Tschuchnigg, F. & Schweiger, H.F., 2015. Performance of strength reduction finite element techniques for slope stability problems. In *Slopes and Geohazards*. pp. 1687–1692. Available at: http://www.icevirtuallibrary.com/doi/abs/10.1680/ecsmge.60678.vol4.

250.
Tschuchnigg, F., Schweiger, H.F. & Sloan, S.W., 2015. Slope stability analysis by means of finite element limit analysis and finite element strength reduction techniques. Part I: Numerical studies considering non-associated plasticity. *Computers and Geotechnics*, 70, pp.169–177.
Vardanega, P. & Bolton, M., 2013. Stiffness of Clays and Silts: Normalizing Shear Modulus and Shear Strain. *Journal of Geotechnical and Geoenvironmental Engineering*, 139(9), pp.1575–1589.
Vermeer, P.A., Bonnier, P.G. & Möller, S.C., 2002. On a smart use of 3D-FEM in tunnelling. In *Proceeding of eighth international symposium on numerical models in geomechanics*. pp. 361–6.
Vermeer, P.A. & Langen, H., 1989. Soil collapse computations with finite elements. *Ingenieur-Archiv*, 59(3), pp.221–236. Available at: http://link.springer.com/10.1007/BF00532252 [Accessed May 31, 2016].
Vermeer, P.A., Ruse, N. & Marcher, T., 2002. Tunnel heading stability in drained ground. *Felsbau*, 20(6), pp.8–18.
Vucetic, M. & Dobry, R., 1991. Effect of soil plasticity on cyclic response. *Journal of geotechnical engineering*, 117(1), pp.89–107.
Walter, H., 2007. Implicit ULS Design using Advanced Constitutive Laws within the Framework of Eurocode 7. In *ECCOMAS Thematic Conference on Computational Methods in Tunnelling (EURO: TUN 2007), Vienna, Austria*.
Walter, H., 2010. Safety concepts in geotechnical engineering then and now–how do the Eurocodes affect tunnelling? *Geomechanics and Tunnelling*, 3(1), pp.24–33.
Yoo, C., 2002. Finite-element analysis of tunnel face reinforced by longitudinal pipes. *Computers and Geotechnics*, 29(1), pp.73–94.
Yoo, C. & Shin, H.-K., 2003. Deformation behaviour of tunnel face reinforced with longitudinal pipes—laboratory and numerical investigation. *Tunnelling and Underground Space Technology*, 18(4), pp.303–319.
Zenti, C.L. et al., 2012. Technical solutions for soil nails in tunnel face reinforcement and drainage. In *Proc. 38th ITA-AITES World Tunnel Congress WTC*.
Zenti, C.L. & Cullaciati, A., 2016. Semi-automatic tubular steel arch support. *TunnelTalk*.
Zenti, C.L. & Perlo, R., 2015. Comparison on different design approaches

applied to a New Tunnel Lining System reinforced by Tubular Arch.

Appendix A. Some details of the used FEM numerical code (Plaxis)

A.1. FEM formulation

The calculation programs used in this thesis (Plaxis 2D AE, Plaxis 2D 2015 and Plaxis 3D 2013) are based on the Finite Element Method. This paragraph provides a brief description of the software basic equations and some calculation details regarding the iterative procedure.

The implemented formulation is founded on a displacement-based finite element solution, where the equilibrium condition is expressed through the principle of virtual works. This principle states that, in order to fulfil the equilibrium condition, the internal work should be equal to the total external work, for any compatible small virtual displacements and can be expressed by the following equation:

$$\int \boldsymbol{\delta \underline{\varepsilon}^{t} \underline{\sigma} dV} = \int \boldsymbol{\delta \underline{u}^{t} \underline{b} dV} + \int \boldsymbol{\delta \underline{u}^{t} \underline{t} dS}$$

Provided that the actual stress state can be written as the sum of the previous stress state and the stress increment

$$\boldsymbol{\underline{\sigma}^{i} = \underline{\sigma}^{i-1} + \Delta \underline{\sigma}}$$

the virtual work equation can be written as

$$\int \boldsymbol{\delta \underline{\varepsilon}^{t} \Delta \underline{\sigma} dV} = \int \boldsymbol{\delta \underline{u}^{t} \underline{b}^{i} dV} + \int \boldsymbol{\delta \underline{u}^{t} \underline{t}^{i} dS} - \int \boldsymbol{\delta \underline{\varepsilon}^{t} \underline{\sigma}^{i-1} dV}$$

where the unknown initial stress does not appear.

The whole problem is discretised into a finite number of continuum elements or volume elements connected to each other through nodes. Depending on the dimensions involved in the problem and on the boundary conditions, it is possible to associate a displacement vector ($\underline{v}$) to each node. The displacements within each element ($\underline{u}$) are obtained by interpolating the node displacements through the shape functions ($\underline{\underline{N}}$) and therefore

$$\underline{\boldsymbol{\varepsilon}} = \underline{\underline{\mathbf{L}}} \cdot \underline{\mathbf{u}} = \underline{\underline{\mathbf{L}}} \cdot \underline{\underline{\mathbf{N}}} \cdot \underline{\mathbf{v}} = \underline{\underline{\mathbf{B}}} \cdot \underline{\mathbf{v}}$$

Where $\underline{\underline{L}}$ is the differential operator and $\underline{\underline{B}} = \underline{\underline{L}} \cdot \underline{\underline{N}}$.
This equation allows rewriting the equilibrium condition in a discretized form. This means that only node displacements appear in the equation:

$$\int \delta\underline{\mathbf{v}}^{\mathbf{T}}\underline{\underline{\mathbf{B}}}^{\mathbf{T}}\Delta\underline{\boldsymbol{\sigma}}\mathbf{dV} = \int \delta\underline{\mathbf{v}}^{\mathbf{T}}\underline{\underline{\mathbf{N}}}^{\mathbf{T}}\underline{\mathbf{b}}^{\mathbf{i}}\mathbf{dV} + \int \delta\underline{\mathbf{v}}^{\mathbf{T}}\underline{\underline{\mathbf{N}}}^{\mathbf{T}}\underline{\mathbf{t}}^{\mathbf{i}}\mathbf{dS} - \int \delta\underline{\mathbf{v}}^{\mathbf{T}}\underline{\underline{\mathbf{B}}}^{\mathbf{T}}\underline{\boldsymbol{\sigma}}^{\mathbf{i-1}}\mathbf{dV}$$

Eliminating the node displacements, which appear in all the integrals, the final equation is:

$$\int \underline{\underline{\mathbf{B}}}^{\mathbf{T}}\Delta\underline{\boldsymbol{\sigma}}\mathbf{dV} = \int \underline{\underline{\mathbf{N}}}^{\mathbf{T}}\underline{\mathbf{b}}^{\mathbf{i}}\mathbf{dV} + \int \underline{\underline{\mathbf{N}}}^{\mathbf{T}}\underline{\mathbf{t}}^{\mathbf{i}}\mathbf{dS} - \int \underline{\underline{\mathbf{B}}}^{\mathbf{T}}\underline{\boldsymbol{\sigma}}^{\mathbf{i-1}}\mathbf{dV}$$

When plastic behaviour is involved, both elastic and plastic deformations have to be considered. The constitutive relation can be written as:

$$\Delta\underline{\boldsymbol{\sigma}} = \underline{\underline{\mathbf{D}}}^{\mathbf{e}} \cdot (\Delta\underline{\boldsymbol{\varepsilon}} - \Delta\underline{\boldsymbol{\varepsilon}}^{\mathbf{p}})$$

Where $\underline{\underline{D}}^{e}$ is the elastic material matrix (representing Hook's law) corresponding to the current stress increment and $\Delta\underline{\varepsilon} - \Delta\underline{\varepsilon}^{p}$ is the elastic strain increment calculated as difference between the total strain increment and the plastic strain increment. The total strain increment is calculated from the nodes displacements through the strain interpolation matrix ($\underline{\underline{B}}$).

The plastic strain increment is calculated through the following equation:

$$\Delta\underline{\boldsymbol{\varepsilon}}^{\mathbf{p}} = \Delta\boldsymbol{\lambda}\left(\frac{\partial \mathbf{g}}{\partial \underline{\boldsymbol{\sigma}}}\right)^{\mathbf{i}}$$

Where $\Delta\lambda$ is the increment of plastic multiplier, derived from the yield condition $f(\underline{\sigma}^{i})=0$, and g is the plastic potential function. The so-written

equation implies the adoption of an implicit integration scheme to locally integrate stresses. In fact, while explicit integration methods involves a direct computation exploiting the stress state of the previous step (i-1), the implicit method is based on the current stress state and requires the solving of simultaneous equations.
Non-linear hardening models such as the Hardening Soil Model require an iterative procedure for calculating the increment of the plastic multiplier ($\Delta\lambda$). In this case, a Newton-type procedure, requiring the fulfilment of a convergence criterion, is adopted. The equilibrium stress, calculated during the previous iteration from the external forces, should get as close as possible (depending on the tolerance) to the constitutive stress. The latter is calculated starting from a trial stress and applying a plastic correction through a so-called return mapping algorithm. The trial stress correspond to the elastic stress, calculated by assuming a purely elastic strain increment as follows:

$$\underline{\sigma}^{i}_{trial} = \underline{\sigma}^{i-1} + \underline{\underline{D}}^{e} \cdot \Delta\underline{\varepsilon}$$

If the trial stress does not violate the yield condition, then it corresponds to the actual stress. On the contrary, if $f(\underline{\sigma}^{trial})>0$ the plastic corrector should be applied to map the point back to the yield surface.

$$\underline{\sigma}^{i,j} = \underline{\sigma}^{trial} - \Delta\lambda\underline{\underline{D}}^{e}\left(\frac{\partial g}{\partial \underline{\sigma}}\right)^{i}$$

where j=1,2,…,n indicates the global iteration. The so-calculated stress represents the constitutive stress, from which, through an integration procedure, it is possible to obtain the vector of internal forces

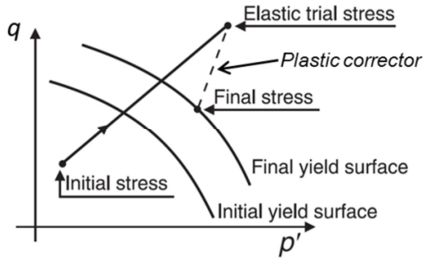

Figure 124. Graphical representation of a return mapping algorithm (modified after Potts 2002)

A certain number of global iterations (j=1,2,…,n) is necessary when dealing with non-linear materials. The relation between material stiffness matrix and global stiffness matrix can be written as follows:

$$\underline{\underline{\mathbf{K}}} = \int \underline{\underline{\mathbf{B}}}^{\mathbf{T}}\, \underline{\underline{\mathbf{D}}}\, \underline{\underline{\mathbf{B}}}\, \mathbf{dV}$$

Neither the soil stiffness matrix nor the global stiffness matrix is known beforehand. The global iterative procedure involves a modified Newton-Raphson scheme.
For each incremental step Δf^i, in which the total load is divided, the global iteration process (j=1,2,…,n) can be written as:

$$\mathbf{\Delta v^i} = \sum_{\mathbf{j=1}}^{\mathbf{n}} \mathbf{\delta v^j}; \qquad \underline{\underline{\mathbf{K}}}^{\mathbf{j}} \cdot \mathbf{\delta v^j} = \Delta \mathbf{f^j} = \mathbf{f_{ext}^i} - \mathbf{f_{in}}$$

The modified Newton-Raphson integration scheme corresponds, for the first iteration, to the tangent stiffness method. Afterwards, a constant global stiffness matrix is assumed for each iteration ($\underline{\underline{K}}^j = \underline{\underline{K}}^i$). The incremental displacements, calculated through the previous equations, are used to recalculate the unbalanced force Δf^j at each iteration. The iterations proceed until both the global and local convergence criteria are satisfied. The global criterion is described by the following inequality:
$|\Delta\, \mathrm{f_j}|/(\Sigma|\text{active loads}| + \text{CSP}\ |\text{inactive loads}|) < \text{tolerance}$

where CSP is the Stiffness parameter and represents the amount of plasticity occurring during the calculation ($CSP = \int \frac{\Delta\varepsilon \cdot \Delta\sigma}{\Delta\varepsilon \cdot D^e \Delta\varepsilon}$).
The local criterion is described by the following inequality:
$|\sigma_c - \sigma_{eq}| / |T_{max}|$
where T_{max} represents the maximum value of shear stress. The local error check represents a further check concerning the error at each stress point. In Figure 125, a calculation scheme is presented to summarise the iterative procedures and the corresponding error checks.

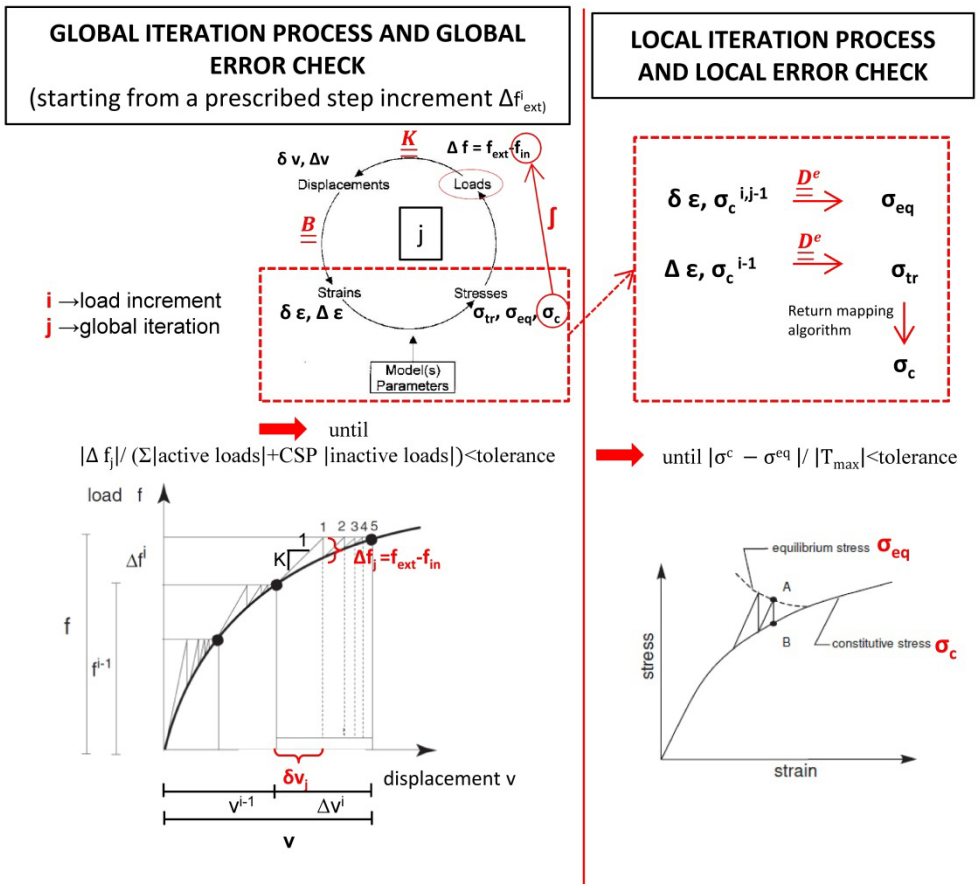

Figure 125. Scheme of the global and local iteration procedures

A.2. Accuracy of the FEM calculation

The accuracy of the calculation, from a numerical point of view, depends mainly on the tolerance criteria adopted and on the mesh refinement.
As already highlighted by **Moller (2006)** the tolerance required to the FEM calculation procedure, has an important effect especially on the accuracy of the calculated displacements. On the contrary, it results less important for the magnitude of the calculated forces on structural elements. However, as underlined in the thesis, especially for 3D models, the mesh refinement can have a remarkable influence on the quality of the structural forces profiles. A good compromise should be reached between accuracy and computational time, being these two inversely proportional.
In Plaxis, the convergence procedure is ruled by both the global and local error. The adoption of both criteria allows, for very large meshes where the unbalanced force is normally much smaller than the total external forces, to guarantee an accurate solution. Default values of tolerance are set to 1%, and the global tolerance coincides with the local one.
Regarding the local iteration, besides the fulfilment of the local tolerance, two further criteria must be fulfilled before ending the iteration process:

$$Number\ of\ inaccurate\ soil\ points \leq 3 + \frac{Number\ of\ plastic\ soil\ points}{10}$$

$$Number\ of\ inaccurate\ interface\ points \leq 3 + \frac{Number\ of\ plastic\ interface\ points}{10}$$

The mesh influence is strictly related to the specific problem. Problems involving considerable stress concentrations like tunnel supported with open arch lining, pile foundations, anchors, etc. might suffer from a certain mesh dependency. In these cases, the mesh refinement should be higher where high stress gradients are expected.
A special tool enabling a more precise as well as a faster (in most cases) calculation is the arc-length control procedure (Figure 126). In particular, the improvement in the calculation precision is remarkable when failure is approached. Therefore for failure analyses, it should always be used.

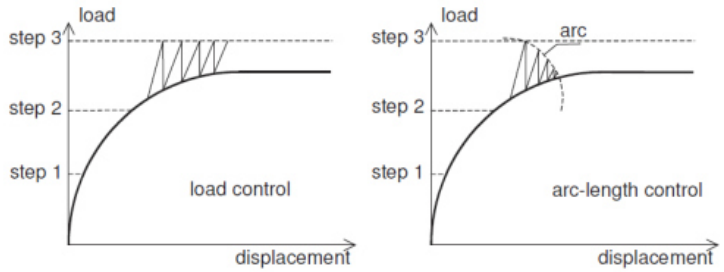

Figure 126. Normal load control (left) and arc-length control (right), from Brinkgreve et al. (2014)

The arc-length control is combined with the automatic failure detection that assumes failure when the load has to be decreased in 5 successive steps. In this case, failure is assumed, and the calculation stops. However, it might happen that the failure detected is just a local mechanism and not a global failure. If the user, after checking the calculation output, realises that the detected failure mechanism is not geotechnically relevant and excessive displacements do not occur, a possible option is to increase the number of unloading steps to enable a further stress redistribution.

Appendix B. Hardening Soil Model

A constitutive relation is a description of the material behaviour connecting stresses and strains and therefore providing a link between equilibrium and compatibility. It is implemented in a FEM software through equations involving stresses, strains and state variables.
The Hardening Soil Model used in the present thesis belongs to the third generation of constitutive models. In such models, the development of the plastic yield surface is due to both volumetric and shear strains.
Besides including the irreversible material behaviour due to deviatoric loading, the HS model adopts an advanced formulation for the soil stiffness. In particular, the model involves three different soil stiffnesses and takes into account their stress dependency. All these features allow the user to realistically model a wide range of stress paths.
The model implemented in Plaxis was proposed by **(Schanz et al. 1999)** and enhanced by **(Benz 2007)**. The double-hardening formulation allows the yield surface to expand almost homotetically, with changes in dimensions but not in shape.
The main features of the HS model can be summarised as follows:

- Mohr-Coulomb failure criterion;
- Rankine failure criterion (tension);
- dilatancy;
- shear hardening;
- volumetric hardening;
- three independent stiffnesses (deviatoric, oedometric and unloading-reloading stiffness);
- stress-dependency of stiffness;
- possibility to consider the soil stress history (overconsolidation).

B.1. Hyperbolic stress-strain relationship

The basic idea of the HS model is the possibility to reproduce the hyperbolic stress-strain relationship observed in primary triaxial loading. This behaviour was first represented by **Duncan & Chang (1970)**. However, the Duncan-Chang model is formulated within the theory of elasticity, whereas the HS model considers soil plasticity. Allowing for irreversible strains, this model can distinguish between loading and unloading stress paths.

The basic constitutive behaviour of the soil undergoing primary triaxial loading in drained conditions can be described by the following equations:

$$\varepsilon_1 = \varepsilon_{50} \frac{q}{q_a - q} = \frac{q_a}{2E_{50}} \frac{q}{q_a - q}$$

Where q_a is the asymptotic value of the deviatoric stress, E_{50} is the shear modulus associated with a mobilisation of 50% of the final shear strength and ε_{50} is the corresponding principal strain.
The final deviatoric stress q_f and the asymptotic stress are related through the failure ratio R_f as follows:

$$q_a = \frac{q_f}{R_f}$$

With $q_f = (\sigma'_3 + a)\frac{2\text{sen}\varphi}{1-\text{sen}\varphi}$ and $a = c' \cdot \cot\varphi$ from the Mohr-Coulomb failure criterion. The coefficient R_f is set to 0.9 in Plaxis. The above described hyperbolic relationship holds for $q < q_f$; as soon as $q = q_f$ perfectly plastic yielding occurs.
This formulation can reproduce the decreasing of soil stiffness with the increase in deviatoric loading and the development of plastic strains. The material behaviour during drained triaxial loading is represented in Figure 127.

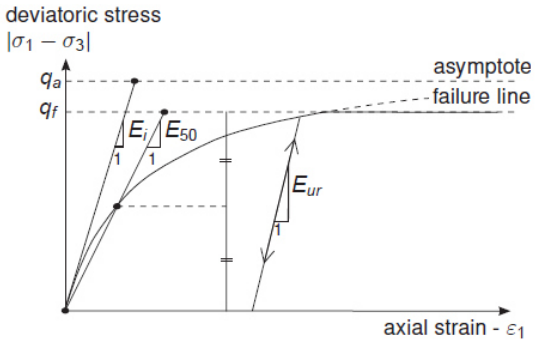

Figure 127. Hyperbolic relation between deviatoric stress and axial strain in drained triaxial loading and unloading, from Brinkgreve et al. (2014)

B.2. Stress-dependent moduli

The HS model describes the stiffness stress dependency using the following power laws:

$$E_{50} = E_{50}^{ref}\left(\frac{\sigma'_3 + c\cdot\cot\varphi}{\sigma_{ref} + c\cdot\cot\varphi}\right)^m$$

$$E_{oed} = E_{oed}^{ref}\left(\frac{\sigma'_1 + c\cdot\cot\varphi}{\sigma_{ref} + c\cdot\cot\varphi}\right)^m$$

$$E_{ur} = E_{ur}^{ref}\left(\frac{\sigma'_3 + c\cdot\cot\varphi}{\sigma_{ref} + c\cdot\cot\varphi}\right)^m$$

The deviatoric and the unloading-reloading modulus depend on the minor principal stress σ'_3, while the oedometric modulus is linked to the major principal stress σ'_1. The coefficient m regulates the amount of stress dependency and can be approximately assumed equal to 0.5 for sand and 0.8 for clays. Alternatively it can be derived for triaxial and oedometric tests.

In contrast with elasticity models, in the HS model, there is no link between the oedometric modulus and the deviatoric modulus. They can be entered separately and govern different deformation behaviours.

The unloading-reloading modulus E_{ur} is the only purely elastic modulus, whereas E_{oed} and E_{50} govern both elastic and plastic behaviour in primary loading. The elastic strains during an unloading-reloading stress path can be calculated according to an Hook's relation. For drained triaxial stress paths, where E_{ur} remains constant, the elastic strains are calculated as follows:

$$\varepsilon_1^e = \frac{q}{E_{ur}} \quad \varepsilon_2^e = \varepsilon_2^e = \nu_{ur}\frac{q}{E_{ur}}$$

Figure 128 shows, on the q-p' space, the areas associated with the previously introduced stiffnesses. These areas are delimited by the hardening surfaces that will be introduced in the following paragraph.

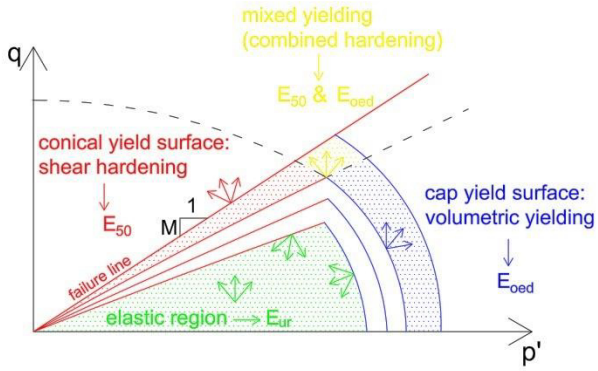

Figure 128. Delimitation of the areas associated with shear hardening, volumetric hardening, combined hardening and elastic behaviour in the q-p' space

B.3. Shear hardening, volumetric hardening and evolution laws

The HS model calculates plastic strains on the basis of two main yield surfaces and of an isotropic hardening criterion.

Volumetric hardening dominates the behaviour of NC-clays and loose sands whereas shear hardening is dominant for OC-clays and dense sands. In order to evaluate the importance of having both hardening mechanisms, it is necessary to consider the stress paths characterising a specific engineering problem. Excavation problems such as the construction of tunnels or retaining walls are likely to involve a significant amount of plastic straining under deviatoric loading.

Considering both volumetric and deviatoric plastic strains, the total strain rate can be written as follows:

$$d\varepsilon = d\varepsilon^e + d\varepsilon^p = d\varepsilon^e + d\varepsilon^{ps} + d\varepsilon^{pc} = \underline{\underline{D}}^{e-1}\underline{\sigma} + \lambda^s \frac{\partial g^s}{\partial \underline{\sigma}} + \lambda^v \frac{\partial g^c}{\partial \underline{\sigma}}$$

Where $d\varepsilon^e$ represents the elastic strain rate, $d\varepsilon^{ps}$ the plastic shear strain rate and $d\varepsilon^{pc}$ the plastic volumetric strain rate. g^s and g^c are the corresponding plastic potential funtions, whereas λ^s and λ^c are the plastic multipliers, calculated by solving the consistency equations $f^s = 0$ and $f^c = 0$, with f^s and f^c representing the conical and and cap yield surfaces, which can expand due to shear and volumetric hardening respectively.

Deviatoric or shear hardening is combined with a non-associated flow rule $f^s \neq g^s$, whereas volumetric or cap hardening assumes an associated flow rule $f^c = g^c$.
The choice of a non-associated plasticity for the deviatoric yield surface is due to the fact that FE analyses with associated plasticity do not give satisfactory results when compared to experimental tests.
The mathematical equations governing shear and compression hardening are summarised in Table 26. The model uses two state variables to define the yield surfaces and their evolution: the plastic shear strain γ^{ps} and the pre-consolidation stress p_p. The latter is defined as the maximum equivalent isotripic stress experienced from a certain stress point.

Table 26. Mathematical formulation of yield surface, plastic potential and hardening law for shear and compression hardening

	Shear hardening	**Volumetric hardening**
Yield surface	$f^s = \frac{q_a}{E_{50}}\frac{q}{q_a - q} - \frac{2q}{E_{ur}} - \gamma^{ps}$	$f^c = \frac{\tilde{q}^2}{\alpha^2} - p'^2 - p_p^2$ *1
Plastic potential	$g^s = (3 - \sin\psi_m)\cdot q - 6\cdot \sin\psi_m \cdot p'$ *2	$f^c = g^c$
Hardening law	$d\varepsilon_v^{ps} = \sin\psi_m \cdot d\gamma^{ps}$	$d\varepsilon_v^{pc} = \frac{K_s/K_c - 1}{K_s - K_c}\left[\left(\frac{p_p + c\cot\varphi}{p^{ref} + c\cot\varphi}\right)^{-m}\right] dp_p$ *3

*1 $\tilde{q}$ is a special stress measure defined as $\tilde{q} = \sigma_1 + (\delta - 1)\sigma_2 - \delta\sigma_3$ with $\delta = \frac{3 - sin\varphi}{3 + sin\varphi}$;

*2 ψ_m is the mobilised dilatancy angle;

*3 K_s/K_c is the ratio between the bulk modulus in isotropic swelling and the bulk modulus in isotropic compression and can be approximated as follows:

$K_s/K_c \approx \frac{E_{ur}^{ref}}{E_{oed}^{ref}} \frac{K_0^{nc}}{(1+2K_0^{nc})(1-2\upsilon_{ur})}$.

The yield function associated with volumetric hardening is an ellipse, and its shape is determined by p_p and α. The first determines its magnitude by fixing the length on the x-axis, whereas the second determines its aspect ratio by fixing the length on the y-axis. The evaluation of p_p is carried out through the initial stress procedure that will be dealt with in one the following paragraphs.

A further yield surface is the Rankine Yield surface, which represents a tensile cut-off and limits the stress state with respect to the tensile stress.
The Rankine yield condition can be written as follows:

$$f^r = \sigma_1 - f_t = 0$$

Where f_t represents the assumed tensile strength. In this case, an associated flow rule is assumed.
Figure 129 is a representation, in the three-dimensional space, of the yield surfaces. Both of them have a hexagonal shape due to the adoption of the Mohr-Coulomb failure criterion. The deviatoric yield surface can expand until the Mohr-Coulomb surface is reached, whereas the cap yield surface is a function of the pre-consolidation stress.

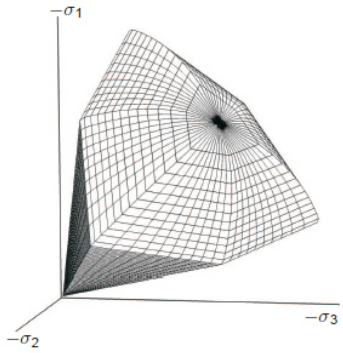

Figure 129. Representation of the HS yield surface in the space of the principle stresses (Brinkgreve et al. 2013)

B.4. Initial conditions

The HS input parameters defining the initial conditions are K_0, $K_{0,nc}$ and OCR (or alternatively the pre-overburden pressure POP as shown in Figure 130).

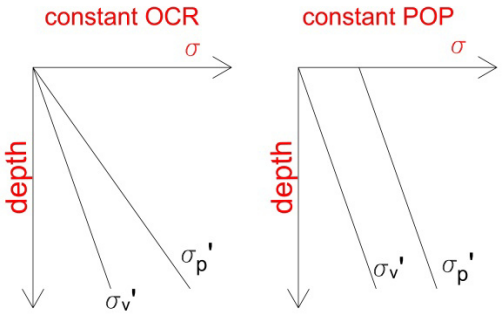

Figure 130. Vertical stress and pre-consolidation stress vs depth, in case a constant OCR or POP is assumed

If the calculation is set as automatic, K_0 is calculated according to the following equation:

$$K_{0,x} = K_{0,y} = K_0^{NC} OCR - \frac{\nu_{ur}}{1-\nu_{ur}}(OCR-1) + \frac{K_0^{NC} POP - \frac{\nu_{ur}}{1-\nu_{ur}} POP}{|\sigma_{zz}^0|}$$

Otherwise $K_{0,}$ as well as $K_{0,nc}$ can be defined by the user. Also the preconsolidation pressure is computed according to the entered OCR or POP. The so-calculated value of p_p defines the magnitude of the cap yield surface delimiting the elastic region. Both OCR and POP cause a shifting of the initial volumetric yield surface.

The so-called equivalent pressure of p_{eq} is associated with the actual initial stress state and represents the intersection of the stress contour on which the current stress state is located and the x-axis. This value can be calculated as:

$$p^{eq} = \sqrt{(p')^2 + q^2/\alpha^2}$$

The ratio between pre-consolidation pressure and equivalent pressure can be defined as isotropic OCR. A graphical representation of the cap yield surface and of the initial stress state in an overconsolidated material is given in Figure 131.

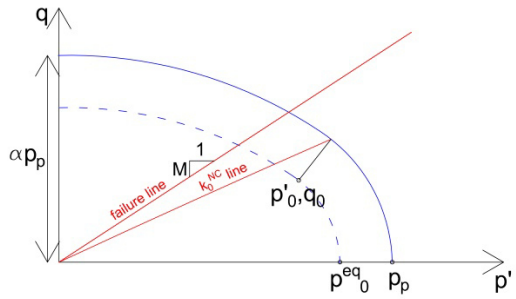

Figure 131. Definition of the cap yield surface and initial stress state for the case OCR>1

Besides using the K_0 procedure, the initial stress state can also be computed according to the gravity loading procedure. This is a particularly suitable method in case of non-horizontal ground surface or non-horizontal stratification. The procedure entails the application of the soil unit weight in the initial phase, which is, therefore, an actual calculation phase and has to fulfil equilibrium conditions. The main drawbacks of this procedure are the necessity to simulate the loading history and the dependency of K_0 on the Poisson's ratio according to the equation $K_0 = \frac{\nu}{1-\nu}$.

B.5. Input parameters

The principal input parameters required for defining the HS model are listed in Table 27.

Table 27. Input parameters of the HS model

Parameter	Symbol	Unit
Triaxial secant stiffness	E_{50}^{ref}	kN/m^2
Oedometric tangent stiffness	E_{oed}^{ref}	kN/m^2
Unloading-reloading stiffness	E_{ur}^{ref}	kN/m^2
Power of stress dependency	m	-
Cohesion	c	kN/m^2
Friction angle	φ	°
Dilatancy angle	ψ	°
Poisson's ratio	υ	-
K_0 value for normal consolidation	K_0^{nc}	-
Failure ratio	R_f	-

The user can also enter a limit value of the tensile strength (kN/m^2) and define the position of the cap yield surface with respect to the actual stress

by entering an OCR value (-) or a POP (kN/m^2), as described in the previous paragraph.

B.6. Influence of model parameters on soil test curves

The following graphs show the influence of the most important HS parameters on the experimental curves of triaxial and oedometric tests.
Such a sensitivity analysis represents a good starting point for a model calibration based on laboratory tests. All the tests have been simulated considering a mean effective pressure of 100 kPa.

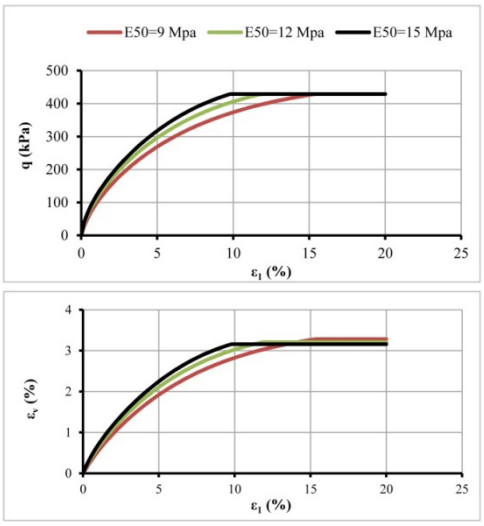

Figure 132. Influence of the deviatoric modulus on a drained triaxial test

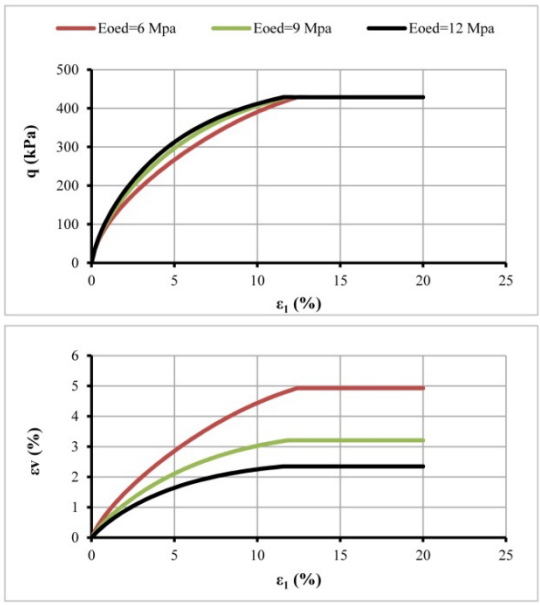

Figure 133. Influence of the oedometric modulus on a drained triaxial test

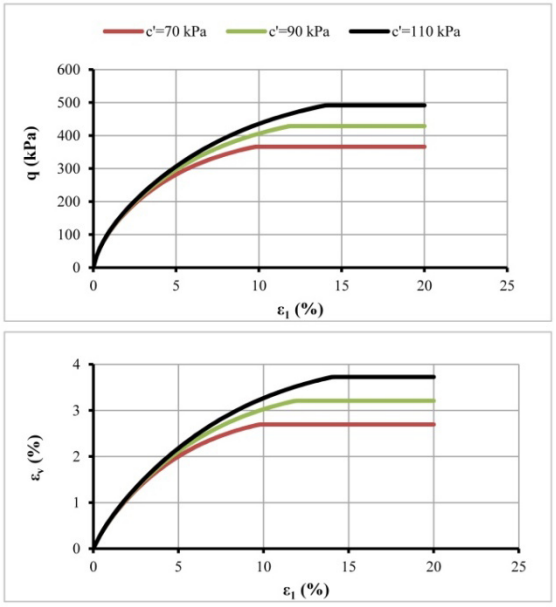

Figure 134. Influence of the cohesion on a drained triaxial test

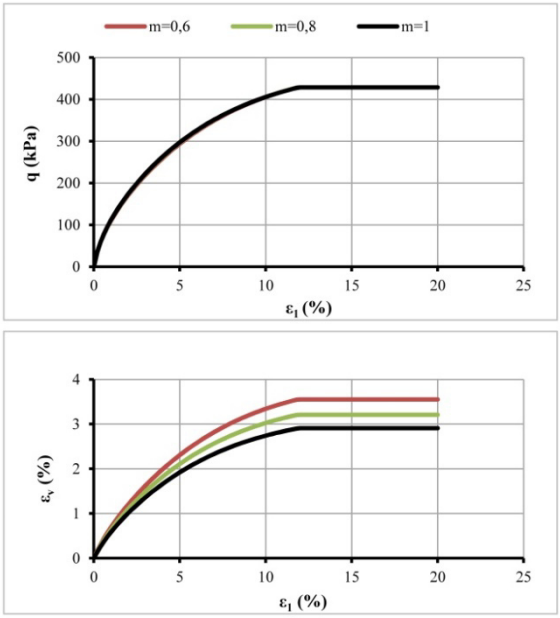

Figure 135. Influence of the stress dependency coefficient on a drained triaxial test

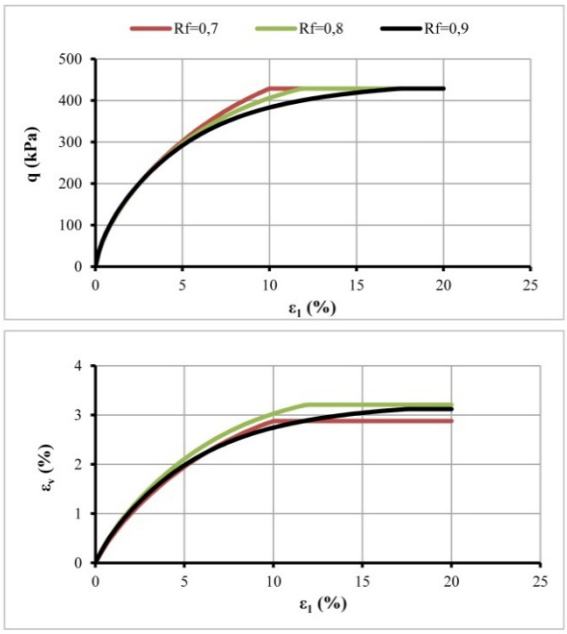

Figure 136. Influence of the failure ratio on a drained triaxial test

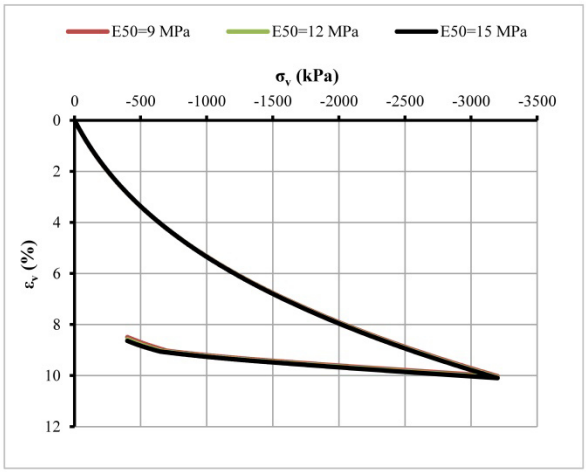

Figure 137. Influence of the deviatoric modulus on an oedometric test

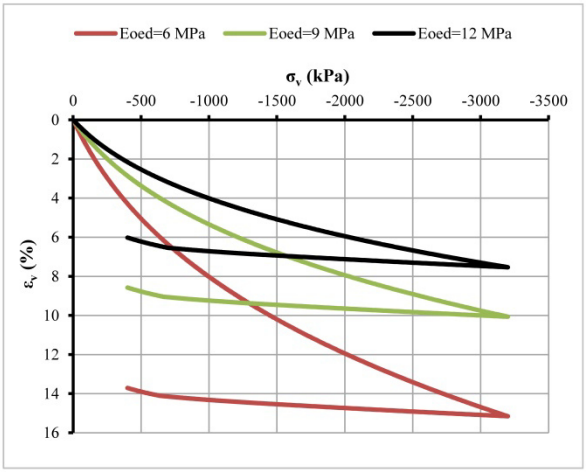

Figure 138. Influence of the oedometric modulus on an oedometric test

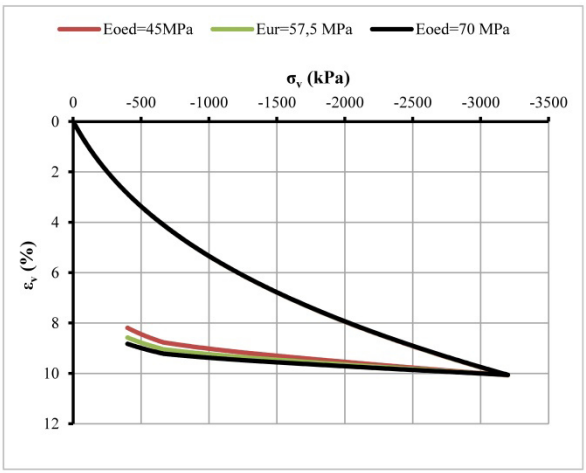

Figure 139. Influence of the unloading-reloading modulus on an oedometric test

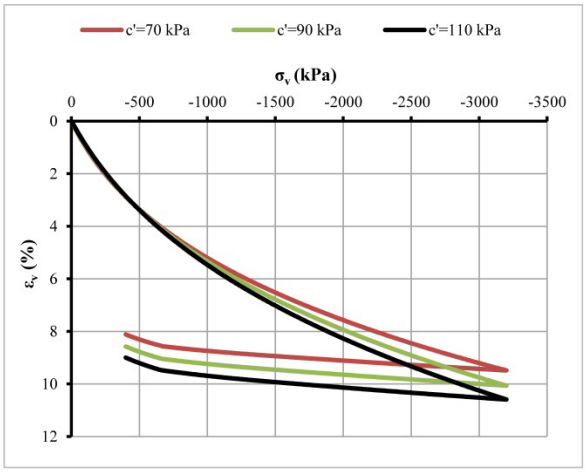

Figure 140. Influence of the cohesion on an oedometric test

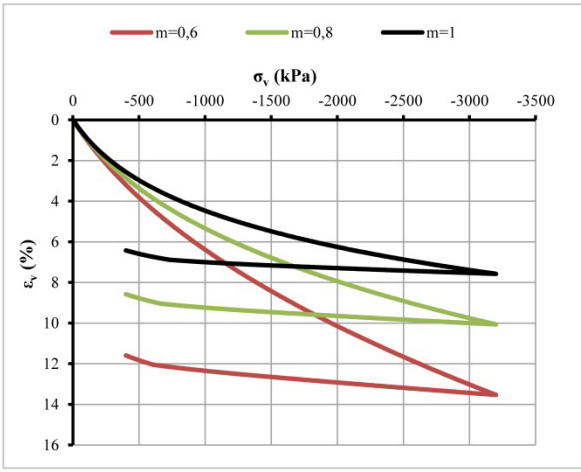

Figure 141. Influence of the stress dependency coefficient on an oedometric test

B.7. Small Strain Stiffness

The Hardening Soil Model with Small Strain Stiffness **(Benz 2007)** is an enhanced version of the Hardening Soil Model.

The implementation model of the small strain stiffness, which represents an important aspect of the soil pre-failure behaviour, into the HS enables more accurate displacement predictions. The new features that the model introduces are the stiffness variation in the small strain domain according to the well-known S-shaped stiffness degradation curve and a hysteretic, non-linear elastic stress-strain relationship in the range of small strains. These features, already known from previous studies focused on the soil dynamic response, were relatively recently recognised to play an important role also in static problems. In fact, the stiffer response under dynamic load is due to the specific deformation range the soil the soil is subjected to rather than to the load type.

Small strain stiffness can be directly estimated only through geophysical methods or with laboratory devices properly equipped for measuring in the small strain range. Stiffness decay can be attributed primarily to the break-up of bonding forces between soil particles or to frictional particle forces exceeding the elastic limit. The implementation of small strain in numerical models tends to concentrate deformations around the source of disturbance

(tunnel excavation, foundation and so forth) while reduces deformations at a certain distance from the loaded or unloaded zone.
The account for small strain stiffness makes the model particularly suitable for predicting displacements behind retaining walls or subsidence due to tunnel construction.

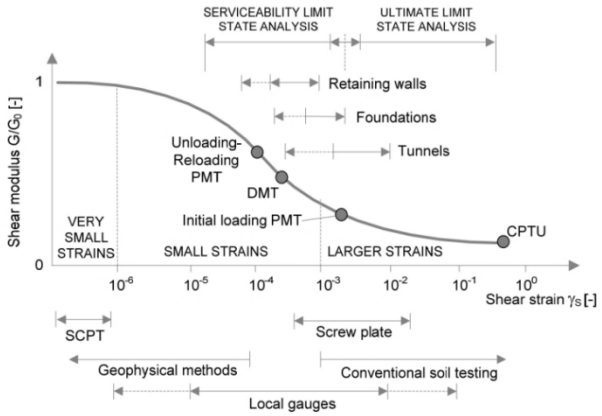

Figure 142. Typical soil stiffness degradation curve with strain ranges characterising the most common geotechnical problems or soil tests (after Obrzud & Eng 2010)

The equations characterising the HSS implemented in Plaxis are almost the same of the HS model.
The stiffness degradation is described through the hyperbolic law suggested by **Dos Santos & Correia (2001)** on the basis of the well-known model proposed by **Hardin & Drnevich (1972)**.

Table 28. Hyperbolic law for the secant shear modulus

(Hardin & Drnevich 1972)	(Dos Santos & Correia 2001)
$G_S = G_0/(1 + \lvert\gamma/\gamma_R\rvert)$	$G_S = G_0/(1 + 0.385\lvert\gamma/\gamma_{0.7}\rvert)$
where $\gamma_R = \tau_{max}/G_0$	where $\gamma_{0.7}$ is the strain value at
and τ_{max}= shear tress at failure	which $G_S = 0.7G_0$

G_S represents the secant shear modulus. In order to derive the tangent shear modulus, it is necessary to calculate the derivative of the shear stress ($\tau = \gamma \cdot G_s$) with respect to the shear strain:

$$G_t = G_0/(1 + 0.385\lvert\gamma/\gamma_{0.7}\rvert)^2$$

The shear strain is expressed using the invariant

$$\gamma = \frac{1}{\sqrt{2}} \cdot \sqrt{(\varepsilon_1 - \varepsilon_1)^2 - (\varepsilon_2 - \varepsilon_3)^2 - (\varepsilon_3 - \varepsilon_1)^2}$$

As well as the three stiffnesses of the HS model also the maximum shear modulus G_0 is stress dependent according to the following equation:

$$G_0 = G_0^{ref} \cdot \left(\frac{\sigma'_3 + c' \cdot cot\varphi'}{\sigma_{ref} + c' \cdot cot\varphi'} \right)^m$$

While the stiffness degradation in the small strain range is modelled by implementing a stiffness decay curve, the stiffness degradation due to plastic behaviour is modelled through the hardening yield surface. The cut-off between the two material behaviours is represented by the value of G_{ur}, namely the unloading-reloading modulus (Figure 143). The latter can be derived from the elastic constants $E_{ur}$and v_{ur} ($G_{ur} = E_{ur}/2(1 + v_{ur})$).
The cut-off shear strain is calculated as:

$$\gamma_{cut-off} = \frac{1}{0.385}\left(\sqrt{G_0/G_{ur}} - 1\right)\gamma_{0.7}$$

Regarding the soil behaviour under cyclic load, the HSS model follows the Masing's rules, confirmed by experimental results:

- the shear modulus in unloading is equal to the initial tangent modulus characterising the loading curve (Figure 144);
- the unloading and reloading curve is twice (in terms of size) the initial loading curve (this second rule is fulfilled by imposing $\gamma_{0.7,re-loading=}2\gamma_{0.7,virgin-loading}$).

With respect to the HS model, the HSS model requires only two further parameters: G_0^{ref} and $\gamma_{0.7}$.

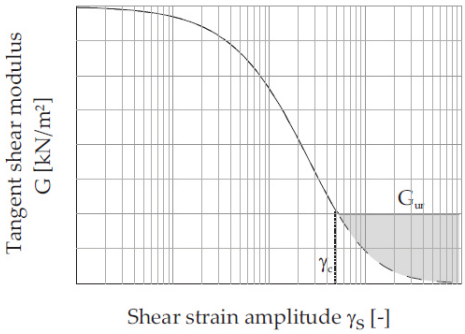

Figure 143. Small strain behaviour cut-off (after Benz 2007)

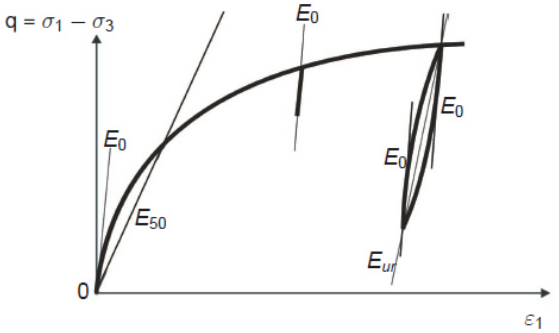

Figure 144. Behaviour of the HSS model under triaxial loading/unloading (from (Brinkgreve et al. 2013)

For further details about the model, one can refer to **Benz (2007)** and **Brinkgreve et al. (2013)**.

Appendix C. Sensitivity analyses

Sensitivity Analysis and Parameter variation are new features of PLAXIS 2D. They enable the user to analyse the influence of the variation of different parameters on the computational results. Generally speaking, sensitivity analyses provide useful information about which aspect of the material behaviour should be further investigated, according to its variability and its influence on the model response.

Given a specific set of material parameters, it is possible to set both minimum and maximum values for all them. The program will perform a series of analyses by changing each time one of the chosen parameters (i.e. the parameters that the user wants to include in the sensitivity analysis).

In order to compare the results, one or more criteria have to be chosen (e.g. displacements, stresses, safety factors and so forth).

After setting both minimum/maximum values and comparison criteria, the program runs all the different permutations and returns as a result a sensitivity score. This value represents the sensitivity of a specific criterion (e.g., node displacements, stresses, safety factors and so forth) to changes in a parameter value.

In the following paragraphs, the results of sensitivity analyses carried out on the basis of a 2D single tunnel analysis are shown. The tunnel, characterised by H/D=2, is full face excavated. Table 29 lists the phases of the reference analysis and indicates the corresponding stress relaxation factor. Figure 145 shows the position, within the FE mesh, of the reference nodes and stress points.

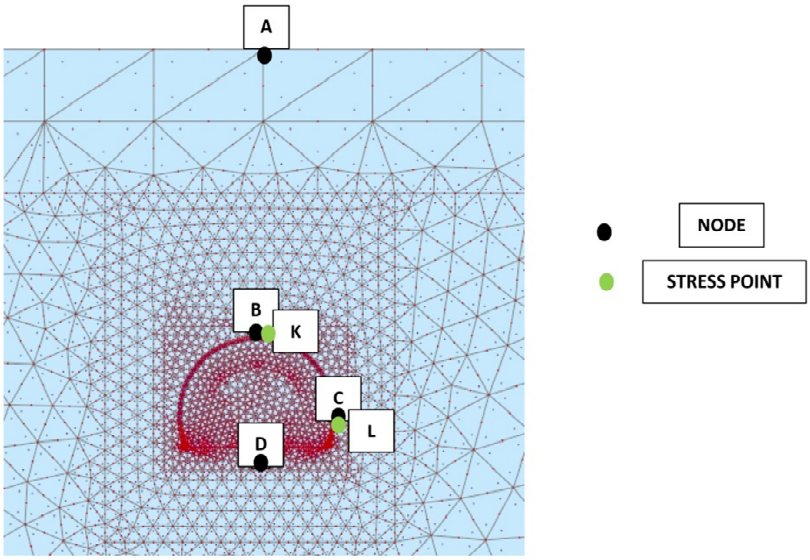

Figure 145. Location of nodes and stress points used for the sensitivity analyses

Table 29. Phase description and stress relaxation factor for the reference analysis

Phase	Description	λ
0	K_0 procedure	-
1	Deactivation of the upper cluster of the core	0.3
2	Primary support activation (open arch)	1
3	Deactivation of the lower cluster of the core	0.2
4	Invert activation	1

The adopted criteria are listed in Table 30. The soil and tunnel lining parameters adopted in the reference analyses are listed in Table 31 and Table 32 respectively.

Table 30. Criteria adopted for the sensitivity analyses

	CRITERIA
1	Vertical displacement - node A
2	Vertical displacement - node B
3	Horizontal displacement - node C
4	Vertical displacement - node D
5	Vertical stress - point K
6	Horizontal stress - point L

Table 31. Soil parameters for the reference analysis

Soil parameter		value
γ_{unsat}	kN/m^3	19
γ_{sat}	kN/m^3	20
$E_{50,ref}$	kPa	12,000
$E_{oed,ref}$	kPa	19,000
$E_{ur,ref}$	kPa	57,500
m	-	0.8
v'_{ur}	-	0.2
k_0	-	0.75
k_0^{nc}	-	0.5774
$G_{0,ref}$	kPa	100,000
$\gamma_{0.7}$	-	0.0002
c'	kPa	90
ϕ'	°	25
ψ	°	0
R_f	-	0.8

Table 32. Lining stiffness parameters for the reference analysis

Stiffness	Primary lining	Invert arch
EA (kN)	3E+06	2.4E+07
EJ (kN*m²)	1.75E+04	1.3E+06

C.1. HSS parameters

The figures below depict the sensitivity score calculated for the different criteria (Table 30) varying some of the soil parameters between a minimum and a maximum value. The variation range was evaluated with reference to the case study included in this thesis. All these evaluations refer to the final phase of the simulation (phase 4, Table 29).
In the lower part of the window all the analysed permutations are listed. From the sensitivity score, it seems that the deviatoric modulus ($E_{50,ref}$) and the cohesion (c') have the highest influence on the computed settlements and stresses. From the results of the different permutation, it turns out that a

variation of these soil parameters within the prescribed range cause a high variation in the computed displacements and stresses (as it can be seen in the lower part of the figures, where the results of all the calculated permutations are listed). However, also the initial stress state plays a very important role.

Criterion: vertical displacement – point A

Type	Material	Parameter	Min	Ref	Max	SensiScore
Soil	hss	E_{50}^{ref}	8000	12,00E3	16,00E3	26
Soil	hss	E_{oed}^{ref}	6000	9000	12,00E3	11
Soil	hss	E_{ur}^{ref}	45,00E3	57,50E3	70,00E3	2
Soil	hss	G_0^{ref}	80,00E3	100,0E3	120,0E3	7
Soil	hss	power (m)	0,6000	0,8000	1,000	1
Soil	hss	c'_{ref}	70,00	90,00	110,0	19
Soil	hss	POP	100,0	300,0	500,0	17
Soil	hss	$K_{0,x}$	0,6000	0,7500	0,9000	18

E_{50}^{ref} [hss]	E_{oed}^{ref} [hss	E_{ur}^{ref} [hss]	G_0^{ref} [hss]	power (m) [h	c'_{ref} [hss]	POP [hss]	$K_{0,x}$ [hss]	Criterion 1
16,00E3	9000	57,50E3	100,0E3	0,8000	90,00	300,0	0,7500	-0,02630
8000	9000	57,50E3	100,0E3	0,8000	90,00	300,0	0,7500	-0,06322
12,00E3	12,00E3	57,50E3	100,0E3	0,8000	90,00	300,0	0,7500	-0,04311
12,00E3	6000	57,50E3	100,0E3	0,8000	90,00	300,0	0,7500	-0,02743
12,00E3	9000	70,00E3	100,0E3	0,8000	90,00	300,0	0,7500	-0,03874
12,00E3	9000	45,00E3	100,0E3	0,8000	90,00	300,0	0,7500	-0,03643
12,00E3	9000	57,50E3	120,0E3	0,8000	90,00	300,0	0,7500	-0,03410
12,00E3	9000	57,50E3	80,00E3	0,8000	90,00	300,0	0,7500	-0,04406
12,00E3	9000	57,50E3	100,0E3	1,000	90,00	300,0	0,7500	-0,03918
12,00E3	9000	57,50E3	100,0E3	0,6000	90,00	300,0	0,7500	-0,03740
12,00E3	9000	57,50E3	100,0E3	0,8000	110,0	300,0	0,7500	-0,02938
12,00E3	9000	57,50E3	100,0E3	0,8000	70,00	300,0	0,7500	-0,05716
12,00E3	9000	57,50E3	100,0E3	0,8000	90,00	500,0	0,7500	-0,03419
12,00E3	9000	57,50E3	100,0E3	0,8000	90,00	100,0	0,7500	-0,05831
12,00E3	9000	57,50E3	100,0E3	0,8000	90,00	300,0	0,9000	-0,03048
12,00E3	9000	57,50E3	100,0E3	0,8000	90,00	300,0	0,6000	-0,05640
12,00E3	9000	57,50E3	100,0E3	0,8000	90,00	300,0	0,7500	-0,03788

Reference analysis

Figure 146. Sensitivity analysis (HSS parameters – vertical displacement, node A)

Criterion: vertical displacement – point B

Type	Material	Parameter	Min	Ref	Max	SensiScore
Soil	hss	E_{50}^{ref}	8000	12,00E3	16,00E3	25
Soil	hss	E_{oed}^{ref}	6000	9000	12,00E3	10
Soil	hss	E_{ur}^{ref}	45,00E3	57,50E3	70,00E3	0
Soil	hss	G_0^{ref}	80,00E3	100,0E3	120,0E3	11
Soil	hss	power (m)	0,6000	0,8000	1,000	2
Soil	hss	c'_{ref}	70,00	90,00	110,0	20
Soil	hss	POP	100,0	300,0	500,0	15
Soil	hss	$K_{0,x}$	0,6000	0,7500	0,9000	17

E_{50}^{ref} [hss]	E_{oed}^{ref} [hss	E_{ur}^{ref} [hss]	G_0^{ref} [hss]	power (m) [h	c'_{ref} [hss]	POP [hss]	$K_{0,x}$ [hss]	Criterion 1
16,00E3	9000	57,50E3	100,0E3	0,8000	90,00	300,0	0,7500	-0,04373
8000	9000	57,50E3	100,0E3	0,8000	90,00	300,0	0,7500	-0,08502
12,00E3	12,00E3	57,50E3	100,0E3	0,8000	90,00	300,0	0,7500	-0,06234
12,00E3	6000	57,50E3	100,0E3	0,8000	90,00	300,0	0,7500	-0,04516
12,00E3	9000	70,00E3	100,0E3	0,8000	90,00	300,0	0,7500	-0,05663
12,00E3	9000	45,00E3	100,0E3	0,8000	90,00	300,0	0,7500	-0,05582
12,00E3	9000	57,50E3	120,0E3	0,8000	90,00	300,0	0,7500	-0,04894
12,00E3	9000	57,50E3	80,00E3	0,8000	90,00	300,0	0,7500	-0,06677
12,00E3	9000	57,50E3	100,0E3	1,000	90,00	300,0	0,7500	-0,05565
12,00E3	9000	57,50E3	100,0E3	0,6000	90,00	300,0	0,7500	-0,05841
12,00E3	9000	57,50E3	100,0E3	0,8000	110,0	300,0	0,7500	-0,04654
12,00E3	9000	57,50E3	100,0E3	0,8000	70,00	300,0	0,7500	-0,07959
12,00E3	9000	57,50E3	100,0E3	0,8000	90,00	500,0	0,7500	-0,05280
12,00E3	9000	57,50E3	100,0E3	0,8000	90,00	100,0	0,7500	-0,07800
12,00E3	9000	57,50E3	100,0E3	0,8000	90,00	300,0	0,9000	-0,04915
12,00E3	9000	57,50E3	100,0E3	0,8000	90,00	300,0	0,6000	-0,07701
12,00E3	9000	57,50E3	100,0E3	0,8000	90,00	300,0	0,7500	-0,05646

Reference analysis

Figure 147. Sensitivity analysis (HSS parameters – vertical displacement, node B)

Criterion: horizontal displacement – point c

Type	Material	Parameter	Min	Ref	Max	SensiScore
Soil	hss	E_{50}^{ref}	8000	12,00E3	16,00E3	33
Soil	hss	E_{oed}^{ref}	6000	9000	12,00E3	16
Soil	hss	E_{ur}^{ref}	45,00E3	57,50E3	70,00E3	5
Soil	hss	G_0^{ref}	80,00E3	100,0E3	120,0E3	6
Soil	hss	power (m)	0,6000	0,8000	1,000	4
Soil	hss	c'_{ref}	70,00	90,00	110,0	22
Soil	hss	POP	100,0	300,0	500,0	10
Soil	hss	$K_{0,x}$	0,6000	0,7500	0,9000	5

E_{50}^{ref} [hss]	E_{oed}^{ref} [hss	E_{ur}^{ref} [hss]	G_0^{ref} [hss]	power (m) [h	c'_{ref} [hss]	POP [hss]	$K_{0,x}$ [hss]	Criterion 1
16,00E3	9000	57,50E3	100,0E3	0,8000	90,00	300,0	0,7500	-0,05026
8000	9000	57,50E3	100,0E3	0,8000	90,00	300,0	0,7500	-0,1007
12,00E3	12,00E3	57,50E3	100,0E3	0,8000	90,00	300,0	0,7500	-0,07595
12,00E3	6000	57,50E3	100,0E3	0,8000	90,00	300,0	0,7500	-0,05212
12,00E3	9000	70,00E3	100,0E3	0,8000	90,00	300,0	0,7500	-0,06541
12,00E3	9000	45,00E3	100,0E3	0,8000	90,00	300,0	0,7500	-0,07254
12,00E3	9000	57,50E3	120,0E3	0,8000	90,00	300,0	0,7500	-0,06430
12,00E3	9000	57,50E3	80,00E3	0,8000	90,00	300,0	0,7500	-0,07414
12,00E3	9000	57,50E3	100,0E3	1,000	90,00	300,0	0,7500	-0,06546
12,00E3	9000	57,50E3	100,0E3	0,6000	90,00	300,0	0,7500	-0,07214
12,00E3	9000	57,50E3	100,0E3	0,8000	110,0	300,0	0,7500	-0,05744
12,00E3	9000	57,50E3	100,0E3	0,8000	70,00	300,0	0,7500	-0,09055
12,00E3	9000	57,50E3	100,0E3	0,8000	90,00	500,0	0,7500	-0,06530
12,00E3	9000	57,50E3	100,0E3	0,8000	90,00	100,0	0,7500	-0,08065
12,00E3	9000	57,50E3	100,0E3	0,8000	90,00	300,0	0,9000	-0,07296
12,00E3	9000	57,50E3	100,0E3	0,8000	90,00	300,0	0,6000	-0,06597
12,00E3	9000	57,50E3	100,0E3	0,8000	90,00	300,0	0,7500	-0,06854

Reference analysis

Figure 148. Sensitivity analysis (HSS parameters –horizontal displacement, node C)

Criterion: vertical displacement – point D

Type	Material	Parameter	Min	Ref	Max	SensiScore
Soil	hss	E_{50}^{ref}	8000	12,00E3	16,00E3	18
Soil	hss	E_{oed}^{ref}	6000	9000	12,00E3	11
Soil	hss	E_{ur}^{ref}	45,00E3	57,50E3	70,00E3	15
Soil	hss	G_0^{ref}	80,00E3	100,0E3	120,0E3	16
Soil	hss	power (m)	0,6000	0,8000	1,000	22
Soil	hss	c'_{ref}	70,00	90,00	110,0	3
Soil	hss	POP	100,0	300,0	500,0	4
Soil	hss	$K_{0,x}$	0,6000	0,7500	0,9000	11

E_{50}^{ref} [hss]	E_{oed}^{ref} [hss	E_{ur}^{ref} [hss]	G_0^{ref} [hss]	power (m) [h	c'_{ref} [hss]	POP [hss]	$K_{0,x}$ [hss]	Criterion 1
16,00E3	9000	57,50E3	100,0E3	0,8000	90,00	300,0	0,7500	0,06584
8000	9000	57,50E3	100,0E3	0,8000	90,00	300,0	0,7500	0,08498
12,00E3	12,00E3	57,50E3	100,0E3	0,8000	90,00	300,0	0,7500	0,07803
12,00E3	6000	57,50E3	100,0E3	0,8000	90,00	300,0	0,7500	0,06671
12,00E3	9000	70,00E3	100,0E3	0,8000	90,00	300,0	0,7500	0,06840
12,00E3	9000	45,00E3	100,0E3	0,8000	90,00	300,0	0,7500	0,08422
12,00E3	9000	57,50E3	120,0E3	0,8000	90,00	300,0	0,7500	0,06723
12,00E3	9000	57,50E3	80,00E3	0,8000	90,00	300,0	0,7500	0,08438
12,00E3	9000	57,50E3	100,0E3	1,000	90,00	300,0	0,7500	0,06471
12,00E3	9000	57,50E3	100,0E3	0,6000	90,00	300,0	0,7500	0,08826
12,00E3	9000	57,50E3	100,0E3	0,8000	110,0	300,0	0,7500	0,07401
12,00E3	9000	57,50E3	100,0E3	0,8000	70,00	300,0	0,7500	0,07679
12,00E3	9000	57,50E3	100,0E3	0,8000	90,00	500,0	0,7500	0,07315
12,00E3	9000	57,50E3	100,0E3	0,8000	90,00	100,0	0,7500	0,07725
12,00E3	9000	57,50E3	100,0E3	0,8000	90,00	300,0	0,9000	0,08719
12,00E3	9000	57,50E3	100,0E3	0,8000	90,00	300,0	0,6000	0,07503
12,00E3	9000	57,50E3	100,0E3	0,8000	90,00	300,0	0,7500	0,07525

Reference analysis

Figure 149. Sensitivity analysis (HSS parameters – vertical displacement, node D)

Criterion: vertical stress – point K

Type	Material	Parameter	Min	Ref	Max	SensiScore
Soil	hss	E_{50}^{ref}	8000	12,00E3	16,00E3	21
Soil	hss	E_{oed}^{ref}	6000	9000	12,00E3	13
Soil	hss	E_{ur}^{ref}	45,00E3	57,50E3	70,00E3	5
Soil	hss	G_0^{ref}	80,00E3	100,0E3	120,0E3	11
Soil	hss	power (m)	0,6000	0,8000	1,000	3
Soil	hss	c'_{ref}	70,00	90,00	110,0	5
Soil	hss	POP	100,0	300,0	500,0	21
Soil	hss	$K_{0,x}$	0,6000	0,7500	0,9000	20

E_{50}^{ref} [hss]	E_{oed}^{ref} [hss	E_{ur}^{ref} [hss]	G_0^{ref} [hss]	power (m) [	c'_{ref} [hss]	POP [hss]	$K_{0,x}$ [hss]	Criterion 1
16,00E3	9000	57,50E3	100,0E3	0,8000	90,00	300,0	0,7500	-260,6
8000	9000	57,50E3	100,0E3	0,8000	90,00	300,0	0,7500	-288,5
12,00E3	12,00E3	57,50E3	100,0E3	0,8000	90,00	300,0	0,7500	-277,8
12,00E3	6000	57,50E3	100,0E3	0,8000	90,00	300,0	0,7500	-260,9
12,00E3	9000	70,00E3	100,0E3	0,8000	90,00	300,0	0,7500	-275,6
12,00E3	9000	45,00E3	100,0E3	0,8000	90,00	300,0	0,7500	-268,3
12,00E3	9000	57,50E3	120,0E3	0,8000	90,00	300,0	0,7500	-265,8
12,00E3	9000	57,50E3	80,00E3	0,8000	90,00	300,0	0,7500	-280,8
12,00E3	9000	57,50E3	100,0E3	1,000	90,00	300,0	0,7500	-275,8
12,00E3	9000	57,50E3	100,0E3	0,6000	90,00	300,0	0,7500	-271,8
12,00E3	9000	57,50E3	100,0E3	0,8000	110,0	300,0	0,7500	-276,1
12,00E3	9000	57,50E3	100,0E3	0,8000	70,00	300,0	0,7500	-269,0
12,00E3	9000	57,50E3	100,0E3	0,8000	90,00	500,0	0,7500	-264,1
12,00E3	9000	57,50E3	100,0E3	0,8000	90,00	100,0	0,7500	-292,3
12,00E3	9000	57,50E3	100,0E3	0,8000	90,00	300,0	0,9000	-293,1
12,00E3	9000	57,50E3	100,0E3	0,8000	90,00	300,0	0,6000	-266,3
12,00E3	9000	57,50E3	100,0E3	0,8000	90,00	300,0	0,7500	-273,6

Reference analysis

Figure 150. Sensitivity analysis (HSS parameters – vertical stress of point K)

Criterion: horizontal stress – point L

Type	Material	Parameter	Min	Ref	Max	SensiScore
Soil	hss	E_{50}^{ref}	8000	12,00E3	16,00E3	19
Soil	hss	E_{oed}^{ref}	6000	9000	12,00E3	6
Soil	hss	E_{ur}^{ref}	45,00E3	57,50E3	70,00E3	8
Soil	hss	G_0^{ref}	80,00E3	100,0E3	120,0E3	4
Soil	hss	power (m)	0,6000	0,8000	1,000	3
Soil	hss	c'_{ref}	70,00	90,00	110,0	40
Soil	hss	POP	100,0	300,0	500,0	14
Soil	hss	$K_{0,x}$	0,6000	0,7500	0,9000	6

E_{50}^{ref} [hss]	E_{oed}^{ref} [hss	E_{ur}^{ref} [hss]	G_0^{ref} [hss]	power (m) [	c'_{ref} [hss]	POP [hss]	$K_{0,x}$ [hss]	Criterion 1
16,00E3	9000	57,50E3	100,0E3	0,8000	90,00	300,0	0,7500	-108,3
8000	9000	57,50E3	100,0E3	0,8000	90,00	300,0	0,7500	-83,54
12,00E3	12,00E3	57,50E3	100,0E3	0,8000	90,00	300,0	0,7500	-98,73
12,00E3	6000	57,50E3	100,0E3	0,8000	90,00	300,0	0,7500	-106,6
12,00E3	9000	70,00E3	100,0E3	0,8000	90,00	300,0	0,7500	-96,05
12,00E3	9000	45,00E3	100,0E3	0,8000	90,00	300,0	0,7500	-107,1
12,00E3	9000	57,50E3	120,0E3	0,8000	90,00	300,0	0,7500	-105,6
12,00E3	9000	57,50E3	80,00E3	0,8000	90,00	300,0	0,7500	-100,6
12,00E3	9000	57,50E3	100,0E3	1,000	90,00	300,0	0,7500	-101,6
12,00E3	9000	57,50E3	100,0E3	0,6000	90,00	300,0	0,7500	-105,1
12,00E3	9000	57,50E3	100,0E3	0,8000	110,0	300,0	0,7500	-122,4
12,00E3	9000	57,50E3	100,0E3	0,8000	70,00	300,0	0,7500	-70,46
12,00E3	9000	57,50E3	100,0E3	0,8000	90,00	500,0	0,7500	-106,7
12,00E3	9000	57,50E3	100,0E3	0,8000	90,00	100,0	0,7500	-87,79
12,00E3	9000	57,50E3	100,0E3	0,8000	90,00	300,0	0,9000	-101,6
12,00E3	9000	57,50E3	100,0E3	0,8000	90,00	300,0	0,6000	-96,50
12,00E3	9000	57,50E3	100,0E3	0,8000	90,00	300,0	0,7500	-104,3

Reference analysis

Figure 151. Sensitivity analysis (HSS parameters –horizontal stress of point L)

C.2. Lining stiffness

The figures below depict the sensitivity score calculated for the different criteria (Table 30) varying the lining stiffness between a reasonable

minimum and a maximum value. All these evaluations refer to the final phase (phase 4, Table 29) of the simulation.
As it can be seen in the lower part of the figures, where the results of all the calculated permutations are listed, the influence of the lining stiffnesses on soil stresses and displacements is quite low.

Criterion: vertical displacement – point A

Type	Material	Parameter	Min	Ref	Max	SensiScore
Plate	primary lining	EA_1	2,500E6	3,000E6	3,500E6	39
Plate	primary lining	EI	10,00E3	17,50E3	25,00E3	56
Plate	invert	EA_1	18,00E6	24,00E6	30,00E6	1
Plate	invert	EI	500,0E3	1,300E6	2,100E6	4

EA_1 [primar	EI [primary l	EA_1 [invert]	EI [invert]	Criterion 1
3,500E6	17,50E3	24,00E6	1,300E6	-0,03763
2,500E6	17,50E3	24,00E6	1,300E6	-0,03815
3,000E6	25,00E3	24,00E6	1,300E6	-0,03758
3,000E6	10,00E3	24,00E6	1,300E6	-0,03831
3,000E6	17,50E3	30,00E6	1,300E6	-0,03787
3,000E6	17,50E3	18,00E6	1,300E6	-0,03788
3,000E6	17,50E3	24,00E6	2,100E6	-0,03786
3,000E6	17,50E3	24,00E6	500,0E3	-0,03791
3,000E6	17,50E3	24,00E6	1,300E6	-0,03788

Reference analysis

Figure 152. Sensitivity analysis (Lining stiffness – vertical displacement of node A)

Criterion: vertical displacement – point B

Type	Material	Parameter	Min	Ref	Max	SensiScore
Plate	primary lining	EA_1	2,500E6	3,000E6	3,500E6	37
Plate	primary lining	EI	10,00E3	17,50E3	25,00E3	59
Plate	invert	EA_1	18,00E6	24,00E6	30,00E6	1
Plate	invert	EI	500,0E3	1,300E6	2,100E6	3

EA_1 [primar	EI [primary l	EA_1 [invert]	EI [invert]	Criterion 1
3,500E6	17,50E3	24,00E6	1,300E6	-0,05611
2,500E6	17,50E3	24,00E6	1,300E6	-0,05687
3,000E6	25,00E3	24,00E6	1,300E6	-0,05598
3,000E6	10,00E3	24,00E6	1,300E6	-0,05717
3,000E6	17,50E3	30,00E6	1,300E6	-0,05645
3,000E6	17,50E3	18,00E6	1,300E6	-0,05647
3,000E6	17,50E3	24,00E6	2,100E6	-0,05644
3,000E6	17,50E3	24,00E6	500,0E3	-0,05651
3,000E6	17,50E3	24,00E6	1,300E6	-0,05646

Reference analysis

Figure 153. Sensitivity analysis (Lining stiffness – vertical displacement of node B)

Criterion: horizontal displacement – point C

Type	Material	Parameter	Min	Ref	Max	SensiScore
Plate	primary lining	EA_1	2,500E6	3,000E6	3,500E6	38
Plate	primary lining	EI	10,00E3	17,50E3	25,00E3	55
Plate	invert	EA_1	18,00E6	24,00E6	30,00E6	3
Plate	invert	EI	500,0E3	1,300E6	2,100E6	3

EA_1 [primar	EI [primary l	EA_1 [invert]	EI [invert]	Criterion 1
3,500E6	17,50E3	24,00E6	1,300E6	-0,06833
2,500E6	17,50E3	24,00E6	1,300E6	-0,06872
3,000E6	25,00E3	24,00E6	1,300E6	-0,06879
3,000E6	10,00E3	24,00E6	1,300E6	-0,06822
3,000E6	17,50E3	30,00E6	1,300E6	-0,06853
3,000E6	17,50E3	18,00E6	1,300E6	-0,06856
3,000E6	17,50E3	24,00E6	2,100E6	-0,06855
3,000E6	17,50E3	24,00E6	500,0E3	-0,06852
3,000E6	17,50E3	24,00E6	1,300E6	-0,06854

Reference analysis

Figure 154. Sensitivity analysis (Lining stiffness – vertical displacement of node C)

Criterion: vertical displacement – point D

Type	Material	Parameter	Min	Ref	Max	SensiScore
Plate	primary lining	EA_1	2,500E6	3,000E6	3,500E6	39
Plate	primary lining	EI	10,00E3	17,50E3	25,00E3	45
Plate	invert	EA_1	18,00E6	24,00E6	30,00E6	4
Plate	invert	EI	500,0E3	1,300E6	2,100E6	12

EA_1 [primar	EI [primary l	EA_1 [invert]	EI [invert]	Criterion 1
3,500E6	17,50E3	24,00E6	1,300E6	0,07517
2,500E6	17,50E3	24,00E6	1,300E6	0,07518
3,000E6	25,00E3	24,00E6	1,300E6	0,07520
3,000E6	10,00E3	24,00E6	1,300E6	0,07529
3,000E6	17,50E3	30,00E6	1,300E6	0,07526
3,000E6	17,50E3	18,00E6	1,300E6	0,07525
3,000E6	17,50E3	24,00E6	2,100E6	0,07525
3,000E6	17,50E3	24,00E6	500,0E3	0,07523
3,000E6	17,50E3	24,00E6	1,300E6	0,07525

Reference analysis

Figure 155. Sensitivity analysis (Lining stiffness – vertical displacement of node D)

Criterion: vertical stress – point K

Type	Material	Parameter	Min	Ref	Max	SensiScore
Plate	primary lining	EA_1	2,500E6	3,000E6	3,500E6	75
Plate	primary lining	EI	10,00E3	17,50E3	25,00E3	24
Plate	invert	EA_1	18,00E6	24,00E6	30,00E6	0
Plate	invert	EI	500,0E3	1,300E6	2,100E6	1

EA_1 [primar	EI [primary l	EA_1 [invert]	EI [invert]	Criterion 1
3,500E6	17,50E3	24,00E6	1,300E6	-276,8
2,500E6	17,50E3	24,00E6	1,300E6	-269,2
3,000E6	25,00E3	24,00E6	1,300E6	-274,7
3,000E6	10,00E3	24,00E6	1,300E6	-272,3
3,000E6	17,50E3	30,00E6	1,300E6	-273,6
3,000E6	17,50E3	18,00E6	1,300E6	-273,6
3,000E6	17,50E3	24,00E6	2,100E6	-273,6
3,000E6	17,50E3	24,00E6	500,0E3	-273,5
3,000E6	17,50E3	24,00E6	1,300E6	-273,6

Reference analysis

Figure 156. Sensitivity analysis (Lining stiffness – vertical stress of point K)

Criterion: horizontal stress – point L

Type	Material	Parameter	Min	Ref	Max	SensiScore
Plate	primary lining	EA_1	2,500E6	3,000E6	3,500E6	29
Plate	primary lining	EI	10,00E3	17,50E3	25,00E3	50
Plate	invert	EA_1	18,00E6	24,00E6	30,00E6	2
Plate	invert	EI	500,0E3	1,300E6	2,100E6	19

EA_1 [primar	EI [primary l	EA_1 [invert]	EI [invert]	Criterion 1
3,500E6	17,50E3	24,00E6	1,300E6	-103,4
2,500E6	17,50E3	24,00E6	1,300E6	-104,4
3,000E6	25,00E3	24,00E6	1,300E6	-104,9
3,000E6	10,00E3	24,00E6	1,300E6	-103,1
3,000E6	17,50E3	30,00E6	1,300E6	-104,3
3,000E6	17,50E3	18,00E6	1,300E6	-104,2
3,000E6	17,50E3	24,00E6	2,100E6	-104,1
3,000E6	17,50E3	24,00E6	500,0E3	-104,8
3,000E6	17,50E3	24,00E6	1,300E6	-104,3

Reference analysis

Figure 157. Sensitivity analysis (Lining stiffness –horizontal stress of point L)

C.3. Stress relaxation factor

Provided that 2D analyses are still widely used for tunnelling applications, a further set of analyses was carried out to investigate the influence of the stress relaxation factor on both displacements and structural forces. As it can be seen from Table 33 and Figure 158, the variation in the computed values of lining displacements and surface settlements can be very high. On

the other hand, the influence in terms of lining axial force seems to be less remarkable.
It should be considered that the influence of the stress relaxation factor on the model response can vary significantly according to the particular geometry and ground properties considered.

Table 33. Calculated values of the maximum displacements and axial forces

		max u_y surface (mm)	max u_y crown (mm)	max u_x sidewalls (mm)	N_{max} (kN)
comb 1	λ_1=0,3; λ_2=1; λ_3=0,2	38	57	62	1980
comb 2	λ_1=0,5; λ_2=1; λ_3=0,2	41	68	67	1851
comb 3	λ_1=0,3; λ_2=0,8; λ_3=0,2	20	34	36	2055
comb 4	λ_1=0,3; λ_2=1; λ_3=0,5	48	90	75	1942

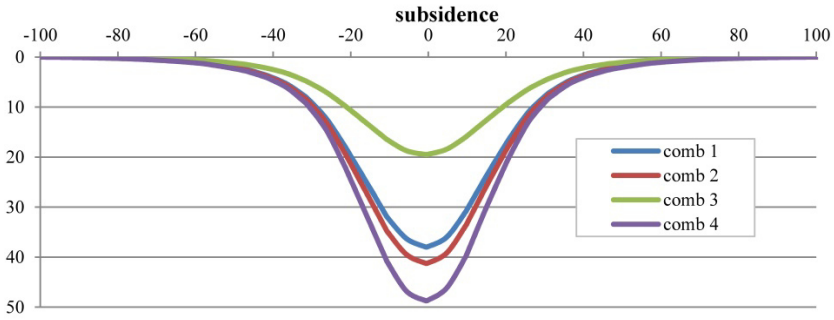

Figure 158. Subsidence for different sets of stress relaxation factors